Ancillary Ligand Effects: from Zirconium(IV)-Catalyzed Homogeneous Propylene Polymerization to Platinum(II)-Mediated C–H Bond Activation

Thesis by

Hong A. Zhong

In Partial Fulfillment of the
Requirements for the Degree of
Doctor of Philosophy

Division of Chemistry
and Chemical Engineering

California Institute of Technology
Pasadena, CA

2001
(Defended May 24, 2001)

For Grandfather

Acknowledgments

My years as a graduate student would not have been possible without the understanding and support of my family. I know how hard it must have been for you to feel disconnected from my life and to be separated from your only child for so long. I appreciate the sacrifice you have made for me, and I am grateful for your allowing me to pursue my own career path. I would also like to thank both Mr. Ron Ayling and Ms. Billie Ayling, my Australian guest parents, for their unwavering friendship and constant encouragement.

I would like to thank Professors Steve Buchwald, Gregory Hillhouse and Kit Cummins for having encouraged my participation in undergraduate research, and Steve for having helped me choose Caltech for my graduate study. My special thanks goes to Dr. Ross Widenhoefer for his invaluable advice (whether asked-for or not) on how to conduct indepedent research, how to advance in one's career without comprimising the personal integrity, and how to be a team player. He was also instrumental in transforming me from a PAW to a QOTM, and had prepared me well for the "abuse" that I was to receive and the "politics" that I was to experience as a graduate student.

I must acknowledge Professor John Bercaw, my advisor, for his wealth of knowledge and his hands-off management style. I am particularly grateful for his patience and understanding when things were going slowly, and for allowing me the flexibility to switch projects in the middle of graduate study. John has been a great teacher, whose fine example of high work standards and work ethics I can only hope to emulate. Dr. Jay Labinger has been my co-advisor on the Pt project, whose suggestion and input have always been enlightening and helpful. I also must thank my committee members – Professors Fred Anson, Bob Grubbs and Dave MacMillan – for their time and suggestions.

The past and present members of the Bercaw group have been a mix of characters, each of whom has taught me something unique in one's own way. Moving into "201" from the infamous "213" at the beginning of my third year was the best decision that I made in my graduate career. Both Antek Wong-Foy and Jeff Yoder were extraordinary lab mates. I have benefited tremendously from discussions with them, who often raised interesting points that forced me to look at problems from a different angle. I have also benefited greatly from their familiarity with existing literature and their insights. I am also indebted to Antek for having taught me the high vacuum line technique, and to Jeff for having helped me setting up my first experiment. I will miss the "yelling match" with Antek and the frequent "noodle runs" to Alhambra.

Many thanks to John Scollard for his ready advice on everything, be it computer-related or chemistry. Your losing streak in poker games is just as legendary as Melanie's

winning streak. Chris Levy, despite being a total "food snob", is an incredibly good cook. Lily Ackmerman, not the least a sharp chemist, but is also brave enough to teach me driving.

Shigenobu Miyake was a wonderful resource when I started the Ziegler-Natta project. He not only taught me the little I know of preparing and characterizing polypropylene, but was forever encouraging. Thank you, Shige, for the speckless Schlenk line you left behind, and I am sorry that I haven't been able to keep it in the top-notch shape that it was first inherited. Dario Veghini also taught me a few things about the high vacuum line and the Ziegler-Natta chemistry. I am particularly grateful for his defending me when I was back-stabbed. Ola Wendt has not only revolutionized the way how kinetics were done at Bercaw group, but was also the one to suggest that I study the cationic zirconium methyl complexes. Steve Miller was also ready to help when asked. Help from Lars greatly eased my transition from Ziegler-Natta project into platinum(II) project. I am also grateful that he continued to share information and progresses with me after he returned to University of Oslo.

Chris Brandow's background in computational chemistry provides him with a unique persepctive on chemistry, and conversations with him often helped clarify my thoughts. Alex Muci was a great resource for organic chemistry, and Joseph Sadighi is a walking encyclopedia on almost anything. Seva Rostovtsev also amazes me with his breadth of knowledge (be it chemistry or not) and his ability to file information away for ready future references.

Jonathan Owen, like it or not, you are going to be a stud like Shannon Stahl. Christoph and Cliff, thank you for doing a great job proof-reading for me. And to the women in the group – Susan, Lily, Sara and Endy - thank you for finally bringing a balance of gender to the Bercaw group.

I am also indebted to people outside the research group. Rick Gerhart, I don't know how I would have survived without your glass-blowing skills. Larry Henling, thank you for solving all those X-ray structures for me and for your "friendly" conversations. Last, but not the least, the thanks go to Dian Buchness and Pat Anderson, who have kept the graduate program and the Bercaw group running as smoothly as possible.

Abstract

A series of C_s- and C_1-symmetric doubly-linked *ansa*-metallocenes of the general formula $\{1,1'\text{-SiMe}_2\text{-}2,2'\text{-E-}(\eta^5\text{-C}_5\text{H}_2\text{-4-R}^1)\text{-}(\eta^5\text{-C}_5\text{H-3}',5'\text{-(CHMe}_2)_2)\}\text{ZrCl}_2$ (E = $SiMe_2$ (**1**), $SiPh_2$ (**2**), $SiMe_2$–$SiMe_2$(**3**); R^1 = H, $CHMe_2$, C_5H_9, C_6H_{11}, C_6H_5) has been prepared. When activated by methylaluminoxane, these are active propylene polymerization catalysts. **1** and **2** produce syndiotactic polypropylenes, and **3** produces isotactic polypropylenes. Site epimerization is the major pathway for stereoerror formation for **1** and **2**. In addition, the polymer chain has slightly stronger steric interaction with the diphenylsilylene linker than with the dimethylsilylene linker. This results in more frequent site epimerization and reduced syndiospecificity for **2** compared to **1**.

C_1-Symmetric *ansa*-zirconocenes $[1,1'\text{-SiMe}_2\text{-(C}_5\text{H}_4)\text{-(3-R-C}_5\text{H}_3)]\text{ZrCl}_2$ (**4**), $[1,1'\text{-SiMe}_2\text{-(C}_5\text{H}_4)\text{-(2,4-R}_2\text{-C}_5\text{H}_2)]\text{ZrCl}_2$ (**5**) and $[1,1'\text{-SiMe}_2\text{-2,2'-(SiMe}_2\text{–SiMe}_2)\text{-(C}_5\text{H}_3)\text{-(4-R-C}_5\text{H}_2)]\text{ZrCl}_2$ (**6**) have been prepared to probe the origin of isospecificity in **3**. While **4** and **3** produce polymers with similar isospecificity, **5** and **6** give mostly hemi-isotactic-like polymers. It is proposed that the facile site epimerization via an associative pathway allows rapid equilibration of the polymer chain between the isospecific and aspecific insertion sites. This results in more frequent insertion from the isospecific site, which has a lower kinetic barrier for chain propagation. On the other hand, site epimerization for **5** and **6** is slow. This leads to mostly alternating insertion from the isospecific and aspecific sites, and consequently, a hemi-isotactic-like polymers. In comparison, site epimerization is even slower for **3**, but enchainment from the aspecific site has an extremely high kinetic barrier for monomer coordination. Therefore, enchainment occurs preferentially from the isospecific site to produce isotactic polymers.

A series of cationic complexes $[(\text{ArN=CR–CR=NAr})\text{PtMe(L)}]^+[\text{BF}_4]^-$ (Ar = aryl; R = H, CH_3; L = water, trifluoroethanol) has been prepared. They react smoothly with benzene at approximately room temperature in trifluoroethanol solvent to yield methane and the corresponding phenyl Pt(II) cations, via Pt(IV)-methyl-phenyl-hydride intermediates. The reaction products of methyl-substituted benzenes suggest an inherent reactivity preference for aromatic over benzylic C–H bond activation, which can however be overridden by steric effects. For the reaction of benzene with cationic Pt(II) complexes, in which the diimine ligands bear 3,5-disubstituted aryl groups at the nitrogen atoms, the rate-determining step is C–H bond activation. For the more sterically crowded analogs with 2,6-dimethyl-substituted aryl groups, benzene coordination becomes rate-determining. The more electron-rich the ligand, as reflected by the CO stretching frequency in the IR spectrum of the corresponding cationic carbonyl complex, the faster the rate of C–H bond activation. This finding, however, does not reflect the actual C–H bond activation process, but rather reflects only the relative ease of

solvent molecules displacing water molecules to initiate the reaction. That is, the change in rates is mostly due to a ground state effect. Several lines of evidence suggest that associative substitution pathways operate to get the hydrocarbon substrate into, and out of, the coordination sphere; *i. e.,* that benzene substitution proceeds by a solvent- (TFE-) assisted associative pathway.

Table of Contents

List of Figures

Chapter 1:

Chapter 2:

Chapter 3:

Chapter 4:

Appendix A:

Appendix H:

List of Tables

Chapter 1:

Chapter 2:

Chapter 3:

Chapter 4:

Appendix B:

Appendix C:

Appendix D:

Appendix E:

Appendix F:

Appendix G:

Chapter 1

Stereochemical Control in Homogeneous Ziegler-Natta Polymerization

Abstract

The mechanism of stereochemical control in homogeneous Ziegler-Natta polymerization is briefly described to provide context for the discussion in Chapters 2 and 3.

Introduction

Transition metal catalysts are ubiquitous in heterogeneous and homogenous reactions due to their high selectivity and activity. One such example is the Ziegler-Natta polymerization of ethylene and propylene. The process is named after Karl Ziegler, who in 1953[1] discovered that $TiCl_4$-$AlEt_3$ was highly efficient in high-density polyethylene production; and Natta,[2] who in the following year revealed that $TiCl_3$-$AlEt_3$ was capable of producing isotactic polypropylene.

Since then, much effort has been put forth to understand the fundamental mechanism of the polymerization reaction and to develop better catalysts. For this reason, a well-defined catalyst system was highly desirable in order to identify the active site and to understand the origins of regio- and stereoselectivity. The discovery that homogeneous mixtures of titanocene dichloride and diethylaluminum chloride effected ethylene polymerization[3] allowed chemists to use metallocene catalysts as homogenous models for Ziegler-Natta polymerization catalysts.

Mechanistic studies on these metallocene catalysts elucidated much information on the basic steps in olefin polymerization, which in turn allowed for a rational design of new generations of catalysts. It is now generally agreed upon that in early transition metal based catalytic system, the active species are 14 e^-, d^0 alkyl complexes with at least two vacant orbitals, one of which is necessary for transition state agostic stabilization[4] in the monomer insertion step (*vide infra*).[5-7]

Further studies revealed a strong correlation between the symmetry of the [Cp_2M] fragment (Cp refers to substituted and /or linked cyclopentadienyl/ indenyl/ fluorenyl ligands) and the microstructure of the resulting polyolefin (Table 1).[8-15] For example, achiral C_{2v}-symmetric zirconocene dichloride produces atactic polypropene when activated by methylaluminoxane (MAO). In contrast, a mixture of MAO and C_2-symmetric catalysts such as *rac*-ethylenebis(tetrahydroindenyl)-zirconium dichloride produces highly isotactic polymers.[8,9,16] C_1-symmetric zirconocenes produce polymers ranging from hemi-isotactic to isotactic,[11,12,15,17-20] depending on both the polymerization conditions and the inherent substituent effects.[12,21,22] In general, polymers produced by C_1-symmetric catalysts are of much lower tacticity.[22,23] Highly syndiotactic polymerizations have been carried out with C_s-symmetric fluorenyl

based zirconocene precursors (**1**),[13,18,19,24] and more recently, with the doubly silylene-bridged cyclopentadienyl based "Thp" systems (**2**).[25-27]

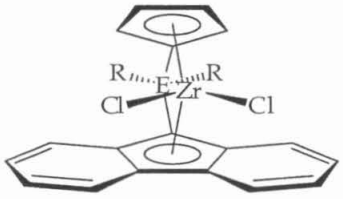

1

(M=Zr, Hf; E=C, Si; R= Me, Ph)

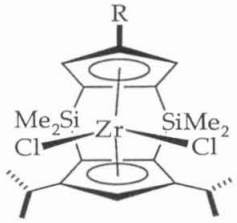

2, (Thp-R)$ZrCl_2$

(R=H, iPr, t-Bu, TMS, etc.)

Table 1. Correlation between catalyst symmetry and polymer tacticity.

Catalyst Symmetry	Polymer Structure (site control)	Polymer Structure (chain-end control)
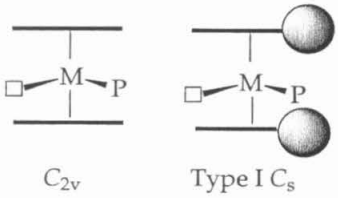 C_{2v} Type I C_s	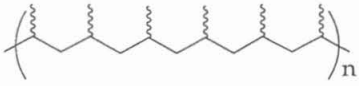 atactic	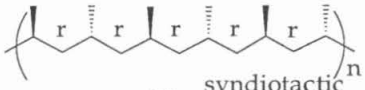 syndiotactic or 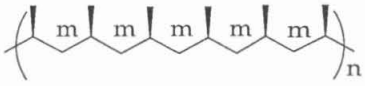 isotactic
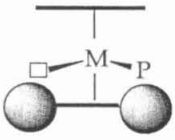 Type II C_s	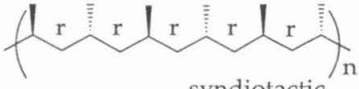 syndiotactic	N/A
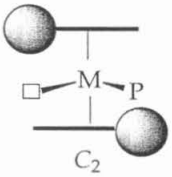 C_2	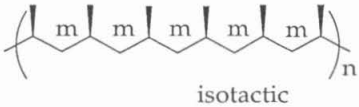 isotactic	N/A
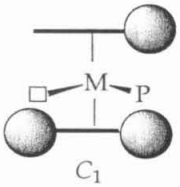 C_1	variable	N/A

Unlike the synthesis of small organic molecules, the polymer chain remains attached to the metal center during chain-growth. Therefore, in theory, both the ligand symmetry and the polymer stereochemistry will have influence on monomer's enantioselectivity during enchainment. Insertion of an α-olefin creates a stereogenic center at the β-carbon, and the subsequent monomer coordination through *re*-face differs in energy from the diastereomer with *si*-face coordination (Scheme 1). If the energy difference between the diastereomers is great enough, then the stereochemical properties of the last inserted unit determines the polymer tacticity. This mode of stereochemical regulation is referred to as "polymer chain-end control",[5] and is predominant at low temperature polymerizations by C_{2v}- and Type 1 C_s-symmetric metallocenes.[13,28]

Scheme 1

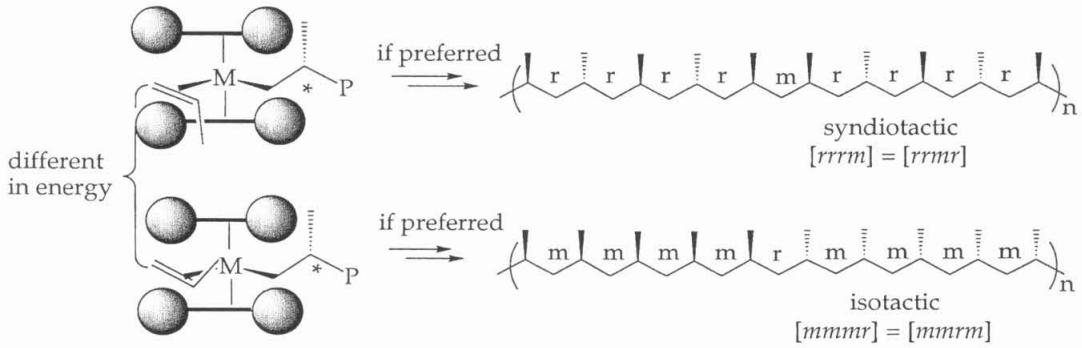

However, if the ligand influence overrides stereochemical preferences exerted by polymer chain end, then polymer stereochemistry is under "enantiomorphic-site control" mechanism (Scheme 2).

Scheme 2

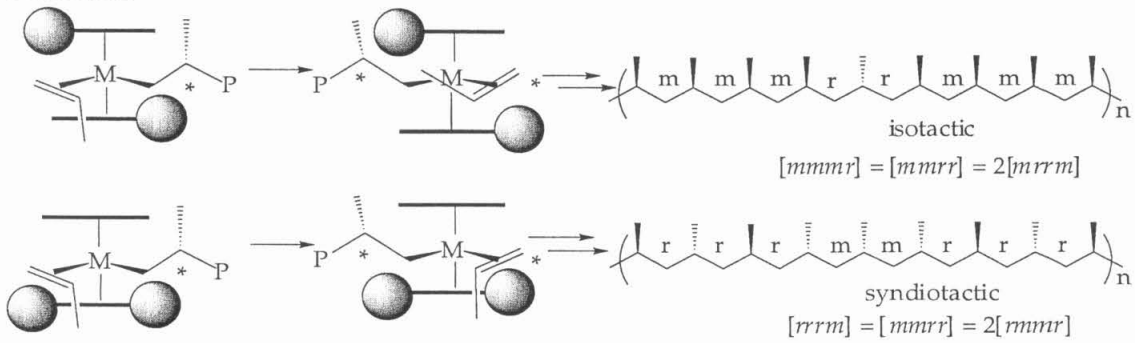

In the "polymer chain-end control" mechanism, the stereo-errors are propagated down the chain (Scheme 1); while in the "enantiomorphic-site control" mechanism, the errors are most often corrected during the next enchainment (Scheme 2). Thus if the polymer chain consists mainly of isolated *m*-dyad (or *r*-dyad) errors, then the chain-end control is operative; whereas if *mm*-triad (or *rr*-triad) errors predominate, then the stereochemistry is under enantiomorphic-site control.

It is now known that enantiomorphic site control is operative for most Group IV metallocene-catalyzed temperatures at ambient temperature and above. However, the enantiofacial selectivity in monomer coordination is not a result of direct interactions with the ligand set. In fact, studies have shown that in the first step of polymerization, when the alkyl group bonded to the metal is a methyl group, the propene insertion is essentially non-enantioselective, which means the energy difference between *re*- or *si*-coordination as a result of direct monomer-ligand interaction is small.[29] Rather the stereochemical control is relayed by the polymer chain.[30] Monomer insertion is assisted by polymer chain's α-agostic interaction with the metal center in the transition state.[31] Of the two possible α-agostic conformation, only one directs the polymer chain away from the steric bulk of the ligand, which determines the preferred orientation of the polymer chain (Figure 1a). To effect the C–C bond formations, it is necessary to bring the monomer and the polymer chain close together. Thus the transition state of monomer insertion involves considerable steric repulsion between the monomer and the polymer chain, which is minimized by orienting the polymer chain and the monomer alkyl substituent trans to each other (Figure 1b). Thus the ligand environment directs the polymer chain orientation, and the polymer chain relays this stereochemical influence on to the monomer through transition state steric interactions. This conclusion has been born out both experimentally[30] and theoretically.[32-34] However, there is still dispute as to which transition structure (**B** or **C**) leads to enantiofacial mis-insertion. Corradini and co-workers favor **C** as the one with lower transition state energy,[35] while Morokuma and Rappe prefer **B**.[33,34,36]

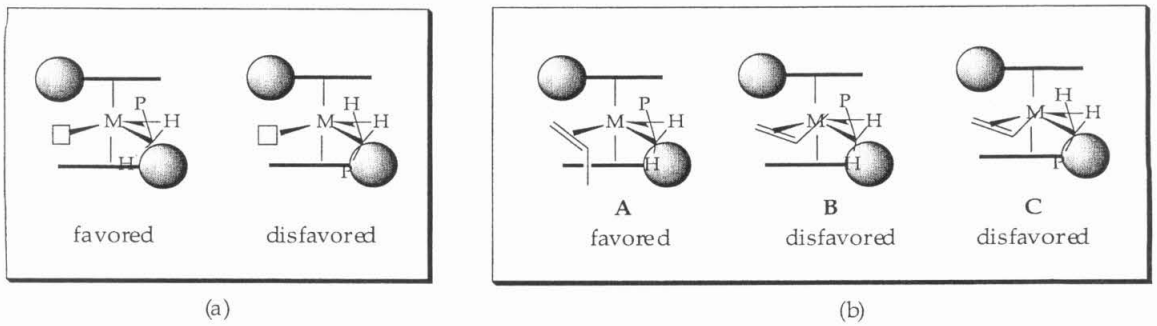

Figure 1. Origin of stereospecificity in enantiomorphic-site control mechanism, using a C_2-symmetric catalyst as an example.

In C_2-symmetric catalysts, the two coordination/insertion sites are homotopic, and monomer insertion thus proceeds with the same enantioface on either side (Scheme 3). This results in isotactic polymers.

Scheme 3

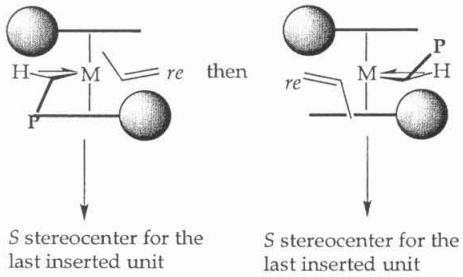

For these C_2-symmetric systems, stereoerrors mainly arise from either enantiofacial mis-insertion (Scheme 4) or chain epimerization (the stereochemistry at the last inserted monomer unit is inverted) (Scheme 5).[7,37–39] The number of stereoerrors produced by enantiofacial misinsertion is independent of monomer concentration, whereas the frequency of stereoerrors produced by chain epimerization process should show a dependence, because this is a uni-molecular process that competes with bimolecular propagation.[7,38,40]

Scheme 4

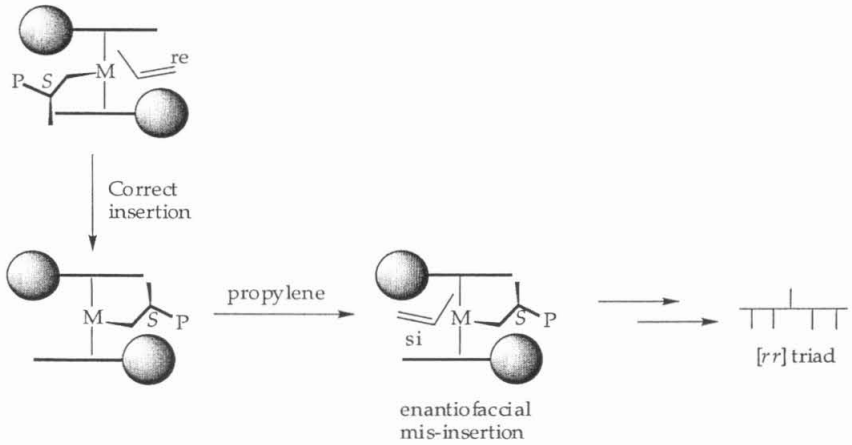

Scheme 5

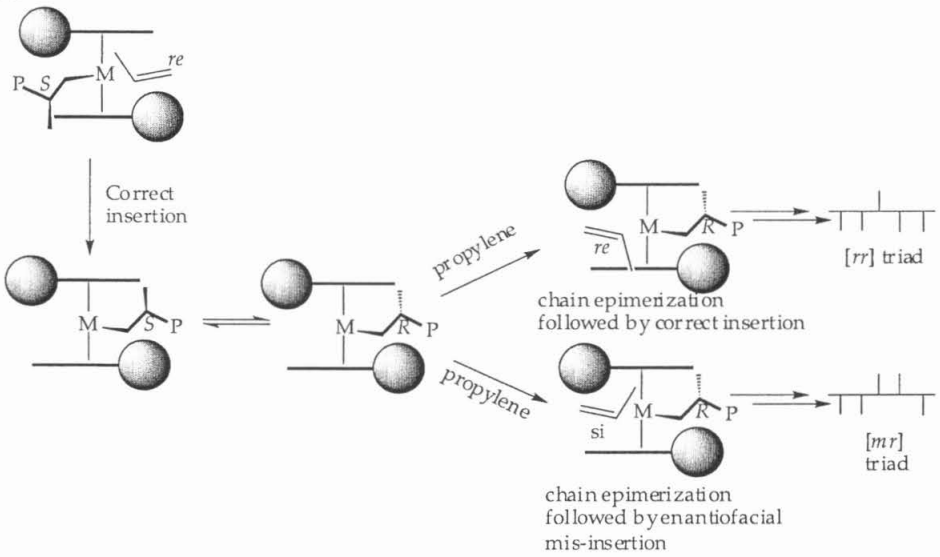

Busico has proposed a tertiary-alkyl mechanism to explain the chain epimerization process.[39,40] According to this mechanism, initial β-H elimination is followed by a 180° in-plane rotation with a subsequent 2,1-insertion to form a quaternary α-carbon center with two diastereotopic methyl groups, which is extremely slow for further monomer insertion.[9,41] This allows time for a 120° bond-rotation around the M–Cα bond and β-H elimination from the methyl group labeled with an asterisk to form a new metal hydride-*gem*-olefin complex. This is followed by an in-plane rotation and a 1,2 olefin insertion, which finally leads to the inversion of the stereocenter at the β-carbon. A direct consequence of the mechanism is that the methylene and methyl carbons are interchanged by

chain-epimerization, and is consistent with the observation that when [1-D]-propylene was used, deuterium is incorporated into the methyl groups of the stereoerrors (Scheme 6).

Scheme 6

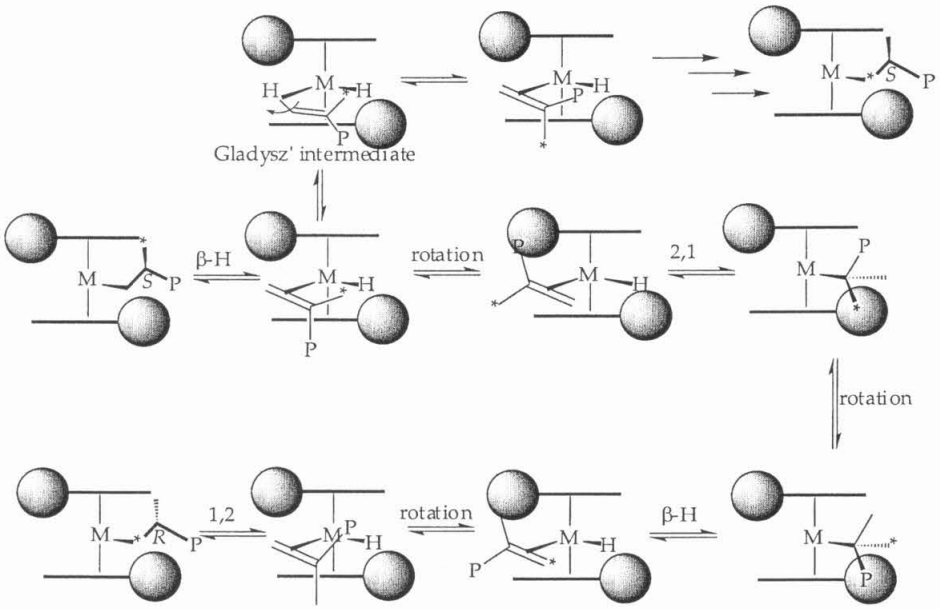

To additionally accommodate the observation that deuterium is also incorporated into the methyl groups with the correct stereochemistry, a Gladysz' type intermediate[42] is proposed. This mechanism has been proved by polymerization with a doubly-labeled propylene.[43] The alternative allyl-mechanism for the chain-epimerization process has been discounted by the same study.[9,44]

Whereas the isospecific metallocene catalysts have highly variable structures, syndiotactic polypropylene traditionally is only made using the system (**1**) developed by Razavi and Ewen.[14] More recently, Herzog *et al.* reported a new class of doubly-linked *ansa*-zirconocenes (**2**) that are capable of promoting highly syndiospecific polymerization in the presence of MAO.[25–27]

The two systems share some common features: (a) C_s-symmetric, with a mirror plane bisecting the two coordination sites; (b) cyclopentadienyl rings of differing sizes; (c) an open region at the front of the metallocene wedge to accommodate the alkyl group of the α-olefins. The third feature seems crucial in

obtaining high syndiotacticity, as exemplified by the lack of stereospecificity displayed by **3**, which lacks an open region in the front.[25]

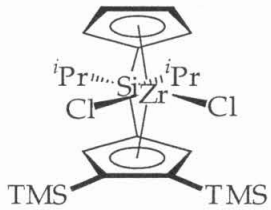

3

The two insertion sites in these C_s-symmetric catalysts (where the mirror plane bisects the Site1–M–Site 2) are enantiotopic. Monomer coordinates and inserts with opposite enantioface from the two sites. Thus alternating insertion from the two sites leads to *rac*-stereochemistry of the two adjacent monomer units, and result in syndiotactic polymers (Scheme 7).

Scheme 7

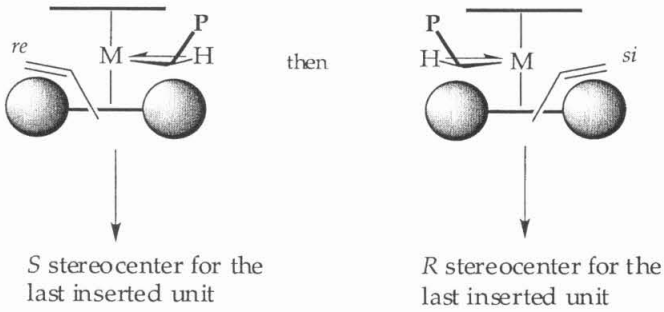

For these C_s-symmetric systems, besides enantiofacial misinsertion and chain epimerization, site epimerization[12,27] can also give rise to stereoerrors. As shown in Scheme 8, the polymer chain switches side after each insertion, and initially sits in the γ-agostic conformation. Then, depending on the rates at which olefin coordinates, the polymer chain may also isomerize to the more stable β-agostic conformation or form an inner-sphere contact pair with a counterion. Occasionally, either through a five- or three-coordinate intermediate, in which the polymer chain resides along the axis bisecting the two coordination sites, the polymer chain may switch side without occurrence of a monomer insertion, and this process is called site-epimerization or chain back-skipping. To obtain highly syndiotactic system, it is therefore important to find a system that has high site epimerization barrier so that conversion between **II** and **II'** only occurs via migratory insertion.

Scheme 8

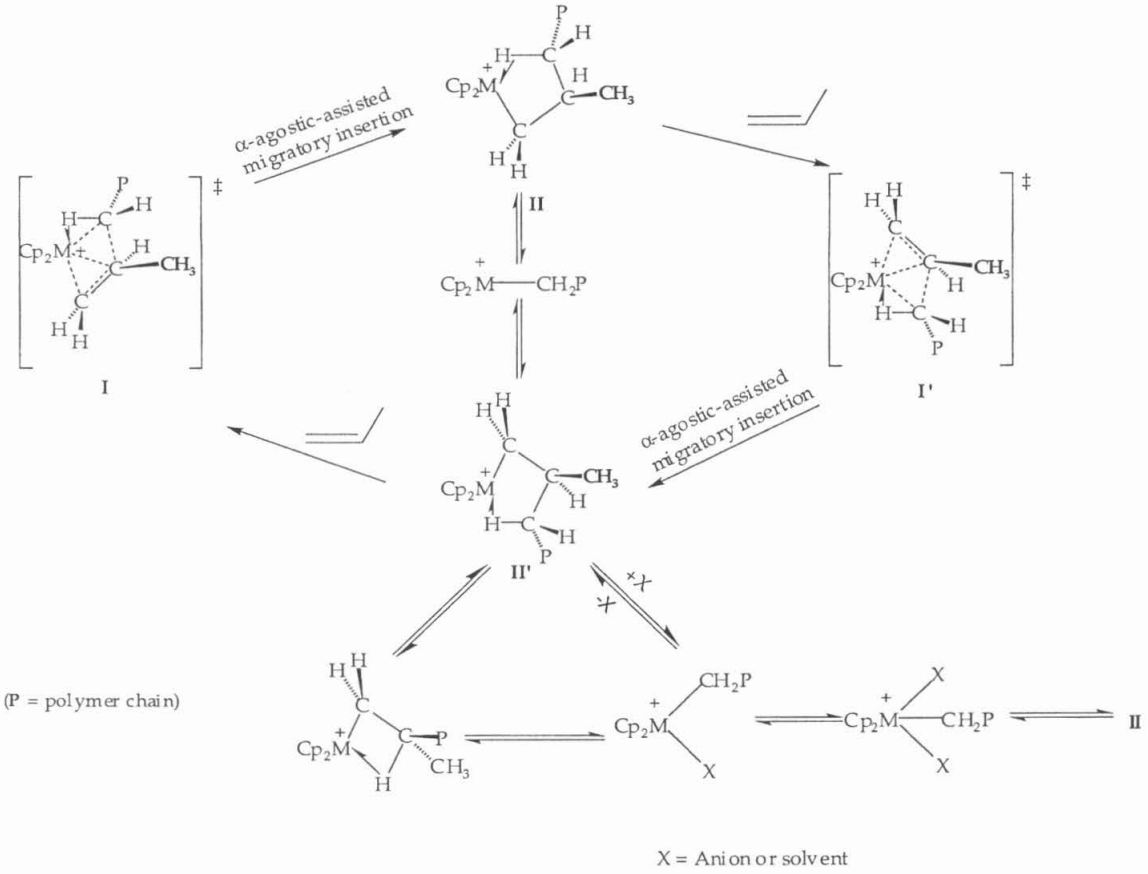

In syndiospecific systems, enantiofacial misinsertion gives rise to [*mm*] triads, the frequency of which should be independent of monomer concentration (Scheme 9). Site epimerization, on the other hand, gives rise to isolated *m* stereoerrors or [*rm*] triads (Scheme 10). Chain epimerization without subsequent site epimerization or enantiofacial misinsertion gives rise to [*mm*] triads, but if chain epimerization is followed by either a site epimerization or an enantiofacial misinsertion, then isolated *m* stereoerrors occur (Scheme 11).

Scheme 9

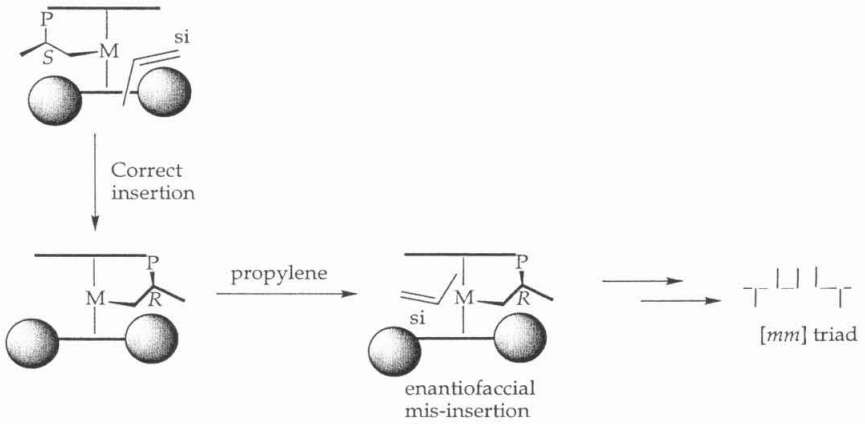

Scheme 10

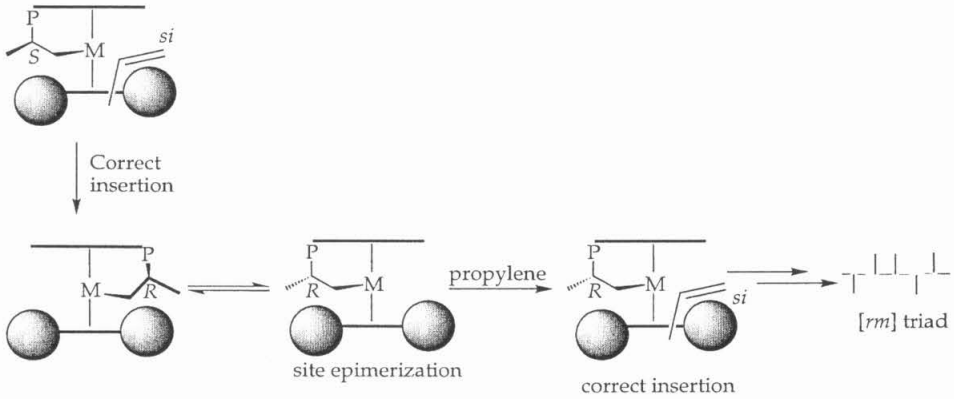

Scheme 11

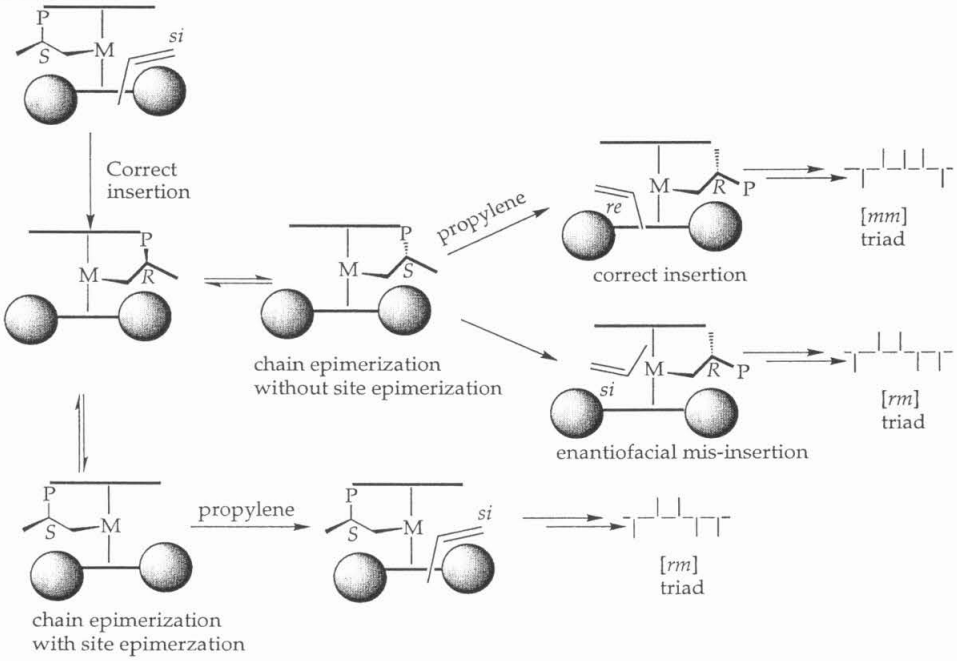

The number of stereoerrors associated with either epimerization process will likely be dependent on monomer concentration. Thus an assay of error distribution in polymers produced at different monomer concentrations can differentiate the three pathways for stereoerror formation. Detailed studies on the mechanism of stereocontrol suggest that site epimerization is the major source of stereoerrors in these systems.[27]

For C_1-symmetric catalysts, the situation is more complicated. In C_1-symmetric catalysts, the two insertion sites (A and B) are diastereotopic, thus depending on the coordination site and the monomer enantioface, four diastereotopic transition states can be envisioned for the enchainment step (Figure 2).

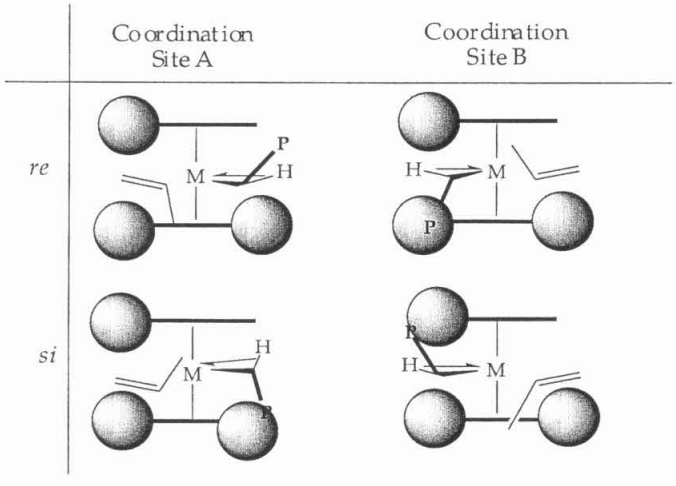

Figure 2. Four diastereotopic transition states for olefin-insertion in C_1-symmetric metallocenes.

The stereochemical outcome of the polymerization will therefore depend on 1) the enantiofacial selectivity at each site; 2) the sequence and the relative rates of insertion at each site. The influence of these two factors on the resulting polymer tacticity is summarized in Table 2.

Table 2. Correlation between polymer tacticity and insertion sequence/enantioselectivity for C_1-symmetric catalysts.

Entry	Insertion Sequence	$P_{re,\,A}$[a]	$P_{re,\,B}$[b]	Polymer Tacticity
1	$(A)_x$	1	-	isotactic
2	$[(A)_n(B)]_x$	1	0.5	mostly isotactic
3	$[(A)_n(B)_m]_x$	1	1	isotactic
4	$(AB)_x$	1	1	isotactic
5	$(AB)_x$	1	0	syndiotactic
6	$(AB)_x$	1	0.5	hemi-iostactic
7	$[(A)_n(B)_m]_x$	1	0.5	stereoblock
8	$[(A)_n(B)_m]_x$	≥ 0.5	≤ 0.5	atactic

[a]. probability of monomer insertion with the *re*-face at Site A. [b]. probability of monomer insertion with the *re*-face at Site B.

To date, the majority of highly stereospecific C_1-symmetric catalysts produce isotactic polymers (see Chart 1 for some representative examples).[11,12,17,19]

Chart 1

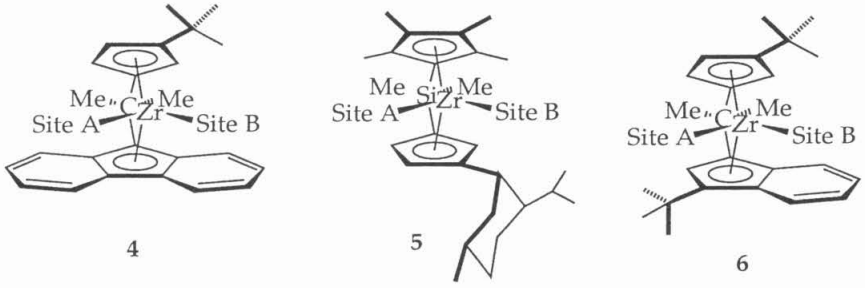

It is not clear which pathways lead to the observed high isospecificity in each individual case, and molecular modeling sometimes leads to conflicting conclusions. For example, theoretical calculations on compound **4** by Morokuma concluded[34] that insertion occurs mostly from a single site B with the polymer chain swinging to the less crowded site A after each insertion (pathway 1 or 2, Scheme 12).

Scheme 12

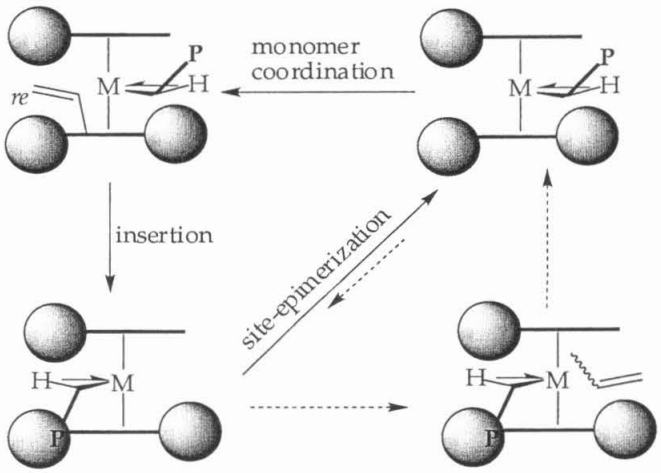

In contrast, calculations by Fink[45] and Corradini[46] both suggested that although the polymer prefers to reside at Site A, the energy difference (1 – 4 kcal/mol) is not large enough to prevent the enchainment from occurring from Site B. Instead, according to their calculation, the olefin inserts with the same enantiofacial preference on either side (pathway 3 or 4, Scheme 13).

Scheme 13

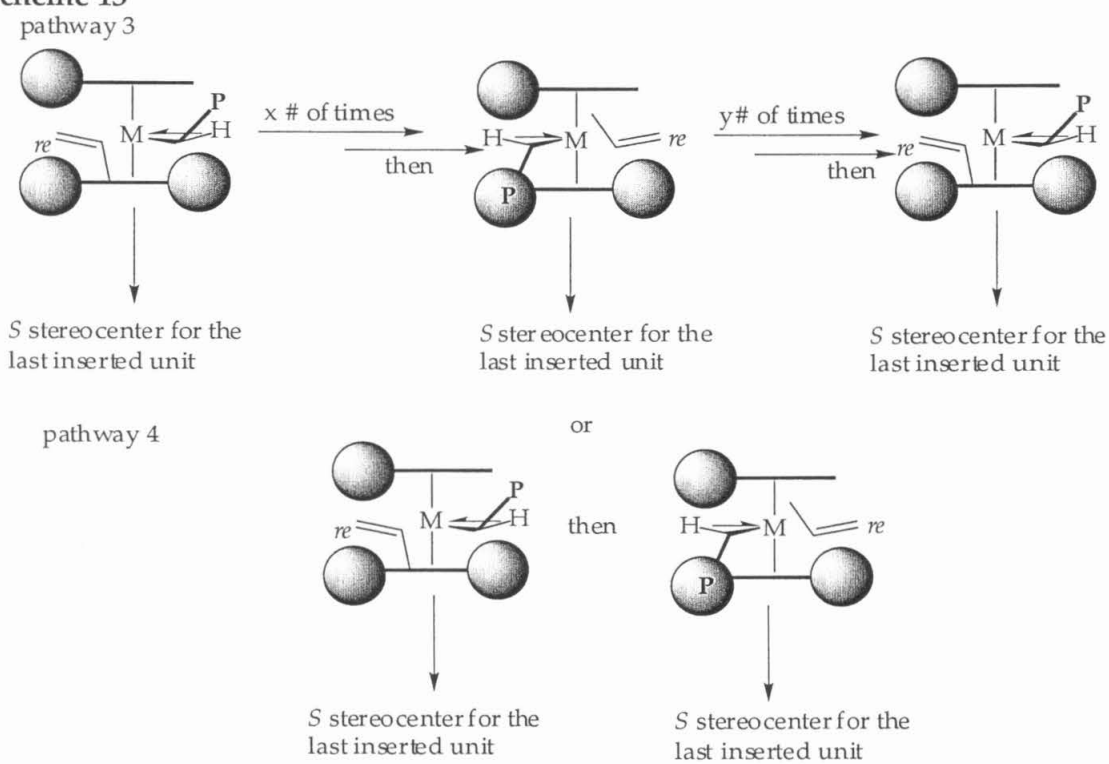

In the following two chapters, we will examine the stereoselectivity in some C_1-symmetric systems. Chapter 2 describes the synthesis and characterization of novel doubly-linked *ansa*-zirconocenes, and the study of their stereoselectivity under various polymerization conditions. The performance of these new catalyst systems will also be compared to the known zirconium polymerization catalysts.

Chapter 3, on the other hand, discusses the different stereoselectivities exhibited by C_1-symmetric zirconocene catalysts with seemingly similar structural features. Through correlation of polypropylene stereoregularities to polymerization conditions as well as examination of cationic zirconium methyl phosphine adducts, we hope to offer a unified explanation that accounts for most if not all experimental observations.

References and Notes

(1) Ziegler, K. *Angew. Chem.* **1955**, *67*, 424.

(2) Natta, G. *J. Polym. Sci.* **1955**, *16*, 424.

(3) (a) Chapman, O. L.; De La Cruz, D.; Roth, R.; Pacansky, J. J. *J. Am. Chem. Soc.* **1973**, *95*, 1337. (b) Chapman, O. L.; McIntosh, C. L.; Pacansky, J. *J. Am. Chem. Soc.* **1973**, *95*, 614. (c) Krantz, A.; Lin, C. Y.; Newton, M. D. *J. Am. Chem. Soc.* **1973**, *95*, 2744.

(4) Brookhart, M.; Green, M. L. H. *J. Organomet. Chem.* **1983**, *250*, 395–408.

(5) Barta, N. S.; Kirk, B. A.; Stille, J. R. *J. Am. Chem. Soc.* **1994**, *116*, 8912–8919.

(6) (a) Krauledat, H.; Brintzinger, H. H. *Angew. Chem. Int. Edit. Engl.* **1990**, *29*, 1412–1413. (b) Piers, W. E.; Bercaw, J. E. *J. Am. Chem. Soc.* **1990**, *112*, 9406–9407.

(7) Leclerc, M. K.; Brintzinger, H. H. *J. Am. Chem. Soc.* **1995**, *117*, 1651–1652.

(8) Coates, G. W. *Chem. Rev.* **2000**, *100*, 1223-1252.

(9) Resconi, L.; Cavallo, L.; Fait, A.; Piemontesi, F. *Chem. Rev.* **2000**, *100*, 1253–1345.

(10) (a) Collins, S.; Gauthier, W. J.; Holden, D. A.; Kuntz, B. A.; Taylor, N. J.; Ward, D. G. *Organometallics* **1991**, *10*, 2061–2068. (b) Kaminsky, W.; Kulper, K.; Brintzinger, H. H.; Wild, F. *Angew. Chem.-Int. Edit. Engl.* **1985**, *24*, 507–508.

(11) Ewen, J. A.; Elder, M. J. In *Ziegler Catalysts*; Fink, G., Mulhaupt, R., Brintzinger, H. H., Eds.; Springer-Verlag: Berlin, 1995; p 99–109.

(12) Ewen, J. A.; Elder, M. J.; Jones, R. L.; Haspeslagh, L.; Atwood, J. L.; Bott, S. G.; Robinson, K. *Makromol. Chem., Macromol. Symp.* **1991**, *48-9*, 253–295.

(13) Ewen, J. A. *J. Am. Chem. Soc.* **1984**, *106*, 6355–6364.

(14) Ewen, J. A.; Jones, R. L.; Razavi, A.; Ferrara, J. D. *J. Am. Chem. Soc.* **1988**, *110*, 6255.

(15) Ewen, J. A. *J. Mol. Catal. A.* **1998**, *128*, 103–109.

(16) Brintzinger, H. H.; Fischer, D.; Mulhaupt, R.; Rieger, B.; Waymouth, R. M. *Angew. Chem., Int. Ed. Engl.* **1995**, *34*, 1143–1170.

(17) (a) Giardello, M. A.; Eisen, M. S.; Stern, C. L.; Marks, T. J. *J. Am. Chem. Soc.* **1995**, *117*, 12114–12129. (b) Miyake, S.; Okumura, Y.; Inazawa, S. *Macromolecules* **1995**, *28*, 3074–3079. (c) Giardello, M. A.; Eisen, M. S.; Stern, C. L.; Marks, T. J. *J. Am. Chem. Soc.* **1993**, *115*, 3326-3327.

(18) Ewen, J. A. *Makromol. Chem., Macromol. Symp.* **1995**, *89*, 181–196.

(19) Ewen, J. A.; Elder, M. J. *Makromol. Chem., Macromol. Symp.* **1993**, *66*, 179–190.

(20) (a) Spaleck, W. *Metallocene-Based Polyolefins* **2000**, *1*, 425–436. (b) Spaleck, W. *Metallocene-Based Polyolefins* **2000**, *1*, 401–424. (c) Spaleck, W.; Antberg, M.; Aulbach, M.; Bachmann, B.; Dolle, V.; Haftka, S.; Kueber, F.; Rohrmann, J.; Winter, A. *Ziegler Catal.* **1995**, 83–97. (d) Spaleck, W.; Kueber, F.; Winter, A.; Rohrmann, J.; Bachmann, B.; Antberg, M.; Dolle,

V.; Paulus, E. F. *Organometallics* **1994**, *13*, 954–963. (e) Spaleck, W.; Antberg, M.; Rohrmann, J.; Winter, A.; Bachmann, B.; Kiprof, P.; Behm, J.; Herrmann, W. A. *Angew. Chem.* **1992**, *104*, 1373–1376 (See also *Angew. Chem., Int. Ed. Engl.* **1992**, *31*, 1347–1350). (f) Spaleck, W.; Antberg, M.; Dolle, V.; Klein, R.; Rohrmann, J.; Winter, A. *New J. Chem.* **1990**, *14*, 499–503.

(21) (a) Chien, J. C. W.; Llinas, G. H.; Rausch, M. D.; Lin, Y. G.; Winter, H. H. *J. Pol. Sci. PC* **1992**, *30*, 2601. (b) Green, M. L. H.; Ishihara, N. *J. Chem. Soc. Dalton Trans.* **1994**, 657.

(22) Rieger, B.; Jany, G.; Fawzi, R.; Steimann, M. *Organometallics* **1994**, *13*, 647–653.

(23) Mise, T.; Kageyama, A.; Miya, S.; Yamazaki, H. *Chem. Lett.* **1991**, 1525–1528. (b) Miya, S.; Mise, T.; Yamazaki, H. *Stud. Surf. Sci. Catal.* **1990**, *56*, 531–534. (c) Mise, T.; Miya, S.; Yamazaki, H. *Chem. Lett.* **1989**, 1853–1856. (d) Gauthier, W. J.; Corrigan, J. F.; Taylor, N. J.; Collins, S. *Macromolecules* **1995**, *28*, 3771–3778. (e) Gauthier, W. J.; Collins, S. *Macromolecules* **1995**, *28*, 3779–3786. (f) Bravakis, A. M.; Bailey, L. E.; Pigeon, M.; Collins, S. *Macromolecules* **1998**, *31*, 1000–1009.

(24) Razavi, A.; Vereecke, D.; Peters, L.; Dauw, K. D.; Nafpliotis, L.; Atwood, J. L. In *Ziegler Catalysts*; Fink, G., Mulhaupt, R., Brintzinger, H. H., Eds.; Springer-Verlag: Berlin, 1995; p 111–147.

(25) Herzog, T. A. thesis: *Department of Chemistry, Division of Chemistry and Chemical Engineering*; California Institute of Technology: Pasadena, CA, **1997**.

(26) Miyake, S.; Bercaw, J. E. *J. Mol. Catal. A: Chem.* **1998**, *128*, 29-39.

(27) Veghini, D.; Henling, L. M.; Burkhardt, T. J.; Bercaw, J. E. *J. Am. Chem. Soc.* **1999**, *121*, 564–573.

(28) (a) Small, B. L.; Brookhart, M. *Macromolecules* **1999**, *32*, 2120–2130. (b) Hagihara, H.; Shiono, T.; Ikeda, T. *Macromol. Chem. Phys.* **1998**, *199*, 2439–2444. (c) Erker, G.; Fritze, C. *Angew. Chem., Int. Ed. Engl.* **1992**, *31*, 199–202.

(29) (a) Longo, P.; Grassi, A.; Pellecchia, C.; Zambelli, A. *Macromolecules* **1987**, *20*, 1015–1018. (b) Zambelli, A.; Locatelli, P.; Sacchi, M. C.; Tritto, I. *Macromolecules* **1982**, *15*, 831–834. (c) Zambelli, A.; Sacchi, M. C.; Locatelli, P.; Zannoni, G. *Macromolecules* **1982**, *15*, 211–212. (d) Karl, J.; Dahlmann, M.; Erker, G.; Bergander, K. *J. Am. Chem. Soc.* **1999**, *121*, 4930. (e) Dahlmann, M.; Erker, G.; Nissinen, M.; Froehlich, R. *J. Am. Chem. Soc.* **1999**, *121*, 2820–2828. (f) Sacchi, M. C.; Barsties, E.; Tritto, I.; Locatelli, P.; Brintzinger, H.-H.; Stehling, U. *Macromolecules* **1997**, *30*, 3955–3957.

(30) (a) Waymouth, R.; Pino, P. *J. Am. Chem. Soc.* **1990**, *112*, 4911–4914. (b) Gilchrist, J. H.; Bercaw, J. E. *J. Am. Chem. Soc.* **1996**, *118*, 12021–12028.

(31) Piers, W. E.; Bercaw, J. E. *J. Am. Chem. Soc.* **1990**, *112*, 9406–9407.

(32) Castonguay, L. A.; Rappe, A. K. *J. Am. Chem. Soc.* **1992**, *114*, 5832–5842.

(33) Kawamura-Kuribayashi, H.; Koga, N.; Morokuma, K. *J. Am. Chem. Soc.* **1992**, *114*, 8687–8694.

(34) Yoshida, T.; Koga, N.; Morokuma, K. *Organometallics* **1996**, *15*, 766–777.

(35) (a) Toto, M.; Cavallo, L.; Corradini, P.; Moscardi, G.; Resconi, L.; Guerra, G. *Macromolecules* **1998**, *31*, 3431–3438. (b) Cavallo, L.; Corradini, P.; Guerra, G.; Resconi, L. *Organometallics* **1996**, *15*, 2254–2263. (c) Guerra, G.; Cavallo, L.; Moscardi, G.; Vacatello, M.; Corradini, P. *J. Am. Chem. Soc.* **1994**, *116*, 2988–2995.

(36) Hart, J. R.; Rappe, A. K. *J. Am. Chem. Soc.* **1993**, *115*, 6159-6164.

(37) (a) Busico, V.; Cipullo, R.; Monaco, G.; Vacatello, M.; Bella, J.; Segre, A. L. *Macromolecules* **1998**, *31*, 8713–8719. (b) Busico, V.; Cipullo, R.; Monaco, G.; Vacatello, M.; Segre, A. L. *Macromolecules* **1997**, *30*, 6251–6263. (c) Busico, V.; Caporaso, L.; Cipullo, R.; Landriani, L.; Angelini, G.; Margonelli, A.; Segre, A. L. *J. Am. Chem. Soc.* **1996**, *118*, 2105–2106. (d) Busico, V.; Cipullo, R.; Chadwick, J. C.; Modder, J. F.; Sudmeijer, O. *Macromolecules* **1994**, *27*, 7538–7543.

(38) Resconi, L.; Fait, A.; Piemontesi, F.; Colonnesi, M.; Rychlicki, H.; Zeigler, R. *Macromolecules* **1995**, *28*, 6667–6676.

(39) Busico, V.; Cipullo, R. *J. Organomet. Chem.* **1995**, *497*, 113–118.

(40) Busico, V.; Cipullo, R. *J. Am. Chem. Soc.* **1994**, *116*, 9329–9330.

(41) (a) Yu, Z. T.; Chien, J. C. W. *J. Polym. Sci. Pol. Chem.* **1995**, *33*, 1085–1094. (b) Resconi, L.; Camurati, I.; Sudmeijer, O. *Top. Catal.* **1999**, *7*, 145–163. (c) Zeigler, R. C.; Rychlicki, H.; Resconi, L.; Piemontesi, F.; Baruzzi, G. *Abstr. Pap. Am. Chem. Soc.* **1997**, *213*, 442-POLY. (d) Resconi, L.; Piemontesi, F.; Balboni, D.; Sironi, A.; Moret, M.; Rychlicki, H.; Zeigler, R. *Organometallics* **1996**, *15*, 5046–5059. (e) Kaminsky, W.; Ahlers, A.; Mollerlindenhof, N. *Angew. Chem. Int. Edit. Engl.* **1989**, *28*, 1216–1218. (f) Grassi, A.; Ammendola, P.; Longo, P.; Albizzati, E.; Resconi, L.; Mazzocchi, R. *Gazz. Chim. Ital.* **1988**, *118*, 539–543. (g) Kaminsky, W. *Angew. Makromol. Chem.* **1986**, *145*, 149–160.

(42) Peng, T. S.; Gladysz, J. A. *J. Am. Chem. Soc.* **1992**, *114*, 4174–4181.

(43) Yoder, J. C. thesis: *Department of Chemistry, Division of Chemistry and Chemical Engineering*; California Institute of Technology: Pasadena, CA, **2000**.

(44) Resconi, L. *J. Mol. Catal. A.* **1999**, *146*, 167–178.

(45) van der Leek, Y.; Angermund, K.; Reffke, M.; Kleinschmidt, R.; Goretzki, R.; Fink, G. *Chem.-Eur. J.* **1997**, *3*, 585–591.

(46) Corradini, P.; Cavallo, L.; Guerra, G. In *Metallocene Catalysts*; Kaminsky, W., Scheirs, J., Eds.; Wiley: New York, 1999; Vol. 2, p 3.

Chapter 2

C_s- and C_1-Symmetric Syndio- and Isospecific Doubly Linked *Ansa*-Metallocenes: Synthesis, Characterization and Polymerization Studies

Abstract

The preparations of C_s-symmetric {1,1',2,2'-$(SiMe_2)_2$-(η^5-C_5H_2-4-R^1)(η^5-C_5H-3',5'-$(CHMe_2)_2$)}$ZrCl_2$ (**1**) and C_1-symmetric {1,1'-$SiMe_2$-2,2'-$SiPh_2$-(η^5-C_5H_2-4-R^1)-(η^5-C_5H-3',5'-$(CHMe_2)_2$)}$ZrCl_2$ (**2**) and {1,1'-$SiMe_2$-2,2'-($SiMe_2$–$SiMe_2$)-(η^5-C_5H_2-4-R^1)(η^5-C_5H-3',5'-$(CHMe_2)_2$)}$ZrCl_2$ (**3**) are reported. X-ray structures of **1c**, **1e** and **3a** have been determined. When activated by MAO, these metallocenes rapidly polymerize propylene to afford stereoregular polypropylenes. Catalysts **1** and **2** produce highly syndiotactic polypropylene at 0 °C in neat propylene. In contrast, under the same polymerization conditions, catalysts **3** yield moderately to highly isospecific polypropylenes. Analysis of pentad distributions indicates that the stereochemistry of polymerization follows "enantiomorphic-site" control mechanism. The major pathway for the occurrence of stereoerrors in catalyst systems **1** and **2** is site epimerization; while that in **3b** is enantiofacial misinsertion and chain epimerization (at high polymerization temperatures). The origin of stereospecificity in **3a** will be discussed in Chapter 3, and occurs presumably *via* kinetic trapping of the pre-insertion intermediate that leads to isospecific monomer insertion.

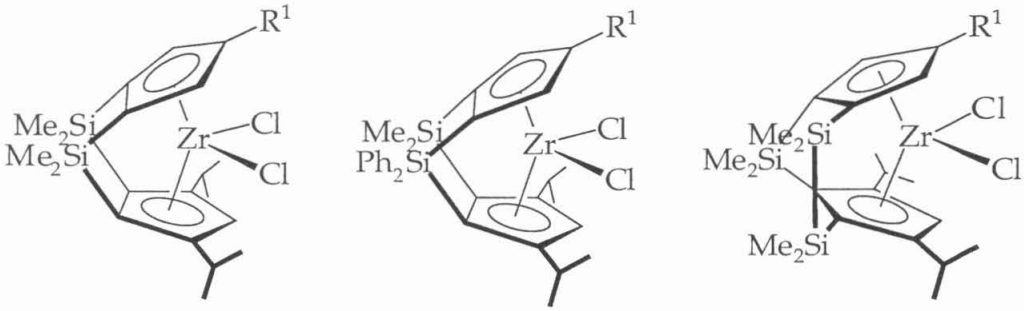

1c $R^1 = C_5H_9$ (Cy5)
1d $R^1 = C_6H_{11}$ (Cy6)
1e $R^1 = C_6H_5$ (Ph)

2a $R^1 = H$
2b $R^1 = CHMe_2$

3a $R^1 = H$
3b $R^1 = CHMe_2$

Introduction

Polymerization of α-olefins by single-site transition metal systems is of intense current interest.[1-3] Despite the recent development in late-transition-metal based olefin polymerization catalysis,[4] major attention has been directed toward polymerization catalyzed by early transition-metals.[2,5–8] Among these, metallocene-based catalysts have been most thoroughly studied, and have been used as model complexes to elucidate the mechanism for heterogeneous Ziegler-Natta catalysts.[2,5,6,9,10] Numerous Group 3 and 4 singly-bridged *ansa*-metallocene catalysts have been prepared and tested for their stereospecificity and activity in propylene polymerization.

More recently, doubly-bridged metallocenes have been synthesized[11,12] and evaluated as potential olefin polymerization catalyst precursors.[12] In particular, we have recently reported the preparation of a class of doubly silylene-bridged zirconocene catalyst precursors $\{1,1',2,2'\text{-}(SiMe_2)_2\text{-}(\eta^5\text{-}C_5H_2\text{-}4\text{-}R^1)\text{-}(\eta^5\text{-}C_5H\text{-}3,5\text{-}R^2{}_2)\}ZrCl_2$ (**1**, abbreviated as $(^{R1}Thp)ZrCl_2$ for $R^2 = CHMe_2$).[13,14] These catalysts, when activated with methylaluminoxane (MAO), exhibit high activity, and produce high molecular weight polypropylenes. R^1 and R^2 have been systematically varied in order to elucidate the impact of differing ligand substitution on the catalyst activity and stereospecificity.[13-15]

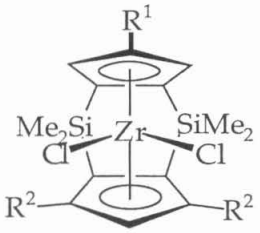

1

R^1= H, $CHMe_2$, CMe_3, $SiMe_3$, $CH(Me)(CMe_3)$, menthyl
R^2 = $CHMe_2$, $SiMe_3$

It has been found that C_s-symmetric systems can display a high degree of syndiospecificity with a *rrrr* content of up to 98.9%.[13,14] The syndiospecificity seems optimal for **1b** ($R^1 = R^2 = CHMe_2$), and a rocking motion about the methine carbon-cylopentadienyl bond has been invoked to explain the

observation (Scheme 1). Thus, as the enchainment proceeds, the methyl group (of the isopropyl substituent on the less substituted Cp ring) rotates around the methine carbon, and switches to the other side of the wedge to minimize steric interactions with the polymer chain. This synchronized motion of the methyl group and the polymer chain then maintains the enantiotopicity of the two sides of the wedge and encourages proper enantiofacial approach of the propylene monomer.

Scheme 1

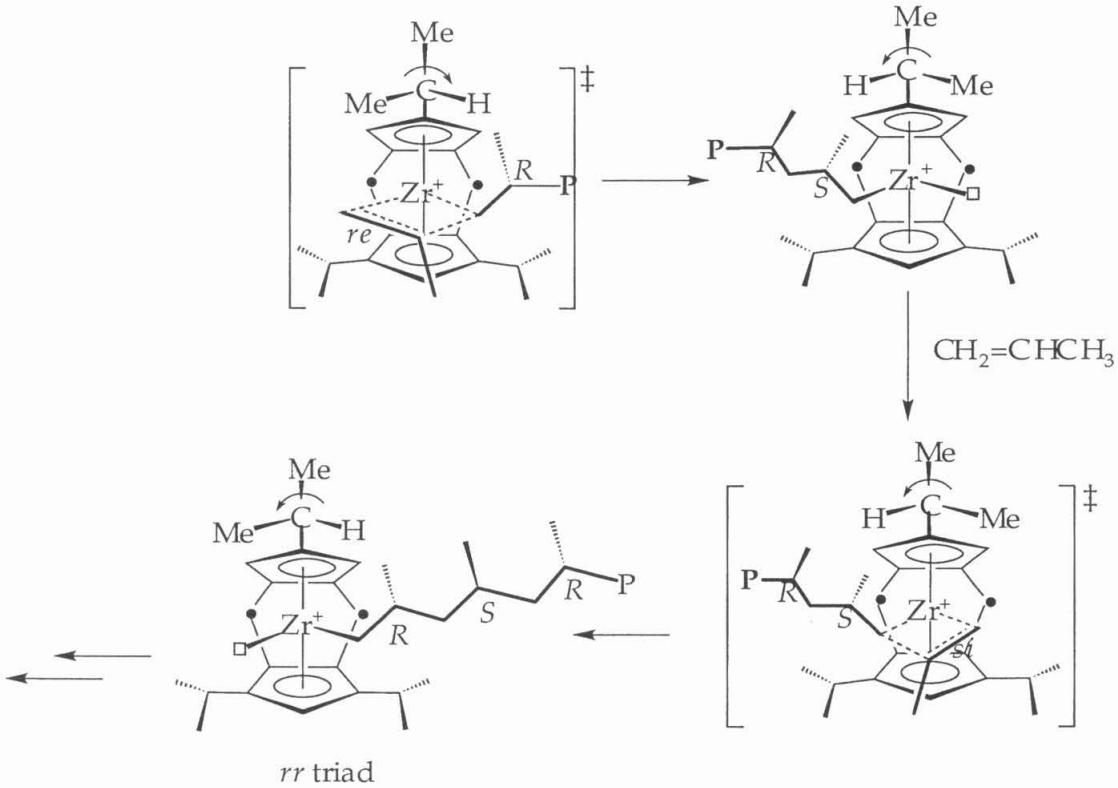

In contrast, C_1-symmetric variants of **1**, where R^1 = CH(Me)(CMe_3) or menthyl and R^2 = $CHMe_2$, produce polypropylenes ranging from modestly syndiotactic to hemi-isotactic and isotactic depending on the propene concentrations.[13-15] This observation has been rationalized as follows: the polymer chain has an inherent preference to migrate to the less hindered side of the metallocene wedge (eq 1). However, at higher monomer concentrations, the bimolecular insertion process is much faster than the uni-molecular site epimerization (chain swinging to the other side of the wedge), and monomer insertion occurs mostly from alternating sides of the metallocene wedge. As a

result, the polymer is predominantly syndiotactic. When the monomer concentration is lowered, site epimerization occurs at a greater rate than migratory insertion, allowing the polymer chain to swing to the less hindered side. Monomer then mostly inserts from one side of the wedge with one enantioface, producing primarily isotactic polymer.

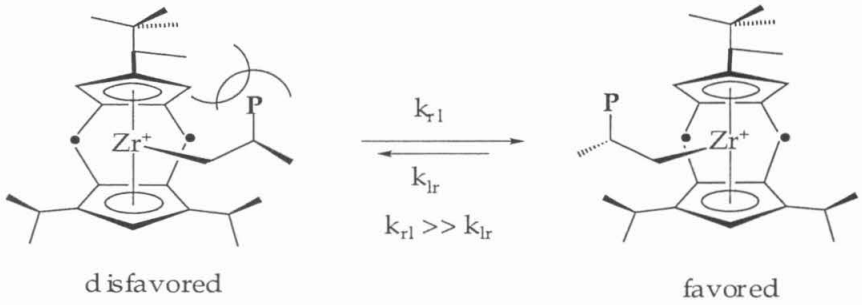

(1)

Based on earlier results and our hypothesis for the origin of especially high syndiospecificity of **1b**, we felt preparation of additional C_s-symmetric compounds was warranted in an attempt to realize perfect syndiospecificity. Among the potential candidates, we felt that catalysts with R^1 = phenyl or ortho,ortho-disubstituted phenyl groups held particular promise. It was anticipated that these substituents will undergo a rocking motion similar to that of isopropyl (Figure 1), and the ortho-substitutents could be easily modified both electronically and sterically to afford catalysts that can actively produce polymers with desired physical properties.

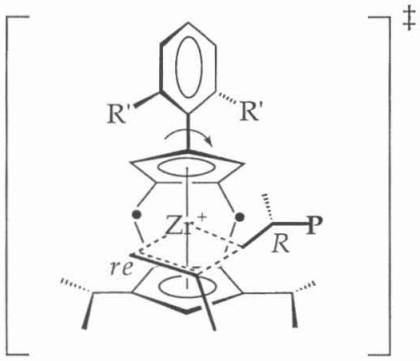

Figure 1. The rocking motion of ortho,ortho-disubstituted phenyl rings can potentially lead to perfect syndiospecificity.

Other promising candidates included cyclohexyl and cyclopentyl groups as the R^1 substituents. We hoped that these 2° cycloalkyl substituents would not only undergo the rocking motion but by virtue of their conformation, would extend far enough to discourage β-H elimination and subsequently further increase the molecular weights of the polypropylenes (Figure 2). For the $(Thp)ZrCl_2$ system, M_w has been shown to depend on R^1, and decrease in the order $CHMe_2 > SiMe_3 > H$ for C_s-symmetric systems (Figure 2).[15]

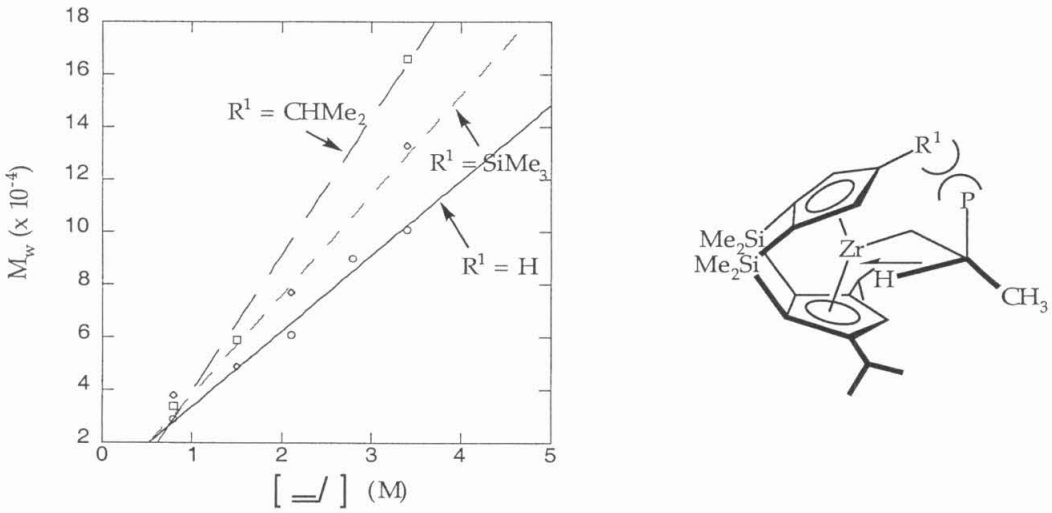

Figure 2. M_w of polypropylene depends on the steric size of R^1. So by extending the R^1 substituent far into the space to interact with the polymer, β-H elimination can be discourage, leading to increased polymer molecular weights.

The unanticipated "ambi-specificity" displayed by C_1-symmetric $(^{R1}Thp)ZrCl_2$ also motivated us to examine other chiral systems so as to find catalyst systems capable of displaying greater extremes of monomer-concentration-dependent stereospecificity. In particular we wondered whether the same monomer-concentration-dependent tacticity change would be observed, if we replaced one dimethylsilylene bridge with a different linker (eq 2). We also wondered what effects different linkers would have on the relative rates of site epimerization and insertion.

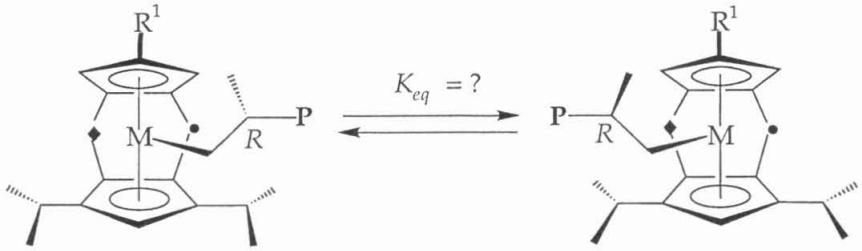

(2)

• = $SiMe_2$; ♦ = linker ≠ $SiMe_2$

With these objectives in mind, we decided to synthesize **1c–e**, **2** and **3**. **1c–e** are variations of C_s-symmetric Thp-type zirconocenes. Zirconocenes **2** have one dimethylsilylene linker in **1** replaced by a diphenylsilylene bridge; whereas in **3**, the dimethylsilylene linker is replaced by a tetramethyldisilylene linker. Herein, the synthesis of these novel zirconocenes is reported, and their polymerization performance - in particular the stereospecificity- is compared to that of **1a** and **1b**.

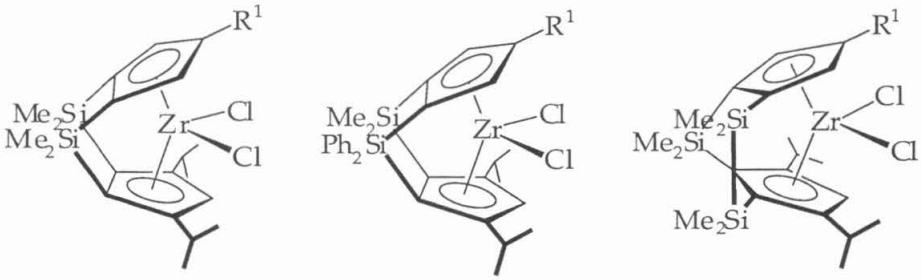

1a $R^1 = H$*
1b $R^1 = CHMe_2$*
1c $R^1 = C_5H_9$ (Cy5)
1d $R^1 = C_6H_{11}$ (Cy6)
1e $R^1 = C_6H_5$ (Ph)
* Reference # 13, 15 & 16

2a $R^1 = H$
2b $R^1 = CHMe_2$

3a $R^1 = H$
3b $R^1 = CHMe_2$

Results and Discussion

Synthesis of Zirconocene Complexes

Synthesis of Complexes 1a – c. Zirconocenes **1a – c** were prepared according to the general protocol developed by Herzog,[13,16] as shown in Scheme 2.

Scheme 2

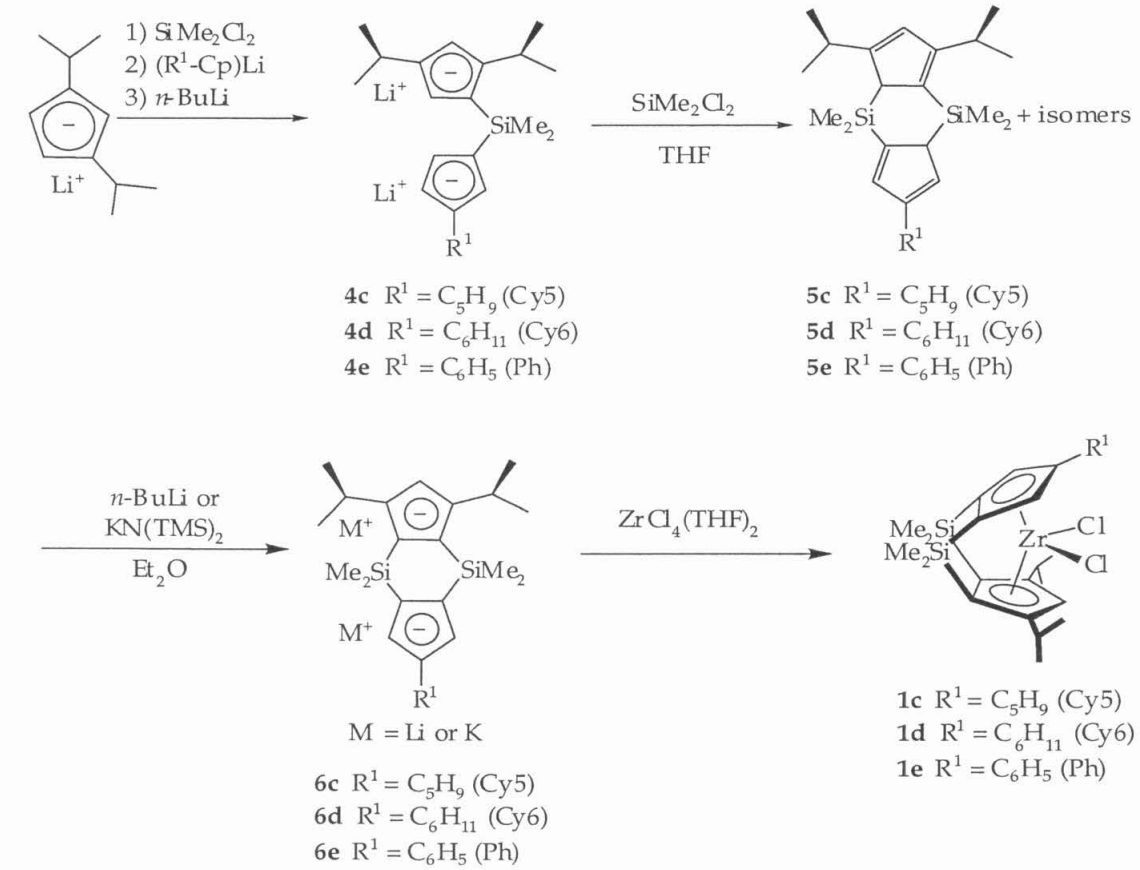

The singly substituted cyclopentadienes, R^1-CpH, were synthesized *via* the fulvene route[17] for R^1 = cyclopentyl and cyclohexyl (Scheme 3), and *via* 1,2 reduction of the 2-cyclopentenone followed by dehydration for R^1 = phenyl[18] (Scheme 4).

Scheme 3

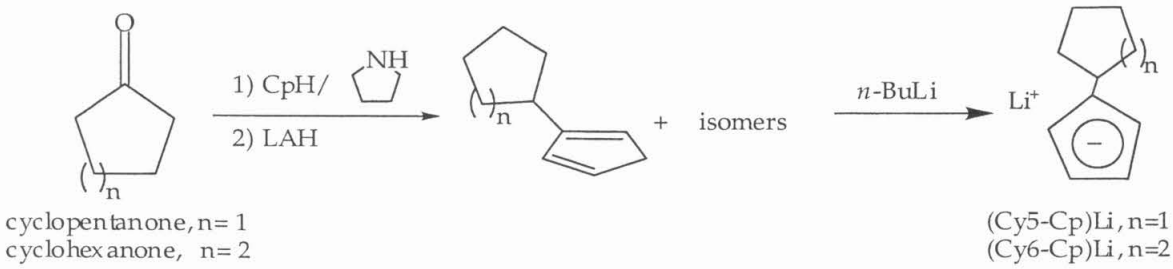

Scheme 4

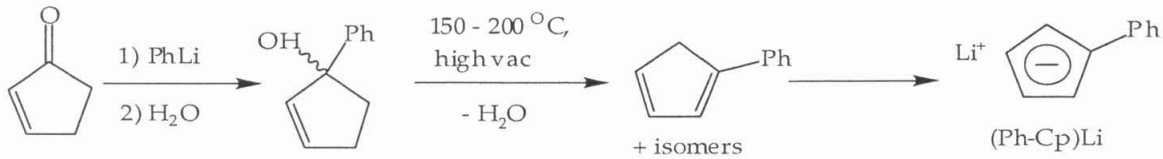

The synthesis of phenylcyclopentadiene was problematic and irreproducible due to its tendency to polymerize and Diels-Alder dimerize under dehydration reaction conditions. In addition, phenyl-substituted Thp ligand (**5e**) appeared thermally less stable than its alkyl-substituted analog. For example, when the crude reaction mixture for the synthesis of **5e** (yellow solid) was Krugelrohr distilled at 110 °C under high vacuum, instead of the expected white solid, an orange waxy material was collected in the receiving bulb, whose ^1H NMR spectrum appeared much more complicated than that of the original reaction mixture.

The zirconocene can be obtained either by reacting **6** with $ZrCl_4(THF)_2$ or by the amine elimination route (Scheme 5).[19] The latter procedure, however, doesn't always yield the zirconocene. For example, when a mixture of **5c** and $Zr(NMe_2)_4$ was refluxed in xylene under argon for 20 hours, an appreciable amount of black precipitate formed at the bottom and on the sides of the reaction flask, with dimethylamine continuously evolving. Treatment of the resulting dark brown mixture with excess trimethylchlorosilane gave no desired zirconocene **1c**.

Scheme 5

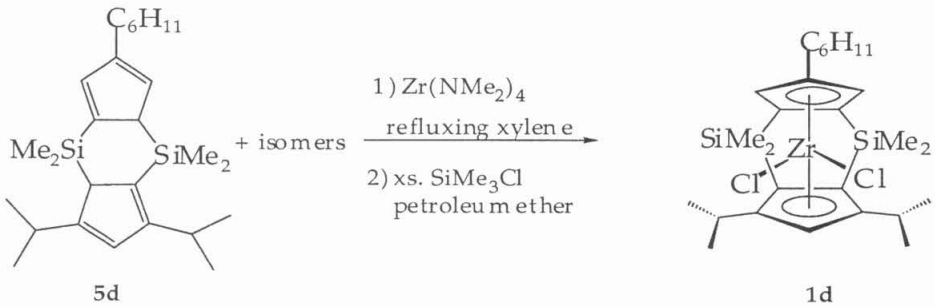

The X-ray structures of **1c** and **1e** have been determined. The structural parameters of **1c** (Figure 3) are nearly identical to that of **1b**.[16] The cyclopentyl ring adopts the low-energy envelope conformation. The dihedral angle between

the two Cp rings is ~ 72°. The selected bond distances and bond angles are reported in Table 1.

Table 1. Selected bond distances and bond angles for **1c**.

	Distance (Å)		Angle (°)
Zr – Cp1 (centroid)	2.233	Pln1 – Zr – Pln2	108.16(6)
Zr – Cp2 (centroid)	2.201	Cent1–Zr–Cent2	121.6
Zr – Cl1	2.4291(5)	Cp1 – Cp2	71.84
Zr – Cl2	2.4348(5)	Cl1 – Zr – Cl2	99.536(7)
C9–C21	1.505(2)	C6 – Si1 – C1	91.92(8)
Si1 – C1	1.8854(18)	C7 – Si2 – C2	92.26(8)
Si1 – C6	1.8768(18)		
Si2 – C2	1.8879(18)		
Si2 – C7	1.8768(19)		
C3 – C11	1.511(2)		
C5– C14	1.511(2)		

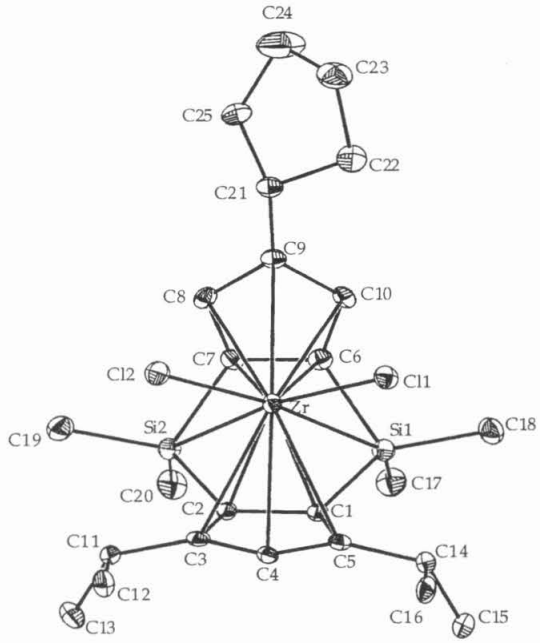

Figure 3. ORTEP drawing of **1c** with 50% probability ellipsoids showing the numbering scheme.

1e was recrystallized as a 1:1 adduct of **1e** and C_6D_6. Each asymmetric unit contains two half–molecules of benzene (Figure 4). The zirconocene molecules are arranged in layers separated by sheets of benzene molecules, which show considerable in–plane rotation and disorder. The other type of benzene molecules lie between the phenyl groups of **1e**. The phenyl ring in **1e** is rotated 13.5° with respect to the cyclopentadienyl ring to which it is bonded (Figure 5). In solution, the phenyl ring must be in rapid rotation around the ipso–carbon bond, because only three resonances in the ratio of 2:2:1 are observed for the aryl protons. The dihedral angle between the two Cp planes is 73°, slightly smaller than the 73.9° dihedral angle observed for (*i*Pr-Thp)$ZrCl_2$ (**1b**).[16] The bond distance between Cp–R^1 (C4–C15, 1.478(2) Å) is noticeably shorter than that observed in **1b** (1.518(8) Å), but this may simply be a result of a shorter C_{sp2}–C_{sp2} (in **1e**) bond distances than a C_{sp2}–C_{sp3} bond (in **1b**). For example, a typical C_{sp2}–C_{sp2} bond distance is 1.459 ± 0.005 Å, whereas a typical C_{sp2}–C_{sp3} bond distance is 1.505 ± 0.005 Å.[20] The selected bond distances and angles are summarized in Table 2.

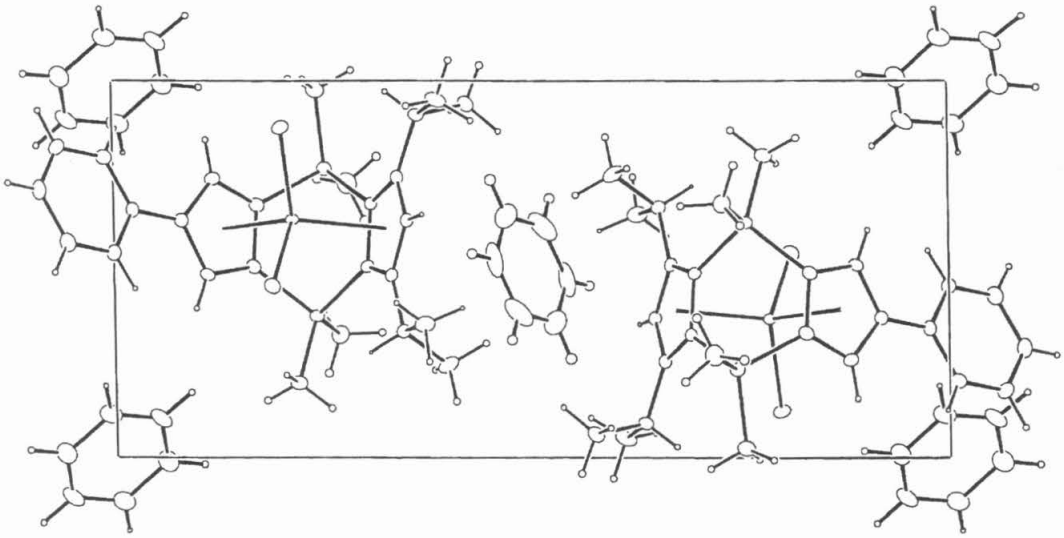

Figure 4. ORTEP representation of the unit cell contents of **1e** with 50% probability ellipsoids, viewed along the a–axis.

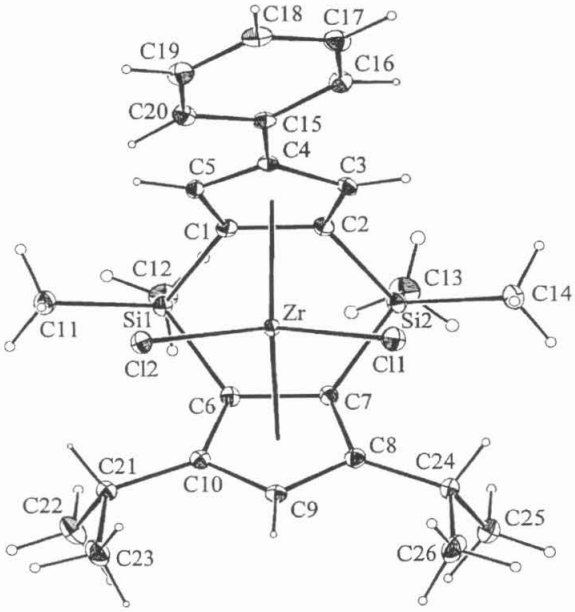

Figure 5. ORTEP drawing of **1e** with 50% probability ellipsoids showing the numbering scheme. Hydrogen atoms are shown at 1/10 scale.

Table 2. Selected bond distances and bond angles for **1e**.

	Distance (Å)		Angle (°)
Zr – Cp1 (centroid)	2.208	Cent1 – Zr – Cent2	121.8
Zr – Cp2 (centroid)	2.244	Cp1 – Cp2	73.0
Zr – Cl1	2.4280(5)	Cl1 – Zr – Cl2	101.24(2)
Zr – Cl2	2.4343(4)	Cp1 – Zr – Cl1	108.4
C4 – C15	1.478(2)	Cp1 – Zr – Cl2	108.3
Si1 – C1	1.874(2)	Cp2 – Zr – Cl1	107.6
Si1 – C6	1.892(2)	Cp2 – Zr – Cl2	107.6
Si2 – C2	1.873(2)	C6 – Si1 – C1	92.0(1)
Si2 – C7	1.888(2)	C7 – Si2 – C2	92.4(1)
C8 – C24	1.515(3)	Ph – Cp1	13.5
C10 – C21	1.512(2)		

Synthesis of Complexes 2a – b. {(1,1'-$SiMe_2$-2.2'-$SiPh_2$-(η^5–C_5H_2–4–R^1)(η^5–C_5H–3',5'–$(CHMe_2)_2$)}$ZrCl_2$ (**2**), where R^1 = H (**2a**) or $CHMe_2$ (**2b**), were prepared according to the procedure analogous to that of complexes **1**.[13-16] The steps shown in Scheme 6 proceeded with moderate to high yields with the exception of the final metallation step.

Scheme 6

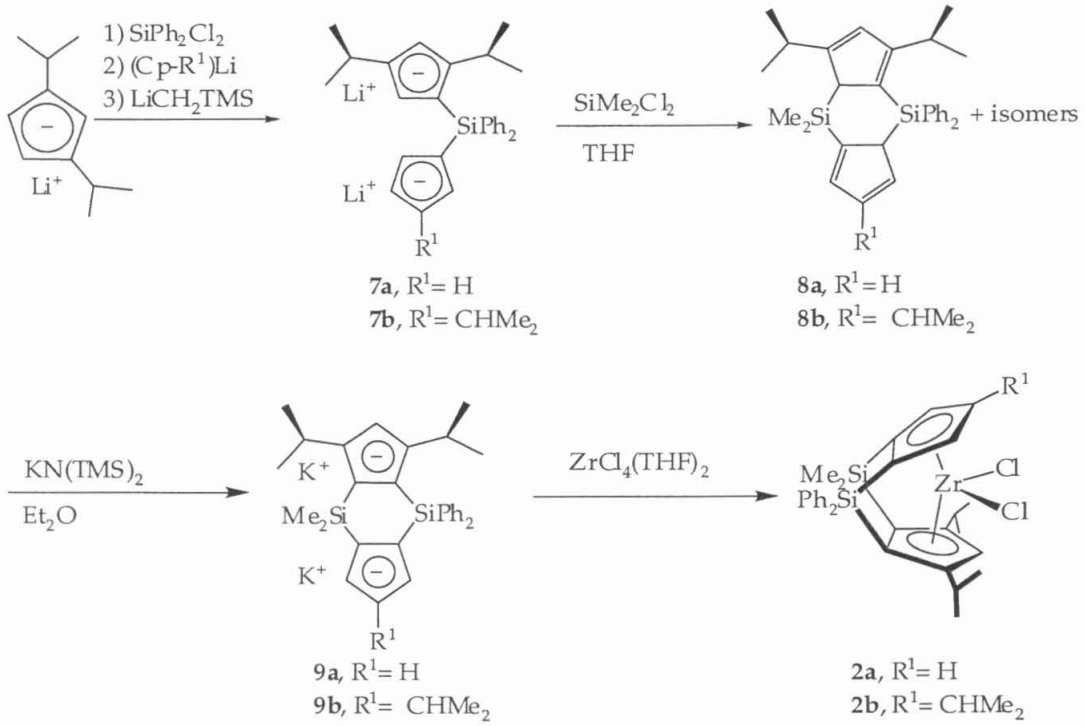

The dilithio salts, **7**, always contained 5–15% unidentifiable side products, which could be removed in the subsequent steps. The zirconocene **2** may be obtained by metalating **9** with either zirconium tetrachloride or its THF adduct. ^{1}H NMR spectrum of **2a** in benzene–d_6 showed two silyl methyl peaks in the ratio of 1:1 at -0.35 and 0.39 ppm respectively, confirming the coordination of the ligand to the metal. The four sets of doublets in the region of 0.75 to 1.40 ppm were assigned to the four diastereotopic isopropyl methyl groups. The methine protons appeared as two sets of overlapping septets at 2.95 ppm. The four chemically non-equivalent Cp protons had chemical shifts of 6.54 (t), 6.57(s), 6.82 (dd) and 7.47 (dd) ppm respectively. The Cp resonance at 7.47 ppm was assigned to the proton next to the diphenylsilylene linker. The singlet at 6.57 ppm was assigned to the Cp proton on the more substituted Cp ring. The triplet at 6.54 ppm was assigned to the proton at 4–position of the less substituted Cp ring; and the remaining peak at 6.82 ppm, to the proton next to the dimethylsilylene linker.

Most phenyl resonances are not well-resolved, except the two doublets at 7.56 and 7.93 ppm that are integrated to one proton each. The multiplicity of

these resonances implies that these are the ortho-protons. Should the phenyl rings on the silicon-linker be rotating freely, we would expect to see two sets of signals for the ortho–protons, integrated to two protons each. On the other hand, hindered rotation of the phenyl rings is expected to give rise to four sets of resonances for the ortho-protons, integrated to one proton each. Thus, separate signals for ortho-protons that are integrated to one proton each is more consistent with hindered rotation of the phenyl rings about Si–C_{ipso}, even though we cannot identify with certainty the remaining two sets of ortho-proton signals. More conclusive evidence for hindered rotation around Si–C_{ipso} bond is furnished by the ^{13}C NMR spectrum of the complex, in which 22 peaks can be identified in the Cp and aryl carbon region. Should the phenyl rings be freely rotating around the Si–C_{ipso} bond, one would only observe 18 distinguishable resonances; whereas 22 peaks are expected for a system with hindered phenyl rotation.

The ^{1}H NMR spectrum of **2b** showed similar features. In addition, consistent with the C_1-symmetry, two sets of doublets were observed for the diastereotopic methyl groups of the isopropyl group on the less substituted Cp ring (R^1). Its methine proton was *ca.* 0.35 ppm downfield from the methine protons of isopropyl group on the more substituted Cp ring.

We were interested in learning the orientation of the phenyl ring that is pointing forward, because this will affect the effective steric influence of the $SiPh_2$ relative to $SiMe_2$. If this phenyl ring lies in a plane parallel to the Cl–Zr–Cl plane, then the forward-extending phenyl ring will have stronger steric interactions with the polymer chain than a $SiMe_2$ group (Figure 6, **A1**). On the other hand, if the phenyl ring is orthogonal to the Cl–Zr–Cl plane, then it will have less steric interactions with the polymer chain than the $SiMe_2$ group (Figure 6, **A2**).

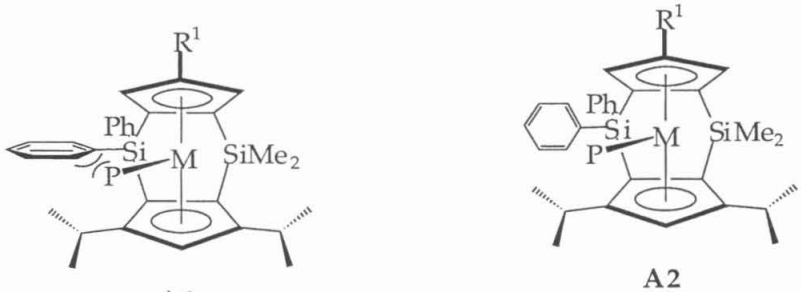

A1 **A2**

Figure 6. The orientation of the phenyl ring determines the effective size of a phenyl ring relative a methyl group.

Unfortunately, attempts to obtain X-ray quality crystals for either **2a** or **2b** have so far been unsuccessful, but the lowest-energy structure for **2a** has been calculated using molecular mechanics programs in CAChe and MacSpartan Pro software (Figure 7). Both CAChe and MacSpartan Pro had accurately predicted the general features of several zirconocenes, as later confirmed by X-ray structures. Thus, we may assume that the structure shown in Figure 7 at least approximates the true solid-state structure. As shown in the figure, the phenyl ring at the back is orthogonal to the Cl–Zr–Cl plane, while the other phenyl ring is nearly parallel to the Cl–Zr–Cl plane. On the other hand, calculation also showed that the alternative ring conformation, where the front phenyl ring is perpendicular to the Cl–Zr–Cl plane, lies only 1–2 kcal/mol above the minimized structure. Therefore, both **A1** and **A2** are likely structures for **2a**.

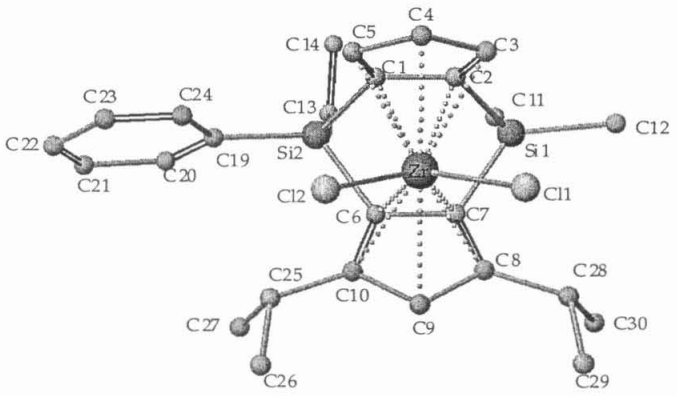

Figure 7. Structure of **2a** (front view) as calculated by CAChe.

Synthesis of Complexes 3a–b. Zirconocenes of the type {1,1'-$SiMe_2$-2,2'-($SiMe_2$–$SiMe_2$)-(η^5–C_5H_2–4–R^1)-(η^5–C_5H–3',5'–$R^2{}_2$)}$ZrCl_2$ (**3**) (R^1 = H or $CHMe_2$) were prepared according to Scheme 7. Either linker can be attached first, but if the disilylene bridge is to be linked first, diisopropylcyclopentadienide must be added slowly to a stirring THF solution of 1,2-dichlorotetramethyldisilane at low temperatures (-78 °C – -20 °C). Otherwise a substantial amount of double addition product, (1,3-$(CHMe_2)_2$-C_5H_3)-($SiMe_2$–$SiMe_2$)-(1,3–$(CHMe_2)_2$-C_5H_3), forms.

Scheme 7

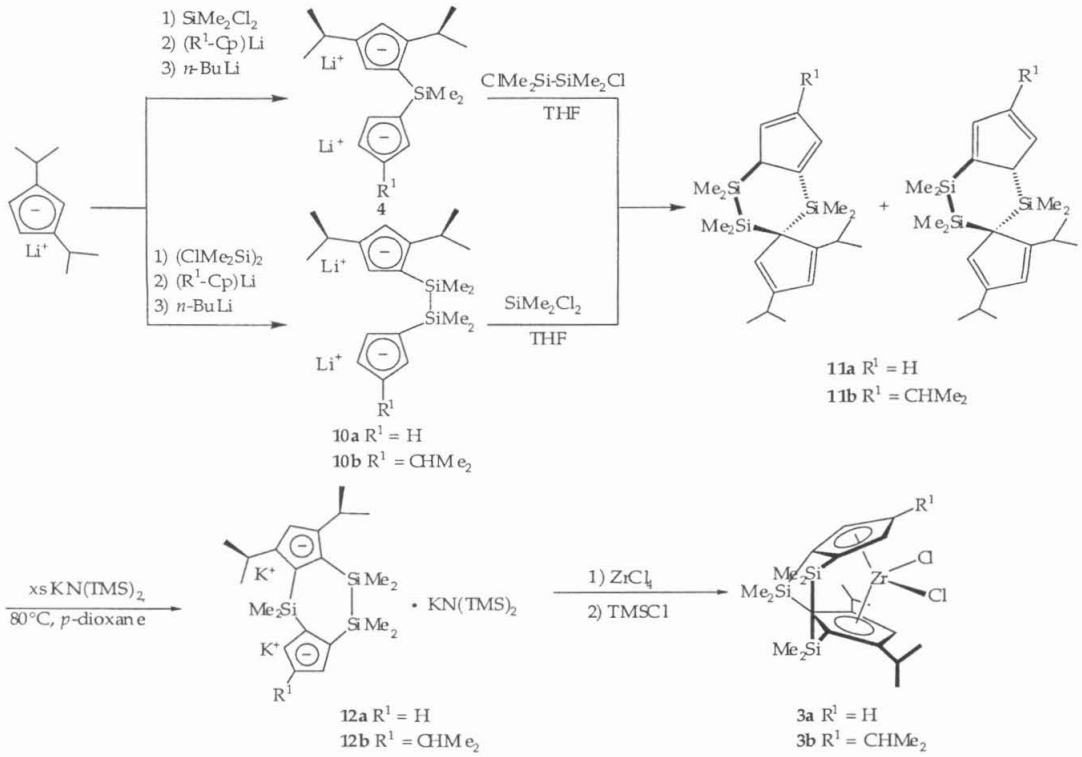

The doubly linked ligand **11** was obtained as a high-boiling orange oil consisting of several isomers. The approximately 1:3 ratio of allyl protons to vinyl protons suggests that the structures shown in the scheme is the major species present in the mixture. Because under mild reaction conditions where the less substituted Cp ring can be deprotonated, the more substituted Cp ring remains in its protonated form, we do not believe that the other possible structures (**11'**) are present in large quantity. In addition, the interconversion between **11** and **11'** must be slow. Should **11'** be the major isomers, we would expect the more substituted Cp ring be deprotonated first, since it contains a sp^3 proton for deprotonation while silyl migration is required for the deprotonation of the less substituted Cp ring. By the similar argument, should **11** and **11'** be in fast equilibrium, then both Cp rings should have been deprotonated under the same mild conditions. The harsh reaction conditions (excess base and high reaction temperatures) required to generate the dipotassium salts **12 (a** and **b)** may reflect the higher energy barrier for the silyl substituents to migrate from an sp^3 carbon to an sp^2 carbon (next to a relatively bulky isopropyl group in **11**) in sterically crowded 1,3-diisopropylcyclopentadienyl ring.[21]

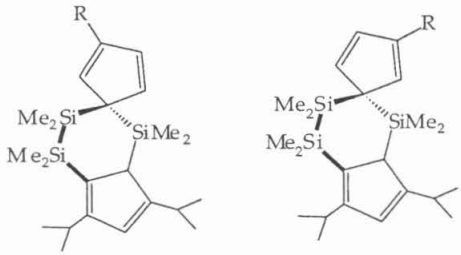

11'

The dipotassium salt **12** may be metallated using $ZrCl_4$ in a mixture of diethyl ether and toluene (1:3 – 1:5). Although the resulting zirconocenes are only slightly soluble in petroleum ether in their pure forms, the solubility is greatly increased in the presence of impurities or residue *p*-dioxane from the deprotonation step. This accounts partially for the poor yields (15 – 30%) in the metallation step.

Suitable crystals of **3a** were obtained from a mixture of toluene and hexane for X–ray structural analysis. The structure is shown in Figure 8. The selected bond lengths and angles are given in Table 3.

Table 3. Selected bond distances (Å) and angles (°) for **3a**.

Bond Lengths		Bond Angles	
Zr – Cent (1)	2.2086(8)	Cent(1)–Zr–Cent(2)	126.34(2)
Zr – Cent (2)	2.2315(7)	Pln(1)–Zr–Pln(2)	118.44(7)
Zr – Pln (1)	2.2066(11)	Pln(1) – Pln(2)	61.56
Zr – Pln (2)	2.2206(11)	Cl(1) – Zr – Cl(2)	99.26(2)
Zr – Cl(1)	2.4280(7)	C(1)–Si(1)–Si(2)	104.13(6)
Zr – Cl(2)	2.4446(7)	C(6)–Si(2)–Si(1)	106.05(6)
Si(1) – C(1)	1.8750(18)	C(2)–Si(3)–C(7)	93.70(8)
Si(1) – Si(2)	2.3630(11)	C(21)–Si(3)–C(22)	105.27(9)
Si(2) – C(6)	1.9022(18)	C(17)–Si(1)–C(18)	107.60 (10)
Si(3) – C(2)	1.8737(18)	C(19)–Si(2)–C(20)	104.32(9)
Si(3) – C(7)	1.8878(18)		

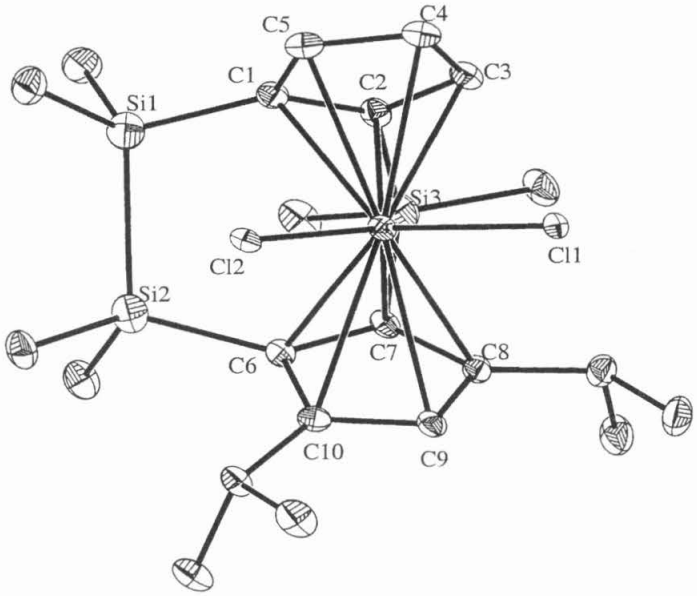

(a)

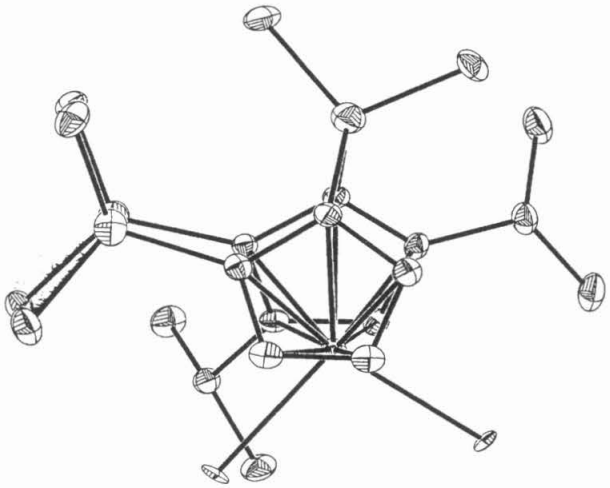

(b)

Figure 8. (a) ORTEP drawing of **3a** (front view) with 50% probability ellipsoids showing the numbering scheme. (b) ORTEP drawing of **3a** (top view) with 50% probability ellipsoids showing the numbering scheme.

The catalyst structure distorts significantly from that of **1** and resembles singly-bridged *ansa*-metallocenes, which explains the difference between **3** and **1** in stereoselectivity as polymerization catalysts (*vide infra*). The side of the wedge where the tetramethyldisilylene linker (and the frontal isopropyl group) resides is narrower and more sterically crowded than the other side. For example, the distance between C5 and C10 is 4.842 Å versus 5.053 Å between C4 and C9; and the distance between C1 and C6 is 3.347 Å versus 3.808 Å between C3 and C8. However, zirconium atom is of equal distance to C9 (C4) and C10 (C5).

The structural parameters of **3a** is fairly similar to those of known dimethylsilylene-linked *ansa*-zirconocene dichlorides. The difference between Cn(1)–Zr–Cn(2) and Pln(1)–Zr–Pln(2) angles is, however, slightly larger – 8° versus 5 – 6°. However, because both the Zr–Cn(1) and Zr–Cn(2) distances and the Cn(1)–Zr–Cn(2) in **3a** are almost the same as those in normal dimethylsilylene–linked *ansa*–zirconocene dichlorides, the relative position of the Zr atom (in the cleft defined by the two Cp ligands) are almost identical in **3a** and known silylene–bridged *ansa*–zirconocenes (Figure 9).

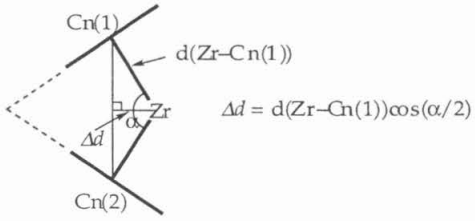

Figure 9. Displacement of Zr (IV) with respect to Cp centroids.

Polymerization Studies with Zirconocenes 1–3

Polymerization with 1c–e/MAO. (^{R}Thp)$ZrCl_2$ (**1c–e**) were activated with MAO for propylene polymerization. The data are summarized in Tables 4 and 5. Polypropylene prepared with these catalysts at 0 °C in neat propene show comparable syndiotacticity to that of **1b**. However, polypropylene prepared with **1c**/MAO showed bimodal distribution of molecular weight (Figure 10), and the higher molecular weight portion consists of polypropylene with M_w well over 1 million, which is considered extremely high for metallocene–based polymerization catalysts.

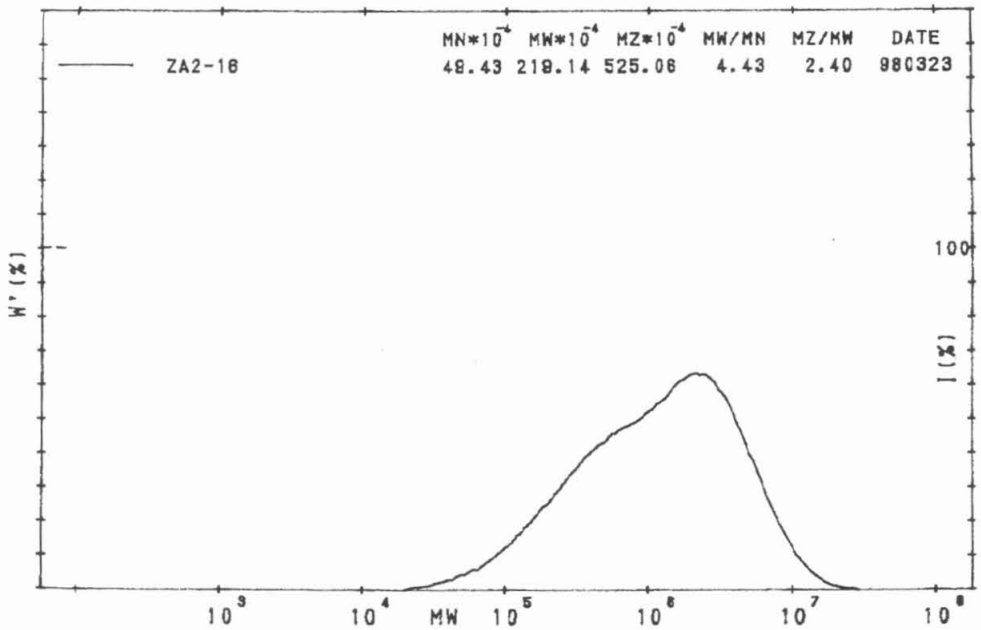

Figure 10. GPC trace for polypropylene prepared by **1c**/MAO at 0 °C in neat propene.

Room temperature propylene polymerization with **1c**/MAO at various monomer concentrations was also briefly investigated. The tacticities of the polymers are compared to those prepared with **1b**/MAO under comparable conditions,[15] and the two systems show similar trends in monomer-concentration-dependent syndiotacticity (Figure 11). No regioerrors have been detected by ^{13}C NMR for any of the polymers produced by these catalysts under conditions investigated. Such observations are consistent with polymerization behavior exhibited by **1a–b**/MAO,[15] but contrasts those exhibited by fluorenyl/cyclopentadienyl based "Ewen catalyst."[3,10,22]

Table 4. Polymerization data for **1c – e**/MAO.

	cat.	T_p (°C)	Propene Pressure/ Concentration	catalyst/ MAO (mg)	melting point (°C)	%[r] ± 5 %	M_W (10^4 g/mol)	PDI	activity (10^6 g PP/mol cat hr)[a]
1	**1c**	22	1 atm (0.8 M)	0.26/130	-	90%	8.26	2.17	6.3
2	**1c**	22	10 psig (1.5 M)	0.26/130	-	94.2%	13.65	2.13	12
3	**1c**	22	20 psig (2.1 M)	0.26/130	-	94.7%	13.2	2.31	16
4	**1c**	22	30 psig (2.8 M)	0.13/80	-	97.5%	26.11	2.33	47
5	**1c**	22	40 psig (3.4 M)	0.13/80	-	97.8%	42.57	2.35	42[b]
6	**1c**	0	80 psig (neat)	0.13/80	142	>99%	219.1	4.43	9.1
7	**1d**	0	80 psig (neat)	0.21/155	151	>99%	77.3	1.98	4.3
8	**1e**	0	80 psig (neat)	0.20/135	152	98.8%	-	-	25.1[c]

a. MAO used to activate **1a** and **1b** is of a different batch from that used to activate **1c**, **2a** and **2b**. b. The lower than expected activity could be due to much shorter reaction time. c. The temperature within the reactor rose above 5 °C at the end of the polymerization.

Table 5. Pentad distributions (%) for the polypropene samples produced by **1c – e**/ MAO.

entry	catalyst	[*mmmm*]	[*mmmr*]	[*rmmr*]	[*mmrr*]	[*rmrr*]+ [*mrmm*]	[*rmrm*]	[*rrrr*]	[*rrrm*]	[*mrrm*]
1	**1c**		0.5	2.5	3.8	16.9	4.0	51.5	20.8	<1
2	**1c**			0.7	1.9	9.6	1.5	74.0	14	
3	**1c**			<1	1.7	8.5	0.4	78.0	11	
4	**1c**			0.4	1.5	5.8		84.0	8.3	
5	**1c**			<0.5	0.8	3.6		89.0	6.3	
6	**1c**				0.5	0.8		97.7	1.0	
7	**1d**				2.4			97.6		
8	**1e**				0.94	1.29	0.26	96.0	1.52	

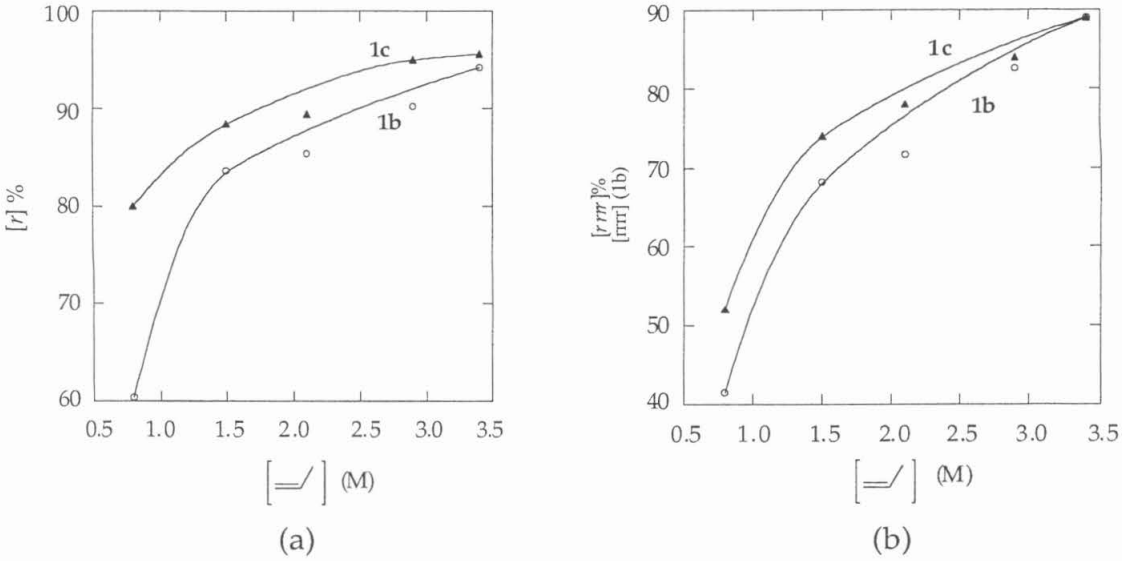

Figure 11. Dependence of [*r*] and [*rrrr*] on propylene concentration for C_S-symmetric **1c** versus **1b**.

In general, stereoselectivity increases with increasing propylene concentration. Percentages of [*mm*] and [*rm*] triads increase with decreasing monomer concentration, but under all conditions investigated, the [*rm*] stereoerrors are the major ones. This implies that site epimerization or chain epimerization followed by site epimerization is the main mechanism for stereoerrors. However, previous studies found that poly-d_0-propylene and poly-2-d_1-propylene produced under the same reaction conditions (RT, [propylene] = 0.8 M) have almost identical microstructures.[15] Because the first step of chain epimerization involves β–H(D) elimination, one would expect that if chain epimerization followed by site epimerization is the major pathway for [*rm*] stereoerrors, poly-2-d_1-propylene should have a lower percentage of [*rm*] than poly–d_0–propylene based on a normal KIE for β–H(D) elimination. The fact that the microstructures of the two polymers are essentially the same leads to the conclusion that site epimerization is the principal process for stereoerror formation.

Because **1b** and **1c** not only have structurally similar features, but also produced polymers with similar microstructures under comparable polymerization conditions, we expect that the mechanism for stereoerror formation is the same for both systems. That is, the majority of the errors are

produced by site epimerization, with chain epimerization becoming increasingly important at lower monomer concentrations (as evidenced by the increasing # of [*mm*] errors). Enantiofacial misinsertion does not seem to be a major contributor to the stereoerrors since the percentage of [*mm*] triads at high monomer concentrations is low (<1%).

Polymerization with 2a–b/MAO. Polymerization with these catalysts under various conditions is briefly investigated and the results are compared to **1a–b**/MAO systems. The polymerization results and pentad distributions are summarized in Tables 6 and 7 respectively. Plots have also been constructed to illustrate the dependence of [*r*] diads, [*rrrr*] pentads (Figure 12) and [*rm*]/[*mm*] triads (Figure 13) on monomer concentration.

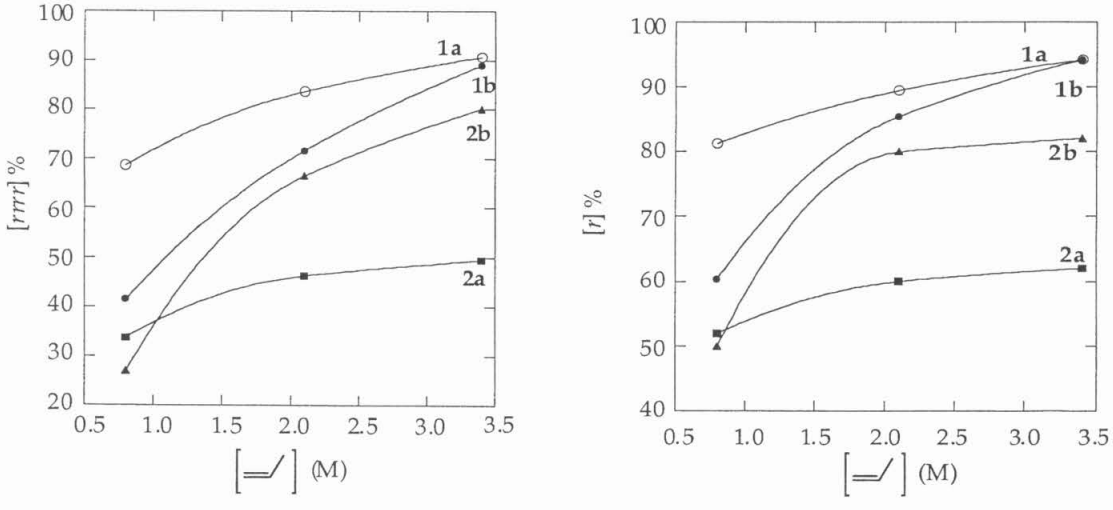

Figure 12. Dependence of [*r*] and [*rrrr*] on propylene concentration for C_1-symmetric **2a – b** versus C_s-symmetric **1a – b**.

Table 6. Propylene polymerization data for **2a – b**/MAO.

entry	cat.	T_p (°C) ± 3 °C	Propene Pressure/ Concentration	catalyst loading/MAO (mg)	Tacticity % [*rrrr*] ± 5 %	% [*r*]	activity[a]
9	**2a**	22	1 atm (0.8 M)	0.20/128	34%	79%	2.49
10	**2a**	22	20 psig (2.1 M)	0.20/135	46%	80%	55.9
11	**2a**	22	40 psig (3.4 M)	0.20/135	50%	81%	53.7
12	**2a**	0	80 psig (neat)	0.25/150	92%	97%	18.2
13	**2b**	22	1 atm (0.8 M)	1.0/480	27%	75%	0.60
14	**2b**	22	20 psig (2.1 M)	0.35/212	67%	90%	5.37
15	**2b**	22	40 psig (3.4 M)	0.20/135	80%	91%	16.8
16	**2b**	0	80 psig (neat)	0.25/152	95%	98%	6.03

a. activity given in 10^4 gPP/g·Zr·hr.

Table 7. Pentad distributions (%) for the polypropene samples produced by **2a – b**/ MAO.

entry	catalyst	[*mmmm*]	[*mmmr*]	[*rmmr*]	[*mmrr*]	[*rmrr*]+ [*mrmm*]	[*rmrm*]	[*rrrr*]	[*rrrm*]	[*mrrm*]
9	**2a**	-	2.0	2.4	10.9	21.4	7.4	33.8	21.4	3.8
10	**2a**	-	1.6	3.1	6.6	15.8	6.1	46.3	16.2	4.1
11	**2a**	-	1.1	2.8	6.4	16.2	4.3	49.5	16.1	1.4
12	**2a**	-	-	1.3	2.4	0.7	-	92.3	3.3	
13	**2b**	-	0.8	3.9	14.4	22.9	7.0	27.0	21.0	4.8
14	**2b**	-	0.2	0.9	3.9	13.7	2.8	66.5	12.1	1.1
15	**2b**	-	-	0.8	2.1	6.8	-	80.1	6.8	-
16	**2b**	-	-	0.8	1.9	0.6	-	94.3	2.4	-

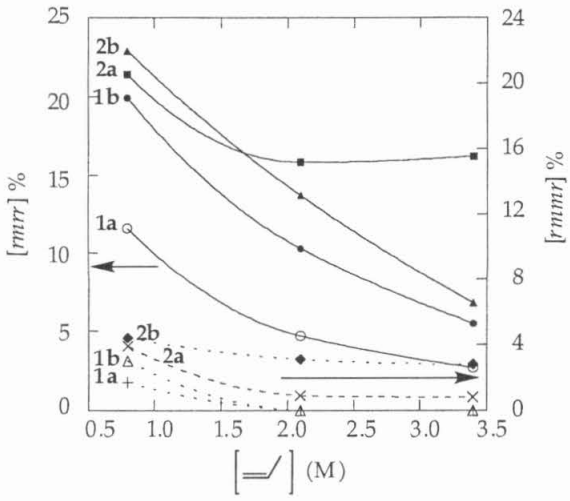

Figure 13. Dependence of [*rmrr*] and [*rmmr*] pentads on propylene concentration for C_1-symmetric **2a – b** versus C_s-symmetric **1a – b**.

At 0 °C in neat liquid propylene, when activated by MAO, **2a** and **2b** produced polypropylenes of slightly lower syndiotacticity than those produced by **1a** and **1b** respectively. But at higher temperatures, complexes **2** showed significantly lower stereospecificity (Tables 6 and 7, Figure 12).[15] At monomer concentration of 0.8 *M* and T_p = 22 °C, **1a**/MAO produced polypropylenes with [*rrrr*] ([*r*]) contents of 68.6% (90.5%) vs. 33.8% (76.0%) by **2a**/MAO. At the same polymerization temperatures, the [*r*] diad contents of the polypropylene produced by **2a**/MAO showed a smaller monomer concentration dependence than **2b**/MAO, which is similar to what was observed for **1a**/MAO vs. **1b**/MAO.[15] The change in [*r*] content upon lowering the monomer concentration is slightly smaller in **2** than in **1**. For example, at T_p = 22 °C, upon lowering the monomer concentration from 3.4 *M* to 0.8 *M*, **2a**/MAO showed a drop of ~ 2% in [*r*]% compared to 6.5% in **1a**/MAO.

In contrast to the trend observed for **1a** and **1b**, **2a**/MAO had a more pronounced decrease in syndiotacticity at higher temperatures than **2b**/MAO. For example, when the polymerization temperature was raised from 0 °C to 22 °C, the optimal [*r*] diad contents dropped from 98% (0 °C) to ca. 81% (22 °C) for **2a** vs. 98% (0 °C) to ca. 91% (22 °C) for **2b**.[23] Also in contrast to **1**/MAO systems, some residual [*mm*] triads are produced by **2**/MAO even in neat propene at 0 °C (Table 7), suggesting a higher probability of enantiofacial misinsertion in these

systems.[15] *However*, regioerrors again seem absent from polymers produced by these catalysts.

But in contrast to **1**/MAO where no chain-end resonances (corresponding to propyl end group) could be observed, such resonances are observable (< 0.3 – 0.5%) for polymers produced at room temperature with a monomer concentration of 0.8 *M* (1 atm). This implies that under comparable conditions, the ratio between r_{ct} and r_p (r_{ct}, rate of chain transfer; r_p, rate of chain propagation) in **2**/MAO is larger than that in **1**/MAO. In addition, the chain end resonance is more prominent in polymers produced by **2a**/MAO than in those produced by **2b**/MAO, implying that the latter has a higher molecular weight. This trend is similar to that observed for **1a**/MAO and **1b**/MAO, where GPC analysis showed that **1b**/MAO in general produced higher molecular weight polymers than **1a**/MAO under comparable conditions. Therefore, substituting hydrogen with an isopropyl group on the less substituted Cp ring seems to have a moderate effect on decreasing the ratio of $r_p : r_{ct}$.

As in **1**/MAO systems, the isolated [*m*] diads (or [*rm*] triads) constitutes the main stereoerrors, implying that site epimerization is the major mechanism for stereo-irregularity (Table 7, Figure 13).[15] The probability of site epimerization from each site is determined by the difference in transition energy of site epimerization and enchainment (the higher the transition state energy for site epimerization relative to that for enchainment, the less likely it is for site epimerization to occur), the lower syndiotacticity observed for catalysts **2** compared to **1** imply that this difference is smaller in **2** (at least at one insertion site) than in **1**. This could be caused by either a decrease in the transition state energy for site epimerization, or an increase in the transition state energy for enchainment, or a combination of two.

Scheme 8 shows the general reaction sequence for catalysts **1** and **2**. In the following discussion, we will assume that the steric interactions between the $SiMe_2$ group and the polymer chain or incoming olefin is the same in **2** as in **1**. Then the ground state energy for **C** should be approximately the same in **2** as in **1**. **E**, the transition state energy for site epimerization, should also be approximately the same in **2** and **1**, because the polymer chain experiences little steric interaction with either linker when it resides in the middle. If $SiPh_2$ is sterically less demanding than $SiMe_2$, then **A**, **B** and **D** are stabilized in **2** relative to in **1**. This means that the difference in transiton state energy between **E** and **B** as well as that between **E** and **D** will both increase, and that as a consequence, the

probability of site epimerization from either side decreases. Such a situation should have resulted in more syndiotactic polypropylenes, contrary to the experimental result. On the other hand, if $SiPh_2$ is sterically more demanding than SiMe2, then **A, B** and **D** are destabilized in **2** compared to in **1**. This translates to smaller differences in transiton state energies between both **E** and **B** and **E** and **D**, which leads to more frequent site epimerization and increased stereoirregularities in the resulting polymers. The experimental results are therefore more consistent with a sterically more demanding $SiPh_2$ than $SiMe_2$, which implies that structure **A1** (*vide supra*) is the more likely one than **A2**, and that the phenyl ring extends at least partially forward to have a stronger steric interaction with both the polymer chain and the incoming monomer. Unfortunately, this steric influence does not appear strong enough to switch the system to isospecific at low monomer concentrations. In fact, the presence of a significant amount of [*rmrm*] implies that site epimerization occurs in both directions at rates on the same order of magnitude. That is, the steric repulsion between the polymer chain and $SiPh_2$ does not seem much greater than that between the polymer chain and $SiMe_2$.

Scheme 8

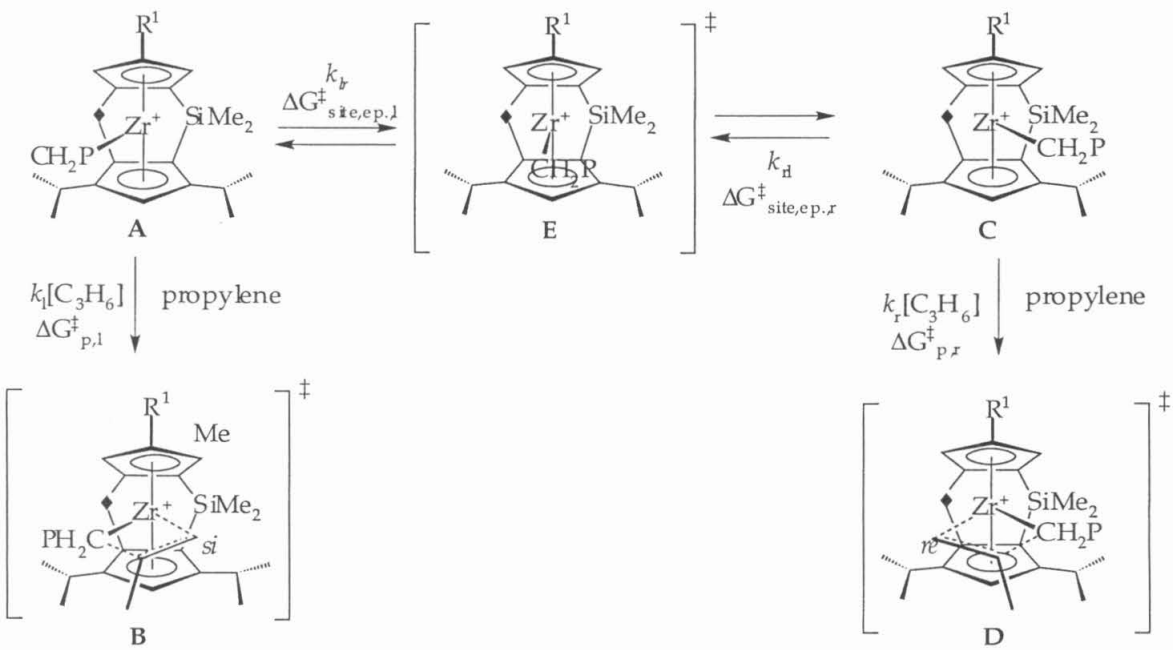

♦ = $SiMe_2$ (**1**), $SiPh_2$ (**2**)

Polymerization with 3a–b/MAO. Catalysts **3a–b** were activated by MAO for the polymerization of propylene. Polymerization with **3a** was carried out at 0 °C under various propylene concentrations (Table 8, entries 1–4). With **3b**, polymerization at variable temperatures was also performed (Table 8, entries 6–8). These catalysts produced polypropylene with much lower molecular weights than those prepared by **1**/MAO. For example, at 20 °C in neat propylene, **1b**/MAO produced polypropylene with molecular weight of 980,000.[15] In comparison, under the same condition, **3b**/MAO could only afford polypropylene with a molecular weight of 43,700. Similarly, at 70 °C in neat propylene, **1b**/MAO catalyzed production of polypropylene with a molecular weight of 130,000[15] compared to a molecular weight of 5600 for those prepared by **3b**/MAO. **1**/MAO was *ca.* five-fold more active catalytically,[15] but because different batches of MAO were employed, a direct comparison of activities by these systems may not be valid.

Under all conditions investigated, the catalyst system produced isotactic polypropylene. The approximately 2:2:1 ratio of [*mmmr*] : [*mmrr*] : [*mrrm*] established enantiomorphic site control as the main stereo–control mechanism. The tacticity of the polymer dropped slightly upon lowering the monomer concentration. For example, the percentage of [*mmmm*] pentad dropped from 75% to 68% upon lowering the monomer concentration from $x_{propylene} = 1$ to 0.17; and for **3b**, a 3% decrease in [*mmmm*] distribution has been observed for the same concentration range.

The isotacticity decreased more significantly when the polymerization temperature was raised. For example, for **3b**/MAO, polypropylenes with [*mmmm*] = 99% and a melting point of 161.5 °C has been obtained at 0 °C in neat propene. But [*mmmm*] dropped to 72% at $T_p = 70$ °C. The drop in isotacticity at higher temperature was probably due to the increased flexibility of the ligand frame work at higher temperatures[24] as well as an increase in the rates of chain–epimerization.

For polymers made in run 24, resonances corresponding to mostly propyl and vinylidene end groups can be observed,[6,25] and they exist in approximately 1:1 ratio. In addition, a small amount of isobutyl chain end groups[6] can also be observed. The propyl and vinylidene end–groups are most likely formed by β–H transfer to monomer or zirconium (Scheme 9),[6,26] and the isobutyl end–group formation mostly proceed through chain–transfer to aluminum or proton (Scheme 10).[6]

Table 8. Propylene polymerization data for **3a** – **b**/MAO.

entry	cat.	$T_p \pm 5$ °C	propene pressure	$x_{propylene}$	[propylene] (M)	catalyst(mg)/ MAO (mg)	% [*m*]	% chain-end[25]	activity[a]
17	**3a**[b]	0	1 atm	0.17 ± 0.01	1.7	1.50/530	87%	<0.6	0.43
18	**3a**	0	20 psig	0.40 ± 0.02	4.1	1.50/505	87%	<0.2	0.99
19	**3a**	0	40 psig	0.62 ± 0.03	6.8	1.50/535	88%	<0.2	3.7
20	**3a**	0	80 psig	1	12.2	1.50/505	90%	<0.2	2.5
21	**3b**	0	1 atm	0.17 ± 0.01	1.7	2.20/536	99%	<0.5	0.38
22	**3b**	0	80 psig	1	12.2	1.00/500	>99%	<0.2	1.7
23	**3b**[c]	20	neat	1	12.2	0.3/60[e]	98%	<0.2	6.6
24	**3b**[d]	70	neat	1	12.2	0.2/40[e]	89%	0.9	34.9

[a.] activity given in 10^4 gPP/g·Zr·hr. [b.] contains ~0.5% regioerrors. [c.] Polymerization performed at Exxon. M_W = 43,700 g/mol, PDI = 1.9; m.p. = 155.4 °C. [d.] Polymerization performed at Exxon. M_W = 5,600, PDI = 1.8, m.p. = 116.7 °C. [e.] Al:Zr ratio is ~2000:1.

Table 9. Pentad distributions (%) for the polypropene samples produced by **3a–b**/ MAO.

entry	catalyst	[*mmmm*]	[*mmmr*]	[*rmmr*]	[*mmrr*]	[*rmrr*]+ [*mrmm*]	[*rmrm*]	[*rrrr*]	[*rrrm*]	[*mrrm*]
17	**3a**	68.3	12.9	<0.3[a]	10.8	1.8	0.6	<0.6 [b]	0.7	4.9
18	**3a**	69.8	11.4	<0.2[a]	11.9	1.6	0.2	<0.2	0.5	4.3
19	**3a**	71.0	11.8	<0.2[a]	11.2	1.1	0.2	<0.2	0.5	4.2
20	**3a**	75.0	10.2	<0.2[a]	9.1	0.5	<0.2	<0.2	0.4	4.5
21	**3b**	96.6	1.5	1.5				<0.2		0.6
22	**3b**	99.2	0.3	0.3				<0.2		0.2
23	**3b**	94.9	2..1	2.2						0.8
24	**3b**	72.3	10.1	<0.1	8.5	2.5	0.3	<0.9[b]	0.3	4.3

[a.] could overlap with the isobutyl chain-end group. [b.] may overlap with propyl chain-end group.

Scheme 9

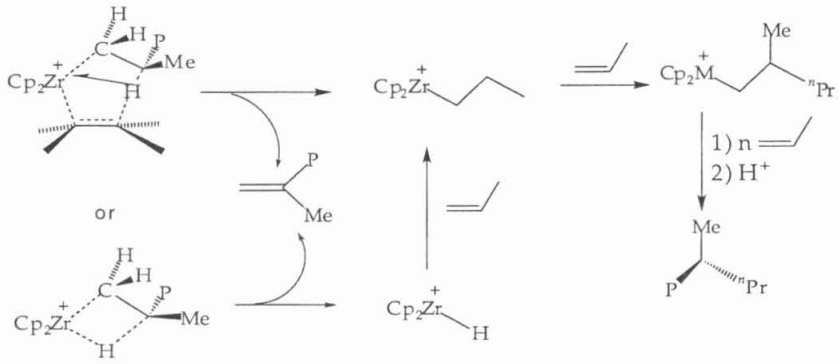

Scheme 10

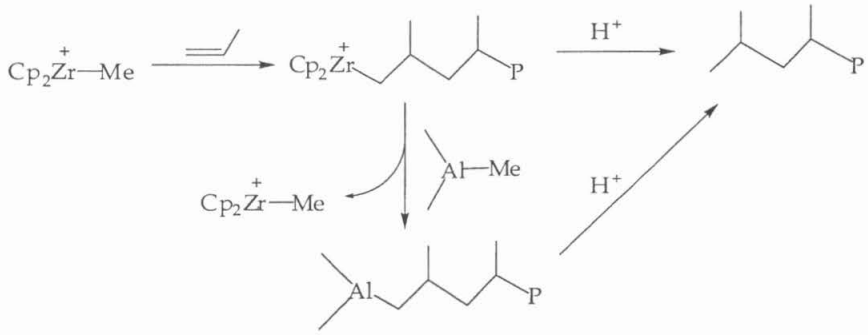

But why are these systems isospecific rather than syndiospecific like **1** and **2**? X–ray crystal structure of **3a** has provided part of the answer. In **1**, the mirror plane that bisects the two enantiotopic coordination/insertion sites also bisects the two silicon linkers. In contrast, in **3**, the plane bisecting the two diastereotopic sites actually passes through (or nearly so) the dimethylsilylene linker. The longer tetramethyldisilylene linker has swung to the side. The structure now resembles a singly–linked *ansa*–metallocene.

Although no crystal structure has been obtained for **3b**, if we assume that **3b** and **3a** have similar structural framework, then **3b** can be depicted as structures shown in Figure 14.

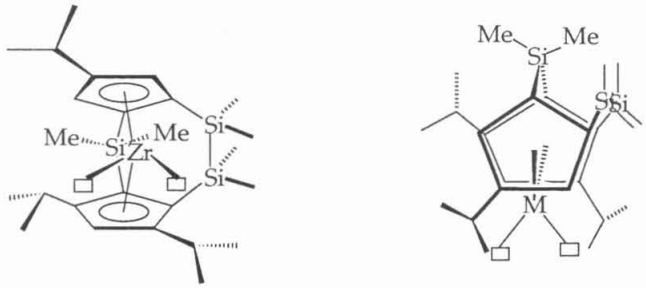

Figure 14. Front and top view of **3b**.

It is commonly accepted that the polymer stereochemistry is mostly controlled by substitutents in the front of the metallocenes (at β–position to the silylene linker in this case).[6,27] In **3b**, the four quadrants in the front are occupied alternatively by the isopropyl groups and the hydrogen atoms in an arrangement similar to that found in many C_2-symmetric isospecific catalysts (Figure 15). This implies that the stereochemical control mechanism followed by **3b** will be similar to many C_2-symmetric catalysts, or more specifically, monomer insertion will involve the same enantioface on either side of the wedge, resulting in highly isotactic polymers.

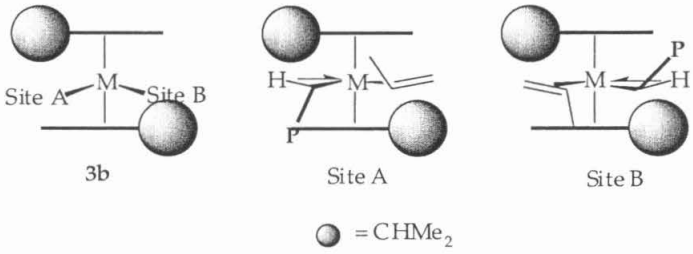

Figure 15. The two coordination sites in **3b** are "homotopic" as in C_2-symmetric catalysts.

While the rear-substituents of the Cp ring (α to the silylene linker in this case) have only a secondary effect in stereocontrol, they are important for regiocontrol and lead to increased molecular weights of the resulting polymers.[6,27,28] The relatively few regioerrors detected may thus be attributed to the unfavorable steric interactions between propylene's methyl groups and either the α-isopropyl group or the tetramethyldisilylene linker (Figure 16).

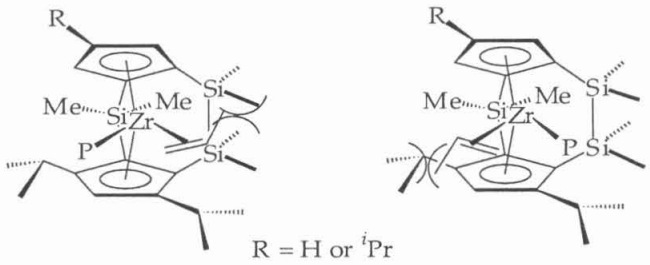

Figure 16. Substituents α to the dimethylsilylene linker disfavor 2,1–insertion.

More perplexing is the fact that in **3a**, of the four quadrants in the front of the wedge, three are occupied by H's and only one is occupied by an isopropyl group (Figure 17). In other words, when the polymer resides at Site A, there is steric differentiation between the two Cp rings, which directs the polymer chain to adopt the α-agostic conformation that minimizes the steric interaction between the polymer chain and the isopropyl group.[29] This in turn directs the enantiofacial selectivity of the monomer unit by placing the propylene methyl group anti to the polymer chain[29,30](**Ia** is favored over **Ib**, see Chapter 1). On the other hand, when the polymer resides at Site B, there does not appear to be any steric differentiation between the two Cp rings, and monomer insertion should therefore have proceeded with little or no selectivity (Scheme 11).

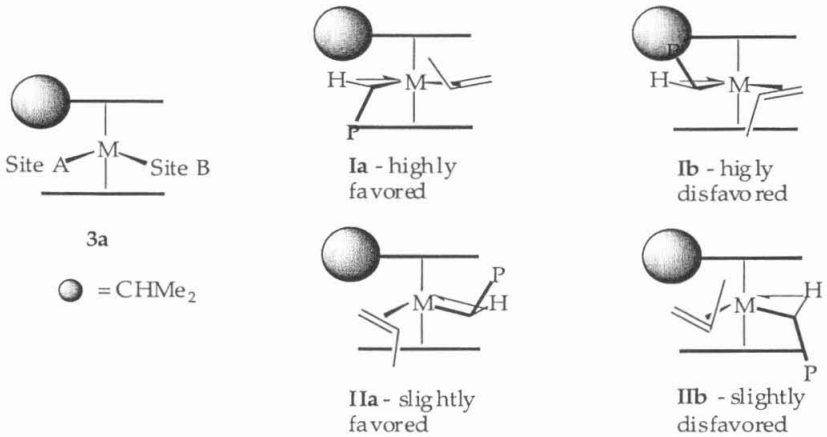

Figure 17. The four diastereotopic transtion states for monomer insertion in **3a**.

Scheme 11

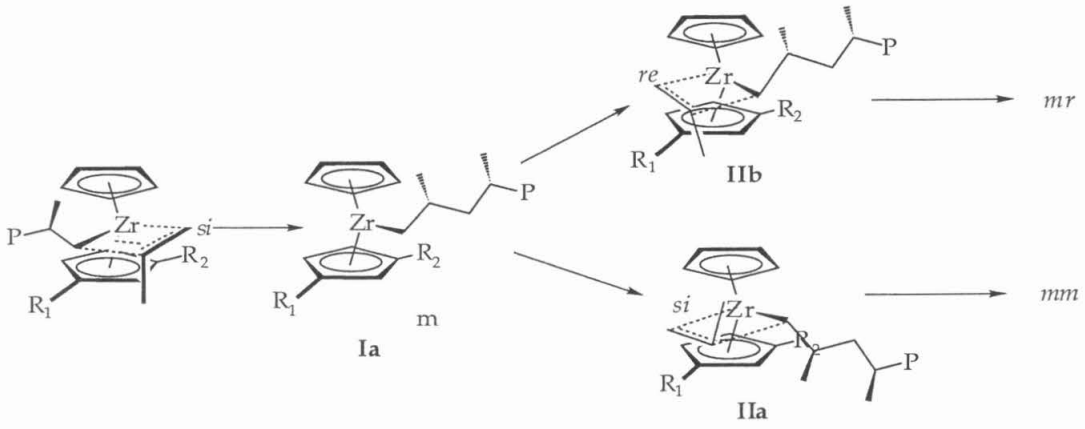

Bridging atoms are omitted for clarity.

Granted, in this case, the enantiofacial selection of the monomer can be determined by its interaction with ligand frame work (Figure 17, **IIa**). However, previous studies have shown that in similar ligand frame work, monomer–ligand interaction results in at most a modest ~ 2:1 ratio of enantioselectivity.[29-31] That is, **IIa** is preferred over **IIb** by a factor of approximately 2, which is not sufficient to result in a [*m*] diad content of >90%. Can there be attractive interactions between the polymer chain and the isopropyl groups so that the preference for **IIa** over **IIb** is much enhanced? Although such interactions have been proposed by Rappe and co–workers to rationalize the polymerization behavior of the so–called "Spaleck catalysts",[32] the interaction is between an aryl ring and an alkyl chain, whose interactions would be fairly different both electrostatically and sterically from interactions between two alkyl groups. Thus, in the absence of additional experimental and theoretical evidence, such a speculation is not extremely plausible.

To rationalize the experimental results, one may also argue that insertion occurs mostly from site B (with polymer chain residing at site A). Occasional insertion does occur from Site A, which has a slight preference for producing a *mm* triad over *mr* triad. The preferred insertion from Site B may arise from the lower ground state structure of **I** than **II** (Scheme 12, pathway a) with similar insertion barrier from either site. The rate of equilibration between **I** and **II** and the rates of chain propagation are comparable ($r_{\mathbf{II-I}} \sim r_{p,A}$; $r_{\mathbf{I-II}} \sim r_{p,B}$). Alternatively, if a fast equilibrium can be established between **I** and **II**, then

lower transition state energy for enchainment from structure **I** than that from **II** (Scheme 12, pathway b) can also lead to selective insertion from site A ($r_{\mathbf{II-I}} \sim r_{\mathbf{I-II}} >> r_{p,A} > r_{p,B}$). The third scenario (Scheme 12, path c) is that the enchainment barrier from the aspecific site is prohibitively high, so that more often than not, the chain swings to the isospecific site before an insertion occurs. According to pathway a, the uni–molecular equilibration between **I** and **II** competes with secondary monomer insertion process. The tacticity of the resulting polymer should therefore show a dependence on the monomer concentration, and should increase with decreasing monomer concentrations. Pathway b, in turn, assumes a fast pre-equilibrium between **I** and **II**. This pathway predicts that the number of stereoerrors (in the absence of chain epimerization) will be determined by the difference in transition-state energy for chain propagation from the aspecific site and that from the isospecific site, which should remain constant at a given temperature. The outcome in pathway c will depend on the relative stability of **I** and **II**. If **I** is more stable than **II**, then the tacticity should increase with decreasing monomer concentration; conversely, if **II** is more stable than **I**, the tacticity should decrease with decreasing monomer concentration. In the extreme case that insertion never takes place on the aspecific site, however, no concentration dependence is expected. But this could not be the case for the current system, because otherwise polymers with tacticities similar to those produced by **3b** would have been obtained. The observation of a slight decrease in [*mmmm*] is most consistent with pathway c and a more stable **II**. But because chain epimerization at low monomer concentrations also lowers resultant tacticities and the change is small, we cannot rule out pathway b either.

Scheme 12

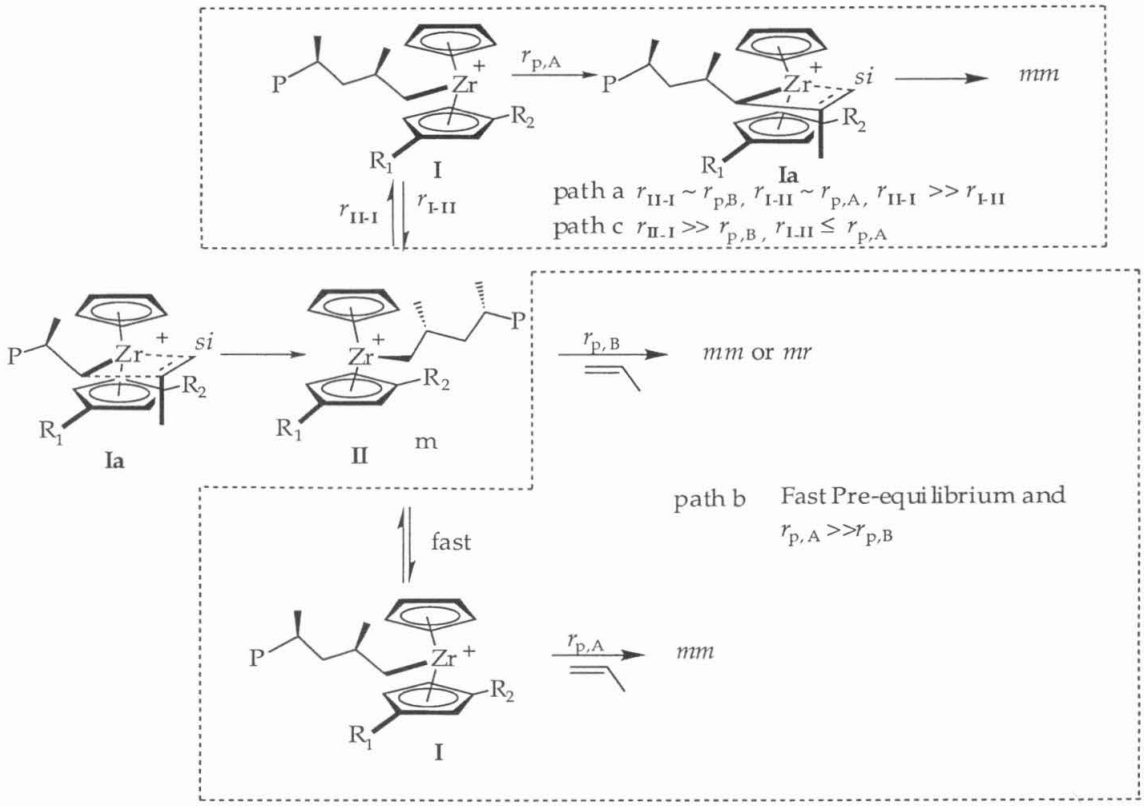

Bridging atoms are omitted for clarity.

It should be noted that *ansa*–zirconocenes with similar frontal structural features to **3a** have also been found to produce isotactic polymers. For example, Miya and Mise reported that zirconocene **13** produced polypropylene with [*mmmm*] content up to 78% at 30 °C under 3 bar of propylene pressure (in toluene). Collins also reported that polypropylene prepared by hafnocene complex **14** at 25 °C under 15 psig of propylene pressure in toluene had a [*mmmm*] content of 53%, although under the same condition, its zirconocene analog **15** is much less stereoselective ([*mmmm*]% = 30%).[33] In order to shed some light on the origin of isospecificity for **3a** and related complexes, several model zirconocene complexes were synthesized and used for propylene polymerization. The results of these studies are reported in Chapter 3.

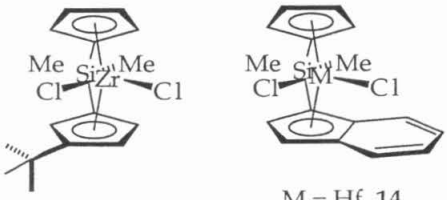

13

M = Hf, **14**
M = Zr, **15**

Conclusions

Several C_s- and C_1-symmetric doubly linked zirconocene have been prepared and tested for stereoselectivity in propylene polymerization. C_s-symmetric **1c–e** are highly syndiospecific catalysts, and their syndiospecificity rivals that of previously reported **1b.** We have also found that by replacing one dimethylsilylene linker in **1** with a bulkier diphenylsilylene linker, the C_1-symmetric system **2** remained syndiotactic, but with higher rates of site epimerization. In both catalyst systems **1** and **2**, the principal mechanism for stereoerror formation is site-epimerization. More interestingly, by replacing one dimethylsilylene linker with a tetramethyldisilylene linker, the zirconocenes **3** adopt a configuration resembling that of single silylene bridged *ansa*–zirconocenes and the stereoselectivity switches to isospecific. However, while we have a plausible explanation for the original of isospecificity for **3b**, whose frontal structural features resemble many C_2–symmetric catalysts, we are still striving to shed light on the origin of the modest isospecificity exhibited by **3a**.

Experimental Section

General considerations. All air and/or moisture sensitive compounds were manipulated using standard high–vacuum line, Schlenk line, or cannula techniques, or in a glove box under a nitrogen atmosphere. Argon was purified and dried by passage through columns of MnO on vermiculite and activated 4 Å molecular sieves. All solvents (except CH_2Cl_2) were stored under vacuum over titanocene or sodium benzophenone ketyl. CH_2Cl_2 was stored under vacuum over CaH_2. CMe_3-C_5H_4 was prepared by Jeff Yoder. 1,3-$(CHMe_2)_2$-C_5H_4 was prepared by Shigenobu Miyage. $SiMe_2Cl_2$ and TMSCl were purchased from

Aldrich, and stored over CaH_2 under vacuum. $SiMe_2Cl–SiMe_2Cl$ was purchased from Aldrich and stored in a Strauss flask under nitrogen in the glove box. *n*-Butyllithium was purchased from Aldrich and stored under argon. Pyrrolidine was purchased from Aldrich and used as received. $LiN(TMS)_2$, $KN(TMS)_2$ and $LiCH_2TMS$ were purchased from Aldrich, purified by sublimation and stored under nitrogen in the glove box. $Li(R\text{-}C_5H_4)$ (R = H, *tert*–Bu, *i*Pr) and $Li(1,3\text{-}iPr_2\text{-}C_5H_2)$ were prepared by deprotonation of the corresponding substituted cyclopentadienes with *n*-BuLi in diethylether, and worked up using standard procedure. $Li_2[1,1'\text{-}(SiMe_2)\text{-}\{3\text{-}R\text{-}C_5H_3\}\text{-}\{2,4\text{-}(CHMe_2)_2\text{-}C_5H_2\}]$ (R=H, *i*Pr), $Li_2[1,1'\text{-}(SiMe_2)\text{-}\{C_5H_4\}\text{-}\{3\text{-}R\text{-}C_5H_3\}]$ (R = tert–Bu, *i*Pr) and $Li_2[1,1'\text{-}(SiMe_2)\text{-}\{C_5H_4\}\text{-}\{3\text{-}R_2\text{-}C_5H_2\}]$ (R = *tert*–Bu, *i*Pr) are prepared according to known procedures.[13,15,16]

^1H NMR spectra were recorded on General Electric QE300 (^1H, 300.1 MHz) and Inova 500 (^1H, 499.852 MHz; ^{19}F, 470.256 MHz; ^{13}C, 125.701 MHz). ^{13}C for polypropene were recorded on Bruker AM500 spectrometers. Elemental analyses were carried out at the Caltech Elemental Analysis Facility by Fenton Harvey, with a run–to–run variation of 0.5% – 1.0%. X–ray diffraction studies were performed by Lawrence Henling at 85K on either a CAD–4 diffractometer or a Bruker SMART 1000 CCD area detector. CRYM programs and Bruker SMART programs were used for data processing and the structures were solved with SHELXS–86.

Synthesis of 1–phenyl–2–cyclopentenol. A 50 ml diethylether solution of 2-cyclopentenone (7 g, 85.4 mmol) was cannula transferred under argon to a 200 ml solution of PhLi (7.5 g, 89.3 mmol) at -78 °C over half an hour. The mixture was allowed to warm to 0 °C over 10 hours, and was then stirred at 0 °C for two more hours. 20 ml of saturated Na_2CO_3 aqueous solution was injected with vigorous stirring. The mixture was then neutralized with NH_4Cl. The mixture was extracted with 2 x 50 ml hexane, and the combined organic layer was dried over $MgSO_4$. The supernatant was filtered away from the salt, and rotavaped to concentrate. It was further dried under high vacuum at 50 °C for 1 hour. Pale yellow oil slowly solidified to waxy white solids. 12g collected and stored in -80 °C freezer (88%). ^1H NMR (300 MHz, C_6D_6): δ = 1.50 (s, 1H, O*H*), 2.00 (m, 2 allyl proton + 1 diastereotopic α proton), 2.30 (m, 1H, α proton), 6.1 (m, 1H, vinyl proton), 6.2 (m, 1H, vinyl proton), 7.1 (m, 1H), 7.2 (m, 2H), 7.5 (m, 2H).

Synthesis of Li(Ph–C_5H_4) ((Ph–Cp)Li). 17 g of 1-phenyl-2-cyclopentenol was loaded into a sublimator. The sublimator was evacuated to 1 torr and heated in a silicon oil bath to 160 °C. The cold finger was cooled by cold water. Under dynamic vacuum, 1–phenyl–2–cyclopentenol underwent dehydration. The red oily material collected on the cold finger was subjected to two more sublimation at 1μ torr at 120 °C. 4 g collected (23%). The yellow waxy material 2.2g (15.5 mmol) was dissolved in diethylether 150 ml, and was deprotonated with *n*-BuLi (20 ml, 1.6 *M* in hexanes, 32 mmol). The reaction mixture was stirred for 7 hours, and then filtered. The white powder was washed three times, and dried under vacuum overnight. 1.25g (54%) collected. ^{1}H NMR (300 MHz, THF–d_8): δ = 5.74 (t, 2.6 Hz, 2H, Cp*H*), 6.15 (t, 2.7 Hz, 2H, Cp*H*), 6.71 (t, 7.4 Hz, 0.5 Hz, 1H, PhH_p), 7.04 (td, 7.6 Hz, 2H, PhH_m), 7.43 (dd, 7.4 Hz, 0.7 Hz, 2H, PhH_o).

Synthesis of Li(C_6H_{11}–C_5H_4) ((Cy6–Cp)Li). To 80 ml of methanol in a 500 ml round bottom flask, cyclohexanone (2.2 ml, 212.3 mmol), cyclopentadiene (19 ml, 230.5 mmol) and pyrrolidine (3 ml, 35.82 mmol) were added in the order specified. The color turned immediately to bright yellow. The solution was cloudy after two hours. The mixture was stirred overnight. Second day, 6 ml of glacial acid was added, and the mixture was stirred for 1 minute. Afterwards, 100 ml of water and 100 ml of diethylether was added to the mixture. The aqueous layer was extracted with 3 x 100 ml of diethylether, and the combined organic layer was washed with 75 ml water and 75 ml of brine. The organic layer was dried over $MgSO_4$, and concentrated on rotavap. 29.8 g collected (97.5%). ^{1}H NMR (300 MHz, C_6D_6): δ = 1.25 (m, 1H), 1.42 (m, 2 H), 2.30 (m, 2H), 6.60 (m, 2H), 6.65 (m,2H).

The above fulvene (14.6g, 100 mmol) was dissolved in diethylether 125 ml. Inside inert atmosphere glove box, 6g of LAH was added to a 3 neck flask equipped with a dry ice/acetone condenser and a nitrogen inlet. 400 ml of diethyl ether was added to the 3–neck flask under argon on the Schlenk line. With cooling (to ~0 °C), fulvene was added dropwise with vigorous stirring. The yellow color quickly disappeared, and large quantities of white precipitate appeared. The mixture was stirred overnight, and then quenched with 10 ml water using a syringe pump (0.34 ml/min.) + 10 ml of 15% NaOH aqueous solution. After hydrogen stopped evolving, 40 ml more water was added. The mixture was filtered, and extracted with 2 x 100 ml diethyl ether. The combined

organic layer was then dried over $MgSO_4$, and rotavaped to concentrate. It was further dried under high vacuum for 1 hour. 14.9 g collected, 95%. 5 gram of the resultant ^{Cy6}CpH (33.8 mmol) was dissolved in diethylether in a swivel–frit assembly, and was treated with *n*-BuLi (33.6 mmol). After stirring overnight, the slurry was filtered, the white precipitate was washed three times and dried under vacuum. 4.5 g, 86.5%. ^{1}H NMR (300 MHz, THF–d_8): δ = 1.25 (m, 1H), 1.35 (m, 5H), 1.63 (m, 1H), 1.73 (m, 1H), 1.91 (m, 2H), 2.40 (m, 1H), 5.50 (s, 4H).

Synthesis of Synthesis of Li(C_5H_9–C_5H_4) ((Cy5–Cp)Li). (Cy5–Cp)Li was synthesized analogously using the fulvene route. Cyclopentanone (20 ml, 226 mmol), cyclopentadiene (20 ml, 242 mmol) and pyrrolidine (3 ml, 36 mmol) were reacted in 80 ml MeOH and worked up after 2 hours to yield 29.2 g of fulvene (97.7%). ^{1}H NMR (300 MHz, C_6D_6): δ = 1.30 (m, 2H), 2.42 (m, 2 H), 6.45 (m, 2H), 6.50 (m, 2H).

After reduction of the above fulvene with LAH and hydrolysis, the resultant ^{Cy5}CpH (9.1g, 67.5 mmol) was deprotonated with *n*-BuLi (52 ml, 83.2 mmol) in diethylether. 9.05 g white powder was collected (95.7%). ^{1}H NMR (300 MHz, THF–d_8): δ = 1.54 (m, 2H), 1.70 (m, 1H), 1.90 (m, 1H), 2.90 (m, 1H), 5.47 (s, 4H).

Synthesis of Li_2[1,1'-$SiMe_2$-{4-C_5H_9-C_5H_4}-{2',4'-$(CHMe_2)_2$-C_5H_2}] (4c). **4c** was prepared by reaction of (Cy5–Cp)Li (4.5 g, 32.1 mmol) and $iPr_2CpSiMe_2Cl$ (7.83 g, 32.2 mmol) in THF followed by deprotonation with *n*-BuLi. The orange product obtained from the reaction of (Cy5-Cp)Li and $iPr_2CpSiMe_2Cl$ was treated with 42 ml of *n*-BuLi solution (67.2 mmol) in diethylether/petroleum ether (3:1). After work–up, white powder (9.8 g, 94%) was collected. ^{1}H NMR (300 MHz, THF–d_8): δ = 0.30 (s, 6H, Si(CH_3)$_2$), 1.16 (m, 12H, CH(CH_3)$_2$), 1.54 (m, 4H), 1.64(m, 2H), 1.87(m, 2H), 2.78 (sept, 1H, C*H*Me_2), 2.90(m, 1H), 3.23 (sept, 1H, C*H*Me_2), 5.62(m, 1H), 6.67(m, 2H), 5.83(m, 2H).

Synthesis of Li_2[1,1'-$SiMe_2$-{4-C_6H_{11}-C_5H_4}-{2',4'-$(CHMe_2)_2$-C_5H_2}] (4d). **4d** was prepared analogously by reaction of (Cy6–Cp)Li (4.5g, 29.2 mmol) and iPr_2Cp-$SiMe_2$–$SiMe_2Cl$ (7.10 g, 29.3 mmol) in THF. 4 g (11.3 mmol) of the 9.5 g orange oil collected was treated with 15.5 ml of *n*–BuLi solution (24.8 mmol) in diethylether. After work–up, 3.2 g (77%) white powder collected. ^{1}H NMR (300 MHz, THF–d_8): δ = 0.30 (s, 6H, Si(CH_3)$_2$), 1.16 (two overlaying doublets, 12H,

$CH(CH_3)_2$), 1.36 (m, 6H), 1.78 (m, 2H), 1.87 (m, 2H), 2.45 (m, 1H), 2.78 (sept, 1H, $CHMe_2$), 3.23 (sept, 1H, $CHMe_2$), 5.62 (m, 1H), 5.67 (m, 2H), 5.83 (m, 2H).

Synthesis of Li_2[1,1'-$SiMe_2$-{4-Ph-C_5H_4}-{2,4-$(CHMe_2)_2$-C_5H_2}] (4e). **4e** was prepared analogously by reaction of (Ph–Cp)Li (1.0g, 7.1 mmol) and iPr_2Cp–$SiMe_2$–$SiMe_2Cl$ (1.72g, 7.1 mmol) in THF. The orange oil was purified by Kugelrohr distillation (1.83 g, 74%), and was treated with 7.4 ml of *n*-BuLi solution (11.8 mmol) in diethylether. After work–up, 1.57 g, 83% white powder collected. ^{1}H NMR (300 MHz, THF–d_8): δ = 0.36 (s, 6H, $Si(CH_3)_2$), 1.16 (m, 12H, $CH(CH_3)_2$), 2.78 (sept, 1H, $CHMe_2$), 3.23 (sept, 1H, 6.9 Hz, $CHMe_2$), 5.65 (m, 1H), 5.70 (m, 1H), 6.02 (m, 1H), 6.25 (m, 1H), 6.42 (m, 1H), 6.72 (m, 1H), 7.06 (m, 2H), 7.42 (m, 2H).

Synthesis of K_2{[1,1',2,2'-$(SiMe_2)_2$-[4-C_5H_9-C_5H_3]-[(3',5'-$CHMe_2)_2$-C_5H]} (6c). $SiMe_2Cl_2$ (1.55 ml, 12.8 mmol) was vacuum transferred into a 150 ml THF solution of **4c** at -78 °C. The mixture was allowed to warm to room temperature overnight and stirred at room temperature overnight. THF solvent was then replaced with petroleum ether. After removal of LiCl, the supernatant was concentrated to give an off–white solid, which was treated with 2 equivalents of $KN(TMS)_2$ in diethylether at room temperature overnight. Filtration, washing the precipitate with cold diethylether and drying under high vacuum afforded a white powder in 91% overall yield. ^{1}H NMR (300 MHz, THF–d_8): δ = 0.12 (brs, 12H, $Si(CH_3)_2$), 1.03 (d, 1.8 Hz, 12H, $CH(CH_3)_2$), 1.5 – 1.75 (m, 10H), 2.00 (m, 1H), 3.05 (sept, 2H, $CHMe_2$), 5.70 (br s, 1H), 5.90 (brs, 2H).

Synthesis of Li_2{[1,1',2,2'-$(SiMe_2)_2$-[4-C_6H_{11}-C_5H_3]-[(3',5'-$CHMe_2)_2$-C_5H]} (6d). $SiMe_2Cl_2$ (1 ml, 8.2 mmol) was vacuum transferred to a 150 ml THF solution of **4d** (3 g, 8.2 mmol) at -78 °C. The mixture was allowed to warm to room temperature overnight and stirred at room temperature overnight. THF solvent was then replaced with petroleum ether. After removal of LiCl, the supernatant was concentrated to give an off–white solid, which was treated with 2 equivalents of *n*-BuLi in diethylether at room temperature overnight. Filtration, washing the precipitate with cold diethylether and drying under high vacuum afforded a white powder in 86% overall yield. ^{1}H NMR (300 MHz, THF–d_8): δ = 0.24 (br, 12H, $Si(CH_3)_2$), 1.19 (d, 6.8 Hz, 12H, $CH(CH_3)_2$), 1.35 (m, 4H), 1.75 (m, 4H), 1.90 (m, 2H), 2.50 (m, 1H), 3.05 (sept, 2H, $CHMe_2$), 5.91 (s, 1H), 6.03(br, 2H).

Synthesis of $K_2\{[1,1',2,2'-(SiMe_2)_2-[4-Ph-C_5H_3][(3',5'-CHMe_2)_2-C_5H]\}$ (6e). $SiMe_2Cl_2$ (0.55 ml, 6.4 mmol) was vacuum transferred to a 150 ml THF solution of **4e** (1.57 g, 6.4 mmol) at -78 °C. The mixture was allowed to warm to room temperature overnight and stirred at room temperature overnight. THF solvent was then replaced with petroleum ether. After removal of LiCl, the supernatant was concentrated to give a yellow solid, which was Kugelrohr distilled under high vacuum at 120 °C to give an orange gel The gel was treated with 2 equivalents of $KN(TMS)_2$ in diethylether at room temperature overnight. Filtration, washing the precipitate with cold diethylether and drying under high vacuum afforded a yellow powder in 72% overall yield. ^1H NMR of the major product (~80%) (300 MHz, THF-d_8): $\delta = 0.22$ (br, 12H, $Si(CH_3)_2$), 1.15 (d, 6.8 Hz, 12H, $CH(CH_3)_2$), 3.20 (sept, 2H, $CHMe_2$), 5.75 (s, 1H), 6.51 (s, 2H), 6.64 (t, 6.8 Hz, 1H), 7.03 (t, 7.5 Hz, 2H), 7.48 (dd, 8 Hz, 1 Hz, 2H).

Synthesis of $Li_2[1,1'-SiPh_2-\{C_5H_4\}-\{2',4'-(CHMe_2)_2-C_5H_2\}]$ (7a). A 50 ml THF solution of $Li(1,3-iPr_2-C_5H_2)$ (2.05 g, 13.1 mmol) was added to a 30 ml THF solution of $SiPh_2Cl_2$ (3.24 g, 12.7 mmol) at -78 °C under argon. The solution was allowed to warm to room temperature overnight, and stirred at that temperature for 10 more hours. A THF solution (~ 70 ml) of LiCp (0.924 g, 12.8 mmol) was added to the above mixture under argon. The reaction mixture was stirred overnight. THF was then removed *in vacuo*, and petroleum ether 100 ml was added to the residue. The orange slurry was stirred at room temperature for 30 minutes, then filtered, resulting in a pink powder and an orange supernatant. The pink insolubes were washed three times with cold recycled petroleum ether. After removal of petroleum ether from the supernatant, a red oil (4.76 g, 90%) was left behind. A diethyl ether solution (~ 100 ml) of $LiCH_2TMS$ (2.18g, 23.1 mmol) was added to the red oil, and the mixture was stirred under argon overnight. White precipitate appeared overnight. Filtration gave 2.5 g white solids as product in 90% purity. ^1H NMR (300 MHz, THF-d_8): $\delta = 0.92$ (d, 6.6 Hz, 3H, $CHMe_2$), 1.17 (d, 6.6 Hz, 3H, $CHMe_2$), 2.81 (overlapping septets, 2H, $CHMe_2$), 5.73 (m, 1H, Cp*H*), 5.80 (m, 1H, Cp*H*), 5.91 (m, 2H, Cp*H*), 6.07 (m, 2H, Cp*H*), 7.13 – 7.15 (m, 6H, Ar*H*), 7.63 – 7.64 (m, 4H, Ar*H*).

Synthesis of $Li_2[1,1'-SiPh_2-\{3-CHMe_2-C_5H_3\}-\{2',4'-(CHMe_2)_2-C_5H_2\}]$ (7b). **7b** was prepared analogously. The red oil was first treated with *n*–BuLi in diethylether at room temperature, and then with KO(*t*–Bu) in THF at 50 °C. The

product was precipitated out of diethylether as a pinkish solid in 53% yield. ^{1}H NMR (300 MHz, THF–d_8): δ = 0.89 (d, 6.0 Hz, 3H, CH*Me*$_2$), 1.04 (d, 6.9 Hz, 3H, CH*Me*$_2$), 1.12 (d, 6.9 Hz, 3H, CH*Me*$_2$), 2.70 (sept., 6.9 Hz, 1H, C*H*Me$_2$), 2.82 (sept., 7.2 Hz, 1H, C*H*Me$_2$) 2.91 (sept., 6.3 Hz, 1H, C*H*Me$_2$), 5.55 (m, 1H, Cp*H*), 5.60 (m, 1H, Cp*H*), 5.75 (m, 1H, Cp*H*), 5.91 (m, 1H, Cp*H*), 5.98 (m, 1H, Cp*H*), 7.18 (m, 6H, Ar*H*), 7.93 (m, 4H, Ar*H*).

Synthesis of K$_2$[1,1'-SiMe$_2$-2,2'-SiPh$_2$-{C$_5$H$_3$}-{3',5'–(CHMe$_2$)$_2$–C$_5$H}]] (9a). SiMe$_2$Cl$_2$ (0.67 ml, 5.52 mmol) was vacuum transferred onto a THF solution (~100 ml) of **7a** (2.2g, 5.39 mmol) at -78 °C with vigorous stirring. The mixture was allowed to warm to room temperature overnight. THF was then removed *in vacuo*, and petroleum ether 50 ml was added to the resulting yellow paste to give a yellow slurry. The mixture was stirred for 30 minutes before filtration. The yellow filtrate was concentrated to give a yellow foam (2.077 g, 84%). The yellow foam was re–dissolved in THF with KN(TMS)$_2$ (1.868 g, 9.36 mmol), and heated at 50 °C overnight. THF was then removed *in vacuo*, and diethylether 50 ml was vacuum transferred onto the paste to give an orange supernatant and a white precipitate. The precipitate was collected (1.854 g, 75%). ^{1}H NMR (300 MHz, THF–d_8): δ = 0.29 (s, 6H, Si*Me*$_2$), 0.87 (d, 6.6 Hz, 6H, CH*Me*$_2$), 1.24 (d, 6.6 Hz, 6H, CH*Me*$_2$), 2.86 (sept, 6.6 Hz, 1H, C*H*Me$_2$), 3.21 (sept, 6.8 Hz, 1H, C*H*Me$_2$), 6.01 (s, 1H, (CHMe$_2$)$_2$–C$_5$*H*), 6.09 (dd, 2.4 Hz, 1.2 Hz, 1H, C$_5$*H*$_3$), 6.14 (t, 2.7 Hz, 1H, C$_5$*H*$_3$), 6.26 (dd, 2.4 Hz, 1.5 Hz, 1H, C$_5$*H*$_3$), 7.150 (6H, Ar*H*), 7.64 (4H, Ar*H*).

Synthesis of K$_2$[1,1'-SiMe$_2$-2,2'-SiPh$_2$-{4-CHMe$_2$-C$_5$H$_3$}-{3',5'-(CHMe$_2$)$_2$-C$_5$H}]] (9b). **9b** was prepared analogously in 74% yield based on **7b**. ^{1}H NMR (300 MHz, THF–d_8): δ = 0.23 (br s, 6H, Si(C*H*$_3$)$_2$), 0.90 (d, 6.6 Hz, 6H, CH(C*H*$_3$)$_2$), 1.16 (d, 6.9 Hz, 6H, CH(C*H*$_3$)$_2$), 1.21 (d, 6.9 Hz, 6H, CH(C*H*$_3$)$_2$), 2.89 (overlapping sept, 6.6 Hz, 2H, CH(C*H*$_3$)$_2$), 3.22 (sept, 6.6 Hz, 1H, C*H*(C*H*$_3$)$_2$), 5.85 (d, 1.5 Hz, 1H, CHMe$_2$–C$_5$*H*$_2$), 5.89 (s, 1H, C$_5$*H*), 6.09 (d, 1.5 Hz, 1H, C$_5$*H*$_2$), 7.12 (6H, Ar*H*), 7.69 (4H, Ar*H*).

Synthesis of 1-chloro-2-(2',5'-(CHMe$_2$)$_2$-C$_5$H$_3$)-tetramethyldisilane (16). 1,2–dichlorotetramethyldisilane (5.39 g, 28.8 mmol) was weighed into a 250 ml round bottom flask, and attached to a swivel frit assembly equipped with another 250 ml round bottom flask and one 90° needle valve. 1,3-(CHMe$_2$)$_2$-C$_5$H$_3$Li (4.5 g, 28.8 mmol) was weighed into a 150 ml round bottom flask equipped with a 180° needle valve. On the vacuum line, tetrahydrofuran 120 ml

was added via cannula to the dilithio salt. Another 30 ml of THF was added under Ar to 1,2–dichlorotetramethyldisilane. Over 2 to 3 hrs with vigorous stirring, the THF solution of the dilithio salt was added dropwise to 1,2–dichlorotetramethyldisilane at -78 °C. The solution was allowed to warm to room temperature overnight, and was stirred at this temperature for an additional 8 hrs. THF was then removed *in vacuo*, and the resulting yellow oily residue was dried under high vacuum for 30 minutes. Afterwards, petroleum ether 100 ml was added *via* vacuum transfer. The yellow slurry was stirred at room temperature for 30 minutes. and then filtered, resulting in a white powder and a yellow supernatant. The white insolubes were washed three times with cold recycled petroleum ether. After removal of petroleum ether from the supernatant, a yellow oil was left behind. It was dried under vacuum for 1 hour and collected in the glove box (8.07 g, 26.8 mmol, 93%). ^{1}H NMR (300 MHz, C_6D_6): δ = 6.22 (s, 1H, vinyl Cp), 5.91 (brs, 1H, vinyl Cp), 3.25 (br s., 1H, allyl), 2.56 (m, 2H, 6.6 Hz, C*H*Me$_2$), 1.16 (d, 6.6 Hz, CH(C*H*$_3$)$_2$) & 1.00 (br, total 12H) 0.35 (s, 6H, Si(C*H*$_3$)$_2$Cl), 0.1 & 0.2 (br, 6H, Si(C*H*$_3$)$_2$Cp).

Synthesis of Li$_2$[1,1'-(SiMe$_2$–SiMe$_2$)-{3-CHMe$_2$-C$_5$H$_3$}-{2',4'-(CHMe$_2$)$_2$-C$_5$H$_2$}] (11b). A 50 ml THF solution of Li[CHMe$_2$-C$_5$H$_4$] (1.82 g, 16.0 mmol) was added via cannula over 20 minutes to a 100 ml THF solution of **16** (4.5 g, 14.5 mmol) with stirring. The reaction mixture was kept at -78°C for half an hour, and afterwards the dry–ice/acetone bath was replaced with an ice bath. The reaction mixture was allowed to warm to room temperature gradually and stirred overnight. Second day, THF was removed in vacuo, and petroleum ether ~75 ml was vacuum transferred onto the resulting yellow paste. The yellow slurry was stirred at room temperature for an hour, and then filtered to leave behind a white precipitate and a yellow supernatant. The precipitate was washed three times with cold recycled petroleum ether. The solvent was then evaporated from the supernatant, leaving behind a sticky yellow oil, whose ^{1}H NMR consisted of many broad peaks, but none seem to correspond to those of **16**. A new swivel assembly was assembled in the glove box. On the high-vacuum line, diethylether 100 ml was added via vacuum transfer to the yellow oil. After replacing the dry–ice/acetone bath with an ice-bath, *n*-BuLi (1.6M in hexane, 20 ml, 32 mmol) was added over 20 minutes via a syringe. White solids started to precipitate during the course of addition, and the light yellow solution turned to slightly orange at the end of addition. The mixture was stirred

overnight at room temperature. The following day, the white precipitate was filtered away from the yellow/orange supernatant, and was washed three time with recycled diethylether (~20 ml each time). Diethylether was then removed *in vacuo*, and dried under high vacuum for 1 hour. The white solid was collected in green box (5.5 g, 14.3 mmol, 98%). ^{1}H NMR (300 MHz, THF–d_8): δ = 0.23 (s, 6H), 0.237 (s, 6H), 1.03–1.10 (3 sets of overlapping doublets, 18H), 3.58 (m, overlapping septets, 3H), 5.07 (m, 1H), 5.28 (m, 1H), 5.38 (m, 2H), 5.43 (m, 1H).

Synthesis of Li_2[1,1'–($SiMe_2$–$SiMe_2$)–{C_5H_4}–{2',4'–$(CHMe_2)_2$–C_5H_2}] (11a). **11a** was prepared analogously by reaction of **16** (2 g, 6.65 mmol) and LiCp (480 mg, 6.66 mmol) in THF. After work–up, the orange oil was treated with $LiN(TMS)_2$ (2.22 g, 13.3 mmol) in diethylether. The solution was stirred at room temperature for 3 nights, and the resulting orange slurry was filtered, the precipitate was washed twice and the solvent was removed *in vacuo*. The product was dried under vacuum for 5 hours and collected in the glove box (1.65 g, 72%). Deprotonation can also be carried out with 2 equivalents of *n*-BuLi, which resulted in much faster deprotonation and improved yield (84%, but with ca 5% impurity). ^{1}H NMR (300 MHz, THF–d_8): δ = 0.24 (s, 6H), 0.26 (s, 6H), 1.03 (d, 6H, 6.9 Hz, $CH(CH_3)_2$), 1.06 (d, 6H, 6.9 Hz, $CH(CH_3)_2$), 2.58 (sept, 6.6 Hz, 1H, $CHMe_2$), 2.66 (sept, 6.9 Hz, 1H, $CHMe_2$), 5.06(d, 2.1 Hz, 1H, $iPr_2C_5H_2$), 5.25(d, 2.1 Hz, 1H, $iPr_2C_5H_2$), 5.59(d, 2.4 Hz, 2H, C_5H_4), 5.61(d, 2.4 Hz, 2H, C_5H_4).

Synthesis of K_2[1,1'-($SiMe_2$)-2,2'-($SiMe_2$–$SiMe_2$)-(C_5H_3)-{3',5'-$(CHMe_2)_2$-C_5H}]] (12a). A THF solution (~100 ml) of **4a** (1.77g, 6.22 mmol) was added dropwise over 3 hours to a 125 ml THF solution of 1,2-dichlorotetramethyldisilane (1.165g, 6.22 mmol) under argon at 50 °C. The reaction mixture was stirred at room temperature overnight. THF was then removed *in vacuo*, and petroleum ether 100 ml was added. The yellow slurry was stirred for 30 minute, and then filtered to give a white solid and a yellow solution. The white solid was washed three times with cold petroleum ether. Petroleum ether was then removed *in vacuo*, leaving a sticky yellow oil. The yellow oil was dried under high–vacuum for 30 minutes. The resulting yellow oil was then deprotonated with $KN(TMS)_2$ (5 g, 25 mmol) in dioxane at 78 °C over two nights. The product was collected as an off–white solids in 60% yield. ^{1}H NMR (300 MHz, THF–d_8): δ = 0.26 (s, 6H, $Si(CH_3)_2$), 0.36 (s, 6H, $Si(CH_3)_2$), 0.62 (s, 6H, $SiMe_2$), 1.07 – 1.12 (2 sets of overlapping doublets, 12H, $CH(CH_3)_2$), 3.03

(sept, 6.6 Hz, 1H, C*H*Me$_2$), 3.21 (sept, 6.9 Hz, 1H, C*H*Me$_2$), 5.07 (s, 1H, C$_5$*H*), 5.87 (t, 2.4 Hz, 1H, C$_5$*H*$_3$), 6.08 (br s, 1H, C$_5$*H*$_3$), 6.15 (s, 1H, C$_5$*H*$_3$).

Synthesis of K$_2$[1,1'-SiMe$_2$-2,2'-(SiMe$_2$–SiMe$_2$)-{3-CHMe$_2$-C$_5$H$_2$}-{3',5'-(CHMe$_2$)$_2$-C$_5$H}]] (12b). SiMe$_2$Cl$_2$ (0.64 ml, 5.28 mmol) was condensed onto 150 ml THF solution of **10b** (2.023 g, 5.26 mmol) at -78 °C. The solution was allowed to warm to room temperature over night, and then stirred at that temperature for 4 more hours. Afterwards, THF was removed *in vacuo*, and the residue was dried for 30 minutes. 50 ml petroleum ether was added to the residue, and the resulting slurry was stirred for 30 minutes. The yellow supernatant was separated from the white precipitate by filtration. After removal of solvent, a sticky yellow oil was left behind.

A 50 ml THF solution of KN(TMS)$_2$ (3.7 g, 18.5 mmol) was added to the yellow oil, and stirred overnight. The solvent was then removed, and *p*–dioxane 50 ml was vacuum transferred onto the residue to form a slurry. The mixture was then heated to 80 °C to form a brown solution. After three days, there were tan precipitates in the solution. The mixture was cooled, and solvent removed *in vacuo*. Diethylether 50 ml was added to the mixture, and stirred for several hours. Filtration gave the desired product in 67% yield as a tan solid. ^{1}H NMR (300 MHz, THF–*d*$_8$): δ = 0.28 (s, 6H, Si(C*H*$_3$)$_2$), 0.37 (s, 6H, Si(C*H*$_3$)$_2$), 0.61 (s, 6H, Si(C*H*$_3$)$_2$), 2.83(sept, 6.6 Hz, 1H, C*H*Me$_2$), 3.10 (sept, 6.9 Hz, 1H, C*H*Me$_2$), 3.22 (sept, 6.9 Hz, 1H, C*H*Me$_2$), 5.73 (s, 1H, C$_5$*H*), 5.95 (br s, 1H, C$_5$*H*$_2$), 6.03 (br s, 1H, C$_5$*H*$_2$).

Synthesis of (Thp–C$_5$H$_9$) ZrCl$_2$ (1c). 1c was prepared by reaction of **6c** (3 g, 6.3 mmol) and ZrCl$_4$ (1.48 g, 6.3 mmol) in 150 ml toluene. The mixture was filtered through a bed of celite in box, and the precipitate was washed with 2 × 20 ml toluene. The combined toluene solution was transferred to a swivel frit assembly, and concentrated down to 2 ml. Petroleum ether 50 ml was added via vacuum transfer, the mixture was stirred for 1 hour and then filtered. The white powder was washed three times with solvent. 1.40 g collected (40%). Elemental analysis Found (Calculated): H 6.88% (7.14%), C 53.92% (53.78%). ^{1}H NMR (300 MHz, C$_6$D$_6$): δ 0.44 = (s, 6H, Si(C*H*$_3$)$_2$), 0.56 (s, 6H, SiMe$_2$), 0.95 (d, 6.9 Hz, 6H, CH(C*H*$_3$)$_2$), 1.30 (d, 6.6 Hz, 6H, CH(C*H*$_3$)$_2$), 1.35 – 1.75 (m, 6H), 2.21(m, 2H), 2.90 (sept, 2H, C*H*Me$_2$), 3.35 (m, 1H, Cy5's ipso carbon), 6.49 (s, 1H), 6.71 (s, 2H)

Synthesis of (Thp–C_6H_{11}) $ZrCl_2$ (1d). 5d (1.62 g, 3.95 mmol) and $Zr(NMe_2)_4$ (1.07 g, 3.95 mmol) were weighed into a 100 ml round bottom flask equipped with a condenser and a 180° needle valve. The mixture heated to 100 °C in xylene under Ar purge. The reaction was stopped when no more $HNMe_2$ evolved. Xylene was removed *in vacuo*, and the red residue was taken up in petroleum ether. Excess TMSCl (5.5 ml) was vacuum transferred into the reaction flask. Light–colored precipitate appeared. The reaction was stirred overnight, and then filtered. The yellow solid was washed three times, and dried under vacuum. To purify further, the solid was taken up in petroleum ether, and stirred overnight. Second day, it was filtered, washed and dried under vacuum to give a off–white solid (1.49 g, 65%). Elemental analysis Found (Calculated): H 7.06% (7.67%), C 54.7% (54.3%). ^{1}H NMR (300 MHz, C_6D_6, contains petroleum ether): δ = 0.44 (s, 6H, Si$CH_3)_2$), 0.56 (s, 6H, Si$CH_3)_2$), 0.90 (d, 6.9 Hz, 6H, CH($CH_3)_2$), 1.30 (d, 6.5 Hz, 6H, CH($CH_3)_2$), 1.2 – 1.5 (m, 6H), 1.70 (m, 2H), 2.43 (m, 2H), 2.90 (m, 3H, $CHMe_2$ + Cy6's ipso carbon), 6.48 (s, 1H), 6.66 (s, 2H)

Synthesis of (Thp–Ph) $ZrCl_2$ (1e). 1e was prepared by reaction of **6e** (960 mg, 2 mmol) and $ZrCl_4(THF)_2$ (700 mg, 1.86 mmol) in a mixture of diethylether and methylene chloride (10:1, ~ 70 ml total). The solvent was removed after five nights. Toluene was used to remove unreacted starting material and KCl. The remaining red mixture was washed repeatedly with an etheral solvent and petroleum ether. 30 mg yellow powder collected (3%). ^{1}H NMR in C_6D_6: δ = 0.54 (s, 6H, Si($CH_3)_2$), 0.62 (s, 6H, $SiMe_2$), 0.95 (d, 7.2 Hz, 6H, CH($CH_3)_2$), 1.3 (d, J 6.6 Hz, 6H, CH($CH_3)_2$), 2.95 (sept., 7.0 Hz, 2H, $CHMe_2$), 6.44 (s, 1H), 7.13 (s, 2H), 7.21(t, J = 7.5 Hz, 2H), 7.10 (tt, 7.5 Hz, 1.5 Hz, 1H), 7.90 (dd, 7.2, 1.2 Hz, 2H).

Synthesis of 2a.. Toluene 75 ml was vacuum transferred onto **9a** (1.854 g, 3.5 mmol) and $ZrCl_4$ (0.187 g, 3.5 mmol). The mixture was stirred at room temperature for 3 days, and then filtered to give a white solid and a yellow filtrate. The yellow filtrate was concentrated *in vacuo*, and petroleum ether 50 ml was added to the resulting yellow paste. The resulting slurry was stirred for 1 hour, and then filtered. 0.875 g of white insolubles were collected (41%). ^{1}H NMR (500 MHz, C_6D_6): δ = -0.35 (s, 3H, Si($CH_3)_2$), 0.38 (s, 3H, Si($CH_3)_2$), 0.78 (d, 3H, 7.0 Hz, CH($CH_3)_2$), 0.90 (d, 3H, 7.0 Hz, CH($CH_3)_2$), 1.32 (d, 3H, $^3J_{H-H}$ = 6.5 Hz, CH($CH_3)_2$), 1.34 (d, 3H, $^3J_{H-H}$ = 6.5 Hz, CH($CH_3)_2$), 2.91 (sept, $^3J_{H-H}$ = 7.0 Hz, 1H, $CHMe_2$), 2.97 (sept, $^3J_{H-H}$ = 6.5 Hz, 1H, $CHMe_2$), 6.55 (t, 1H, $^4J_{H-H}$ = 1.5

Hz, CpH), 6.57 (s, 1H, Cp*H*), 6.82 (dd, 1H, $^3J_{H-H}$ = 3.0 Hz, $^4J_{H-H}$ = 1.5 Hz, Cp*H*), 7.47 (dd, 1H, $^3J_{H-H}$ = 3.0 Hz, $^4J_{H-H}$ = 1.5 Hz, Cp*H*), 7.09 (m, 3H, Ar*H*), 7.12–7.22 (m, 3H, Ar*H*), 7.56 (d, $^3J_{H-H}$ = 7.0 Hz, 1H, Ar*H*), 7.89 (overlapping peaks, $^3J_{H-H}$ = 7.0 Hz, 6.5 Hz, 2H), 7.93 (d, $^3J_{H-H}$ = 7.0 Hz, 1H, Ar*H*). ^{13}C NMR (125 MHz, C_6D_6): δ = –0.442, 1.584 ($SiCH_3$), 20.96, 21.07 ($CHMe_2$), 28.74, 28.88, 29.62, 29.88 ($CH(CH_3)_2$), 108.47, 110.96, 112.70, 114.60, 116.44, 118.41, 128.50, 128.69, 128.87, 129.24, 129.70, 131.64, 131.68, 131.89, 135.72, 136.50, 137.05, 138.65, 138.81, 139.67, 165.94, 165.97.

Synthesis of 2b. **2b** was prepared analogously in 35% yield. ^{1}H NMR (300 MHz, C_6D_6): δ = -0.28 (s, 3H, Si(CH_3)$_2$), 0.42 (s, 3H, Si*Me*$_2$), 0.79 (d, 6.9 Hz, 3H, CH(CH_3)$_2$), 0.92 (d, 7.2 Hz, 3H, CH(CH_3)$_2$), 1.32 – 1.41 (overlapping doublets, 12H, CH*Me*$_2$), 2.95 (overlapping sept, 6.9 Hz, 2H, C*H*Me$_2$), 3.30 (sept, 6.6 Hz, 1H, C*H*Me$_2$), 6.62 (br s, 1H, Cp*H*), 6.78 (br s, 1H, Cp*H*), 7.42 (br s, 1H, Cp*H*), 7.08 – 7.22 (6H, Ar*H*), 7.69 (d, 6.0 Hz, 1H, Ar*H*), 7.982 (3H, Ar*H*). Elemental analysis Found (Calculated): H 6.28% (6.16%), C 60.09% (60.52%).

Synthesis of 3a. **3a** was prepared analogously in a 1:3 mixture of diethylether and toluene in 41% yield. ^{1}H NMR (300 MHz, C_6D_6): δ 0.28 (s, 3H, Si(CH_3)$_2$), 0.32 (s, 3H, Si(CH_3)$_2$), 0.48 (s, 6H, Si(CH_3)$_2$), 0.52 (s, 3H, Si(CH_3)$_2$), 0.68 (s, 3H, Si(CH_3)$_2$), 0.95 (d, 6.9 Hz, 3H, CH(CH_3)$_2$), 1.03 (d, 6.9 Hz, 3H, CH(CH_3)$_2$), 1.40(d, 6.6 Hz, 3H, CH(CH_3)$_2$), 1.47 (d, 6.6 Hz, 3H, CH(CH_3)$_2$), 2.68 (sept, 6.9 Hz, 1H, C*H*Me$_2$), 3.29 (sept, 6.6 Hz, 1H, C*H*Me$_2$), 5.95 (dd, 2.7 Hz, 1.8 Hz, 1H, C_5H_3), 6.80 (m, 2H, C_5H & C_5H_3), 7.102 (dd, 3.0 Hz, 1.8 Hz, 1H, C_5H_3). Elemental analysis Found (Calculated): H 6.67% (6.63%), C 48.30% (48.32%).

Synthesis of 3b. **3b** was prepared analogously in a 3:1 mixture of diethylether and toluene in 15% yield. ^{1}H NMR (300 MHz, C_6D_6): δ = 0.32 (s, 3H, Si(CH_3)$_2$), 0.360 (s, 3H, Si(CH_3)$_2$), 0.49 (s, 3H, Si(CH_3)$_2$), 0.54 (s, 3H, Si(CH_3)$_2$), 0.54 (s, 3H, Si(CH_3)$_2$, 0.73 (s, 3H, Si(CH_3)$_2$), 0.97 (d, 6.9 Hz, 3H, CH(CH_3)$_2$), 1.057 (d, 6.9 Hz, 3H, CH(CH_3)$_2$), 1.16 (d, 7.2 Hz, 3H, CH(CH_3)$_2$), 1.474 (d, 6.3 Hz, 3H, CH(CH_3)$_2$), 1.432 (d, 6.6 Hz, 3H, CH*Me*$_2$), 1.414 (d, 6.6 Hz, 3H, CH(CH_3)$_2$), 2.67 (sept, 6.6 Hz, 1H, C*H*Me$_2$), 3.30 (sept, 6.9 Hz, 1H, C*H*Me$_2$), 3.44 (sept, 6.9 Hz, 1H, C*H*Me$_2$), 5.79 (d, 1.8 Hz, 1H, C_5H_2), 6.88 (s, 1H, C_5H), 7.06 (d, 1.8 Hz, 1H, C_5H_2).. Elemental analysis Found (Calculated): H 7.35% (7.19%), C 50.70% (50.98%).

Recrystallization and X–ray diffraction studies of 1c, 1e and 3a. ~12 mg of the zirconocenes and ~ 0.6 ml of C_6D_6 were added to a J–Young NMR tube. The tube was immersed in a 80°C oil bath with occasional shaking to effect the dissolution of the solids. The tube was then inserted through a hole in a foam lid to ~80°C hot water contained in a Dewar flask. The water was allowed to cool down gradually to room temperature (>24 hours). Afterwards, the NMR tube was inverted with care to separate the crystals from supernatant. After two days, the supernatant was removed in box. The yellow needle–like crystals of **3a** were freeze dried, whereas the colorless prismatic crystals of **1c** and **1e** were used as was. For **1e**, the benzene adducts were modeled with two benzene molecules in an 85:15 ratio with the two rings rotated about 30° with respect to each other. All three structures were refined by full-matrix-least-squares with anisotropic thermal parameters for all non–hydrogen atoms and isotropic parameters for hydrogens. For **1c**, $GOF(F^2) = 1.894$ For **1e**, $GOF_{merge} = 0.99$ for 6788 multiples, $R_{merge} = .018$ for 6360 duplicates, final $R(F_0)$ 0.024 for 6085 reflections with $F_0^2 > 3\sigma(F_0^2)$ and $GOF(F^2) = 1.46$. For **3a**, $GOF(F^2) = 1.334$.

General polymerization procedures. In the glove box, MAO and toluene was added to the 100 ml high pressure glass reactor equipped with a septa port, a large stir bar and pressure gauge. Out of the box, the reactor was placed in a water (or ice/water) bath. The reactor was then connected a propylene line and was purged with slightly over 1 atm propylene for 20 minutes with stirring. The outlet was then shut, and pressure was then adjusted to that desired in the experiment, and the reactor was kept closed for 20 – 30 more minutes to reach a steady state. Afterwards, a toluene solution of the catalyst was injected using a 1 ml gas tight syringe through the septa with vigorous stirring. The mixture was stirred for 20 – 60 minutes before propylene was released from the reactor. The mixture was then quenched with MeOH. After gases stopped evolving, the reaction mixture was poured into an acidified MeOH solution (20% HCl by volume), and stirred for 1 hour before filtering. In the case of low–pressure polymerization with **3a/b**, toluene was evaporated and the residue was then treated with MeOH/HCl. The precipitate was washed with several portions of MeOH, and dried at high vacuum overnight.

References and Notes

(1) (a) Buchmeiser, M. R. *Chem. Rev.* **2000**, *100*, 1565–1604. (b) Britovsek, G. J. P.; Gibson, V. C.; Wass, D. F. *Angew. Chem., Int. Ed. Engl.* **1999**, *38*, 428–447. (c) Bochmann, M. *J. Chem. Soc., Dalton Trans.* **1996**, 255-270.

(2) (a) Brintzinger, H. H.; Fischer, D.; Mulhaupt, R.; Rieger, B.; Waymouth, R. M. *Angew. Chem., Int. Ed. Engl.* **1995**, *34*, 1143–1170. (b) Coates, G. W. *Chem. Rev.* **2000**, *100*, 1223–1252.

(3) Ewen, J. A.; Elder, M. J.; Jones, R. L.; Haspeslagh, L.; Atwood, J. L.; Bott, S. G.; Robinson, K. *Makromol. Chem., Macromol. Symp.* **1991**, *48-9*, 253–295.

(4) (a) Wang, C. M.; Friedrich, S. K.; Younkin, T. R.; Li, R. T.; Grubbs, R. H.; Bansleben, D. A.; Day, M. W. *Organometallics* **1998**, *17*, 3149–3151. (b) Younkin, T. R.; Connor, E. F.; Henderson, J. I.; Friedrich, S. K.; Grubbs, R. H.; Bansleben, D. A. *Science* **2000**, *288*, 1750–1751. (c) Younkin, T. R.; Conner, E. F.; Henderson, J. I.; Friedrich, S. K.; Grubbs, R. H.; Bansleben, D. A. *Science* **2000**, *287*, 460–462. (d) Tempel, D. J.; Johnson, L. K.; Huff, R. L.; White, P. S.; Brookhart, M. *J. Am. Chem. Soc.* **2000**, *122*, 6686–6700. (e) Ittel, S. D.; Johnson, L. K.; Brookhart, M. *Chem. Rev.* **2000**, *100*, 1169–1203. (f) Small, B. L.; Brookhart, M.; Bennett, A. M. A. *J. Am. Chem. Soc.* **1998**, *120*, 4049–4050. (g) Killian, C. M.; Tempel, D. J.; Johnson, L. K.; Brookhart, M. *J. Am. Chem. Soc.* **1996**, *118*, 11664–11665. (h) Johnson, L. K.; Killian, C. M.; Brookhart, M. *J. Am. Chem. Soc.* **1995**, *117*, 6414–6415.

(5) (a) Alt, H. G.; Koppl, A. *Chem. Rev.* **2000**, *100*, 1205–1221. (b) Fink, G.; Steinmetz, B.; Zechlin, J.; Przybyla, C.; Tesche, B. *Chem. Rev.* **2000**, *100*, 1377–1390. (c) Rappe, A. T.; Skiff, W. M.; Casewit, C. J. *Chem. Rev.* **2000**, *100*, 1435–1456.

(6) Resconi, L.; Cavallo, L.; Fait, A.; Piemontesi, F. *Chem. Rev.* **2000**, *100*, 1253–1345.

(7) (a) Scollard, J. D.; McConville, D. H.; Vittal, J. J.; Payne, N. C. *J. Mol. Catal. A.* **1998**, *128*, 201–214. (b) Scollard, J. D.; McConville, D. H.; Vittal, J. J. *Organometallics* **1997**, *16*, 4415–4420. (c) Scollard, J. D.; McConville, D. H.;

Rettig, S. J. *Organometallics* **1997**, *16*, 1810–1812. (d) Scollard, J. D.; McConville, D. H. *J. Am. Chem. Soc.* **1996**, *118*, 10008–10009. (e) Scollard, J. D.; McConville, D. H.; Payne, N. C.; Vittal, J. J. *Macromolecules* **1996**, *29*, 5241–5243.

(8) (a) Stevens, J. C. *Stud. Surf. Sci. Catal.* **1996**, *101*, 11–20. (b) Shapiro, P. J.; Cotter, W. D.; Schaefer, W. P.; Labinger, J. A.; Bercaw, J. E. *J. Am. Chem. Soc.* **1994**, *116*, 4623–4640. (c) Shapiro, P. J.; Bunel, E.; Schaefer, W. P.; Bercaw, J. E. *Organometallics* **1990**, *9*, 867–869.

(9) Angermund, K.; Fink, G.; Jensen, V. R.; Kleinschmidt, R. *Chem. Rev.* **2000**, *100*, 1457–1470.

(10) Ewen, J. A. *J. Mol. Catal. A.* **1998**, *128*, 103–109.

(11) (a) Barriola, A. M.; Cano, A. M.; Cuenca, T.; Fernandez, F. J.; Gomez-Sal, P.; Manzanero, A.; Royo, P. *J. Organomet. Chem.* **1997**, *542*, 247–253. (b) Cano, A.; Cuenca, T.; Gomez-Sal, P.; Manzanero, A.; Royo, P. *J. Organomet. Chem.* **1996**, *526*, 227–235. (c) Cuenca, T.; Galakhov, M.; Royo, E.; Royo, P. *J. Organomet. Chem.* **1996**, *515*, 33–36. (d) Dorer, B.; Prosenc, M.-H.; Rief, U.; Brintzinger, H. H. *Organometallics* **1994**, *13*, 3868–3872. (e) Halterman, R. L.; Tretyakov, A.; Combs, D.; Chang, J.; Khan, M. A. *Organometallics* **1997**, *16*, 3333–3339. (f) Grossman, R. B.; Tsai, J.-C.; Davis, W. M.; Gutierrez, A.; Buchwald, S. L. *Organometallics* **1994**, *13*, 3892–3896.

(12) (a) Stehling, U.; Diebold, J.; Kirsten, R.; Roell, W.; Brintzinger, H. H.; Juengling, S.; Muelhaupt, R.; Langhauser, F. *Organometallics* **1994**, *13*, 964–970. (b) Mengele, W.; Diebold, J.; Troll, C.; Roell, W.; Brintzinger, H. H. *Organometallics* **1993**, *12*, 1931–1935. (c) Ihara, E.; Nodono, M.; Katsura, K.; Adachi, Y.; Yasuda, H.; Yamagashira, M.; Hashimoto, H.; Kanehisa, N.; Kai, Y. *Organometallics* **1998**, *17*, 3945–3956.

(13) Herzog, T. A.; Zubris, D. L.; Bercaw, J. E. *J. Am. Chem. Soc.* **1996**, *118*, 11988–11989.

(14) Miyake, S.; Bercaw, J. E. *J. Mol. Catal. A: Chem.* **1998**, *128*, 29-39.

(15) Veghini, D.; Henling, L. M.; Burkhardt, T. J.; Bercaw, J. E. *J. Am. Chem. Soc.* **1999**, *121*, 564–573.

(16) Herzog, T. A. In *Department of Chemistry, Division of Chemistry and Chemical Engineering*; California Institute of Technology: Pasadena, CA, **1997**.

(17) Stone, K. J.; Little, R. D. *J. Org. Chem.* **1984**, *49*, 1849–1853.

(18) (a) Singh, P.; Rausch, M. D.; Bitterwolf, T. E. *J. Organomet. Chem.* **1988**, *352*, 273–282. (b) Riemschineider, R. *Monatsh. Chem.* **1960**, *91*, 829–832.

(19) (a) Diamond, G. M.; Jordan, R. F.; Petersen, J. L. *Organometallics* **1996**, *15*, 4045–4053. (b) Diamond, G. M.; Jordan, R. F.; Petersen, J. L. *Organometallics* **1996**, *15*, 4030–4037. (c) Diamond, G. M.; Jordan, R. F.; Petersen, J. L. *J. Am. Chem. Soc.* **1996**, *118*, 8024–8033. (d) Diamond, G. M.; Rodewald, S.; Jordan, R. F. *Organometallics* **1995**, *14*, 5–7.

(20) Gordon, A. J.; Ford, R. A. In *The Chemist's Companion: A Handbook of Practicaldata, Techniques, and References*; Gordon, A. J., Ford, R. A., Eds.; John Wiley & Sons: New York, 1972; p 108.

(21) Jutzi, P.; Burford, N. *Chem. Rev.* **1999**, *99*, 969–990. ( ) Jutzi, P. *Chem. Rev.* **1986**, *86*, 983–996.

(22) (a) Razavi, A.; Vereecke, D.; Peters, L.; Dauw, K. D.; Nafpliotis, L.; Atwood, J. L. In *Ziegler Catalysts*; Fink, G., Mulhaupt, R., Brintzinger, H. H., Eds.; Springer-Verlag: Berlin, 1995; p 111–147. (b) Ewen, J. A.; Elder, M. J. In *Ziegler Catalysts*; Fink, G., Mulhaupt, R., Brintzinger, H. H., Eds.; Springer-Verlag: Berlin, 1995; p 99–109. (c) Ewen, J. A. *Makromol. Chem., Macromol. Symp.* **1995**, *89*, 181–196. (d) Ewen, J. A.; Elder, M. J. *Makromol. Chem., Macromol. Symp.* **1993**, *66*, 179–190. (e) Ewen, J. A.; Jones, R. L.; Razavi, A.; Ferrara, J. D. *J. Am. Chem. Soc.* **1988**, *110*, 6255.

(23) The [*r*] diad contents were almost identical (less than 1% change) at [C_3H_6] = 2.1 *M* and 3.4 *M* for both **2a** and **2b**. We may thus extrapolate and assume that the [r] diad contents in neat propene are close to 81% and 91% for **2a** and **2b** respectively.

(24) Burger, P.; Diebold, J.; Gutmann, S.; Hund, H. U.; Brintzinger, H. H. *Organometallics* **1992**, *11*, 1319–1327.

(25) (a) Grassi, A.; Zambelli, A.; Resconi, L.; Albizzati, E.; Mazzocchi, R. *Macromolecules* **1988**, *21*, 617–622. (b) Asakura, T.; Nakayama, N.; Demura, M.; Asano, A. *Macromolecules* **1992**, *25*, 4876–4881.

(26) Bravakis, A. M.; Bailey, L. E.; Pigeon, M.; Collins, S. *Macromolecules* **1998**, *31*, 1000–1009.

(27) Cavallo, L.; Corradini, P.; Guerra, G.; Vacatello, M. *Polymer* **1991**, *32*, 1329–1335.

(28) (a) Miya, S.; Mise, T.; Yamazaki, H. *Stud. Surf. Sci. Catal.* **1990**, *56*, 531–534. (b) Mise, T.; Miya, S.; Yamazaki, H. *Chem. Lett.* **1989**, 1853–1856. (c) Roll, W.; Brintzinger, H. H.; Rieger, B.; Zolk, R. *Angew. Chem.-Int. Edit. Engl.* **1990**, *29*, 279–280.

(29) Gilchrist, J. H.; Bercaw, J. E. *J. Am. Chem. Soc.* **1996**, *118*, 12021–12028.

(30) Waymouth, R.; Pino, P. *J. Am. Chem. Soc.* **1990**, *112*, 4911–4914.

(31) (a) Zambelli, A.; Locatelli, P.; Sacchi, M. C.; Tritto, I. *Macromolecules* **1982**, *15*, 831–834. (b) Zambelli, A.; Sacchi, M. C.; Locatelli, P.; Zannoni, G. *Macromolecules* **1982**, *15*, 211–212. (c) Dahlmann, M.; Erker, G.; Nissinen, M.; Froehlich, R. *J. Am. Chem. Soc.* **1999**, *121*, 2820–2828. (d) Sacchi, M. C.; Barsties, E.; Tritto, I.; Locatelli, P.; Brintzinger, H.-H.; Stehling, U. *Macromolecules* **1997**, *30*, 3955-3957.

(32) (a) Spaleck, W.; Kueber, F.; Winter, A.; Rohrmann, J.; Bachmann, B.; Antberg, M.; Dolle, V.; Paulus, E. F. *Organometallics* **1994**, *13*, 954-963. (b) Spaleck, W.; Antberg, M.; Rohrmann, J.; Winter, A.; Bachmann, B.; Kiprof, P.; Behm, J.; Herrmann, W. A. *Angew. Chem.* **1992**, *104*, 1373-1376 (See also *Angew. Chem., Int. Ed. Engl.*, **1992**, *31*, 1347–1350). (c) Spaleck, W.; Antberg, M.; Dolle, V.; Klein, R.; Rohrmann, J.; Winter, A. *New J. Chem.* **1990**, *14*, 499-503.

(33) Gauthier, W. J.; Collins, S. *Macromolecules* **1995**, *28*, 3779–3786.

Chapter 3

Effects of Cp α-Substituents on Propylene Polymerization

Abstract

C_1-symmetric *ansa*-metallocenes [1,1'-$SiMe_2$-(C_5H_4)-(3-R-C_5H_3)]$ZrCl_2$ (**2a**, R = $CHMe_2$; **2b**, R = CMe_3), [1,1'-$SiMe_2$-(C_5H_4)-(2,4-R_2-C_5H_2)]$ZrCl_2$ (**3a**, R = $CHMe_2$; **3b**, R = CMe_3) and [1,1'-$SiMe_2$-2,2'-($SiMe_2$–$SiMe_2$)-(C_5H_3)-(4-R-C_5H_2)]$ZrCl_2$ (**4a**, R = $CHMe_2$; **4b**, R = CMe_3) are prepared. In the presence of MAO, catalysts **2** produce modestly isotactic polypropylenes, whereas catalysts **3** and **4** produce hemi-isotactic polypropylenes. It is proposed that site epimerization *via* an associative pathway is a facile process in catalyst system **2**. The ensuing Curtin-Hammett situation, where chain propagation is much slower than site epimerization, allows the polymer chain to insert preferentially from the isospecific site and leads to polymers with modestly high isotacticities. In contrast, the rates for associative site epimerization are slow in catalysts **3** and **4**. This results in alternating insertion from the isospecific and aspecific sites, and leads to hemi-isotactic polypropylenes.

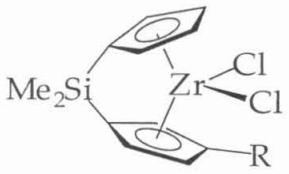

2a R = $CHMe_2$
2b R = CMe_3

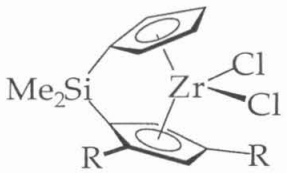

3a R = $CHMe_2$
3b R = CMe_3

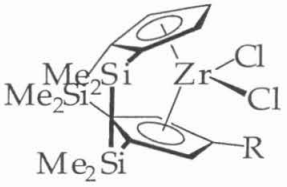

4a R = $CHMe_2$
4b R = CMe_3

Only one enantiomer is shown.

Introduction

Billions of pounds of polyolefins are produced by Ziegler-Natta polymerization catalysts annually over the globe. Traditionally, heterogeneous polymerization catalysts have been the backbone of Ziegler-Natta polymerization. During the past two decades, however, an extraordinary amount of effort has been directed toward homogeneous single-site polymerization catalysts.[1]

Compared to their heterogeneous counterparts, the homogeneous polymerization catalysts can be easily tailored to afford a wide range of polymers with desired molecular weight, molecular weight distribution, co-monomer incorporation content, and both the relative and absolute stereochemistries.[2] The most widely studied single-site catalysts are the Group IV metallocenes.[3,4]

One major reason for the enormous amount of research devoted to metallocene catalysts has been the realization that stereoselectivity in propene polymerization can be controlled to an unprecedented extent by modifying the metal coordination environment. Although the major focus has been to develop isospecific catalysts that can rival the performance of $MgCl_2$-supported Ti catalysts used in commercial production of isotactic polypropene, such a goal remains ambitious at this stage. On the other hand, the well-defined molecular environment allows detailed structural and mechanistic studies, of which, determining the correlation between ligand substitution and polymer stereoregularity has been an important part.

It is now commonly accepted that chiral, stereorigid, *ansa*-C_2-symmetric metallocenes bearing substituents at the 3,4'-positions (also called the β-positions) of the Cp ring can produce polypropylenes with modest to high isotacticities. The rear α-substituents of the Cp ring (i.e., substituents at the 2',5-positions) have only a secondary effect on the stereoselectivity but a major one on regioselectivity and molecular weight control. One major problem associated with these C_2-symmetric metallocenes is that their preparation often involves the generation of the *meso* isomers, which are difficult to separate and often produce low molecular weight atactic polypropylenes with moderate polymerization activity.[3,5]

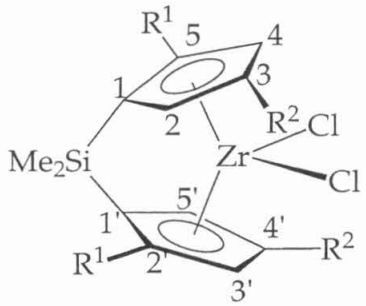

Figure 1. Generic representation of a C_2-symmetric *ansa*-metallocene.

To circumvent the above problem, researchers have investigated the possibility of finding highly isospecific C_1-symmetric metallocenes.[6-8] Along the way, some interesting discoveries have been made.[9-13] By virtue of their diastereotopic coordination sites, these C_1-symmetric metallocenes exhibit a wide range of stereoselectivity. Thus, depending on the size and the positions of the substituents and the linker, polypropylenes ranging from amorphous hemi-isotactic to elastomeric and partially isotactic, also to highly crystallinic and highly isotactic, can be prepared.

Because of the wide variability of ligand environment in C_1-symmetric metallocenes, these catalysts have not only increased the range of properties (e.g. thermoplastic-elastomeric) attainable by homogeneous polymerization of propylene, but have also offered a new stimulus for deeper understanding of the polymerization mechanisms. In particular, they provide more insight at the correlation between polymer microstructures and ligand structures and/or polymerization conditions, as well as the kinetics of insertion versus site epimerization.[3] In addition, they are also perceived as better models for the $MgCl_2/TiCl_4$ heterogeneous catalysts than the C_2-symmetric metallocene systems.[14]

In Chapter Two, we reported the synthesis of isospecific C_1-symmetric zirconocenes **1a** and **1b**. The frontal substituents in **1b** have similar arrangement as those found in C_2-symmetric catalyst systems. However, thanks to the tetramethyldisilylene linker, there is no possibility of forming the aspecific *meso*-like isomer, thus obviating the need to separate the *rac*-isomers from *meso*-isomers.

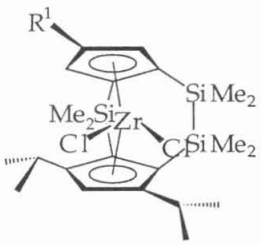

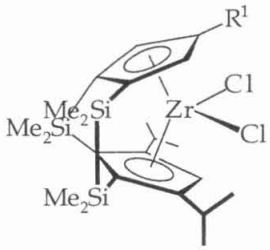

1a $R^1 = H$
1b $R^1 = CHMe_2$

Only one enatiomer is shown.

On the other hand, we are somewhat perplexed by the modestly high isospecificity displayed by **1a** ([*m*]% up to 90% at 0 °C). With few exceptions,[7] C_1-symmetric zirconocenes with similar frontal arrangement as **1a** - that is, with only one sterically demanding frontal substituent on one of the Cp rings - usually produce polypropylenes with much lower isotacticities ([*m*]% ~60–70%).[10,12] We wondered whether the higher stereoselectivity displayed by **1a** is a result of the steric bulk by the frontal isopropyl group, or is unique to the particular ligand structure. We were also interested in learning more about the origin of stereospecificity in **1a**. However, due to the difficulty in ligand synthesis, **1a** could not be prepared in large quantities easily, and was thus not amenable for a detailed mechanistic studies. We therefore decided to synthesize the following metallocenes (**2a/b**, **3a/b** and **4a/b**) as possible model complexes for **1a**.

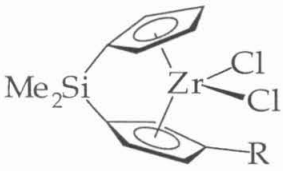

2a $R = CHMe_2$
2b $R = CMe_3$
2c R = Me

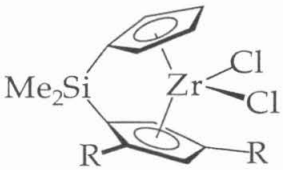

3a $R = CHMe_2$
3b $R = CMe_3$
3c R = Me

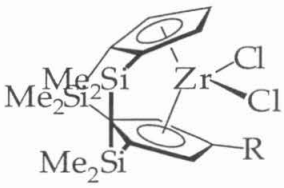

4a $R = CHMe_2$
4b $R = CMe_3$

Only one enantiomer is shown.

Below, we report the synthesis and utilization of **2 – 4** as propylene polymerization catalysts. For catalysts **2a/b** and **3a**, propylene polymerization

with variable monomer concentrations were also performed. The stereoselectivities of these catalyst systems will be compared to that exhibited by **1a** as well to one another.

Results

Synthesis and Characterization of Zirconocenes

The procedures for the preparation of zirconocenes **2 – 4** are outlined in Schemes 1 and 2.

Scheme 1

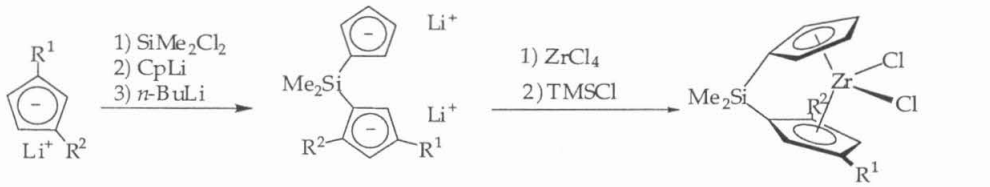

5a R^1 = H, R^2 = $CHMe_2$
5b R^1 = H, R^2 = CMe_3
6a R^1 = R^2 = $CHMe_2$
6b R^1 = R^2 = CMe_3

2a R^1 = H, R^2 = $CHMe_2$
2b R^1 = H, R^2 = CMe_3
3a R^1 = R^2 = $CHMe_2$
3b R^1 = R^2 = CMe_3

Scheme 2

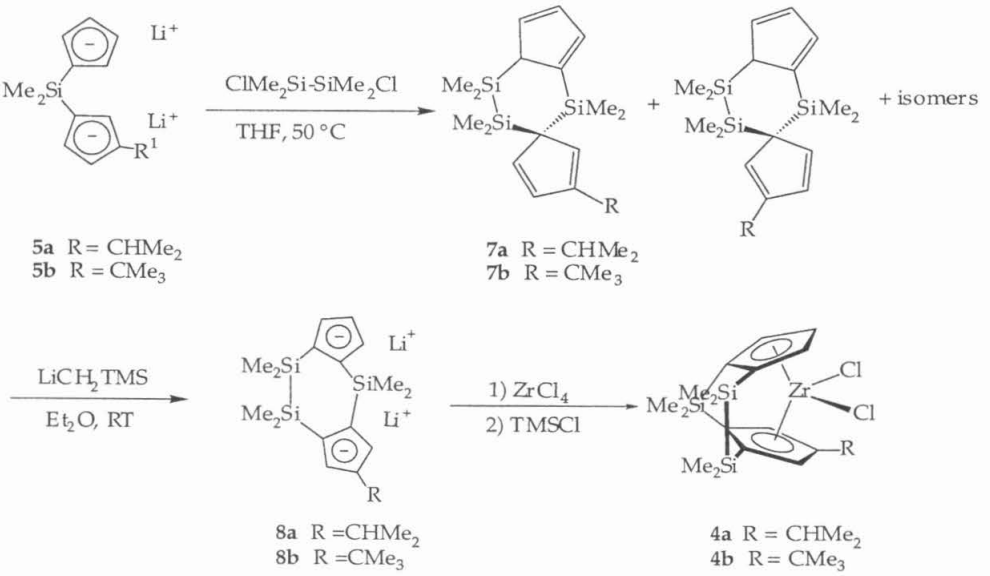

5a R = $CHMe_2$
5b R = CMe_3

7a R = $CHMe_2$
7b R = CMe_3

8a R = $CHMe_2$
8b R = CMe_3

4a R = $CHMe_2$
4b R = CMe_3

Mono- and di-substituted cyclopentadienes were prepared according to literature procedures.[7,15,16] The structure of **7a/b** is tentatively assigned as shown in Scheme 2, based on the structural assignment of similar complexes (e.g., complex **11** in Chapter Two). Dilithio-salts **5**, **6** and **8** can be easily obtained by deprotonation of the corresponding $(CpH)_2$ at room temperature.[17]

The dilithio-salts **5**, **6** and **8** were metallated by $ZrCl_4$ in toluene to afford zirconocenes **2** – **4** respectively in moderate to good yields (38 – 75%). The Cp proton coupling constants, ca 1.5 – 1.8 Hz, are typical of a $^4J_{H\text{-}H}$ in a Cp ring, and are consistent with the proposed regiochemistry for zirconocenes **2** and **4** where the alkyl substituents R are β to the silylene linkers.

Suitable crystals for X-ray diffraction studies have been obtained for **2b** and **3a** from a mixture of toluene and petroleum ether. Unit cells of **2b** contains two molecules per asymmetric cell. The structures for **2b** and **3a** are shown below in Figures 2 and 3. Key bond distances and angles are summarized in Table 1.

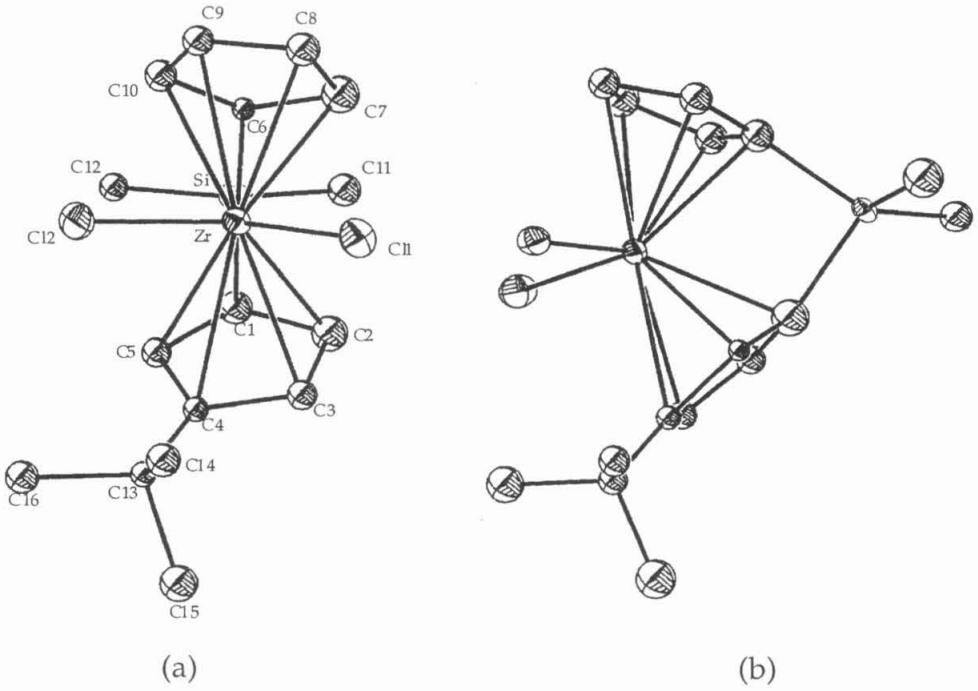

Figure 2. Front (a) and side(b) view of **2b.**

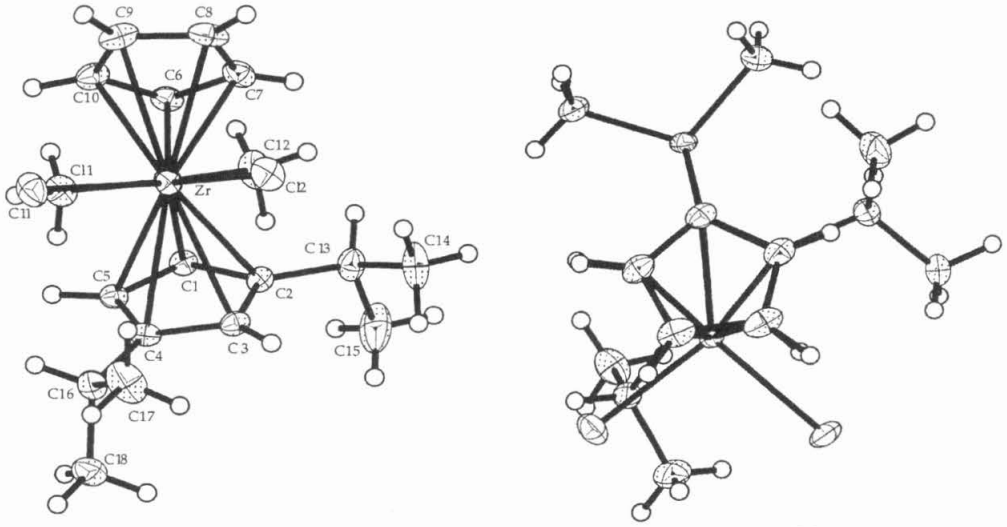

(a) (b)

Figure 3. Front (a) and top(b) view of **3a.**

Table 1. Selected bond distances and angles for compounds **2b** and **3a**.

	Compound **2b**	Compound **3a**
	Bond Distances (Å)	
Zr–Pln(1)	2.2118(10) / 2.2087(10)	2.2054(6)
Zr–Pln(2)	2.1994(10) / 2.1981(10)	2.2072(6)
Zr–Cent(1)	2.220 / 2.217	2.209
Zr–Cent(2)	2.202 / 2.199	2.209
Zr–Cl(1)	2.4411(6) / 2.4294(6)	2.4433(4)
Zr–Cl(2)	2.4413(6) / 2.4365(6)	2.4476(4)
Zr–C(1)	2.462(2) / 2.463(2)	2.4783(13)
Zr–C(2)	2.454(2) / 2.449(2)	2.5074(13)
Zr–C(3)	2.570(2) / 2.562(2)	2.5632(14)
Zr–C(4)	2.629(2) / 2.630(2)	2.5668(14)
Zr–C(5)	2.512(2) /2.510(2)	2.4721(14)
	Bond Angles (°)	
Cl(1)–Zr–Cl(2)	102.44(2) / 98.52(2)	98.383(13)
Cent(1)–Zr–Cent(2)	126.3 / 125.3	125.6
Cp(1)–Zr–Cp(2)	118.51(9) / 118.52(9)	120.34(6)
Cp(1)–Cp(2)	61.49(9) / 61.48(9)	59.68(6)
C(1)–Si–C(6)	94.20(9) / 93.46(9)	93.81(6)
C(11)–Si–C(12)	114.20(13) / 113.55(13)	110.82(8)

One interesting feature common to both complexes is that the side of the wedge where β-alkyl substituents of the Cp ring situate is slightly more open than the other side. For example, in **2b**, the C4–C9 distance is 5.056 Å versus 4.741 Å for C3–C8. Similarly, in **3a**, the C4–C9 distance is 4.984 Å versus 4.827 Å for C3–C8. The planes in which the Cp rings lie intersect at a slightly larger angle in **2b** than in **3a**.

Because no suitable crystals have been obtained for either **4a** or **4b**, we performed molecular mechanics modeling with MacSpartan Pro Software to determine the solid-state geometry. To test the accuracy of the program, we first modeled zirconocene **1a**, and compared the calculated bond distances to those measured by X-ray diffraction studies (see Chapter 2). The numbers are reasonably close to give us confidence in at least the general trend suggested by the molecular mechanics software. For example, the calculated distance between C5–C10 in **1a** is 4.817 Å compared to 4.842 Å determined experimentally, and the distance between C4–C9 is 5.030 Å compared to the experimental value of 5.053 Å. According to the calculation, in both **4a** and **4b**, the C4–C9 distance (5.050 Å and 5.070 Å for **4a** and **4b** respectively) is significantly longer than that between C5–C10 (Figure 4, 4.799 Å and 4.798 Å for **4a** and **4b** respectively). In addition, moving the alkyl group from C10 (in **1a**) to C9 (in **4a** and **4b**) further increases the distances between C4 and C9, and decrease the distance between C5 and C10, although both changes are small (< 0.02 Å).

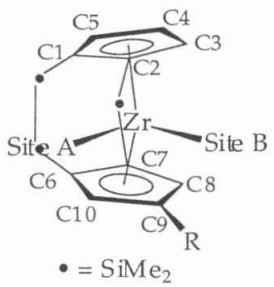

Site A is expected to be narrower than Site B.

Figure 4. MacSpartan Pro software predicted a shorter C5–C10 distance than C4–C9 distance.

Polymerization with Zirconocenes

Zirconocenes **2** – **4** were activated by MAO, and produced polypropylenes with various tacticities in neat propylene at 0 – 5 °C. The polymerization conditions and the pentad distribution for the resulting polypropylenes are reported in Tables 2 and 3 respectively.

Table 2. Propylene polymerization data for **2–4**/MAO.

	cat.	T_p ± 3 °C	Propene Pressure	catalyst loading/ MAO (mg)	% [m]	activity[a]
1	**2a**	5[b]	80 psig[c]	0.73/303	88%	1.43
2	**2b**	5[b]	80 psig[c]	1.40/420	94%	1.02
3	**3a**	5[b]	80 psig[c]	0.7/272	65%	3.06
4	**3b**	5[b]	80 psig[c]	1.17/428	57%	1.64
5	**4a**	5[b]	80 psig[c]	0.92/300	53%	2.66
6	**4b**	5[b]	80 psig[c]	1.13/366	64%	1.02

[a.] activity given in 10^4 gPP/g·Zr·hr. [b.] estimated by the neat propene pressure. [c.] neat propene.

Table 3. Pentad distributions (%) for the polypropene samples produced by **2 – 4**/MAO in neat propene at 0 – 5 °C.

entry	catalyst	[*mmmm*]	[*mmmr*][a]	[*rmmr*][b]	[*mmrr*]	[*rmrr*]+ [*mrmm*][c]	[*rmrm*]	[*rrrr*][d]	[*rrrm*]	[*mrrm*]
1	**2a**	74.6	9.55	-	9.42	1.34	0.21	0.35	0.32	4.25
2	**2b**	83.8	7.08	-	6.41	-	0.10	0.19		2.38
3	**3a**	23.1	17.0	4.92	17.7	12.1	6.66	3.48	6.26	8.82
4	**3b**	17.4	14.5	5.49	15.3	15.3	8.63	5.71	9.01	8.16
5	**4a**	12.8	13.6	5.94	18.4	15.2	7.72	6.22	8.69	11.42
6	**4b**	26.8	16.1	5.59	18.0	9.57	3.97	4.55	5.94	9.49

[a.] overlap with propyl and vinylidene end group resonances, the reported value has the estimated intensity attributable to these chain-end resonances subtracted. [b.] overlap with the isobutyl chain-end group. [c.] may overlap with propyl chain-end group and 1,3-regioerror resonances. [d.] overlap with propyl chain-end resoncances.

The observed stereoselectivity – catalysts **2** showed reasonably high isospecificity, whereas catalysts **3** and **4** produced elastomeric polypropylenes with low percentages of [*mmmm*] and [*m*] – also indicated that at least in these systems, the rear α-substituents of the Cp ring also play an important role in stereochemical control. In addition, in neat propene at 0 – 5 °C, **2a**/MAO and **1a**/MAO produced polypropylenes of comparable tacticities and with similar activities. The stereospecificity displayed by **2** and **3** are reminiscent of the propylene polymerization results obtained by Miya and co-workers, who observed that the [*mmmm*] pentad distribution decreased from 52.4% with [1,1'-$SiMe_2$-(C_5H_4)-(3-Me-C_5H_3)]$ZrCl_2$ (**2c**)/ MAO to 41% with [1,1'-$SiMe_2$-(C_5H_4)-(2,4-Me_2-C_5H_2)]$ZrCl_2$ (**3c**)/ MAO.[7] In addition, it seems that the larger the α-alkyl substitutent of the Cp ring, the larger the decrease in isospecificity. For example, when the α-alkyl group is a methyl substituent, a decrease of 11% in [*mmmm*]% was observed (**3c** versus **2c**).[7] In comparison, decreases of 51% and 66% in [*mmmm*]% respectively were observed when the α-alkyl substituents were isopropyl (**3a** vs. **2a**) and *tert*-butyl (**3b** vs. **2b**).

We were also interested in the correlation between polymer stereoregularity/regioregularity and polymerization conditions, so we performed polymerization at variable monomer concentrations and different temperatures with catalysts **2a**/**b** and **3a**. The results are summarized in Tables 4 – 9. The methyl region of the ^{13}C NMR spectra of polypropylene prepared in these runs are shown in Figures 5 – 7.

An appreciable amount of 1,3-regioerrors was observed for polymers prepared by **2b**/MAO at room temperature. Except at the lowest monomer concentrations (run 16), polymers prepared at 0 – 5 °C contained few or no regioerrors. Run 16 produced polypropylenes containing both the 2,1- and 1,3 regioerrors. In contrast, few regioerrors were detected for polymers made by **2a** at either 0 – 5 °C or at room temperature. Few regioerrors have been detected for polymers made with **3a**/MAO either. Room temperature polymerization results also indicated that **2b** produces higher molecular weight polypropylene than **2a**, as evidenced by the lower percentage of chain-end groups (1:1 propyl : vinylidene) (Figure 8). In addition, comparison of polymerization results at 0 – 5 °C indicates that **3a** produced polymers with the highest molecular weight.

Table 4. Propylene polymerization with **2a**/MAO under various polymerization conditions.

entry	cat.	$T_p \pm 3\,^\circ C$	propene pressure	x propylene	[propylene] (M)	catalyst(mg)/ MAO (mg)	% [*m*]	% chain-end[3,18]
7	**2a**	5[a]	80 psig	1	12.2	0.5 / 102	90	<0.2[b]
8	**2a**	5[a]	40 psig	0.62 ± 0.03	6.8	0.5 / 102	90	<0.3[b]
9	**2a**	5[a]	20 psig	0.40 ± 0.02	4.1	1.0 / 205	90	<0.5[b]
10	**2a**	5[a]	1 atm	0.17 ± 0.01	1.7	1.0 / 203	89	0.5[b]
11	**2a**	22	10 psig	0.18 ± 0.01	1.8	0.5 / 102	81	8[b]

[a.] estimated by the neat propene pressure. [b.] approximately 1:1 propyl to 2-propenyl (vinylidene) ends.

Table 5. Pentad distributions (%) for the polypropylene produced by **2a**/MAO under various polymerization conditions.

entry	catalyst	[*mmmm*]	[*mmmr*][a]	[*rmmr*][b]	[*mmrr*]	[*rmrr*]+ [*mrmm*][c]	[*rmrm*]	[*rrrr*][d]	[*rrrm*]	[*mrrm*]
7	**2a**	74.7	10.5		9.8	<0.5	<0.5	<0.2	<0.3	3.5
8	**2a**	76.3	9.2		9.2	0.7	<0.5	<0.5	<0.5	3.2
9	**2a**	73.9	10.5	<0.5	9.5	0.8	0.4	<0.6	0.5	4.1
10	**2a**	72.9	10.9		9.1	<1	0.8	<0.5	0.5	4.1
11	**2a**	56.9	13.3	1.6	12.4	5.6	2.3		1.5	6.4

[a.] overlap with propyl and vinylidene end group resonances, the reported value has the estimated intensity attributable to these chain-end resonances subtracted. [b.] overlap with the isobutyl chain-end group. [c.] may overlap with propyl chain-end group and 1,3-regioerror resonances. [d.] overlap with propyl chain-end resoncances.

Table 6. Propylene polymerization with **2b**/MAO under various polymerization conditions.

entry	cat.	$T_p \pm 5\,^\circ C$	propene pressure	$x_{propylene}$	[propylene] (M)	catalyst(mg)/ MAO (mg)	% [*m*]	% chain-end[3,18]	% regioerrors[3,18]
12	**2b**	3[a]	75 psig	1	12.2	0.5/120	95	<0.2[b]	-
13	**2b**	3[a]	55 psit	0.76 ± 0.05	8.7	0.5/135	94	<0.3[b]	-
14	**2b**	3[a]	40 psig	0.62 ± 0.03	6.8	0.5/136	95	<0.3[b]	-
15	**2b**	3[a]	20 psig	0.40 ± 0.02	4.1	0.5/156	95	<0.3[b]	-
16	**2b**	3[a]	1 atm	0.17 ± 0.01	1.7	1.0/280	95	<1.0[b]	0.5[c]
17	**2b**	20	65 psig	0.63 ± 0.03	6.8	0.26 /140	94	2.0[b]	0.8[c]
18	**2b**	20	35 psig	0.40 ± 0.02	4.1	0.2/146	93	2.8[b]	0.8[c]
19	**2b**	20	10 psig	0.18 ± 0.01	1.8	0.2/142	87	3.6[b]	0.9[c]

[a]. estimated by the neat propene pressure. [b]. approximately 1:1 propyl to 2-propenyl (vinylidene) ends. [c]. mostly 1,3-regioerros.

Table 7. Pentad distributions (%) for the polypropylene produced by **2b**/MAO under various polymerization conditions.

entry	catalyst	[*mmmm*]	[*mmmr*][a]	[*rmmr*][b]	[*mmrr*]	[*rmrr*]+ [*mrmm*][c]	[*rmrm*]	[*rrrr*][d]	[*rrrm*]	[*mrrm*]
12	**2b**	86.0	5.8		5.4	0.7				2.1
13	**2b**	86.4	4.9	<0.2	4.7	0.7	<0.5			2.0
14	**2b**	86.3	5.2	<0.5	4.8	0.7	<0.5			2.2
15	**2b**	85.2	5.8	<0.5	5.2	0.7	0.5			2.1
16	**2b**	85.3	5.9	<0.2	5.1	1.0	<0.5			2.0
17	**2b**	83.3	6.5	<0.5	5.7	1.2	0.5			2.8
18	**2b**	82.6	6.7	<0.5	5.6	1.6	0.5			2.8
19	**2b**	78.7	7.7	<0.5	6.4	3.1	0.4			3.7

[a]. overlap with propyl and vinylidene end group resonances, the reported value has the estimated intensity attributable to these chain-end resonances subtracted. [b]. overlap with the isobutyl chain-end group. [c]. may overlap with propyl chain-end group and 1,3-regioerror resonances. [d]. overlap with propyl chain-end resoncances.

Table 8. Propylene polymerization with **3a**/MAO under various polymerization conditions.

entry	cat.	$T_p \pm 3\,°C$	propene pressure	x propylene	[propylene] (M)	catalyst(mg)/ MAO (mg)	% [*m*]	% chain-end[3,18]
3	**3a**	5[a]	80 psig	1	12.2	0.7/272	65	-
20	**3a**	5[a]	40 psig	0.62 ± 0.03	6.8	0.5/200	62	-
21	**3a**	5[a]	20 psig	0.40 ± 0.02	4.1	0.5/200	61	-
22	**3a**	5[a]	1 atm	0.17 ± 0.01	1.7	0.5/200	57	-

[a.] estimated by the neat propene pressure. [b.] approximately 1:1 propyl to 2-propenyl (vinylidene) ends.

Table 9. Pentad distributions (%) for the polypropylene produced by **3a**/MAO under various polymerization conditions.

entry	catalyst	[*mmmm*]	[*mmmr*][a]	[*rmmr*][b]	[*mmrr*]	[*rmrr*]+ [*mrmm*][c]	[*rmrm*]	[*rrrr*][d]	[*rrrm*]	[*mrrm*]
3	**3a**	24.8	16.8	5.7	18.8	11.4	6.0	3.2	5.7	7.7
20	**3a**	21.4	18.5	4.8	19.0	10.7	5.7	3.6	6.5	9.8
21	**3a**	18.6	18.0	5.3	18.7	13.2	6.3	3.8	6.2	9.9
22	**3a**	16.8	17.6	3.9	18.7	11.8	6.1	4.4	7.2	13.4

[a.] overlap with propyl and vinylidene end group resonances, the reported value has the estimated intensity attributable to these chain-end resonances subtracted. [b.] overlap with the isobutyl chain-end group [c.] may overlap with propyl chain-end group and 1,3-regioerror resonances. [d.] overlap with propyl chain-end resoncances.

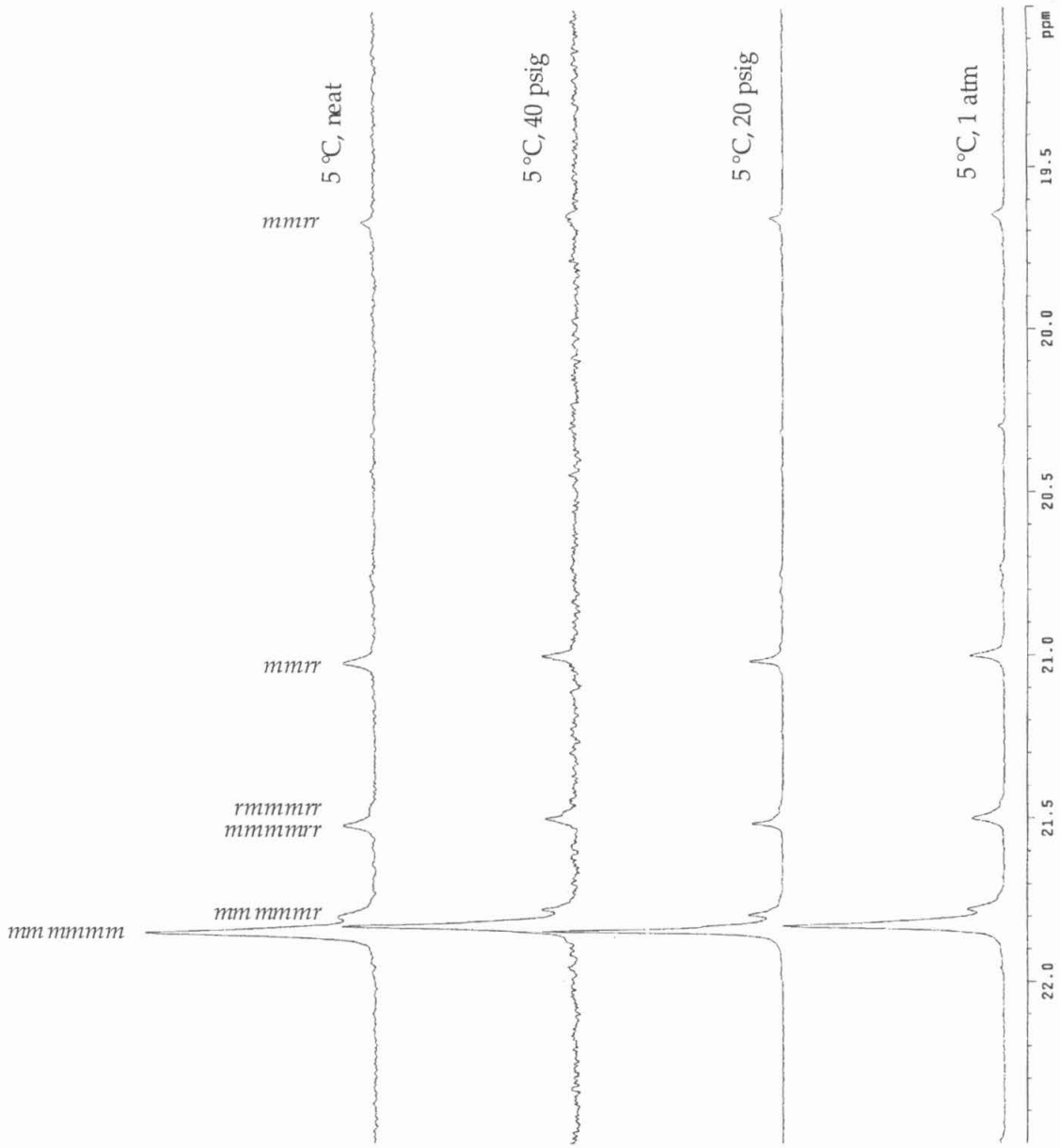

Figure 5. The methyl region of the ^{13}C NMR spectra, showing the pentad distributions of the polypropenes prepared by **2a**/MAO under various propene pressure at 0 – 5 °C.

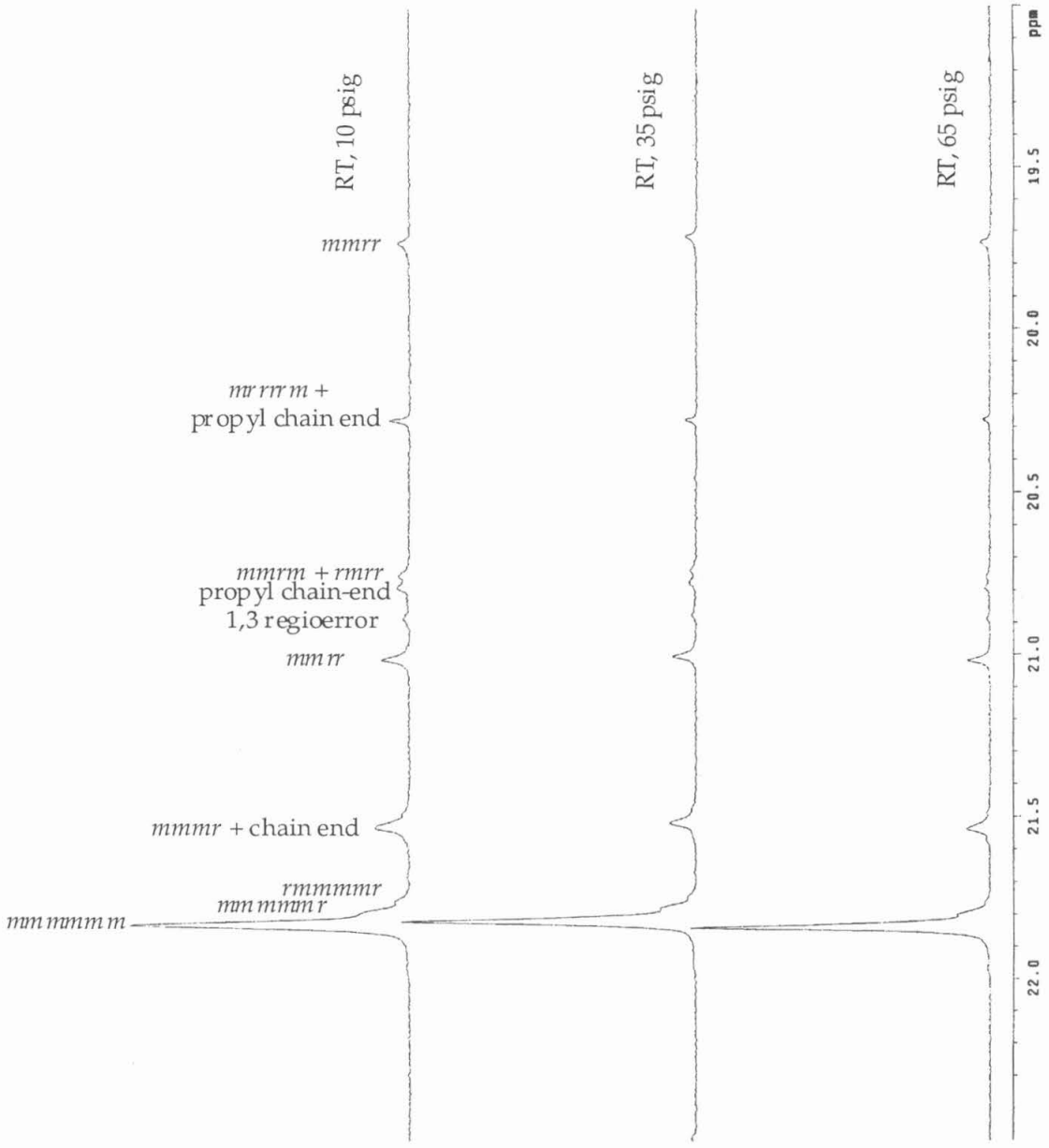

Figure 6. The methyl region of the ^{13}C NMR spectra, showing the pentad distribution of the polypropenes prepared by **2b**/MAO under various propene pressure at room temperature.

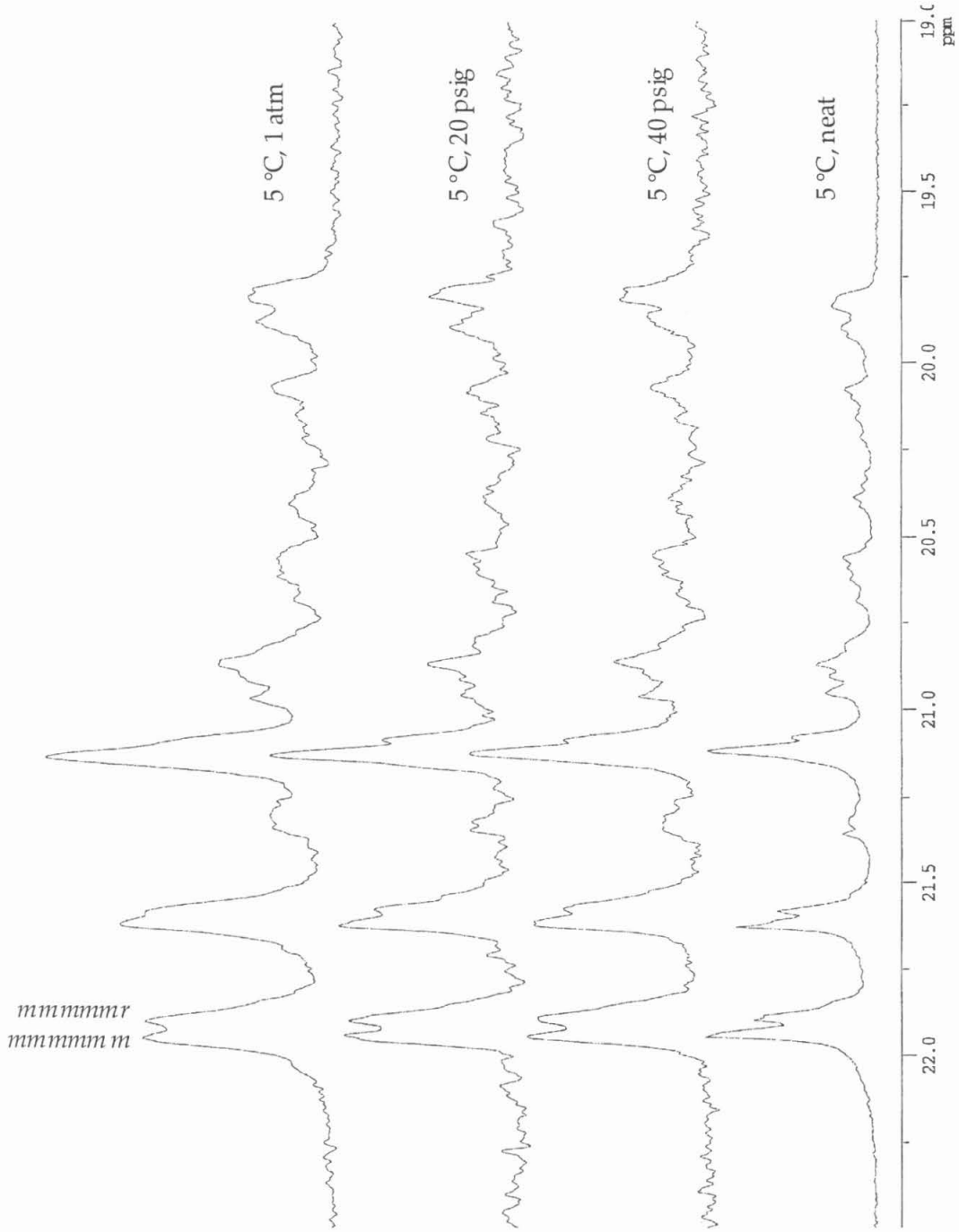

Figure 7. The methyl region of the ^{13}C NMR spectra, showing the pentad distributions of the polypropenes prepared by **3a**/MAO under various propene pressure at 0 – 5 °C.

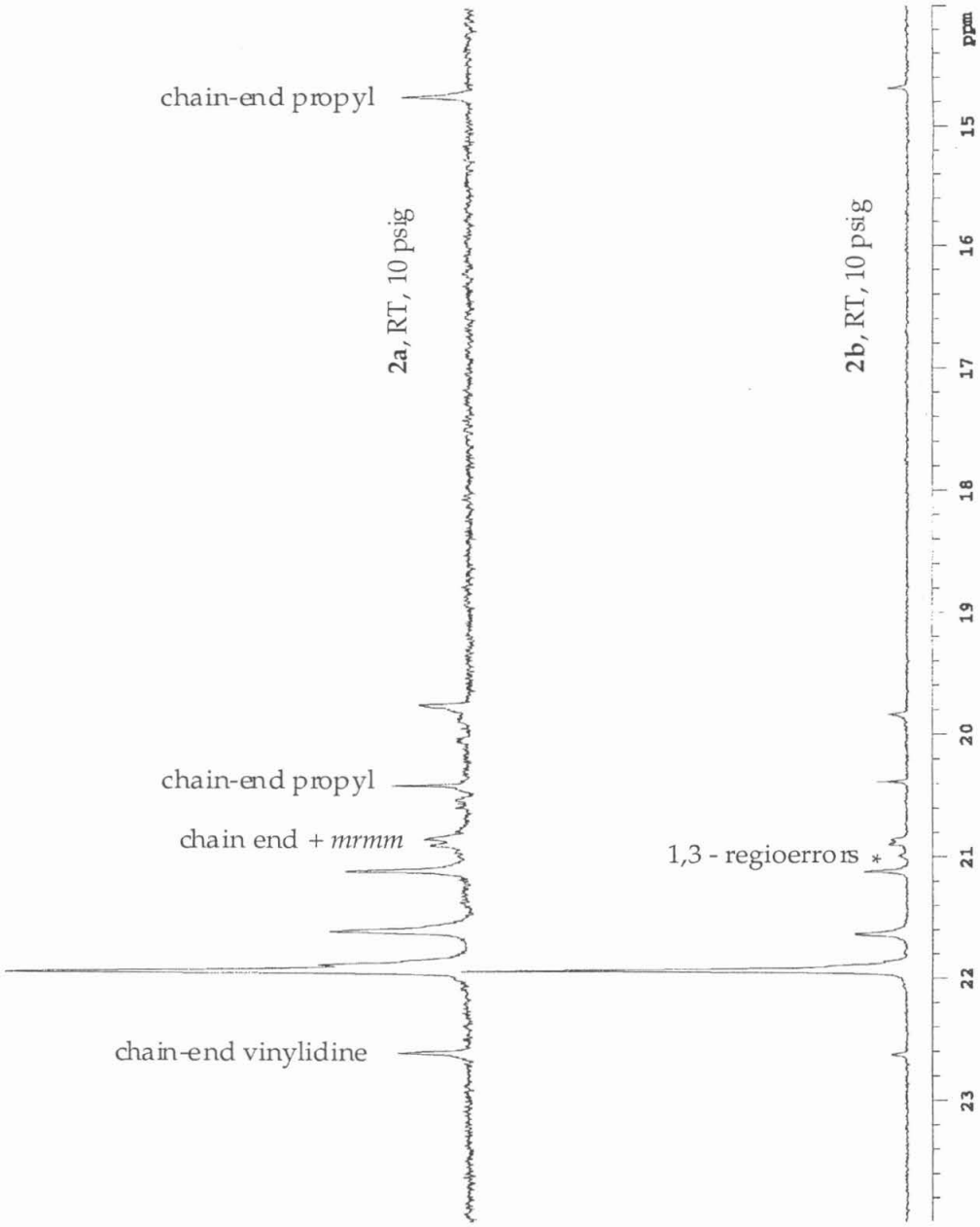

Figure 8. The methyl region of the ^{13}C NMR spectra of polypropene prepared in runs 11 and 20. Under the same polymerization condition, **2b** produced polypropene with both higher M_W (lower intensities of chain-end resonances) and higher isotacticities than those prepared by **2a**. But polymers prepared by **2a** contain fewer regioerrors.

Because of the presence of regioerrors and chain-end groups and/or overlapping of pentad resonances, the pentad distributions reported in the tables have a ± 5% error range. On the other hand, the high-field ^{13}C NMR (125 MHz) allows the resolution of methyl resonances beyond the pentad level. In particular, the *mmmm* pentad can now be resolved into *mmmmmm* and *mmmmmr* heptads. An increased ratio of *mmmmmr* to *mmmmmm* is a good indication of decreased isospecificity of the catalyst systems. A cursory inspection of the *mmmmmm* and *mmmmmr* heptad resonances in Figures 5 and 6 indicated that for catalysts **2a** and **2b**, the isospecificity of the catalyst systems showed little if any change with changing monomer concentrations. In contrast, a modest but noticeable decrease in isotacticity was observed for polypropylene made with **3a**/MAO at lower monomer concentrations, based on the increased intensity of *mmmmmr* resonance relative to *mmmmmm* resonance (Figure 7). For **2a**/**b**, the isospecificity also decreased at higher polymerization temperatures (compare entries 10/11, 14/17, 15/18 and 16/19). However, the change is not as dramatic for **2b** as for **2a** (Tables 4 and 6).

Studies on Cationic Zirconium Complexes

When [1,1'-$SiMe_2$-(C_5H_4)-(3-CMe_3-C_5H_3)]$ZrMe_2$ was treated with 1 equivalent of $B(C_6F_5)_3$, two species were formed in 4.5 : 1 ratio. The two species could either be the two pairs of diastereomers (Scheme 3), or more likely, because tiny droplets of red oil formed in the reaction, the minor species is some form of aggregates of the cation.[19] Irradiation of the *tert*-butyl resonance of the major species induces significant NOE enhancement of the Zr–Me resonance, implying that the diastereomer formed was the one in which the zirconium methyl group resided on the same side of the wedge as the *tert*-butyl group of the Cp ring (**14b**). Irradiation of the *tert*-butyl resonance of one species also resulted in magnetization transfer to the *tert*-butyl resonance of the other complex.

Scheme 3

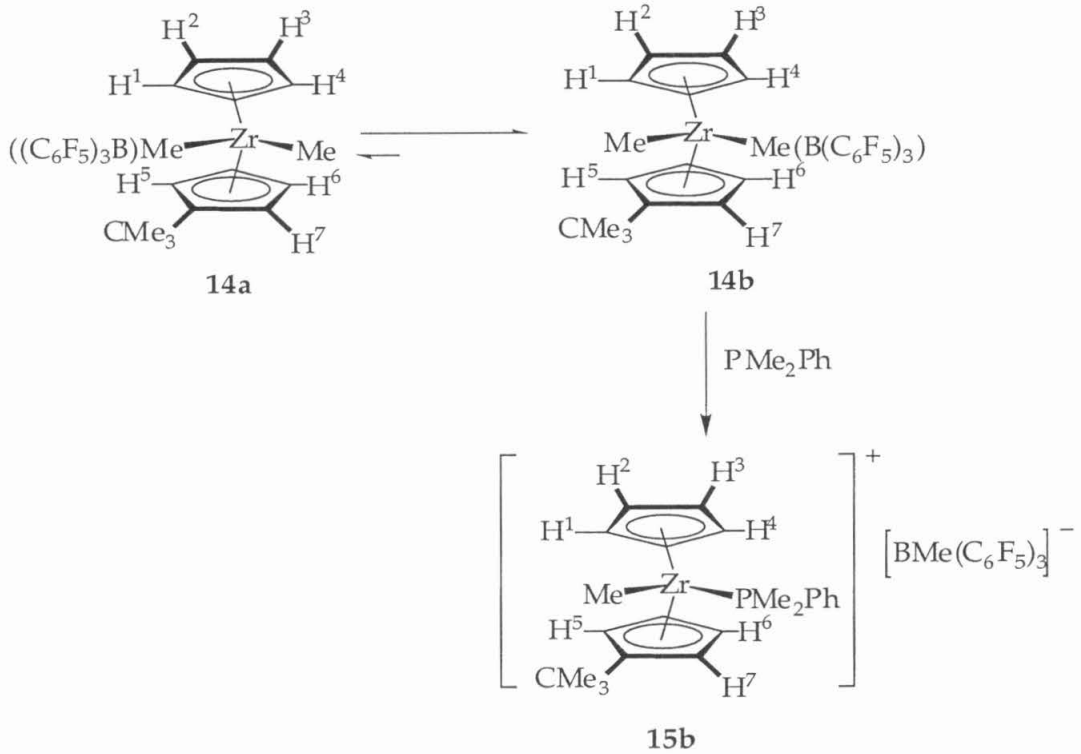

The enantiomers are not shown.
Bridging atoms omitted for clarity.

When dimethylphenylphosphine (PMe_2Ph) was added to the above mixture, one new set of resonances appeared (Scheme 3). NOE studies indicated that there was considerable through-space interactions between the Zr–Me and the *tert*-butyl group of the Cp ring. Thus, **15b** was the likely structure for the new species. When less than one equivalent of the phosphine was added, the diastereotopic splitting of the methyl groups of the coordinated phosphine could be observed. But such splitting disappeared when even a slight excess of phosphine was added. For example, when 5 – 8% excess phosphine was added to the mixture, only one doublet could be observed for the [P–CH_3] signal. That is, resonances for free and coordinated phosphines have coalesced. Furthermore, as more PMe_2Ph was added, the chemical shift of the coordinated phosphine starts to shift toward those of the free phosphine. NOE studies indicated that the P–CH_3 groups were on average of equal distances from H^3 and H^7 or H^4 and H^6 even when less than one equivalent of phosphine was added.

There were also NOE effects between the phenyl protons and the protons on both Cp rings.

Similarly, $\{[1,1'\text{-}SiMe_2\text{-}(C_5H_4)\text{-}(2,4\text{-}(CHMe_2)_2\text{-}C_5H_2)]Zr(Me)(PMe_2Ph)\}^+$ $[MeB(C_6F_5)_3]^-$ (**17**) was generated *in-situ* and studied using CycloNOE technique. Originally, two diastereomers of $[1,1'\text{-}SiMe_2\text{-}(C_5H_4)\text{-}(2,4\text{-}(CHMe_2)_2\text{-}C_5H_2)]Zr(Me)(MeB(C_6F_5)_3)$ were generated in ~10 : 1 ratio with **16b** being the major one (Scheme 4).

Scheme 4

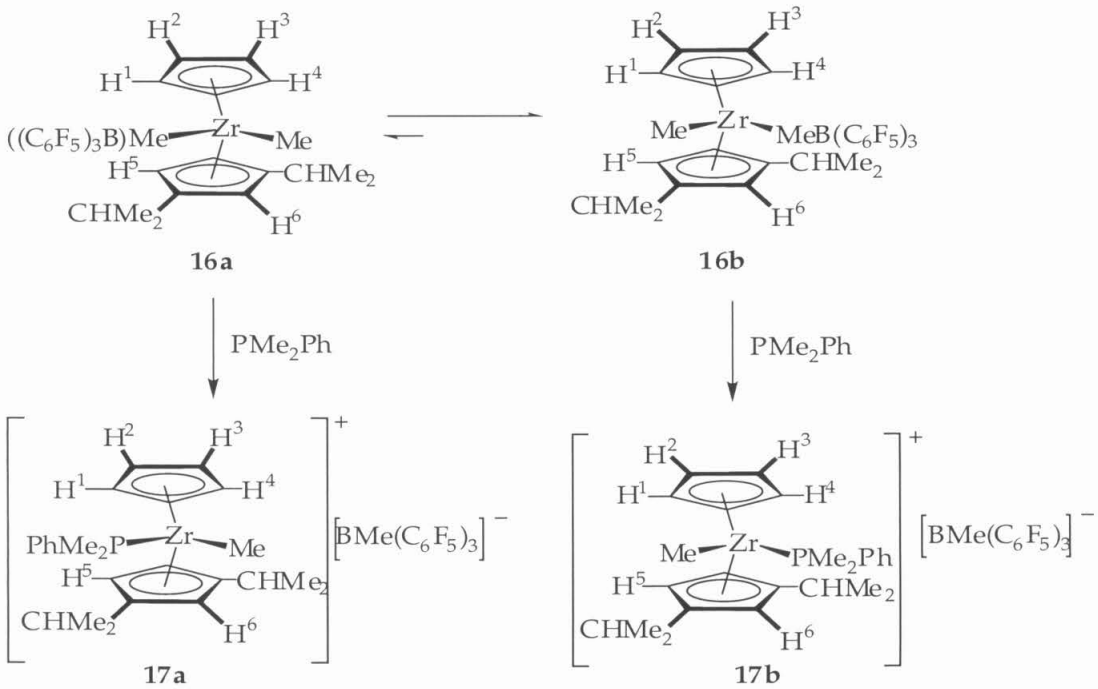

The enantiomers are not shown.
Bridging atoms omitted for clarity.

Upon addition of a slight excess of PMe_2Ph to the mixture of **16**, two complexes (presumably the two pairs of diastereomers) were formed, in ~ 10:1 ratio. In the major isomer, the zirconium methyl and the front β-isopropyl group show considerable NOE effect, indicating that the methyl resides on the same side as the β-isopropyl group of the Cp ring and that **17b** is the major isomer. Two doublets can be observed for the [P–CH_3] resonances. In contrast, only one doublet could be detected for [P–CH_3] in the minor isomer. In addition,

even in the presence of 1 equivalent of free phosphine, **17b** retained the diastereotopic splitting of the phosphine methyl resonances, although significant line broadening did occur under these conditions.

For the [1,1'-$SiMe_2$-2,2'-($SiMe_2$–$SiMe_2$)-(C_5H_3)-(4-($CHMe_2$)-C_5H_2)] ligand system, methyl abstraction by $B(C_6F_5)_3$ resulted in formation of **18b** : **18a** in ~ 2:1 ratio (Scheme 5). Irradiation at one diastereomer's resonances result in magnetization transfer to the corresponding resonances of the other diastereomer.

Scheme 5

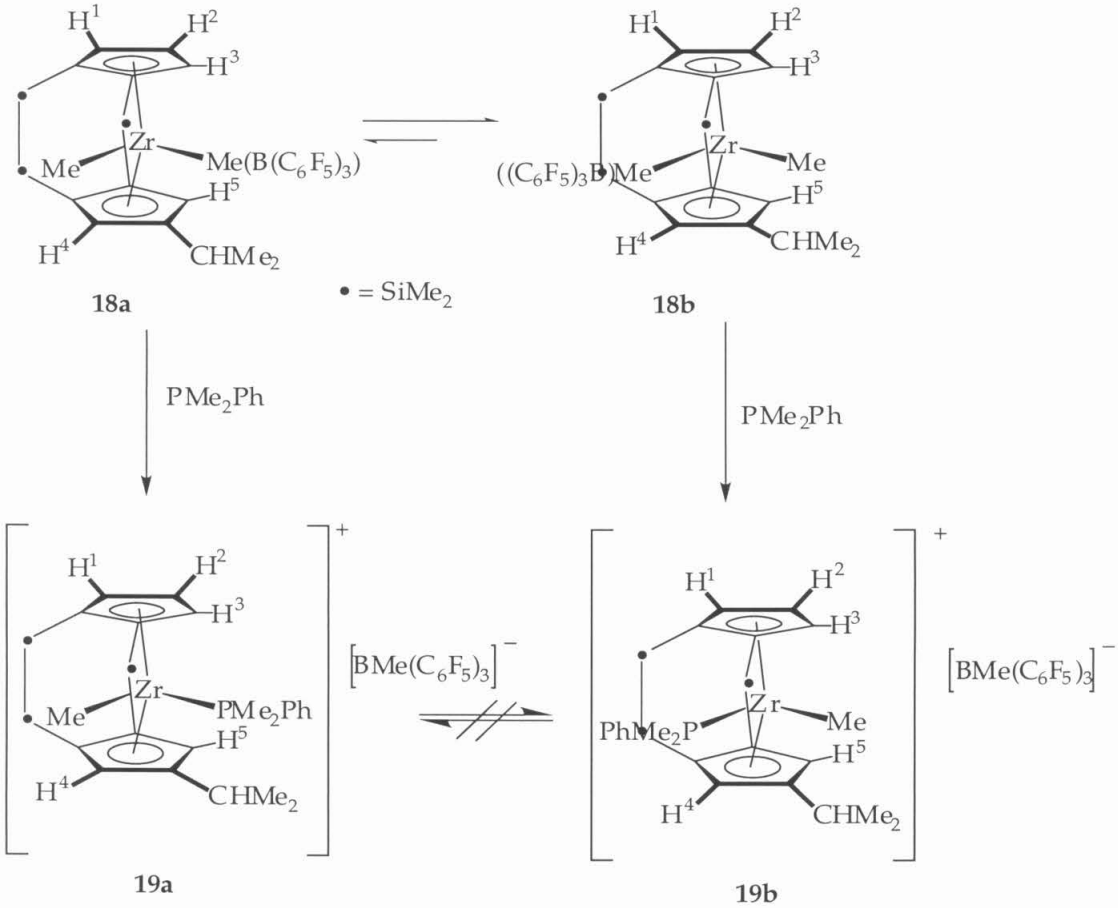

The enantiomers are not shown.

Addition of even a slight excess of PMe_2Ph to the above mixture did not lead to the complete disappearance of **18a** and **18b**. For example, ~10% of **18a/b** remained unreacted after 40 minutes at room temperature, even though under the condition, free phosphine could be observed. At least four new products

were formed, and the two major ones (accounts for 80–90% of the new products) were identified as **19b** and **19a**. Irradiation at **19b**'s isopropyl methine peak resulted in no magnetization transfer to the methine peak of **19a** or **18b**. For both **19a** and **19b**, two sets of doublets could be detected for P–CH_3 resonances even in the presence of large excess phosphine, but the resonances for the minor isomer seemed to have broadened more than those of the major isomer.

Discussion

Deprotonation of 7

The ready formation of **8a/b** is in stark contrast to the harsh reaction conditions required to yield **10** (eq 1, also see Chapter 2). In **7**, silyl group migrates[20] from the sp^3-carbon to an sp^2-carbon γ to the R substituent (eq 2.), which has considerably less steric repulsion than when it migrates to the sp^2-carbon β-to the R substituent as in **9**. The reduced steric effects lowers the barrier for silyl migration, and results in mild deprotonation conditions to produce **8**.

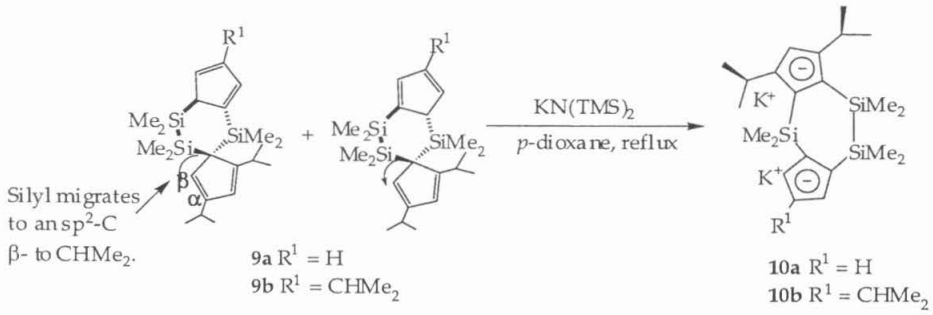

(1)

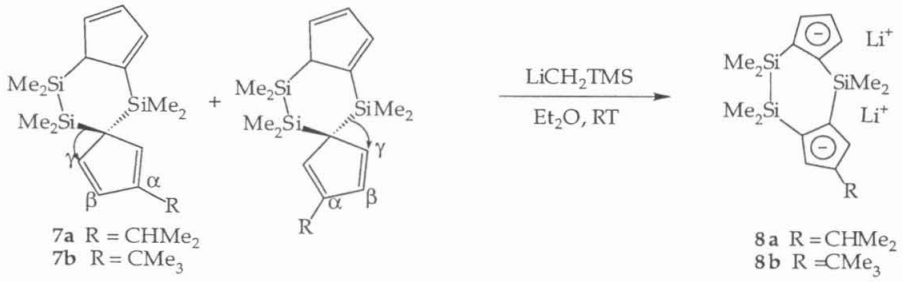

(2)

Structural Features of Zirconocenes

X-ray structures of **2a** and **3b** revealed that C4–C9 distance is longer than C5–C10. This is probably caused by the steric repulsion between the chlorine

atom and the alkyl substituents, and should therefore decrease with decreasing steric bulk of the alkyl substituents. Experimental evidence indeed supports such a conclusion: the difference decreases from 0.31 Å in **2b** where the alkyl substituent is a *tert*-butyl group to 0.16 Å in **3a** where the alkyl substituent is an isopropyl group.

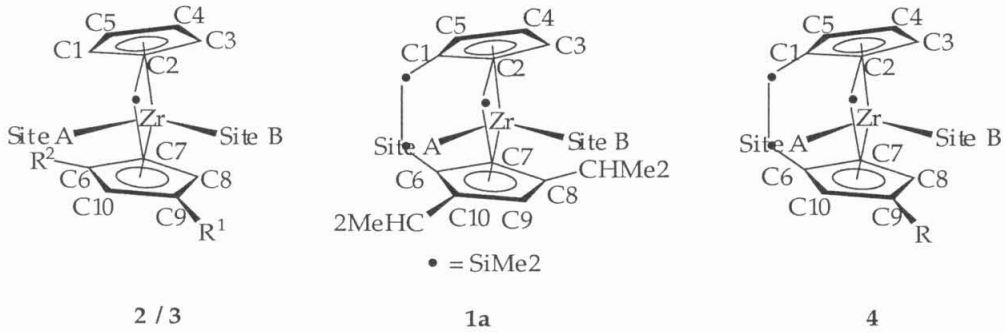

Site A is narrower than Site B.

Figure 9. Site A is sterically more crowded than Site B. This results from steric interaction between the β-alkyl and Zr–*Cl* in **2** and **3**, and from the stereorigidity imposed by the tetramethyldisilylene linker in **1a** and **4**.

In Chapter Two, we described the X-ray structure of **1a**, in which one side of the wedge is also narrower than the other, but in this case, it is the side of the wedge where the frontal isopropyl group of the Cp ring (β-to the dimethylsilylene linker, and α-to the tetramethyldisilylene linker) resides that is narrower (i.e., C5–C10 distance is shorter than C4–C9). Molecular modeling by MacSpartan Pro also predicted that in **4a** and **4b**, the side of the wedge where the tetramethyldisilylene resides is narrower than the side where the β-alkyl substituent of the Cp ring sits (C4–C9 distance is longer than C5–C10). Thus, it appears that unlike in **2b** and **3a** where the difference is caused by chlorine-alkyl interactions, the difference in **1a** and **4** is most likely determined by the stereorigidity imposed by the tetramethyldisilylene linker.

Stereochemical Control in Zirconocenes 1 – 4

In catalysts **1** – **4** (Figure 10), when the polymer resides at Site B, and the monomer coordinates at Site A, the subsequent insertion is enantioselective. On the other hand, insertion is essentially non-enantioselective when the polymer resides at Site A. Thus if insertion occurs alternatively from the two sites with no site epimerization (chain swinging from one site to the other without insertion),

a hemi-isotactic polymer will be produced ([*mmmm*]% ~ 12%). Higher isotacticity of the resulting polymer has often been attributed to the frequent site epimerization to the stereoselective site.[8,10-13,21,22]

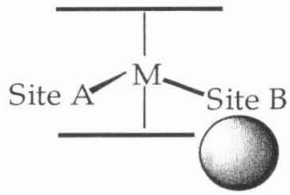

Figure 10. Schematic drawing of the front wedge of zirconocenes **1–4**.

To provide experimental evidence for this hypothesis, variance of stereoregularity as a function of monomer concentration has been investigated by several groups.[10–13] The reasoning has been that if at high monomer concentration, the rate of site epimerization is on the same order or slower than that of monomer insertion, then polymer stereoregularity will increase (or decrease) as the rate of uni-molecular site epimerization exceeds that of binuclear monomer insertion at low monomer concentrations, and insertion occurs increasingly frequently from the isospecific (or aspecific) site. Results of such studies have, however, been as variable as the catalyst structures. For example, Rieger and co-workers have found that at constant polymerization temperature, the stereoregularities of polypropylenes made with *rac*-C_2H_3-1-(*R*,*S*)Ph-(Cp)-((*R*,*S*)-1-Ind)$ZrCl_2$ (**11a**) and *rac*-C_2H_3-1-(*S*,*R*)Ph-(Cp)-((*R*,*S*)-1-Ind)$ZrCl_2$ (**11b**) showed no dependence on propylene concentrations.[10] On the other hand, Collins and co-workers found that as monomer concentration decreased, the isotacticities of polypropylene samples prepared by *rac*-(1,1'-CMe_2-Cp-Ind)$TiCl_2$ (**12a**) decreased while those of polypropeylenes prepared by either *rac*-(1,1'-CMe_2-Cp-Ind)$HfCl_2$ (**12b**) or *rac*-(1,1'-$SiMe_2$-Cp-Ind)$HfCl_2$ (**12c**) increased.[11]

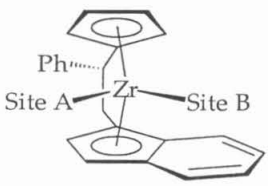

11a

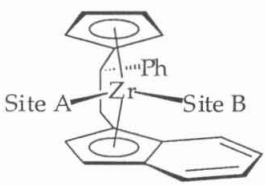

11b

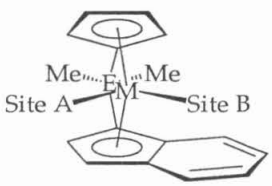

12a M = Ti, E = C
12b M = Hf, E = C
12c M = Hf, E = Si

In the present study, we noticed that the stereoselectivity of **2a/b**, which produce polypropene samples with modestly high isotacticities, showed little dependence on monomer concentrations. On the other hand, the less stereoselective **3a** produced polypropylene of decreasing stereoregularity with decreasing monomer concentrations. The decreased isotacticity of the resulting polypropylene at low monomer concentrations is unlikely a result of chain-epimerization, because under similar polymerization conditions, **3a** produced higher molecular weight polymers than either **2a** or **2b**, suggesting that β-H elimination, the first step in chain-epimerization, is less likely to occur in **3a** than in **2a** or **2b**. We also noticed that of the three types of catalysts studied, **4a/4b** are the least stereoselective. The following sections will try to rationalize and to reconcile these experimental findings.

Implication of NOE Studies with Cationic Zirconocene Complexes. The diastereoselectivities observed for the methyl abstraction reactions and the coordination of phosophine to the zirconium center (Schemes 3 – 5) may simply result from the fact that both the $[Me(B(C_6F_5)_3)]^-$ anion and the PMe_2Ph molecule are bulkier than the (zirconium) methyl group, and prefer to sit on the less crowded metallocene wedge. The much lower diastereoselectivity observed for **18a** (**19a**) and **18b** (**19b**) is probably a result of the unfavorable van der Waals repulsion between the tetramethyldisilylene linker and the borate anion (or PMe_2Ph) (Figure 11).

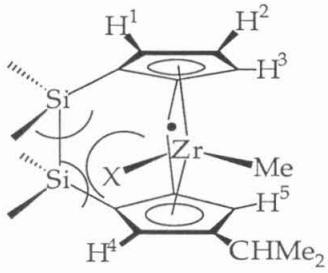

X = $Me(B(C_6F_5)_3)$
or PMe_2Ph

Figure 11. Van der Waals repulsion between the tetramethyldisilylene linker and the methylborate anion or the phosphine resulted in lower diastereoselectivity in the formation of **18** and **19**.

The exchange signals in the CycloNOE spectra for these methylborates, which interconnect the ^{1}H-NMR signals of one diastereomer with the corresponding signals of the other diastereomer, indicate a fast-exchange on the NMR time-scale. This implies that equilibration between the two diastereomers is fast on the NMR-time scale. More important to our discussion in the next section concerns the rates of phosphine exchange in different catalyst systems.

In the dimethylphenylphosphine adduct **15b**, no diastereotopic splitting could be observed for P–CH_3 when greater than one equivalent of phosphine was added to the mixture of **14a/b**, and signals for free and coordinated phosphines coalesce. This is consistent with a rapid associative degenerate exchange between the free and bound phosphine molecules.

In **17b**, no loss of diastereotopic splitting of bound P–CH_3 even in the presence of one equivalent of free phosphine implies that associative phosphine exchange is slower in **17b** than in **15b**. In contrast, the loss of diastereotopic splitting of P–CH_3 signals in **17a** (and the broadness of all other signals) in the presence of even a small amount of free phosphine (<10%) suggest that phosphine exchange is facile in **17a**.

By similar reasoning, the exchange between bound and free phosphine is slow in **19a** and **19b**. Furthermore, the different extent of signal broadening between **19a** and **19b** indicate that phosphine exchange is faster in **19a** than in **19b**. Lack of exchange signal between the isopropyl methine resonance of **19a** and **19b** in the CycloNOE spectra implies that interconversion between **19a** and **19b** is slow on the NMR time-scale. If the extent of line-broadening is attributed solely to phosphine exchange, then at the same free phosphine concentration, it is estimated that the rates of exchange decrease in the order **19b** < **17b** < **19a** << **17a** ~ **15b**. The trend seems to suggest that addition of α-substituents significantly slows down the exchange process. This is probably due to the steric obstacle imposed by the the α-substituent on the approach of the incoming nucleophile. Brintzinger and co-workers have observed a similar trend.[19]

Because of the dependence of line-broadening on free phosphine concentrations, an associative pathway is implicated for the exchange of bound and free phosphine (Scheme 6). An associative mechanism is also the most likely for the displacement of methylborate anions by phosphines.[19] The process most likely involves a five-coordinated intermediate (**A**).

Scheme 6

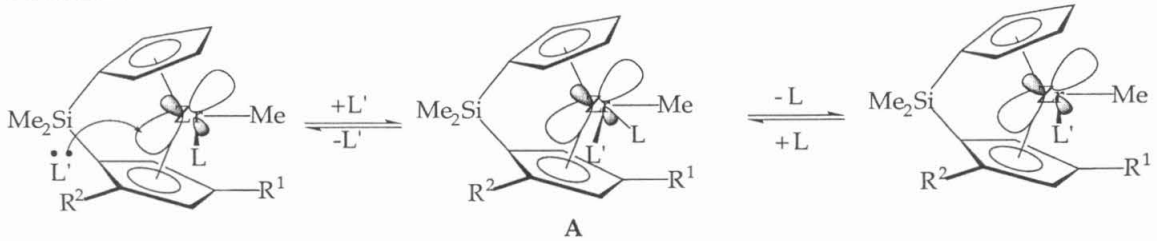

L, L' = PMe_2Ph or $MeB(C_6F_5)_3$ or olefin

In homogenous Zielger-Natta polymerization, olefin coordination presumably occurs via displacement of a bound counterion or a solvent molecule or an agostic C–H bond by the monomer. This process presumably involves an intermediate of similar structural features to **A**. Thus, the trend obtained in the present study should imply that the ease of formation of the following olefin adducts should decrease in the order **i** ~ **ii** ~ **iv** >> **vi** > **iii** > **v** (Chart 1).

Chart 1

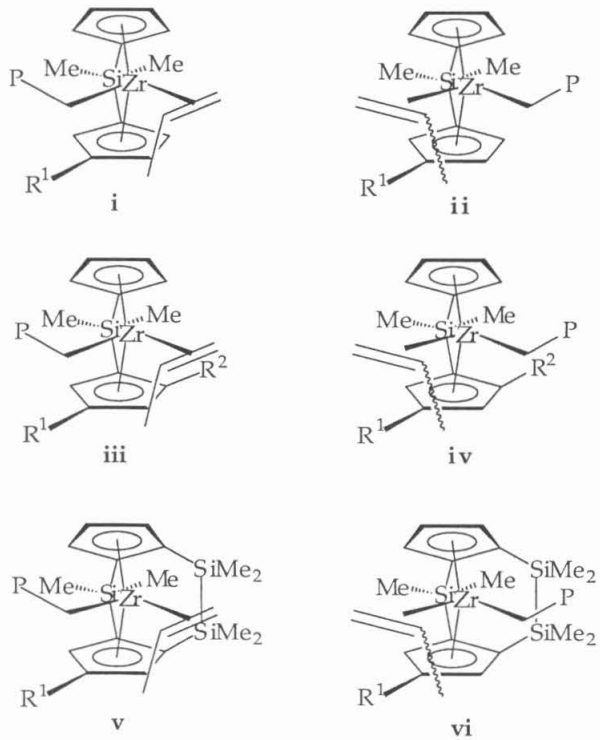

R^1 = $CHMe_2$ or CMe_3
R^2 = H, $CHMe_2$ or CMe_3
Only one enantiomer is shown.

However, the reactivity trend measured in the present study should have an implication not only on olefin coordination, but also on the rates of an *associative* site epimerization, which may involve an intermediate such as **C** (Scheme 7).

Scheme 7

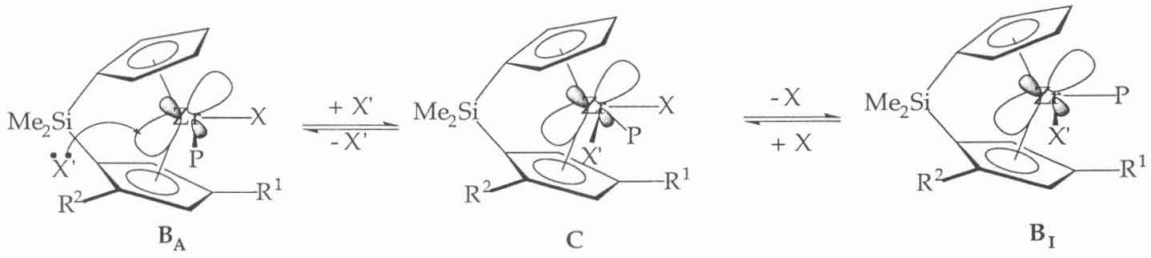

X = anions or solvent or C–H bond of an agostic conformation
X' = solvent molecules or anions
P = polymer chain

If we assume that the phosphine exchange rates reflect the barrier for the formation of the five-coordinate intermediate and that the diastereomer $\mathbf{B_A}$ is slightly lower in energy than $\mathbf{B_I}$ (which may not be true, *vide infra*), then an energy profile for site epimerization can be constructed for the reaction shown in Scheme 7 (using catalysts **3** as an example, Figure 12). Thus the increased kinetic barrier imposed by an α-substituent on the approach of a nucleophile in forming the five-coordinate intermediate not only results in an increase in the activation barrier in forming the olefin-adduct, but also increases the barrier for site-epimerization. It therefore follows that the barrier for site-epimerization decreases in the order **4** > **3** >> **2**. In addition, because *tert*-butyl group is larger than an isopropyl group, we would expect that the barrier for site epimerization is larger in **3b** than in **3a**.

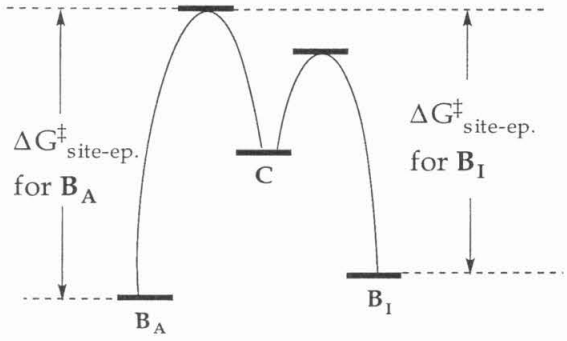

Figure 12. Energy profile for the site-epimerization reaction shown in Scheme 7.

Origin of Different Stereoselectivities in 2 – 4. The chain propagation step in these C_1-symmetric catalysts can be represented, in the simplest form, by the reactions shown in Scheme 8. The probability of the occurrence of site-epimerization will depend on $\Delta\Delta G^{\ddagger}_{p\text{-site-ep.}}$, the difference between the activation energy for site epimerization, $\Delta G^{\ddagger}_{\text{site-ep.}}$, and the activation energy for enchainment, $\Delta G^{\ddagger}_{p}$ (Figure 13).

Scheme 8

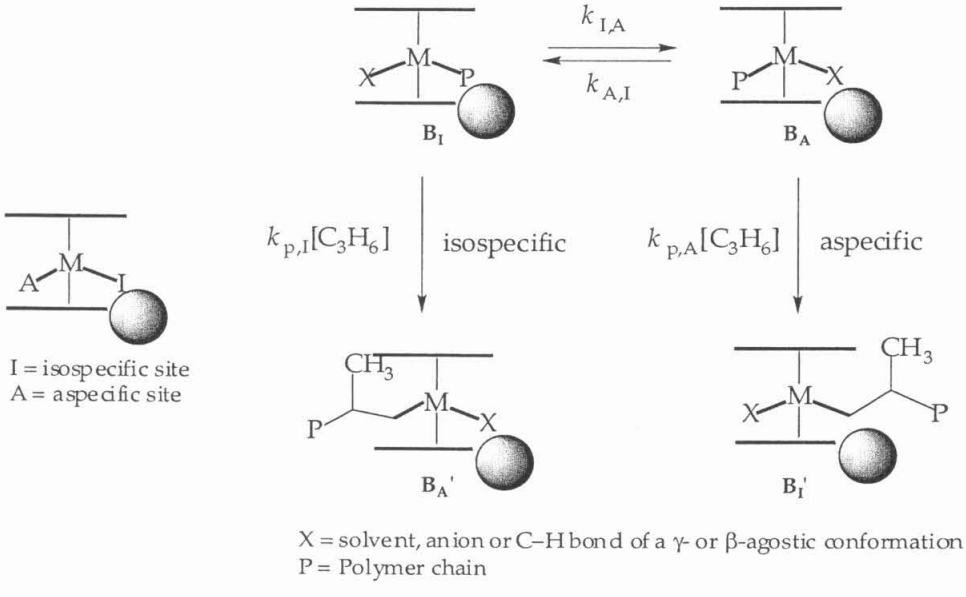

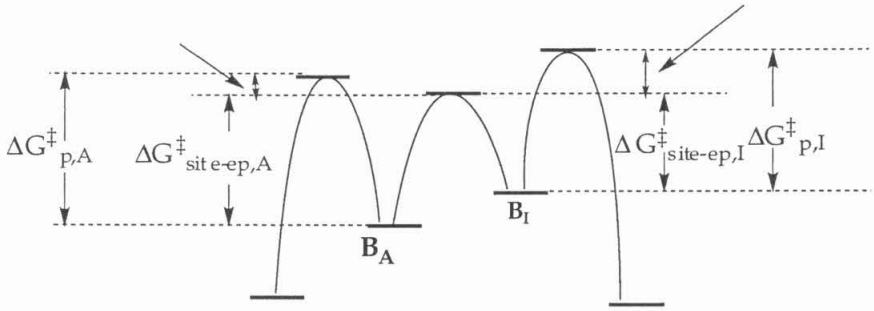

Figure 13. Energy diagram for a simple representation of chain propagation process that shows only the overall barrier for the site epimerization and enchainment step.

Factors determining the magnitude of $\Delta G^{\ddagger}_{site\text{-}ep.}$ have been discussed in the section above, and $\Delta G^{\ddagger}_{p}$ will depend on the aptitude of both olefin coordination and olefin insertion (showing only propagation from the isospecific site, Scheme 9). An expanded energy diagram for the chain propagation step is shown in Figure 14.

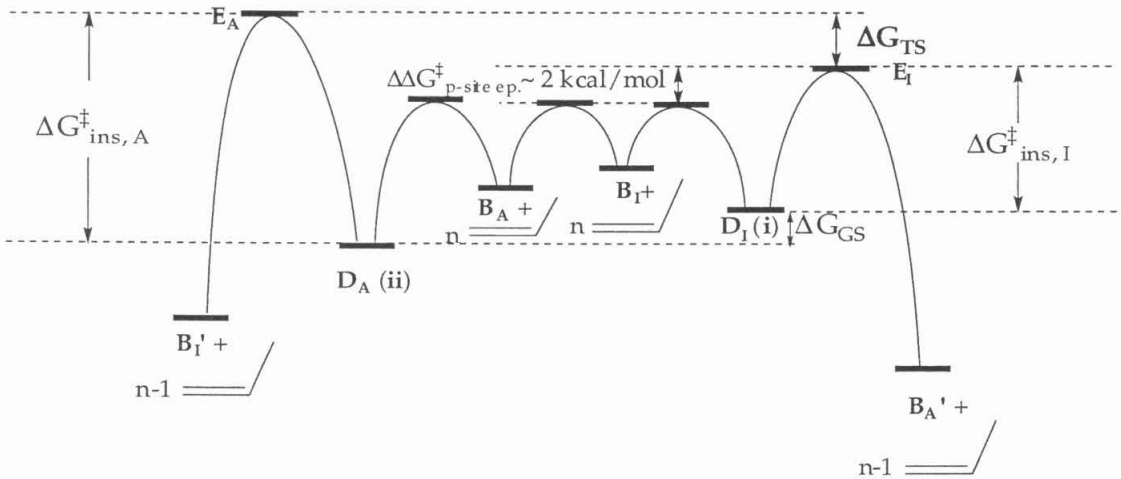

Figure 14. Energy diagram for chain propagation process in **2** that includes barriers for site epimerization, olefin coordination and olefin insertion steps. The relative ground state energy of **B** versus **D** will vary depend on the actual composition of **B**.

Scheme 9

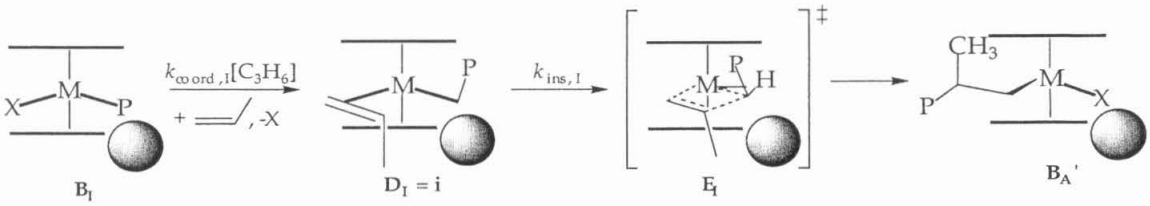

As discussed in the section above, the barrier for olefin coordination depends on the ease of forming a five-coordinate intermediate **A**. For catalysts **2**, this barrier should be of comparable height as the barrier for site-epimerization. Model studies on olefin dissociation in cationic zirconium (IV) complexes with Me_2SiCp_2 ligand indicated that indeed the barrier for olefin re-coordination and site epimerization is of similar magnitude in systems lacking α-substituents. On the other hand, model studies on cationic $(SiMe_2Cp_2)Zr^+$ complexes indicate that at -30 °C olefin insertion is ~ 2 kcal/mol higher than that of olefin dissociation ([monomer] = 1 M).[23] The resulting Curtin-Hammett situation (D_A and D_I and, in particular, B_A and B_I, are in fast pre-equilibria with one another, Figure 14) means that the probability of an insertion from the isospecific site versus thta from the aspecific site will be determined by ΔG_{TS}, the difference in transition-state energy of insertion from the aspecific site (**E_A**) and that of insertion from the isospecific site (**E_I**) (Figure 14). Granted, as monomer concentration is lowered, olefin coordination barrier will likely increase, but under the polymerization conditions, the maximum change in olefin concentration was ~ 6-fold (at ~ 273 K), and this corresponds to ~ 1 kcal/mol increase in olefin coordination barrier, not enough to overcome the ~ 2 kcal/mol difference in $\Delta\Delta G^{\ddagger}_{p\text{-site ep}}$. Consequently, at a given temperature (and in the absence of significant amount of chain epimerization), polypropylene samples prepared by the same catalyst should have the same tacticities, determined by ΔG_{TS}. Experimentally, stereoregularities of polypropylene prepared by either **2a** or **2b** showed no dependence on monomer concentrations.

But what value of ΔG_{TS} is required to achieve the kind of isospecificity attained in **2**? If we assume that olefin adduct **i** (**D_I**) is approximately 0.7 kcal/mol higher in energy than **ii** (**D_A**) (as calculated by Corradini for **11a** [21]), then using the formula (eq 3) developed by Collins[13] and assuming that $P_A \sim 1/2$

and $P_I \sim 1$, we estimate the transition-state energy of insertion from the isospecific site ($\mathbf{E_I}$) to be ~ 1 (**2a**) – 1.5 (**2b**) kcal/mol lower than that of insertion from the aspecific site ($\mathbf{E_A}$) (ΔG_{TS} = 1 – 1.5 kcal/mol) at T_p = 0 °C. In the derivation, we also assume that occasional enantiofacial misinsertion is the only type of stereoerrors present.

$$P_{re} = \frac{K_{eq} P_{A,re} + g P_{I,re}}{K_{eq} + g} \qquad (3)$$

g = ratio of rate of insertion from the isospecific site to that from the aspecific site

K_{eq} = [**ii**]/[**i**]

P_{re} = overall probability of a re-insertion in the catalyst ~ 1 - 0.5 × (1-[*m*]%)

$P_{A,re}$ = probability of a *re*-insertion from the aspecific site

$P_{I,re}$ = probability of a *re*-insertion from the isospecific site

On the other hand, calculations by MacSpartan predicts that **i** ($\mathbf{D_I}$) is actually ~0.8 kcal/mol lower in energy than **ii** ($\mathbf{D_A}$) when the ligand is [1,1'-$SiMe_2$-(C_5H_4)-(3-CMe_3-C_5H_3)]. which translates to ~1.1 kcal/mol difference in $\mathbf{E_I}$ and $\mathbf{E_A}$ ($\mathbf{E_A} > \mathbf{E_I}$) for catalyst **2b**. Since transition-state for monomer insertion is slightly more reactant-like, the relative energies of $\mathbf{E_I}$ and $\mathbf{E_A}$ should be the same as the relative ground state energy of the pre-insertion intermediates **i** ($\mathbf{D_I}$) and **ii** ($\mathbf{D_A}$). In this sense, calculation that predicts a higher ground state energy for **ii** ($\mathbf{D_A}$) than **i** ($\mathbf{D_I}$) seems more reliable.

This prediction seems contradictory to the experimental observation that bulkier ligand prefers to reside on the aspecific site to avoid steric interactions with the β-alkyl substituent of the Cp ring. However, molecular mechanics predicts that an η^2-bound propene molecule occupies about as much space as a PMe_3 molecule.[24] On the other hand, when the growing polymer resides on the same side as the β-alkyl substituent of the Cp ring, it can adopt the conformation shown in Chart 1, with only the two α-methylene protons of the polymer chain interacting with the β-alkyl group of the Cp ring. In this sense, the steric interaction between the polymer chain and the β-alkyl substituent of the Cp ring should not differ greatly from that between a methyl group and the β-alkyl

substituent of the Cp ring. Therefore, propene can be considered a bulkier ligand than CH_2P (P = polymer chain) in this case, and will therefore prefer to occupy the aspecific site (away from the β-alkyl substituent of the Cp ring).

The barrier for site epimerization is much higher in catalysts **3** (and **4**) than in **2**. Without further experimental data, it is hard to estimate how large an increase this is. Furthermore, it is unclear how addition of α-substituents affect the transition-state energy of insertion. But for simplicity, let's assume that the transition state energy for chain propagation is the same in catalyst **3** as in **2** (justified by the similar polymerization activities exhibited by the two systems), and that at high monomer concentrations, monomer insertion is still the rate-determining step in chain propagation (Figure 15).

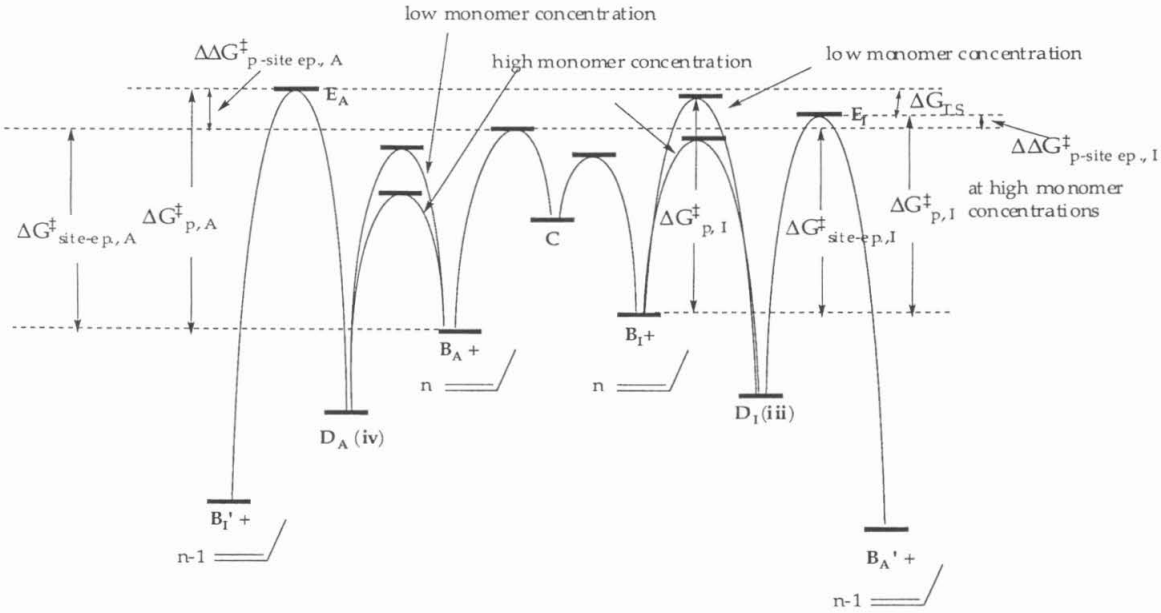

Figure 15. Energy diagram for chain propagation process in **3** (and **4**) that includes barriers for site epimerization, olefin coordination and olefin insertion steps. The transition-state energy for site epimerization can be above either $\mathbf{E_I}$ or $\mathbf{E_A}$.

Thus, an increase in the barrier for site epimerization leads to a decrease in the value of $\Delta\Delta G^{\ddagger}_{\text{p-site ep}}$ (which is the difference between the activation energy for site epimerization, $\Delta G^{\ddagger}_{\text{site-ep.}}$, and the activation energy for enchainment $\Delta G^{\ddagger}_{\text{p)}}$ in **3** (**4**) than in **2**. Because the larger the value of $\Delta\Delta G^{\ddagger}_{\text{p-site ep}}$, the more likely it is for a site epimerization to occur, a decrease in the magnitude of

$\Delta\Delta G^{\ddagger}_{p/site\ ep}$ in **3** (**4**) means that site epimerization occurs less frequently in **3** and **4** than in **2**. That is, the requirement for a Curtin-Hammett regime is no longer satisfied. Thus, even if the difference in transition state energy of chain propagation, ΔG_{TS}, remains the same in **3** and **4** as in **2**, the catalysts cannot fully access the kinetically more favorable insertion from the isospecific site, which results in a more frequent insertion from the aspecific site and consequently lower polymer tacticity. And because site-epimerization barrier is likely to increase with larger α-substituents, site epimerization occurs with decreasing frequency in zirconocenes with larger α–substituents, which translates to more frequent insertion from the aspecific site, and consequently, lower tacticity. This is consistent with the experimental observation that for catalyst series **3**, the isospecificity decreases in the order **3c** (with an α-methyl) > **3a** (with an α-isopropyl > **3c** (with an α-*tert*-butyl). This is also consistent with the observation that **4** (containing tetramethyldisilylene α to the dimethylsilylene linker in both Cp rings) exhibits the lowest isospecificity among the three catalyst systems.

As a side note, in the extreme case that barrier for site epimerization is much higher than insertion from either site, polymers will insert alternatively from the two sites, and ideally a hemi-isotactic polymer will be produced. But occasional enantiofacial misinsertion from the isospecific site and the slight enantioselectivity on the aspecific site will result in polymer microstructures that deviate from ideal hemi-isotactic. This could be what happens in catalysts **4**. Furthermore, for catalysts **4**, even if site epimerization were facile, the resultant polymer would still not contain high percentages of [*mmmm*], because there is little inherent preference for the polymer chain to reside at one particular insertion site.

Because of the higher barrier for the formation of **iii** than that of **iv**, which translates to a smaller difference in transition energy difference between olefin insertion and olefin coordination from the isospecific site, olefin coordination at the isospecific site can become rate-determining at low monomer concentrations, and increases the overall barrier for chain propagation from the isospecific site (Figure 15). On the other hand, barrier for chain propagation from the aspecific site should remain unaffected by change in monomer concentration, as in catalyst system **2**. This implies that the probability of site-epimerization from the isospecific site (to aspecific site) increases at lower monomer concentrations, while the probability of site-epimerization from the aspecific site to the isospecific site remains the same. This should lead to a more frequent insertion from the

aspecific site relative to that from the isospecific site, and should result in decreasing tacticity with decreasing monomer concentrations. This has indeed been observed with **3a**.

Origin of Stereospecificity in 1a. The above argument, however, does not explain why **1a** is isospecific. An inspection of the X-ray crystal structure of **1a** (Chapter 2, Figure 8) indicates that site epimerization *via* an associative pathway will have a prohibitively high barrier. Thus, it is possible that in this case, site epimerization actually occurs *via* a *dissociative* pathway (as in the double-silicon bridged Thp system). Olefin coordination in the three coordinate intermediate **I**, with the polymer chain residing on the aspecific site, is likely to be a slow process due to steric hindrance imposed by both the tetramethyldisilylene linker and the front isopropyl group on the trajectory for coordination. Chain-swinging to the isospecific site, while expected to be of higher barrier than olefin coordination in the absence of outside assistance, can be accelerated if a solvent molecule or monomer or anion coordinates from the backside of the aspecific site, and concertedly pushes the polymer chain to the isospecific site (**I** --> **J** --> **F**). If the incoming ligand is a monomer molecule, **I** will be converted to **H** directly. Consequently, chain-swinging from the aspecific site to the isospecific site occurs more frequently than an enchainment from the aspecific site. On the other hand, when the polymer chain resides on the isospecific site, olefin coordination, while likely to be impeded by the presence of a rear isopropyl group on the Cp ring, can still take place. Chain-swinging, on the other hand, has a considerably higher barrier, because in this case, concerted site epimerization assisted by the backside attack by an incoming ligand from the isospecific site is too sterically hindered to take place; and site epimerization without outside assistance is ~ 5 kcal/mol higher in energy than olefin coordination in "Thp" systems. The ensuing energy profile is such that when the polymer chain resides on the isospecific site, it inserts more often than it site epimerizes; whereas when the polymer chain resides at the aspecific site, site epimerization takes place more frequently than incorporation of a monomer units (Figure 16). This leads to insertion mostly from the isospecific site, and leads to isotactic polypropylene.

Scheme 10

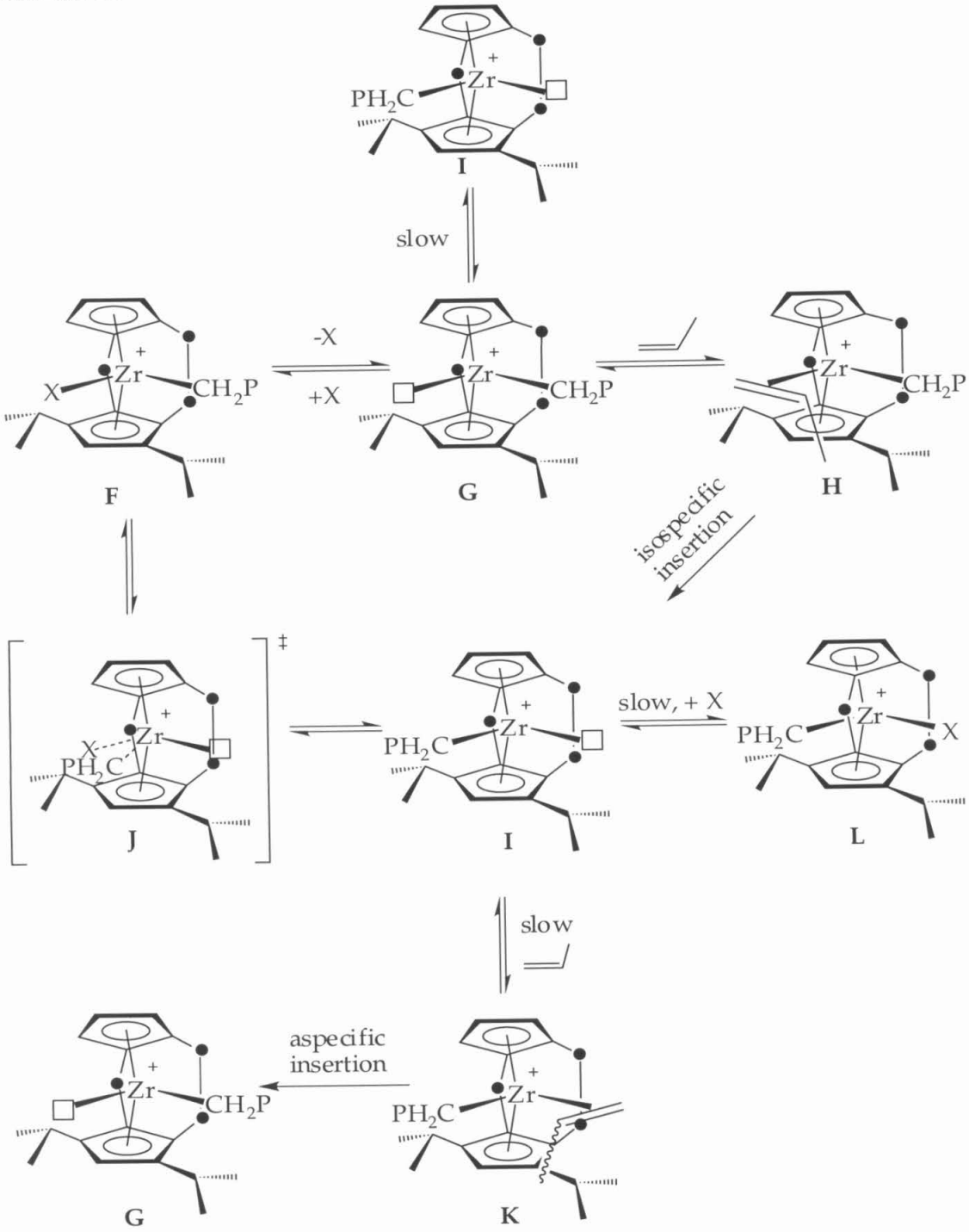
PH2C
Zr
I
slow
-X
+X
X
CH2P
F
G
H
isospecific insertion
J
‡
slow, + X
L
slow
aspecific insertion
K

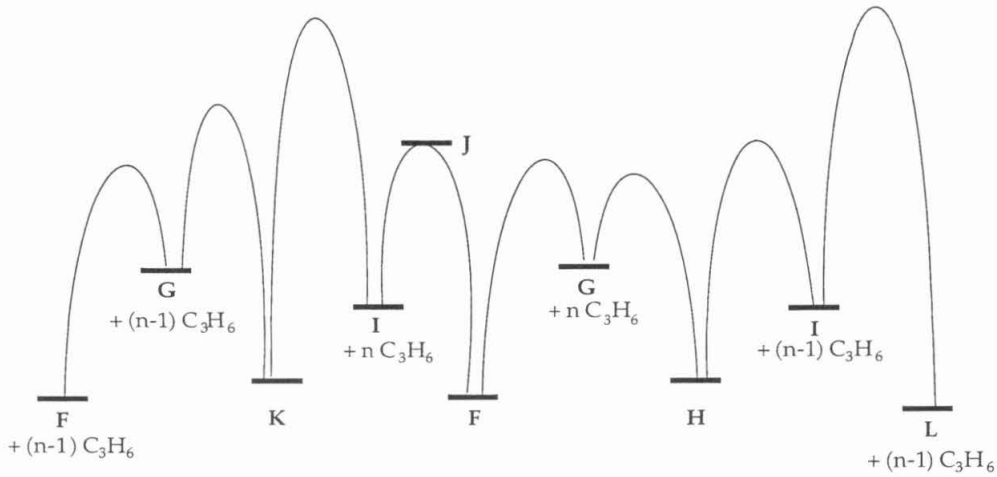

Figure 16. Energy diagram for chain propagation process in **1a**.

Regioselectivity and Polymer Molecular Weight

An increase in the amount of 2,1-insertion at higher polymerization temperatures is to be expected. Because both 2,1- and 1,2-insertions are second order reactions, $\Delta\Delta G^{\ddagger}$ for the two processes is expected to be (nearly) constant at all temperatures. However, since $\ln(k_{1,2}/k_{2,1}) = -\Delta\Delta G^{\ddagger}/RT$, selectivity for 1,2- over 2,1-insertion decreases as temperature increases. This results in a relative increase in regioerrors. On the other hand, by the same argument, there should not be a change in the amount of 2,1-misinsertions at constant temperatures. This appeared true for room temperature polymerizations with **2b** (entries 17–19), but at 0°C, while few regioerrors could be detected at higher monomer concentrations, an observable amount was present for polypropylene made at the lowest monomer concentration (run 16). We did not have a good explanation for this observation.

That **2a** produces fewer regioerrors than **2b** is unexpected but not completely surprising. When the polymer chain resides on the same side as the frontal β-alkyl substituent of the Cp ring, 1,2-insertion (Figure 17, left figure) geometry leads to some steric repulsion between propylene's methyl group and the frontal alkyl substituent. When the alkyl is an isopropyl group (R^1 = H), this interaction is considerably less than if it is a *tert*-butyl group (R^1 = Me). Such steric interaction (as well as that between the polymer chain and the methyl group of propylene molecule) may at times override the inherent electronic preference for 1,2-insertion,[25] unless there is counterbalancing steric interactions in the 2,1-insertion geometry between propylene's methyl group and R^2, α-

substituent of the Cp ring (as in the case of **3a**, Figure 17, right figure). That frontal isopropyl substituent of the Cp ring leads to lower regioerrors has been observed by Brintzinger and co-workers as well, who reported that while polypropylene prepared by **13b** contained 0.4% regioerrors (Tp = 50 °C, 2 bar propene), regioerrors for polypropene prepared by **13a** under the same condition were below detection limit.[26]

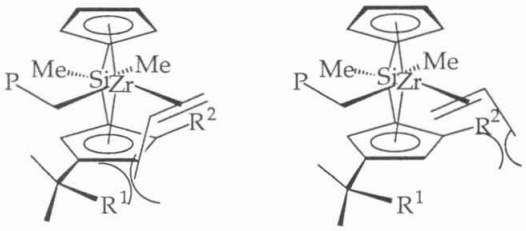

R^1 = H, Me
R^2 = H, $CHMe_2$, CMe_3

Figure 17. Steric interaction between the methyl group of the monomer and the β-substituent increases the frequency of 2,1-insertion; while that between the methyl group and the α-substituent prohibits 2,1-insertion.

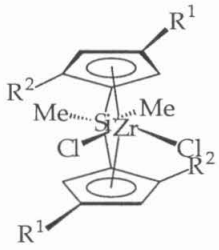

13a $R^1 = CHMe_2$, R^2 = Me
13b $R^1 = CMe_3$, R^2 = Me
13c $R^1 = CMe_3$, R^2 = H

Brintzinger and co-workers have also observed before that under the same polymerization conditions **13b** produces polymers of nearly twice the M_W as those prepared by **13a**, and both produced polymers with significantly high molecular weight than **13c**.[26] This is at least consistent with the observation made in the present study that under the same polymerization conditions, polymers made with **2b** have longer chain-lengths than those made with **2a** (Figure 8 and Tables 4 and 6, entries 11 and 20), but polymers made by **2a**/**2b** both seem to have lower molecular weights than those by **3a** under comparable polymerization conditions.

The increase in molecular weights of polymers prepared by metallocenes containing α-substituents in the Cp ring(s) is due to probably both an increase in the propagation rate and a decrease in the chain termination rate. In the present study, the 1:1 ratio of propyl to vinylidene chain end groups indicates that β-H transfer to monomer or zirconium is the major pathway for chain termination. Theoretical calculations have shown that [$Cp_2Zr(H)$(olefin)] is stable toward olefin dissociation.[3] Thus, even if β-H transfer to zirconium center is a facile process, an associative displacement of the olefin-like chain end by either a monomer or a solvent molecule is required for chain release. Incorporation of an α-substituent into the Cp ring increases the barrier for associative exchanges, and should therefore decreases the rates for both β-H transfer to monomer and β-H transfer zirconium center followed by associative displacement of the chain end. This results in higher molecule weight polymers. In addition, the lower percentages of 2,1-insertion in metallocenes containing α-substituent in the Cp rings also help to enhance the molecule weight, because it is known that 2,1-insertion generates a much slower propagating species. Thus, more regioregular 1,2-insertion should lead to a higher propagation rate, which should also lead to an increase in polymer molecular weights.

Conclusions

Several C_1-symmetric ansa-metallocenes were synthesized, and used in propylene polymerization. Among them, **2a** and **2b** are isospecific polymerization catalysts, while **3a/b** and **4a/b** are hemi-isospecific. Studies of cationic zirconium (IV) complexes as well as examination of polymer stereoregularity as a function of monomer concentration indicate that polymerization in **2** falls in the Curtin-Hammett regime, in which site epimerization is fast relative to monomer enchainment. The lower transition-state energy for monomer insertion from the isospecific site therefore leads to more frequent insertion from the isospecific site, and high isotacticity of the resulting polymers.

On the other hand, incoporation of α-substituents in **3** and **4** results in slow site epimerization. Therefore, the less active aspecific site is kinetically trapped by the monomer, resulting in similar frequency of insertion from either site, and consequently lower isotacticity. Isospecificity in **1a**, on the other hand, is a result of kinetic trapping by the isospecific site.

α-Substituents also help minimize 2,1-misinsertion, resulting in a more regioregular polymer. The decreased number of 2,1-misinsertion also increases overall chain propagation rate. The steric hindrance imposed by α-substituents on associative exchange process reduces the likelihood for both β-H transfer to monomer and β-H transfer zirconium center followed by associative displacement of the chain end. Both the increased chain propagation rate and the decreased β-H transfer rate result in polymers with higher molecular weights.

Experimental Section

General considerations. All air and /or moisture sensitive compounds were manipulated using standard high-vacuum line, Schlenk, or cannula techniques, or in a glove box under a nitrogen atmosphere. Argon was purified and dried by passage through columns of MnO on vermiculite and activated 4 Å molecular sieves. All solvents (except CH_2Cl_2) were stored under vacuum over titanocene or sodium benzophenone ketyl. CH_2Cl_2 was stored under vacuum over CaH_2. CMe_3-C_5H_4 was prepared by Jeff Yoder. 1,3-$(CHMe_2)_2$-C_5H_4 was prepared by Shigenobu Miyage. $SiMe_2Cl_2$ and TMSCl were purchased from Aldrich, and stored over CaH_2 under vacuum. $SiMe_2Cl$-$SiMe_2Cl$ was purchased from Aldrich and stored in a strauss flask under nitrogen in the glove box. *n*-Butyllithium was purchased from Aldrich and stored under argon. Pyrrolidine was purchased from Aldrich and used as received. $LiN(TMS)_2$, $KN(TMS)_2$ and $LiCH_2TMS$ were purchased from Aldrich, purified by sublimation and stored under nitrogen in the glove box. Li(R-C_5H_4) (R=H, *tert*-Bu, *i*Pr) and Li(1,3-iPr_2-C_5H_2) were prepared by deprotonation of the corresponding substituted cyclopentadienes with *n*-BuLi in diethylether, and worked up using standard procedure. Li_2[1,1'-($SiMe_2$)-{C_5H_4}-{3-R-C_5H_3}] (R = *t*-Bu, *i*Pr) and Li_2[1,1'-($SiMe_2$)-{C_5H_4}-{3-R_2-C_5H_2}] (R = *t*-Bu, *i*Pr) are prepared according to known procedures.[16,27]

NMR spectra were recorded on a GE QE300 (^1H, 300.1 MHz), a varian INOVA 500 (^1H, 499.852 MHz; ^{19}F, 470.256 MHz; ^{13}C, 125.701 MHz) or a varian Mercury 300 (^1H, 299.8 MHz; ^{19}F, 282.081 MHz; ^{13}C, 75.4626 MHz) spectrometer. Elemental analyses were carried out at the Caltech Elemental Analysis Facility by Fenton Harvey, with a run-to-run variation of 0.5%–1.0%. X-ray diffraction studies were performed by Lawrence Henling at 85K on a Bruker SMART 1000

CCD area detector. Bruker SMART programs were used for data processing and the structures were solved with SHELXS–86.

Synthesis of $Li_2[1\text{-}(SiMe_2\text{-}SiMe_2)\text{-}2\text{-}(SiMe_2)\text{-}\{C_5H_3\}]\text{-}\{3\text{-}CHMe_2\text{-}C_5H_2\}]$ (8a). 100 ml THF solution of $Li_2[(1\text{-}(SiMe_2)\text{-}\{C_5H_4\}]\text{-}\{2\text{-}CHMe_2\text{-}C_5H_3\}]$ (1.000 g, 4.13 mmol) was added dropwise to 70 ml THF solution of $SiMe_2Cl\text{-}SiMe_2Cl$ (0.773 g, 4.13 mmol) at 50 °C over 3 hours. The mixture was then stirred at room temperature for 12 hours, before removal of THF *in vacuo*. Petroleum ether 50 ml was added to the residue, and the yellow slurry was stirred for 30 minutes. The yellow supernatant was separated from the white precipitate by filtration. The filtrate was concentrated to give a yellow oil, 1.33 gram of which (3.86 mmol) was then deprotonated with *n*-BuLi (1.6 *M* in hexanes, 5 ml, 8 mmol) in diethylether at room temperature. The resultant dilithio salt was isolated as diethylether adduct (0.5 equivalent, 1.2 g, 72%), and was used without further purification. ^1H NMR (300 MHz, THF–d_8): δ = 0.24 (s, 6H, SiMe_2), 0.25 (s, 6H, SiMe_2), 0.42(s, 6H, SiMe_2), 1.2 (d, 6.9 Hz, 6H, CHMe_2), 2.85 (sept, 6.9 Hz, 1H, CHMe$_2$), 5.90 (t, 3 Hz, 1H, C_5H_3), 6.040(br s, 2H, C_5H_2), 6.13 (dd, 2.7 Hz, 1.8 Hz, 1H, C_5H_3), 6.25(dd, 2.7 Hz, 1.8 Hz, 1H, C_5H_3).

Synthesis of $Li_2[1\text{-}(SiMe_2\text{-}SiMe_2)\text{-}2\text{-}(SiMe_2)\text{-}\{C_5H_3\}]\text{-}\{3\text{-}CMe_3\text{-}C_5H_2\}]$ (8b). 100 ml THF solution of $Li_2[(1\text{-}(SiMe_2)\text{-}\{C_5H_4\}]\text{-}\{2\text{-}CMe_3\text{-}C_5H_3\}]$ (1.006 g, 3.925 mmol) was added dropwise to 70 ml THF solution of $SiMe_2Cl\text{–}SiMe_2Cl$ (0.735 g, 3.925 mmol) at 50 °C over 3 hours. The mixture was then stirred at room temperature for 12 hours, before removal of THF *in vacuo*. Petroleum ether 50 ml was added to the residue, and the yellow slurry was stirred for 30 minutes. The yellow supernatant was separated from the white precipitate by filtration. The filtrate was concentrated to give a yellow oil, 1 gram of which (2.79 mmol) was then deprotonated with 550 mg of $LiCH_2TMS$ (5.84 mmol) in diethylether at room temperature. The resultant dilithio salt was soluble even in petroleum ether, and was used without further purification. ^1H NMR (300 MHz, THF–d_8): δ = 0.18 (s, 6H, SiMe_2), 0.21 (s, 6H, SiMe_2), 0.37 (s, 6H, SiMe_2), 1.17 (s, 9H, CMe_3), 5.83 (t, 2.7 Hz, 1H, C_5H_3), 6.04 (br s, 2H, C_5H_2), 6.10 (dd, 2.7 Hz, 1.8 Hz, 1H, C_5H_3), 6.13 (dd, 2.7 Hz, 1.8 Hz, 1H, C_5H_3).

Synthesis of 2a. Toluene 50 ml was vacuum transferred onto a mixture of $Li_2[(1\text{-}(SiMe_2)\text{-}\{C_5H_4\}]\text{-}\{3\text{-}CHMe_2\text{-}C_5H_3\}]$ (1.005 g, 4.13 mmol) and $ZrCl_4$ (0.962 g,

4.13 mmol) with stirring. The slurry was allowed to warm to room temperature (from -78°C) over 2 hours, and stirred at that temperature for 12 more hours. TMSCl (2 ml) was then vacuum transferred into the reaction flask, and the mixture was stirred for 3 hours at room temperature. Afterwards, the yellow solution was filtered away from the white insolubles. The yellow filtrate was concentrated to give a yellow paste. Petroleum ether was added to the yellow paste, and the insoluble off-white solids were collected by filtration (0.554 g, 34.4%). ^{1}H NMR in C_6D_6: δ 0.07 (s, 3H, Si(CH_3)$_2$), 0.15 (s, 3H, Si(CH_3)$_2$), 1.09 (d, 3H, 6.9 Hz, CH(CH_3)$_2$), 1.32 (d, 3H, 6.6 Hz, CH(CH_3)$_2$), 3.30 (sept, 6.9 Hz, 1H, C*H*Me$_2$), 5.27 (t, 2.1 Hz, 1H, Cp*H*), 5.43 (m, 1H, Cp*H*), 5.52 (m, 2H, Cp*H*), 6.67 (dd, 2.7 Hz, 1.8 Hz, 1H, Cp*H*), 6.82 (m, 2H, Cp*H*). Elemental analysis Found (Calculated): H 5.14% (5.16%), C 45.57% (46.13%).

Synthesis of 2b. **2b** was synthesized analogously in 43% yield with Li_2[(1-(SiMe$_2$)-{C_5H_4}]-{3-CMe$_3$-C_5H_3}] (THF adduct, 3g, 9.1 mmol) and $ZrCl_4$ (2.50 g, 10.7 mmol). The zirconocene initially isolated (3.2 g) contained coordinated THF (and maybe lithium chloride), evidenced by broad peaks at ~1.2 and 4 ppm in ^{1}H NMR (C_6D_6) spectrum. THF was removed by repeated (4 – 5) cycles of dissolution of **2b** in toluene, filtration of insolubles and removal of toluene. The yield reported is for product collected after purification (1.57 g, off-white solid) . ^{1}H NMR (300 MHz, C_6D_6): δ = 0.06 (s, 3H, Si(CH_3)$_2$), 0.19 (s, 3H, Si(CH_3)$_2$), 1.43 (s, 9H, C(CH_3)$_3$), 5.44 (m, 1H, Cp*H*), 5.51 (t, 2.7 Hz, 1H, Cp*H*), 5.64 (d, 2.4 Hz, 1H, Cp*H*), 5.72 (m, 1H, Cp*H*), 6.66 (m, 1H, Cp*H*), 6.83 (m, 1H, Cp*H*). Elemental analysis Found (Calculated): H 5.49% (5.48%), C 47.57% (47.50%).

Synthesis of 3a. **3a** was synthesized analogously in 65% yield (2.90 g, green solid) with Li_2[(1-(SiMe$_2$)-{C_5H_4}]-{2, 4-(CHMe$_2$)$_2$-C_5H_2}] (2.95 g, 10.4 mmol) and $ZrCl_4$ (2.42 g, 10.4 mmol). ^{1}H NMR (300 MHz, C_6D_6): δ = 0.07 (s, 3H, Si(CH_3)$_2$), 0.37 (s, 3H, Si(CH_3)$_2$), 0.96 (d, 6.9 Hz, 3H, CH(CH_3)$_2$), 1.11 (d, 6.9 Hz, 3H, CH(CH_3)$_2$), 1.29 (d, 6.6 Hz, 3H, CH(CH_3)$_2$), 1.38 (d, 6.9 Hz, 3H, CH(CH_3)$_2$), 2.63 (sept, 6.9 Hz, 1H, C*H*Me$_2$), 3.42 (sept, 6.9 Hz, 1H, C*H*Me$_2$), 5.33 (d, 2.1 Hz, 1H, C_5H_2), 5.52 (m, 1H, C_5H_4), 5.58 (m, 1H, C_5H_4), 6.69 (d, 2.4 Hz, 1H, C_5H_2), 6.78 (m, 1H, C_5H_4), 6.90 (m, 1H, C_5H_4). Elemental analysis Found (Calculated): H 6.02% (6.06%), C 50.19% (49.97%).

Synthesis of 3b. **3b** (760 mg, yellow) was synthesized analogously in 31% yield with $Li_2[(1\text{-}(SiMe_2)\text{-}\{C_5H_4\})\text{-}\{2, 4\text{-}(CMe_3)_2\text{-}C_5H_2\}]$ (1.66 mmol, 5.31 mmol) and $ZrCl_4$ (1.238g, 5.31 mmol). The product is fairly soluble in petroleum ether, and was collected as a precipitate from a 1:2 mixture of petroleum ether and hexamethyldisiloxane (TMS_2O) or pure TMS_2O. ^1H NMR (300 MHz, C_6D_6): δ = 0.26 (s, 3H, $Si(CH_3)_2$), 0.51 (s, 3H, $Si(CH_3)_2$), 1.24 (s, 9H, CMe_3), 1.38 (s, 9H, $C(CH_3)_3$), 5.44 (dd, 2.7 Hz, 0.6 Hz, 1H, C_5H_4), 5.63 (d, 2.4 Hz, 1H, C_5H_4), 5.74 (dd, 2.7 Hz, 0.6 Hz, 1H, C_5H_2), 6.76 (m, 1H, C_5H_4), 6.77 (d, 2.7 Hz, 1H, C_5H_2), 6.90 (m, 1H, C_5H_4).. Elemental analysis Found (Calculated): H 6.57% (6.56%), C 52.42% (52.15%).

Synthesis of 4a. **4a** (white, 920 mg) was synthesized analogously in 54% yield with **8a** (all from above, ~2.69 mmol) and $ZrCl_4$ (0.78 g, 3.35 mmol) in toluene. Removal of toluene-insolubles was carried out in air. ^1H NMR (300 MHz, C_6D_6): δ = 0.14 (s, 3H, $Si(CH_3)_2$), 0.28 (s, 3H, $Si(CH_3)_2$), 0.290 (s, 3H, $Si(CH_3)_2$), 0.45 (s, 3H, $Si(CH_3)_2$), 0.50 (s, 3H, $Si(CH_3)_2$), 0.51 (s, 3H, $Si(CH_3)_2$) 1.12 (d, 7.2 Hz, 3H, $CH(CH_3)_2$), 1.41 (d, 6.6 Hz, 3H, $CH(CH_3)_2$), 3.43 (sept, 6.9 Hz, 1H, $CHMe_2$), 5.88(d, 1.8 Hz, 1H, C_5H_2), 6.02 (dd, 2.4 Hz, 1.5 Hz, 1H, C_5H_3), 6.74 (t, 2.7 Hz, 1H, C_5H_3), 7.04 (d, 1.8 Hz, 1H, C_5H_2), 7.09 (dd, 3.3 Hz, 1.8 Hz, 1H, C_5H_3). Elemental analysis Found (Calculated): H 5.49% (5.99%), C 45.86% (45.21%).

Synthesis of 4b. **4b** (pale green, 450 mg) was synthesized analogously in 31% yield with **8b** (~ 2.79 mmol) and $ZrCl_4$ (0.78 g, 3.35 mmol). The product is fairly soluble in petroleum ether, and was collected as a precipitate from a 1:5 mixture of petroleum ether and hexamethyldisiloxane (TMS_2O). ^1H NMR (300 MHz, C_6D_6): δ = 0.16 (s, 3H, $Si(CH_3)_2$), 0.22 (s, 3H, $Si(CH_3)_2$), 0.24 (s, 3H, $Si(CH_3)_2$), 0.41 (s, 3H, $Si(CH_3)_2$), 0.48 (s, 3H, $Si(CH_3)_2$, 0.50 (s, 3H, $Si(CH_3)_2$), 1.44(s, 9H, $C(CH_3)_3$), 6.09 (dd, 2.7 Hz, 1.8 Hz, 1H, C_5H_3), 6.14 (d, 1.8 Hz, 1H, C_5H_2), 6.64 (t, 2.7 Hz, 1H, C_5H_3), 7.03 (dd, 3 Hz, 1.5 Hz, 1H, C_5H_3), 7.15 (d, 1.8 Hz, 1H, C_5H_2). Elemental analysis Found (Calculated): H 6.63% (6.22%), C 45.94% (46.30%).

Synthesis of $[1,1'\text{-}SiMe_2\text{-}\{C_5H_4\}\text{-}(3\text{-}CMe_3\text{-}C_5H_3)]ZrMe_2$.(20). In a swivel-frit assembly equipped with a 90° valve, **2b** (635 mg, 1.57 mmol) was dissolved in 1:1 toluene : diethylether (~40 ml total) at -78 °C. After warming to 0 °C, MeLi (2.30 ml, 1.4 *M* in Et_2O, 3.22 mmol) was added to the solution via a syringe under argon. The mixture was stirred at 0 °C for 3 hours and the solvent was removed

at 0 °C under dynamic vacuum. Petroleum ether (~20 ml) was then added to the off-white solids, and the mixture was filtered and washed with recycled petroleum ether twice. After removal of petroleum ether and drying on the high vacuum line for 3 hours, the petroleum-ether soluble solids were collected in an inert-atmosphere glove box. 415 mg collected (72.7%). ^{1}H NMR (300 MHz, C_6D_6): δ = 0.005 (s, 3H, Si(CH_3)$_2$), 0.02(s, 3H, Si(CH_3)$_2$), 0.12 (s, 3H, Zr–CH_3), 0.20 (s, 3H, Zr–CH_3), 1.37(s, 9H, C(CH_3)$_3$), 5.31 (t, 2.7 Hz, 1H, Cp*H*), 5.35 (d, 2.1 Hz, 1H, Cp*H*), 5.58 (d, 1.8 Hz, 1H, Cp*H*), 5.63 (t, 2.1 Hz, 1H, Cp*H*), 6.56 (d, 1.8 Hz, 1H, Cp*H*), 6.68 (t, 2.1 Hz, 1H, Cp*H*), 6.74 (d, 1.8 Hz, 1H, Cp*H*).

Synthesis of [1,1'-SiMe$_2$-(C$_5$H$_4$}-(2, 4-(CHMe$_2$)$_2$-C$_5$H$_2$)]ZrMe$_2$. (21). The complex was prepared analogously with **3a** (356 mg, 0.82 mmol) and MeLi (1.20 ml, 1.4 *M* in Et_2O, 1.68 mmol) in a 1:2 mixture of toluene and diethylether. White solids collected (243 mg, 76%). ^{1}H NMR (300 MHz, C_6D_6): δ = -0.14 (s, 3H, Si(CH_3)$_2$), -0.08 (s, 3H, Si(CH_3)$_2$), 0.13 (s, 3H, Zr–CH_3), 0.39 (s, 3H, Zr–CH_3), 1.068 (d, 6.9 Hz, 3H, CH(CH_3)$_2$), 1.075 (d, 6.9 Hz, 3H, CH(CH_3)$_2$), 1.22 (d, 6.9 Hz, 3H, CH(CH_3)$_2$), 1.295 (d, 6.9 Hz, 3H, CH(CH_3)$_2$), 2.48 (sept, 6.9 Hz, 1H, C*H*Me$_2$), 3.03 (sept, 6.9 Hz, 1H, C*H*Me$_2$), 5.20 (d, 2.1 Hz, 1H, C$_5H_2$), 5.38 (m, 1H, C$_5H_4$), 5.48 (m, 1H, C$_5H_4$), 6.61(m, 2H, C$_5H_2$ & C$_5H_4$), 6.80 (pseudo td, 3.0 Hz, 1.8 Hz, 1H, C$_5H_4$).

Synthesis of [1,1'-(SiMe$_2$-SiMe$_2$)-2,2'-SiMe$_2$-(C$_5$H$_3$)-(3-CHMe$_2$-C$_5$H$_2$)]ZrMe$_2$ (22). The complex was prepared analogously with **4a** (200 mg, 0.40 mmol) and MeLi (0.6 ml, 1.4M in Et_2O, 0.83 mmol) in a 1:3 mixture of toluene and diethylether. white solids collected (115 mg, 62.6%). ^{1}H NMR (300 MHz, C_6D_6): δ = -0.19 (s, 3H, Zr–CH_3), -0.03 (s, 3H, Zr–CH_3), 0.16 (s, 3H, Si(CH_3)$_2$), 0.31(s, 3H, Si(CH_3)$_2$), 0.325 (s, 3H, Si(CH_3)$_2$), 0.334 (s, 3H, Si(CH_3)$_2$), 0.35 (s, 3H, Si(CH_3)$_2$), 0.48 (s, 3H, Si(CH_3)$_2$) 1.24 (d, 6.9 Hz, 3H, CH(CH_3)$_2$), 1.30 (d, 6.6 Hz, 3H, CH(CH_3)$_2$), 3.08 (sept, 6.9 Hz, 1H, C*H*Me$_2$), 5.84 (d, 1.2 Hz, 1H, C$_5H_2$), 5.99 (m, 1H, C$_5H_3$), 6.64 (t, 2.7 Hz, 1H, C$_5H_3$), 6.92 (d, 1.8 Hz, 1H, C$_5H_2$), 7.01 (m, 1H, C$_5H_3$).

Characterization of Minor Species in the Reaction between 20 and B(C$_6$F$_5$)$_3$. ^{1}H NMR (500 MHz, C_6D_6): δ = -0.17 (s, 3H, Si(CH_3)$_2$), -0.05 (s, 3H, Si(CH_3)$_2$), 0.51 (s, 3H, Zr–CH_3), 0.58 (br s, 3H, B–CH_3), 0.66 (s, 9H, C(CH_3)$_3$), 5,10 (m, 1H, Cp*H*), 5.37 (m, 1H, Cp*H*), 5.41 (m, 1H, Cp*H*), 6.29 (m, 1H, Cp*H*), 6.47 (m, 1H, Cp*H*), missing two Cp resonances which could be overlapping with major

isomer's resonances. ^{19}F NMR (470 MHz, C_6D_6/C_6D_5Br): - 156.60 (br s, 6F, F_m), -138.40 (br s, 3F, F_p), -125.32 (br s, 6F, F_o).

Characterization of 14b. ^{1}H NMR (500 MHz, C_6D_6): δ = -0.27 (s, 3H, Si(CH_3)$_2$ - same side as CMe_3), -0.08 (s, 3H, Si(CH_3)$_2$), 0.45 (s, 3H, Zr–CH_3), 0.58 (br s, 3H, B–CH_3), 0.98 (s, 9H, C(CH_3)$_3$), 5.05 (dd, 2.7 Hz, 2.1 Hz, 1H, H_1), 5.18 (dd, 4.5 Hz, 2.1 Hz, 1H, H_4), 5.26 (t, 2.7 Hz, 1H, H_5), 5.35 (t, 2.7 Hz, 1H, H_6), 6.28 (m, 1H, H_2), 6.33 (m, 1H, H_3), 6.40 (dd, 3.0 Hz, 2.1 Hz, 1H, H_7). Key CycloNOE correlations: -0.27 (H_1, H_3, exchange with -0.05), -0.08 (H_4, H_6, exchange with -0.17), 0.45 (H_1, H_2, H_3, C(CH_3)$_3$, exchange signal with B–CH_3), 0.98 (H_5, H_7, Zr–CH_3, exchange with 0.66), 6.40 (H_6). ^{19}F NMR (470 MHz, C_6D_6/C_6D_5Br): -160.87 (br s, 6F, F_m), -155.55 (br s, 3F, F_p), -130.12 (br s, 6F, F_o).

Characterization of 15b. ^{1}H NMR (500 MHz, C_6D_6/C_6D_5Br): δ = 0.11 (s, 3H, Si(CH_3)$_2$, non-CMe_3 side), 0.16 (s, 3H, Zr–CH_3), 0.19 (s, 3H, Si(CH_3)$_2$), 0.93 (d, 7.2 Hz, P(CH_3)$_2$), 0.95 (d, 7.2 Hz, P(CH_3)$_2$), 1.00 (s, 9H, C(CH_3)$_3$), 1.27 (s, 3H, B–CH_3), 4.75 (dd, 5.0 Hz, 2.7 Hz, 1H, H_4), 4.86 (m, 1H, H_6), 5.27 (m, 1H, H_1), 5.44 (t, 2.1 Hz, 1H, H_5), 6.25 (m, H, H_3), 6.27 (m, H, H_7), 6.60 (dd, 5.0 Hz, 2.7 Hz, 1H, H_2), 6.75 (m, 2H, Ph-H_m), 7.12–7.14 (m, 3H, Ph-H_o and Ph-H_p). When slightly more than one equivalent of PMe_2Ph was added, the P(CH_3)$_2$ resonances coalesces to 0.93 ppm (d, 7.2 Hz). Key CycloNOE correlations: 0.11 (H_1, H_3), 0.16 (C(CH_3)$_3$, H_1, H_2, H_3 Ph-H_m), 0.19 (H_4, H_6), 1.00 (H_5, H_7, Zr–CH_3), 0.92 & 0.95 (H_4, H_6, H_3, H_7, Ph-H_m), 4.77 (H_3, 0.11- SiMe, PMe_2), 6.60 (H_1, H_3, Zr–CH_3). ^{19}F NMR (470 MHz, C_6D_6/C_6D_5Br): -163.23 (t, 20.0 Hz, 6F, F_m), -160.81 (t, 20.5 Hz, 3F, F_p), -128.48 (d, 20.9 Hz, 6F, F_o).

Characterization of 16b. ^{1}H NMR (500 MHz, C_6D_6): δ = -0.27 (s, 3H, Si(CH_3)$_2$, front *i*Pr side), 0.16 (s, 3H, Si(CH_3)$_2$), 0.40 (s, 3H, Zr–CH_3), 0.62 (s, 3H, B–CH_3), 0.59 (d, 7.2 Hz, 3H, back CH(CH_3)$_2$), 0.77 (d, 7.0 Hz, 3H, back CH(CH_3)$_2$), 0.93 (d, 7.0 Hz, 3H, front CH(CH_3)$_2$), 1.00 (d, 6.9 Hz, 3H, front CH(CH_3)$_2$), 2.30 (sept, 7.0 Hz, 1H, back $CHMe_2$), 2.79 (sept, 7.0 Hz, 1H, front $CHMe_2$), 4.77 (d, 2.1 Hz, 1H, H_5), 4.94 (dd, 4.5 Hz, 2.1 Hz, 1H, H_1), 5.35 (dd, 4.5 Hz, 2.1 Hz, 1H, H_4), 6.34 (d, 1.5 Hz, H_6), 6.41 (m, 2H, H_2 and H_3). ^{1}H NMR (500 MHz, C_6D_6/C_6D_5Br): δ = -0.75 (s, 3H, Si(CH_3)$_2$), 0.25 (s, 3H, Si(CH_3)$_2$), 0.41 (s, 3H, Zr–CH_3), 0.58 (s, 3H, B–CH_3), 0.60 (d, 7.2 Hz, 3H, CH(CH_3)$_2$), 0.81 (d, 7.0 Hz, 3H, CH(CH_3)$_2$), 0.96 (d, 7.0 Hz, 3H, CH(CH_3)$_2$), 1.00 (d, 6.9 Hz, 3H, CH(CH_3)$_2$),

2.37 (sept, 7.0 Hz, 1H, C*H*Me$_2$), 2.80 (sept, 7.0 Hz, 1H, C*H*Me$_2$), 4.82 (d, 2.1 Hz, 1H, H$_5$), 5.04 (dd, 4.5 Hz, 2.1 Hz, 1H, H$_1$), 5.41 (dd, 4.5 Hz, 2.1 Hz, 1H, H$_4$), 6.33 (d, 2.0 Hz, H$_6$)), 6.41 (dd, 4.5 Hz, 3.0 Hz, 1H, H$_3$), 6.49 (dd, 4.5 Hz, 3.0 Hz, 1H, H$_2$). Key CycloNOE correlations: -0.27 (H$_1$, H$_5$), 0.16 (back C*H*Me$_2$, H$_4$), 0.40 (front C*H*Me$_2$, H$_1$, H$_2$, H$_5$), 2.30 (H$_4$, 0.59, 0.77 - CH(C*H*$_3$)$_2$, 0.16 - Si(C*H*$_3$)$_2$, back *i*Pr side), 0.41 (H$_1$, H$_5$, H$_2$), 2.79 (H$_5$, weak H$_6$, 0.93, 1.00 -CH(C*H*$_3$)$_2$, Zr–C*H*$_3$). ^{19}F NMR (480 MHz, C$_6$D$_6$):

Characterization of 17b. ^{1}H NMR (500 MHz, C$_6$D$_6$/C$_6$D$_5$Br): δ = -0.07 (s, 3H, Zr–C*H*$_3$), -0.05 (s, 3H, Zr–Me side Si(C*H*$_3$)$_2$), 0.40 (s, 3H, back *i*Pr side Si(C*H*$_3$)$_2$), 0.34 (d, 7.0 Hz, 3H, rear front-pointing CH(C*H*$_3$)$_2$), 0.74 (d, 7.0 Hz, 3H, front forward-pointing CH(C*H*$_3$)$_2$), 0.89 (d, 7.0 Hz, 3H, rear back pointing CH(C*H*$_3$)$_2$), 1.00 (d, 7.0 Hz, 3H, front back-pointing CH(C*H*$_3$)$_2$), 1.005 (d, 7.2 Hz, P(C*H*$_3$)$_2$), 0.996 (d, 7.2 Hz, P(C*H*$_3$)$_2$), 1.29 (s, 3H, B–C*H*$_3$), 2.25 (sept, 6.9 Hz, 1H, front C*H*Me$_2$), 2.28 (sept, 6.9 Hz, 1H, back C*H*Me$_2$), 4.95 (d, 2.1 Hz, 1H, H$_5$), 5.03 (dd, 4.5 Hz, 2.5 Hz, 1H, H$_4$), 5.14 (dd, 4.5 Hz, 2.5 Hz, 1H, H$_1$), 6.08 (m, 1H, H$_6$), 6.54 (m, 1H, H$_3$), 6.57 (m, 1H, H$_2$), 6.74 (m, 2H, Ph-H$_m$), 7.11–7.13 (m, 3H, Ph-H$_o$ and Ph-H$_p$). Key CycloNOE correlations: -0.07 (2.23 - front C*H*Me$_2$, P(C*H*$_3$)$_2$, H$_1$, H$_2$, H$_3$, Ph-H$_m$), -0.05 (Si(C*H*$_3$)$_2$, H$_1$, H$_5$), 0.35 (0.89 - rear back pointing CH(C*H*$_3$)$_2$, P(C*H*$_3$)$_2$, back C*H*(CH$_3$)$_2$, H$_4$, H$_6$), 0.40 (Si(C*H*$_3$)$_2$, back C*H*Me$_2$, 0.89 - rear back pointing CH(C*H*$_3$)$_2$, H$_4$), 2.23 (Zr–C*H*$_3$, 0.74, 1.00 - front CH(C*H*$_3$)$_2$, H$_5$, H$_6$, Ph-H$_m$), 2.28 (0.34, 0.89 - rear CH(C*H*$_3$)$_2$, H$_4$). 5.04 (H$_5$, rear C*H*(CH$_3$)$_2$, 0.40 -Si(C*H*$_3$)$_2$, 0.35 - rear front-pointing CH(C*H*$_3$)$_2$), 6.08 (0.35, 0.74, weak 0.89, P(C*H*$_3$)$_2$, front C*H*Me$_2$). ^{19}F NMR (470 MHz, C$_6$D$_6$/C$_6$D$_5$Br): -163.23 (t, 20.0 Hz, 6F, F$_m$), -160.81 (t, 20.5 Hz, 3F, F$_p$), -128.48 (d, 20.9 Hz, 6F, F$_o$).

Characterization of 18a. ^{1}H NMR (500 MHz, C$_6$D$_6$): δ = 0.02 (s, 3H, tetramethyldisilylene top front Si(C*H*$_3$)$_2$), 0.06 (s, 3H, Si(C*H*$_3$)$_2$), 0.07 (s, 3H, Si(C*H*$_3$)$_2$), 0.08 (s, 3H, Si(C*H*$_3$)$_2$), 0.24 (s, 3H, *i*Pr side dimethylsilylene Si(C*H*$_3$)$_2$), 0.32 (s, 3H, Si(C*H*$_3$)$_2$), 0.57 (s, 3H, Zr–C*H*$_3$), 0.61 (s, 3H, B–C*H*$_3$), 0.76 (d, 6.9 Hz, 3H, CH(C*H*$_3$)$_2$), 0.96 (d, 6.6 Hz, 3H, CH(C*H*$_3$)$_2$), 2.18 (sept, 6.9 Hz, 1H, C*H*Me$_2$), 5.82 (d, 2.1 Hz, 1H, H$_5$), 5.98 (t, 2.1 Hz, 1H, H$_3$), 6.53 (t, 2.7 Hz, 1H, H$_2$), 6.86 (dd, 2.8 Hz, 1.6 Hz, 1H, H$_1$), 7.13 (d, 1.7 Hz, 1H, H$_4$). Key CycloNOE correlations: 2.17 (exchange with 2.82, NOE with CH(C*H*$_3$)2, H$_5$,).

Characterization of 18b. ^{1}H NMR (500 MHz, C_6D_6): δ = -0.27 (s, 3H, *i*Pr side dimethylsilylene Si(CH_3)$_2$), -0.08 (s, 3H, tetramethyldisilylene top front Si(CH_3)$_2$), 0.08 (s, 3H, Si(CH_3)$_2$), 0.10 (s, 3H, Si(CH_3)$_2$), 0.12 (s, 3H, Si(CH_3)$_2$), 0.28 (s, 3H, dimethylsilylene Si(CH_3)$_2$), 0.37 (s, 3H, Zr–CH_3), 0.61 (s, 3H, B–CH_3), 0.93 (d, 6.9 Hz, 3H, CH(CH_3)$_2$), 0.95 (d, 6.6 Hz, 3H, CH(CH_3)$_2$), 2.81 (sept, 6.9 Hz, 1H, *C*HMe$_2$), 5.58 (t, 2.1 Hz, 1H, H_3), 5.63 (d, 2.1 Hz, 1H, H_5), 6.55 (t, 2.7 Hz, 1H, H_2), 6.61 (dd, 2.8 Hz, 1.8 Hz, 1H, H_1), 6.63 (d, 1.7 Hz, 1H, H_4). Key CycloNOE correlations: -0.27 (exchange with 0.24, NOE with 0.28 - dimethylsilylene Si(CH_3)$_2$, H_3, H_5), -0.08 (exchange with 0.02, NOE with H_1), 0.37 (*C*H(CH_3)$_2$, weak CH(CH_3)$_2$, H_2, H_3, H_5), 0.61 (Zr–Me, H_1, H_4), 2.82 (exchange with 2.17, CH(CH_3)$_2$, Zr-CH_3, H_5, weak H_2), ^{19}F NMR (480 MHz, C_6D_6):

Characterization of 19a. ^{1}H NMR (500 MHz, C_6D_6/C_6D_5Br): δ = 0.08 (s, 3H, Si(CH_3)$_2$), 0.16 (s, 3H, Si(CH_3)$_2$), 0.17 (s, 6H, Si(CH_3)$_2$ and Zr–CH_3), 0.22 (s, 3H, Si(CH_3)$_2$), 0.29 (s, 3H, Si(CH_3)$_2$), 0.45 (s, 3H, Si(CH_3)$_2$), 0.84 (d, 6.6 Hz, 3H, CH(CH_3)$_2$), 0.87 (d, 6.6 Hz, 3H, CH(CH_3)$_2$), 0.963 (d, 7.6 Hz, P(CH_3)$_2$), 0.957 (d, 7.2 Hz, P(CH_3)$_2$), 1.35 (s, 3H, B–CH_3), 2.31 (sept, 6.9 Hz, 1H, *C*HMe$_2$), 5.32 (m, 2H, H_3 and H_5), 6.21 (q, 3.0 Hz, 1H, H_4 or H_1 or H_2), 6.42 (m, 1H, H_4 or H_1 or H_2) 6.70–6.74 (m, 2H, Ph-H_m), 7.05 (m, 1H, H_4 or H_1 or H_2), 7.11–7.13 (m, 3H, Ph-H_o and Ph-H_p). Key CycloNOE data: 2.31 (both sets of CH(CH_3)$_2$, P(CH_3)$_2$, H_3 or H_5, weak Ph-H_m). ^{19}F NMR (470 MHz, C_6D_6/C_6D_5Br): -163.23 (t, 20.0 Hz, 6F, F_m), -160.81 (t, 20.5 Hz, 3F, F_p), -128.48 (d, 20.9 Hz, 6F, F_o).

Characterization of 19b. ^{1}H NMR (500 MHz, C_6D_6/C_6D_5Br): δ = -0.23 (s, 3H, Si(CH_3)$_2$), -0.15 (s, 3H, Si(CH_3)$_2$), -0.09 (s, 3H, Zr–CH_3), -0.08 (s, 3H, Si(CH_3)$_2$), 0.08 (s, 3H, Si(CH_3)$_2$), 0.21 (s, 3H, Si(CH_3)$_2$), 0.43 (s, 3H, Si(CH_3)$_2$), 0.88(d, 6.6 Hz, 3H, CH(CH_3)$_2$), 1.00 (d, 7.6 Hz, P(CH_3)$_2$), 0.99 (d, 7.2 Hz, P(CH_3)$_2$), 1.09 (d, 7.1 Hz, 3H, CH(CH_3)$_2$), 1.35 (s, 3H, B–CH_3), 2.05 (sept, 6.9 Hz, 1H, *C*HMe$_2$), 5.72 (t, 1.8 Hz, 1H, H_3), 5.74 (d, 1H, H_5), 6.42 (m, 1H, H_4), 6.61 (t, 2.8 Hz, 1H, H_2), 6.74 (m, 2H, Ph-H_m), 7.11–7.13 (m, 4H, H_1, Ph-H_o and Ph-H_p). Key CycloNOE data: -0.22 (P(CH_3)$_2$, H_4,), -0.09 (P(CH_3)$_2$, 1.09 – CH(CH_3)$_2$, *C*H(CH_3)$_2$, H_2, H_3, H_5, weak Ph-H_m), 2.10 (both sets of CH(CH_3)$_2$, P(CH_3)$_2$, Zr–CH3, weak H_4, very weak Ph-H_m). ^{19}F NMR (470 MHz, C_6D_6/C_6D_5Br): -163.23 (t, 20.0 Hz, 6F, F_m), -160.81 (t, 20.5 Hz, 3F, F_p), -128.48 (d, 20.9 Hz, 6F, F_o).

References and Notes

(1) (a) Brintzinger, H. H.; Fischer, D.; Mulhaupt, R.; Rieger, B.; Waymouth, R. M. *Angew. Chem., Int. Ed. Engl.* **1995**, *34*, 1143–1170. (b) Britovsek, G. J. P.; Gibson, V. C.; Wass, D. F. *Angew. Chem., Int. Ed. Engl.* **1999**, *38*, 428–447. (c) Bochmann, M. *J. Chem. Soc., Dalton Trans.* **1996**, 255–270.

(2) Coates, G. W. *Chem. Rev.* **2000**, *100*, 1223–1252.

(3) Resconi, L.; Cavallo, L.; Fait, A.; Piemontesi, F. *Chem. Rev.* **2000**, *100*, 1253–1345.

(4) (a) Alt, H. G.; Koppl, A. *Chem. Rev.* **2000**, *100*, 1205–1221. (b) Fink, G.; Steinmetz, B.; Zechlin, J.; Przybyla, C.; Tesche, B. *Chem. Rev.* **2000**, *100*, 1377–1390. (c) Rappe, A. T.; Skiff, W. M.; Casewit, C. J. *Chem. Rev.* **2000**, *100*, 1435–1456. (d) Angermund, K.; Fink, G.; Jensen, V. R.; Kleinschmidt, R. *Chem. Rev.* **2000**, *100*, 1457–1470. (e) Boffa, L. S.; Novak, B. M. *Chem. Rev.* **2000**, *100*, 1479–1493.

(5) Mitchell, J. P.; Hajela, S.; Brookhart, S. K.; Hardcastle, K. I.; Henling, L. M.; Bercaw, J. E. *J. Am. Chem. Soc.* **1996**, *118*, 1045–1053.

(6) (a) Giardello, M. A.; Eisen, M. S.; Stern, C. L.; Marks, T. J. *J. Am. Chem. Soc.* **1995**, *117*, 12114–12129. (b) Miyake, S.; Okumura, Y.; Inazawa, S. *Macromolecules* **1995**, *28*, 3074–3079. (c) Giardello, M. A.; Eisen, M. S.; Stern, C. L.; Marks, T. J. *J. Am. Chem. Soc.* **1993**, *115*, 3326–3327. (d) Ewen, J. A.; Elder, M. J.; Jones, R. L.; Haspeslagh, L.; Atwood, J. L.; Bott, S. G.; Robinson, K. *Makromol. Chem., Macromol. Symp.* **1991**, *48–9*, 253–295. (e) Spaleck, W.; Kuber, F.; Bachmann, B.; Fritze, C.; Winter, A. *J. Mol. Catal. A: Chem.* **1998**, *128*, 279–287.

(7) (a) Miya, S.; Mise, T.; Yamazaki, H. *Stud. Surf. Sci. Catal.* **1990**, *56*, 531–534. (b) Mise, T.; Miya, S.; Yamazaki, H. *Chem. Lett.* **1989**, 1853–1856.

(8) Ewen, J. A.; Elder, M. J. In *Ziegler Catalysts*; Fink, G., Mulhaupt, R., Brintzinger, H. H., Eds.; Springer-Verlag: Berlin, 1995; p 99–109.

(9) (a) Ewen, J. A. *J. Mol. Catal. A.* **1998**, *128*, 103–109. (b) Chien, J. C. W.; Llinas, G. H.; Rausch, M. D.; Lin, Y. G.; Winter, H. H.; Atwood, J. L.; Bott, S. G. *J. Polym. Sci. Pol. Chem.* **1992**, *30*, 2601–2617. (c) Llinas, G. H.; Dong, S. H.; Mallin, D. T.; Rausch, M. D.; Lin, Y. G.; Winter, H. H.; Chien, J. C. W. *Macromolecules* **1992**, *25*, 1242–1253. (d) Chien, J. C. W.; Llinas, G. H.; Rausch, M. D.; Lin, G. Y.; Winter, H. H. *J. Am. Chem. Soc.* **1991**, *113*, 8569–8570. (e) Mallin, D. T.; Rausch, M. D.; Lin, Y. G.; Dong, S. Z.; Chien, J. C. W. *J. Am. Chem. Soc.* **1990**, *112*, 2030–2031.

(10) Rieger, B.; Jany, G.; Fawzi, R.; Steimann, M. *Organometallics* **1994**, *13*, 647–653.

(11) Gauthier, W. J.; Corrigan, J. F.; Taylor, N. J.; Collins, S. *Macromolecules* **1995**, *28*, 3771–3778.

(12) Gauthier, W. J.; Collins, S. *Macromolecules* **1995**, *28*, 3779–3786.

(13) Bravakis, A. M.; Bailey, L. E.; Pigeon, M.; Collins, S. *Macromolecules* **1998**, *31*, 1000–1009.

(14) Busico, V.; Cipullo, R.; Talarico, G.; Segre, A. L.; Chadwick, J. C. *Macromolecules* **1997**, *30*, 4786–4790.

(15) (a) Stone, K. J.; Little, R. D. *J. Org. Chem.* **1984**, *49*, 1849–1853. (b) Venier, C. G.; Casserly, E. W. *J. Am. Chem. Soc.* **1990**, *112*, 2808–2809.

(16) (a) Herzog, T. A.; Zubris, D. L.; Bercaw, J. E. *J. Am. Chem. Soc.* **1996**, *118*, 11988–11989. (b) Herzog, T. A. In *Department of Chemistry, Division of Chemistry and Chemical Engineering*; California Institute of Technology: Pasadena, CA, 1997.

(17) The dilithio salts of ligands **8a** and **b** were fairly soluble in petroleum ether, so were used without isolation from the excess base in the subsequent metallation step.

(18) (a) Grassi, A.; Zambelli, A.; Resconi, L.; Albizzati, E.; Mazzocchi, R. *Macromolecules* **1988**, *21*, 617–622. (b) Asakura, T.; Nakayama, N.; Demura, M.; Asano, A. *Macromolecules* **1992**, *25*, 4876–4881.

(19) Beck, S.; Prosenc, M.-H.; Brintzinger, H.-H. *J. Mol. Catal. A.* **1998**, *128*, 41–52.

(20) (a) Jutzi, P.; Burford, N. *Chem. Rev.* **1999**, *99*, 969–990. (b) Jutzi, P. *Chem. Rev.* **1986**, *86*, 983–996.

(21) Guerra, G.; Cavallo, L.; Moscardi, G.; Vacatello, M.; Corradini, P. *Macromolecules* **1996**, *29*, 4834–4845.

(22) Razavi, A.; Vereecke, D.; Peters, L.; Dauw, K. D.; Nafpliotis, L.; Atwood, J. L. In *Ziegler Catalysts*; Fink, G., Mulhaupt, R., Brintzinger, H. H., Eds.; Springer-Verlag: Berlin, 1995; p 111–147.

(23) (a) Dahlmann, M.; Erker, G.; Bergander, K. *J. Am. Chem. Soc.* **2000**, *122*, 7986–7998. (b) Karl, J.; Dahlmann, M.; Erker, G.; Bergander, K. *J. Am. Chem. Soc.* **1998**, *120*, 5643–5652.

(24) White, D. P.; Brown, T. L. *Inorg. Chem.* **1995**, *34*, 2718–2724.

(25) Doherty, N. M.; Bercaw, J. E. *J. Am. Chem. Soc.* **1985**, *107*, 2670–2682.

(26) Roll, W.; Brintzinger, H. H.; Rieger, B.; Zolk, R. *Angew. Chem. Int. Edit. Engl.* **1990**, *29*, 279–280.

(27) Veghini, D.; Henling, L. M.; Burkhardt, T. J.; Bercaw, J. E. *J. Am. Chem. Soc.* **1999**, *121*, 564–573.

Chapter 4

C–H Bond Activation by Cationic Platinum(II) Complexes: Ligand Electronic and Steric Effects

Abstract

A series of *bis*(aryl)diimine-ligated methyl complexes of Pt(II) with variously substituted aryl groups has been prepared. The cationic complexes $[(ArN{=}CR{-}CR{=}NAr)PtMe(L)]^+[BF_4]^-$ (Ar = aryl; R = H, CH_3; L = water, trifluoroethanol) react smoothly with benzene at approximately room temperature in trifluoroethanol solvent to yield methane and the corresponding phenyl Pt(II) cations, via Pt(IV)-methyl-phenyl-hydrido intermediates. The reaction products of methyl-substituted benzenes suggest an inherent reactivity preference for aromatic over benzylic C–H bond activation, which can however be overridden by steric effects. For the reaction of benzene with cationic Pt(II) complexes bearing *3,5*-disubstituted aryl diimine ligands, the rate determining step is C–H bond activation; whereas for the more sterically crowded analogs with *2,6*-dimethyl-substituted aryl groups, benzene coordination becomes rate-determining. This switch is manifested in distinctly different isotope scrambling and KIE patterns. The more electron rich the ligand, as assayed by the CO stretching frequency of the corresponding carbonyl cationic complex, the faster the rate of C–H bond activation. Although at first sight this trend appears to be at odds with the common description of this class of reaction as electrophilic, the fact that the same trend is observed for the two different series of complexes, which have different rate-determining steps, suggests that this finding does not reflect the actual C–H bond activation process, but rather reflects only the relative ease of benzene displacing a ligand to initiate the reaction, *i. e.* the change in rates is mostly due to a ground state effect. The stability of the aquo complex ground state in equilibrium with the solvento complex increases as the diimine ligand is made more electron withdrawing. Several lines of evidence, including the mechanism of degenerate acetonitrile exchange for the methyl-acetonitrile Pt(II) cations in alcohol solvents, suggest that associative substitution pathways operate to get the hydrocarbon substrate into, and out of, the coordination sphere; *i. e.* the mechanism of benzene substitution proceeds by a solvent (TFE)-assisted associative pathway.

Introduction

Extensive research over the last 30 years aimed at the selective functionalization of alkanes by transition metal complexes[1] has discovered many examples of inter- and intramolecular C–H bond activation. Relatively few, however, lead to actual alkane functionalization.[2] We have concentrated on an example of electrophilic activation of alkanes by late transition metal complexes,[3] the so-called Shilov system (eq 1), in which Pt(II) catalyzes oxidation of alkanes to alcohols by Pt(IV) at 120 °C.[4] This system is not yet practical — it requires an expensive stoichiometric oxidant, the catalyst is unstable with respect to Pt metal formation, rates are too slow — but it does exhibit patterns of regioselectivity (1° > 2° >> 3°)[1d] as well as chemoselectivity (C–H bonds of RCH_3 are activated in preference to C–H bonds of RCH_2OH)[5] that would be of considerable practical interest if the above problems could be solved.

$$RCH_3 + [PtCl_6]^{2-} + H_2O \xrightarrow[H_2O,\ 120\ °C]{cat.\ [PtCl_4]^{2-}} \underset{(RCH_2Cl)}{RCH_2OH} + [PtCl_4]^{2-} + 2\,HCl \quad (1)$$

Studies by our group[5,6] and others[7] implicate a catalytic cycle consisting of three steps: (*i*) electrophilic activation of the alkane to yield a Pt(II)-alkyl compound; (*ii*) oxidation to a Pt(IV)-alkyl by $[PtCl_6]^{2-}$ via electron transfer; and (*iii*) nucleophilic attack by water or chloride ion at the alkyl to regenerate the Pt(II) complex and release the functionalized alkane (Scheme 1). Studies of protonolysis of R–Pt(II) — the microscopic reverse of C–H activation — were carried out on model systems to shed some light on the nature of step (*i*), and led to the conclusion that two intermediates are involved: a Pt(II)-C,H-η^2-alkane complex and a Pt(IV)-alkyl-hydrido complex.[8] These studies further suggested that cationic complexes of the form $[(N–N)PtR(L)]^+$, where N–N is a bidentate diamine or diimine and L is a weakly-bound solvent molecule or other ligand, should be capable of activating C–H bonds according to eq 2.

Scheme 1

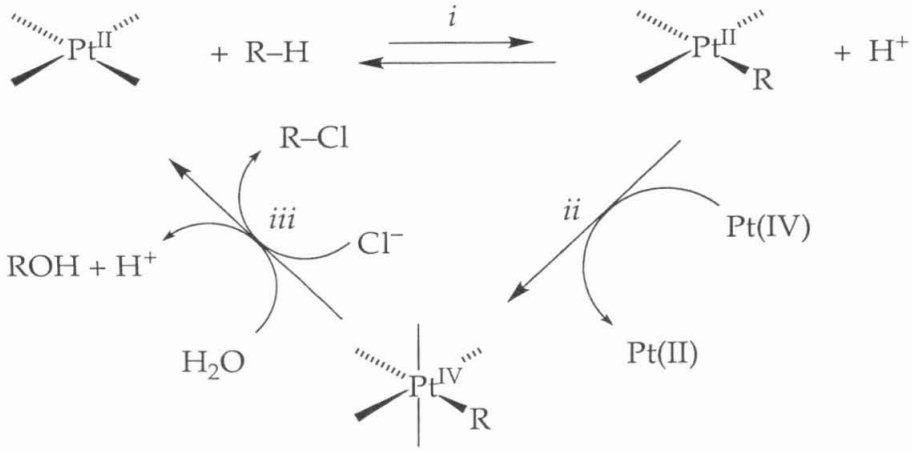

(2)

Two different examples confirming this prediction, where N–N = tetramethylethylenediamine and L = pentafluoropyridine,[9] or N–N = $Ar^fN{=}C(Me){-}C(Me){=}NAr^f$ (Ar^f = *3,5* -$(CF_3)_2C_6H_3$) and L = water and/or trifluoroethanol (TFE),[10] were subsequently reported.

The complexes with N-N = an α-diimine ligand and L = H_2O/TFE are particularly well suited for mechanistic investigation, since many reactions take place at a convenient rate at or near room temperature, and since the steric and electronic properties of the ligands can easily be varied. A detailed kinetics and mechanistic study on the reaction of $[(ArN{=}CMe{-}CMeN{=}Ar)PtMe(L)]^+$ (Ar = *2,6*-$(CH_3)_2C_6H_3$) with benzene supported the involvement of the two intermediates cited above, as well as a Pt(II)-(π-C,C-η^2-benzene) complex, formation of which appears to be the rate-determining step.[11] But several key questions remain unanswered. In particular, how does the reaction depend upon the electronic and steric properties of the metal center? One might intuitively expect that for these formally electrophilic activations, a more electron-deficient metal center would lead to a faster reaction. However, it is not clear whether the term "electrophilic" has real mechanistic significance or merely describes stoichiometry. Indeed, a recent observation for a related reaction of a cationic Ir complex suggests the *opposite* trend: the more electron-rich center

appears to react faster.[12] Changes in ligand properties might even change the rate-determining step, with possible consequences for selectivity. It is also unclear whether hydrocarbon enters the coordination sphere via an associative or dissociative mechanism.

To address some of these issues, we have initiated a series of kinetic and mechanistic investigation on the C–H activation of benzene by $[(ArN{=}C(R)–C(R)N{=}Ar)Pt(Me)(L)]^+(BF_4)^-$ (R = Me or H, L = H_2O/TFE) in which both the steric and electronic properties of Ar, and hence the overall complex, are varied over a significant range. We have also examined substitution reactions in the same system (L = MeCN). Based on these and other recent findings, we can construct a mechanistic description which appears consistent with all observations, even though it may fall somewhat short of a complete explanation.

Results

Synthesis of Diimine Ligands. The diimines ArN=CMe–CMeN=Ar (**1**, Ar = *3*-R^3-*4*-R^4-*5*-R^5-C_6H_2; **2**, Ar = *2,6*-$(CH_3)_2$-4-R^4-C_6H_2) — formally derivatives of 1,4-diazabutadiene — are prepared in moderate to good yields by condensing *2,3*-butanedione and the corresponding anilines in methanol with a catalytic amount of formic acid, or in toluene at 90 °C over 5Å molecular sieves[13] (Scheme 2). The latter procedure is particularly effective for the more electron-withdrawing anilines, and the use of 5Å molecular sieves is crucial in order to obtain a reasonable yield of the products.

Scheme 2

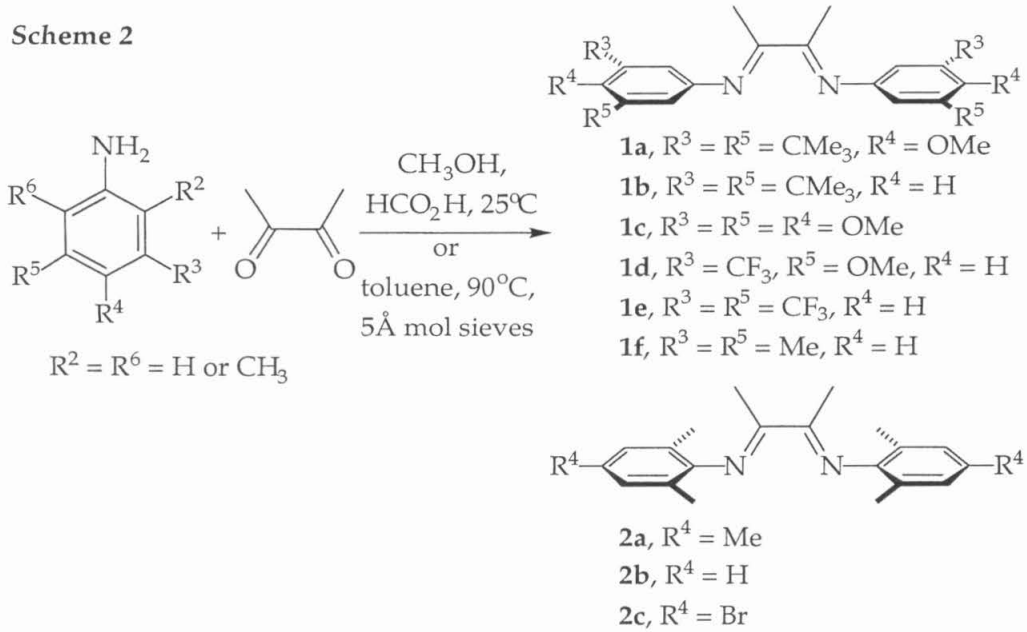

For comparison we wanted to have some examples of the analogous ligands *without* the backbone methyl substituents, ArN=CH–CHN=Ar. However, condensation reactions between *3,5*-disubstituted anilines and glyoxal (either as the trimer or the 40% aqueous solution) invariably yielded mixtures of unidentifiable products.[14] Instead, diimine **3** was prepared by reacting the corresponding iminophosphoranes[15] with glyoxal trimer in refluxing dry THF for 16 – 72 hours under an Ar atmosphere (**3a** and **b**, Scheme 3).[16]

Scheme 3

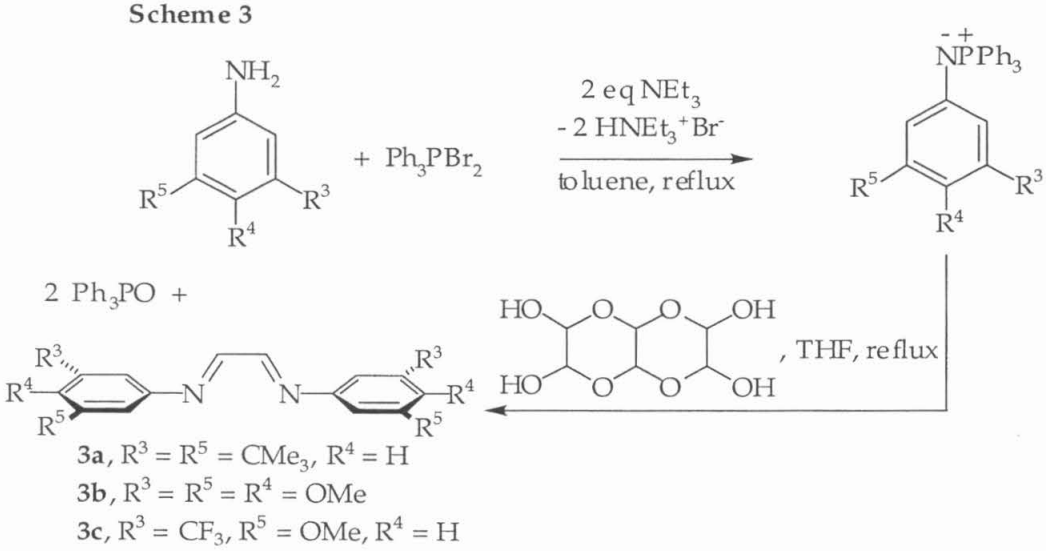

Preparation of Platinum Dimethyl Complexes. Diimine ligands **1–3** react with *bis*(dimethyl(μ-dimethylsulfide)platinum(II))[17] in toluene at room temperature to afford the corresponding platinum dimethyl complexes **4–6** in high yields (Scheme 4). The most useful feature for characterization is the [Pt–CH_3] signal, with its accompanying ^{195}Pt satellites, in the ^{1}H NMR. The shift is somewhat ligand-dependent: the resonance appears between 0.9 and 1.1 ppm for **4** and between 0.7 and 0.8 ppm for **5**, while the resonance for **6** is much further downfield at 1.65 ppm. However, the two bond platinum coupling is virtually the same, ~ 85 Hz, for all these dimethyl complexes.

Scheme 4

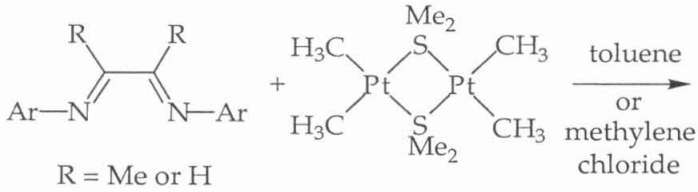

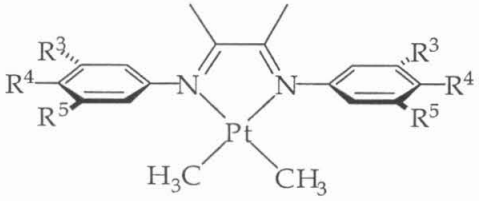

4a, $R^3 = R^5 = CMe_3$, $R^4 = OMe$
4b, $R^3 = R^5 = CMe_3$, $R^4 = H$
4c, $R^3 = R^5 = R^4 = OMe$
4d, $R^3 = CF_3$, $R^5 = OMe$, $R^4 = H$
4e, $R^3 = R^5 = CF_3$, $R^4 = H$
4f, $R^3 = R^5 = Me$, $R^4 = H$

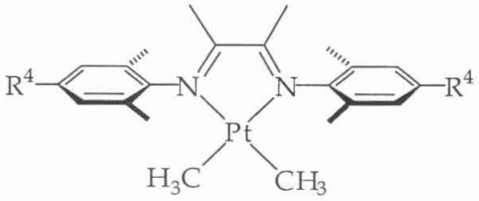

5a, $R^4 = Me$
5b, $R^4 = H$
5c, $R^4 = Br$

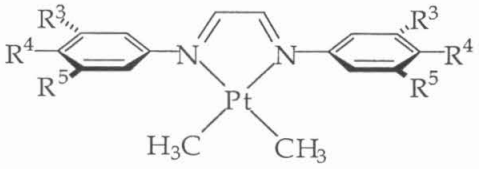

6a, $R^3 = R^5 = CMe_3$, $R^4 = H$
6b, $R^3 = R^5 = R^4 = OMe$
6c, $R^3 = CF_3$, $R^5 = OMe$, $R^4 = H$

Preparation of Platinum (II) Methyl Carbonyl Cations. Addition of one equivalent of HBF_4 (aq) to a solution of **4–6** in trifluoroethanol generates a mixture of solvento and aquo adducts (*vide infra*) of the platinum(II) methyl

cation, which upon exposure to 1 atmosphere of carbon monoxide converts cleanly to the corresponding platinum methyl carbonyl cation **7–9** (Scheme 5).

Scheme 5

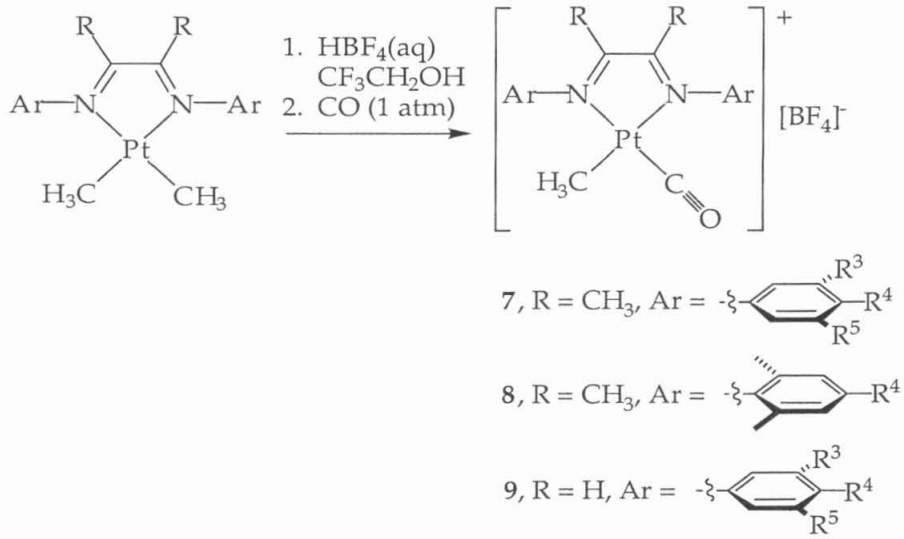

In many instances, addition of CO causes the solution to change from orange or red to yellow almost instantaneously (except for **9b**, in which case the solution turned to wine red). The Pt–C*H*$_3$ resonances (in CD_2Cl_2) shift ~ 0.2 ppm upfield compared to those of the corresponding dimethyl complexes, while $^2J_{Pt-H}$ decreases from ~ 85 Hz to ~ 66 Hz. As a result of the reduced symmetry the backbone R groups are now inequivalent, which is displayed in the NMR spectra, particularly in the $^3J_{Pt-H}$ values. For example, **9a** exhibits R = *H* backbone signals at 9.29 and 9.04 ppm with coupling constants of 38 and 74 Hz, respectively. The difference of $^4J_{Pt-H}$ for the backbone methyl groups in **8** is less dramatic: the lower field resonance has a coupling constant of ~ 6 Hz, while no platinum satellite is discernible for the upper field resonance. For **7**, no platinum satellite can be observed for *either* backbone methyl resonance.

All the carbonyl cations appear to be indefinitely stable in trifluoroethanol under 1 atm of CO, but **7d** and **7e** decompose rapidly in the solid state, or in methylene chloride in the absence of excess CO. In TFE-d_3 the backbone methyls of **7e** became fully deuterated within an hour at room temperature. Isolated **9b** appeared to contain a small amount of paramagnetic material that significantly broadened the spectrum. The carbonyl IR stretching frequencies of complexes **7–9** are reported in Table 1.

Table 1. Infrared carbonyl stretching frequencies for $[(N—N)Pt(CH_3)(CO)]^+[BF_4]^-$ (**7–9**) in methylene chloride solution.

	N—N	ν_{CO} (cm^{-1})		N—N	ν_{CO} (cm^{-1})
7a	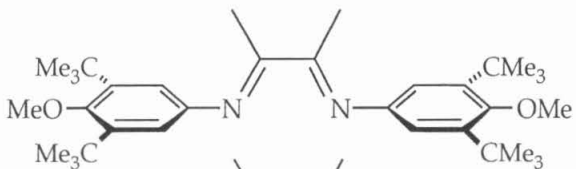	2103.5	**8a**	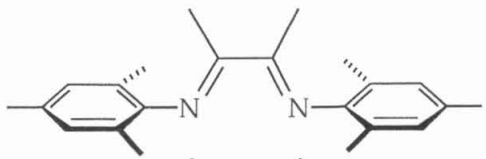	2108.3
7b	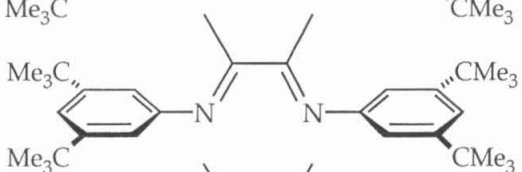	2104.6	**8b**	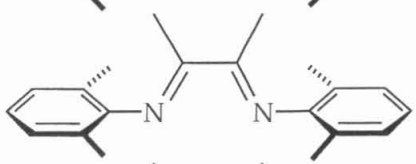	2109.6
7c	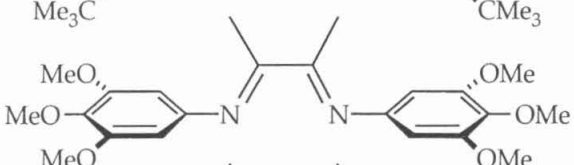	2105.8	**8c**	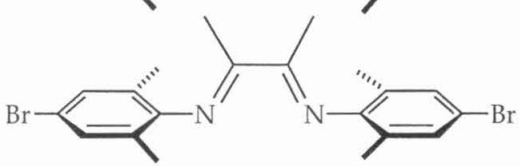	2111.1
7d	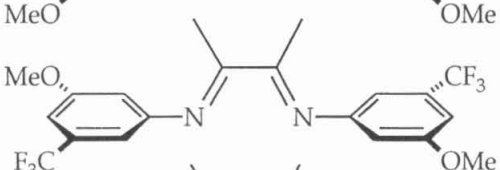	2110.1	**9a**	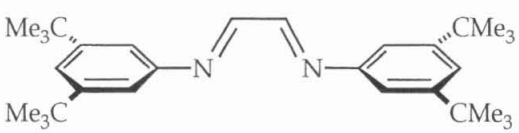	2108.8
7e	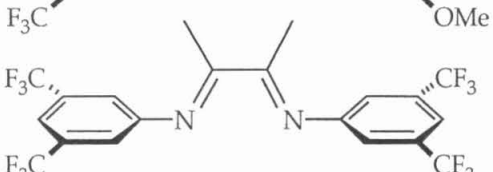	2113.5	**9b**	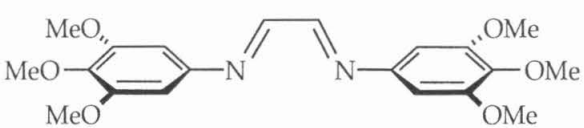	2110.3
7f	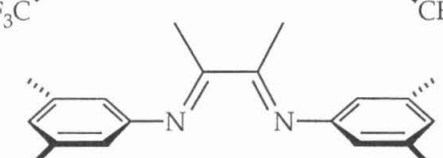	2105.7	**9c**	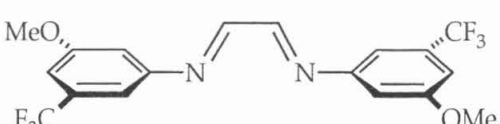	2116.0

Generation of Platinum (II) Methyl-Aquo/Solvento Cations. Protonolysis of Pt(II) dimethyl complexes **4–6** by aqueous HBF_4 in TFE generates the corresponding methyl cations as an equilibrium mixture of aquo and solvento adducts **10–12** (Scheme 6).[10,11]

Scheme 6

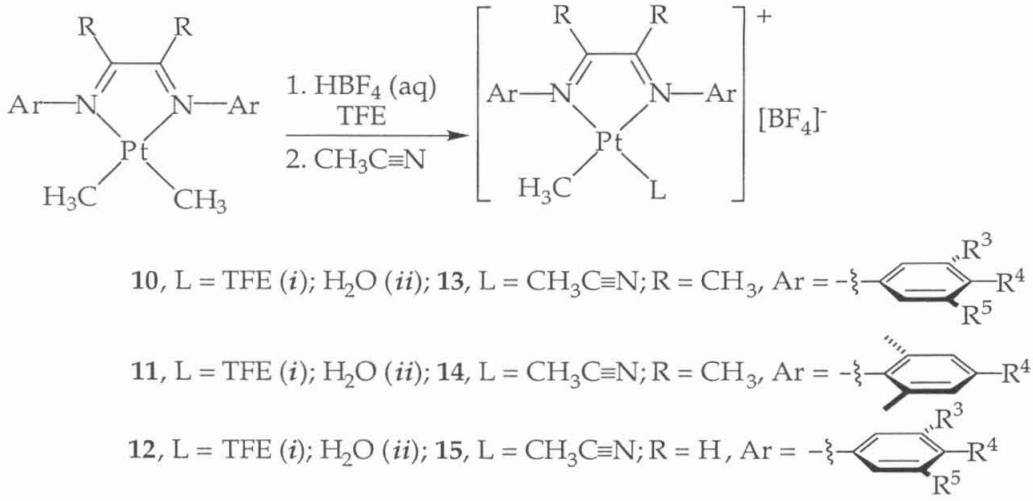

The stoichiometry need not be exactly 1:1, as the Pt–Me groups of cationic complexes do not readily react with the slight excess of acid. Subsequent addition of a slight excess of acetonitrile (or carrying out the initial protonolysis in acetonitrile solution) affords the acetonitrile adducts **13–15**. The platinum satellites for the Pt–CH_3 signals for **10–12** are extremely broad, in contrast to the relatively sharp satellites observed for the corresponding carbonyl (**7–9**) and acetonitrile (**13–15**) adducts.

Protonolysis of **4–6** in TFE-d_3 results in liberation of CH_4 as well as CH_3D, with concomitant formation of [Pt–CH_2D] and [Pt–CH_3] cations (eq 3).

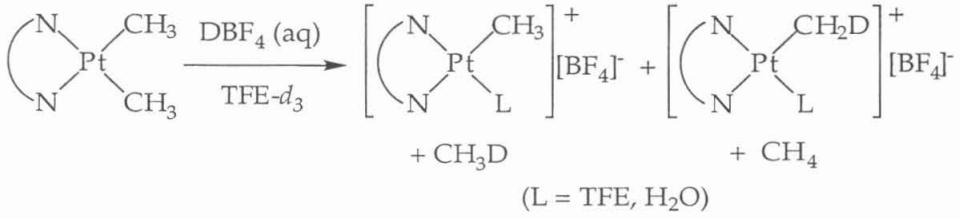

(3)

Within integration error limits, the ratio of CH_4 to CH_3D equals that of [Pt–CH_2D] to [Pt–CH_3]. No multiple deuteration was observed for either the methane or the [Pt-methyl]. When protonolysis of **4b** was carried out in the presence of added acetonitrile, the ratio of CH_3D to CH_4 was found to increase with the acetonitrile concentration (Figure 1).

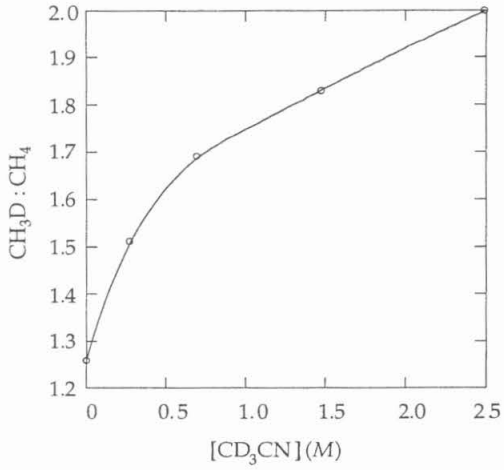

Figure 1. The ratio of CH_3D:CH_4 generated in the protonolysis of **4b** in TFE-d_3 as a function of acetonitrile concentration.

Cations **10–12** decompose over the course of several weeks at room temperature in TFE solution. For **10a/b** and **12a** a single (or major) species is formed, accompanied by methane liberation. NMR (^1H and ^{19}F) is consistent with a $(\mu\text{-OH})_2$ dimeric structure (**16**). This was confirmed for **16b**, the decomposition product of **10b**, by a crystal structure determination.[18] The analogous phenyl complexes **17** and **19** (*vide infra*) react similarly, evolving benzene (eq 4). In contrast, the decomposition of **11** yielded a mixture of unidentifiable products. The decomposition is accelerated by higher platinum concentrations and retarded by added water; the mechanism for the formation of $(\mu\text{-OH})_2$ dimer is not clear.

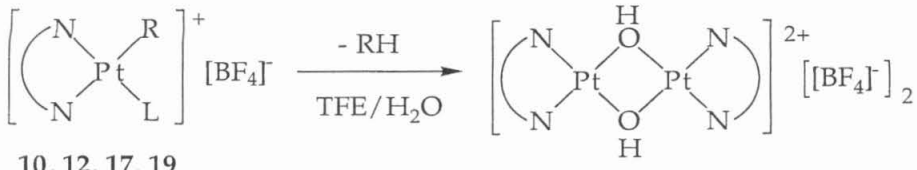

(4)

10, 12, 17, 19
(R = CH_3, C_6H_5;
L = TFE, H_2O)

16

Equilibria between Aquo and Solvento Complexes. Addition of 1 equivalent of aqueous HBF_4 (which contains approximately 5 moles of H_2O per mole of HBF_4) at 25 °C to a suspension of 0.007 mmol of (**4**) in 0.7 mL of TFE-d_3 results in two Pt-CH_3 signals in the ^{1}H NMR, in ratios ranging from ~ 1.5:1 (**10a**) to > 10:1 (**10e**). For **10a**, addition of water further increases the relative intensity of the major peak, which is accordingly assigned to aquo complex **10a*ii***. The equilibrium between the solvento and aquo adducts (eq 5) greatly favors the latter for all ligands examined here. The magnitude of the equilibrium constant depends on the ligands (Table 2): the more electron-withdrawing the diimine substituents (indicated by a higher carbonyl stretching frequency for the analogous methyl-carbonyl cation, *vide supra*), the larger the equilibrium constant. Moreover, for the same diimine ligand, the equilibrium constant for the platinum(II) phenyl cation (**17** and **18**) is greater than for the methyl cation (**10** and **11**). The equilibrium constants for **12** and **19** are too large to be determined accurately; they are all greater than 3×10^3.

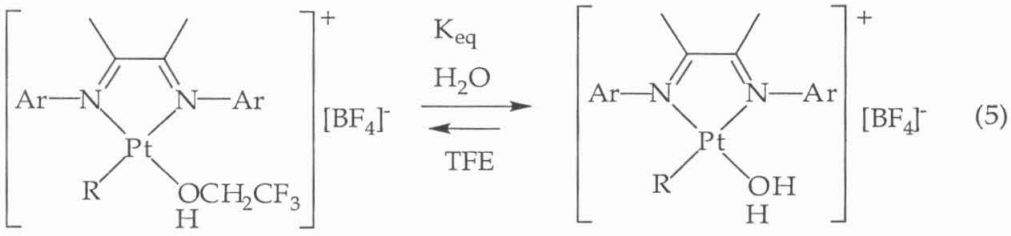

(5)

i *ii*

10, R = CH_3, Ar = 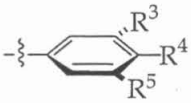

17, R = C_6H_5, Ar = 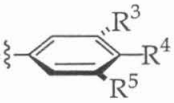

11, R = CH_3, Ar = 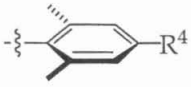

18, R = C_6H_5, Ar = 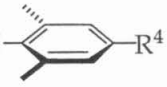

Table 2. Equilibrium constants between ***i*** and ***ii*** for $[(N—N)Pt(R)(L)]^+[BF_4]^-$ (**10** and **11**, R = CH_3, **17** and **18**, R = C_6H_5; ***i***, L = TFE; ***ii***, L = H_2O) in TFE/water mixtures at 20 °C.

	$\mathbf{10}i \underset{}{\overset{K_{eq}}{\rightleftharpoons}} \mathbf{10}ii$	$\mathbf{17}i \overset{K_{eq}}{\rightleftharpoons} \mathbf{17}ii$
a ($R^3 = R^5 = CMe_3$, $R^4 = OMe$)	3.9×10^2	6.6×10^2
b ($R^3 = R^5 = CMe_3$, $R^4 = H$)	4.3×10^2	7.4×10^2
c ($R^3 = R^4 = R^5 = OMe$)	7.5×10^2	9.6×10^2
d ($R^3 = OMe$, $R^5 = CF_3$, $R^4 = H$)	1.4×10^3	1.8×10^3
e ($R^3 = R^5 = CF_3$, $R^4 = H$)	2.8×10^3	4.0×10^3
	$\mathbf{11}i \overset{K_{eq}}{\rightleftharpoons} \mathbf{11}ii$	$\mathbf{18}i \overset{K_{eq}}{\rightleftharpoons} \mathbf{18}ii$
a ($R^2 = R^6 = Me$, $R^4 = Me$)	7.8×10^2	1.5×10^3
b ($R^2 = R^6 = Me$, $R^4 = H$)	9.5×10^2	1.8×10^3
c ($R^2 = R^6 = Me$, $R^4 = Br$)	1.6×10^3	3.1×10^3

Reactions between Platinum(II) Methyl Cations and Benzene. Platinum(II) methyl cations **10–12** react cleanly with benzene, or with partially or completely deuterated benzene (*vide infra*), to form the corresponding platinum(II) phenyl complexes **17–19** respectively, with concurrent production of methane (eq 6).

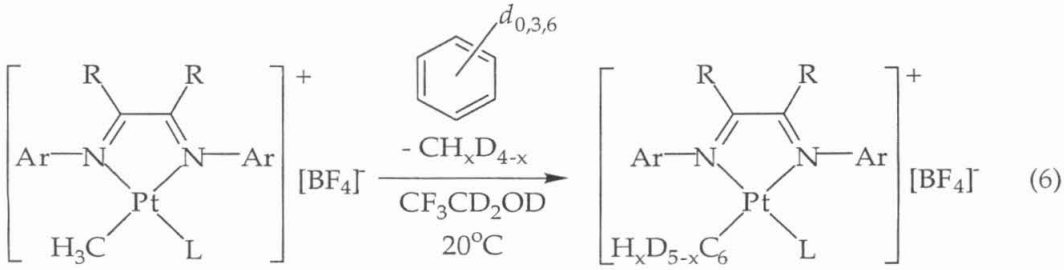

(L = TFE (*i*); H_2O (*ii*))

(L = TFE (*i*); H_2O (*ii*))

10

11

12

17, R = CH_3, Ar = 

18, R = CH_3, Ar = 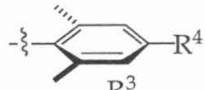

19, R = H, Ar = 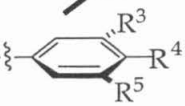

Under reaction conditions where both the solvento and aquo cations are observable by ^{1}H NMR, the two species disappear at the same rate, and the solvento and aquo adducts of the phenyl products appear at the same rate. No other species were observed up to 3 half lives; the (μ-OH)$_2$ dimers **16** can be observed at later stages of reaction. In all cases the rates of (μ-OH)$_2$ dimer formation (eq 4) from either the starting materials **10–12** or the products **17–19** are at least an order of magnitude slower than those of benzene C–H bond activation, so the rate constants reported below should not be affected by this secondary reaction to any significant degree.

At elevated temperatures (> 60 °C), the platinum (II) methyl acetonitrile cations **13b** and **13d** were also able to activate C–H(D) bonds in benzene (benzene-d_6) to form the corresponding platinum (II) phenyl acetonitrile cations **20b** and **20d** (eq. 7). The half life for the reaction between **13b** and 0.82 *M* C_6D_6 in TFE is ~ 12.8 hours at 60 °C and 1.5 hours at 82 °C. Formation of platinum black was observed after prolonged heating at these temperatures(~ 3 hours at 80 °C).

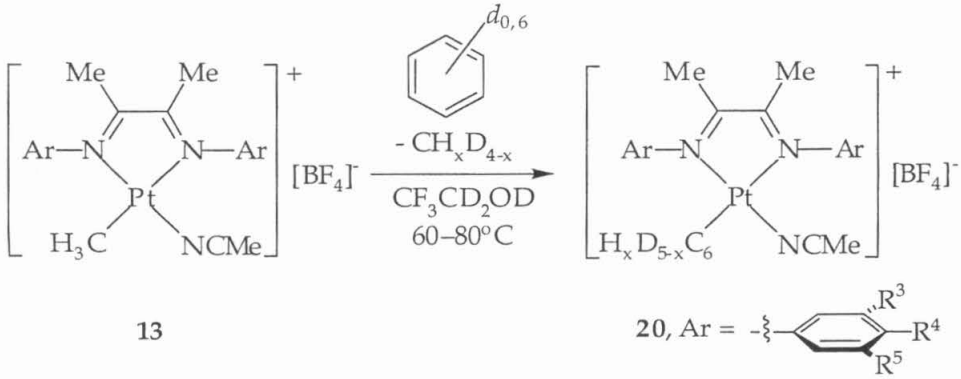

Kinetics of Benzene C-H Bond Activation. ^{1}H NMR was used to monitor the disappearance of starting material and/or the appearance of product, from which rates were determined. Figure 2 shows the results of a typical experiment, for the reaction between **10b** ([H_2O] = 2.72 *M*, where only aquo adducts are detectable) and benzene in TFE-d_3. The values of the calculated rate constants, k_{obs}, for the various complexes under different sets of conditions can be found in the supplementary materials (Appendix B, Tables 1 – 12). Additional kinetics experiments were carried out in several cases, particularly for **10a** and **10b**. The reaction rates are not affected by ionic strength; for example, the observed rate constant for the reaction between **10a** and benzene at [D_2O] = 1.33 *M*, [C_6H_6] = 0.25 *M* and [Pt] = 0.01 *M* is $1.8 \pm 0.2 \times 10^{-4}$ s^{-1} with no added NMe_4BF_4, and $1.9 \pm 0.2 \times 10^{-4}$ s^{-1} with [NMe_4BF_4] = 0.12 *M*. Hence most of the kinetic studies were run without controlling ionic strength. However, it should be noted that the rates did show a slight decrease in the presence of weakly coordinating anions such as triflate (Appendix B, Table 12).

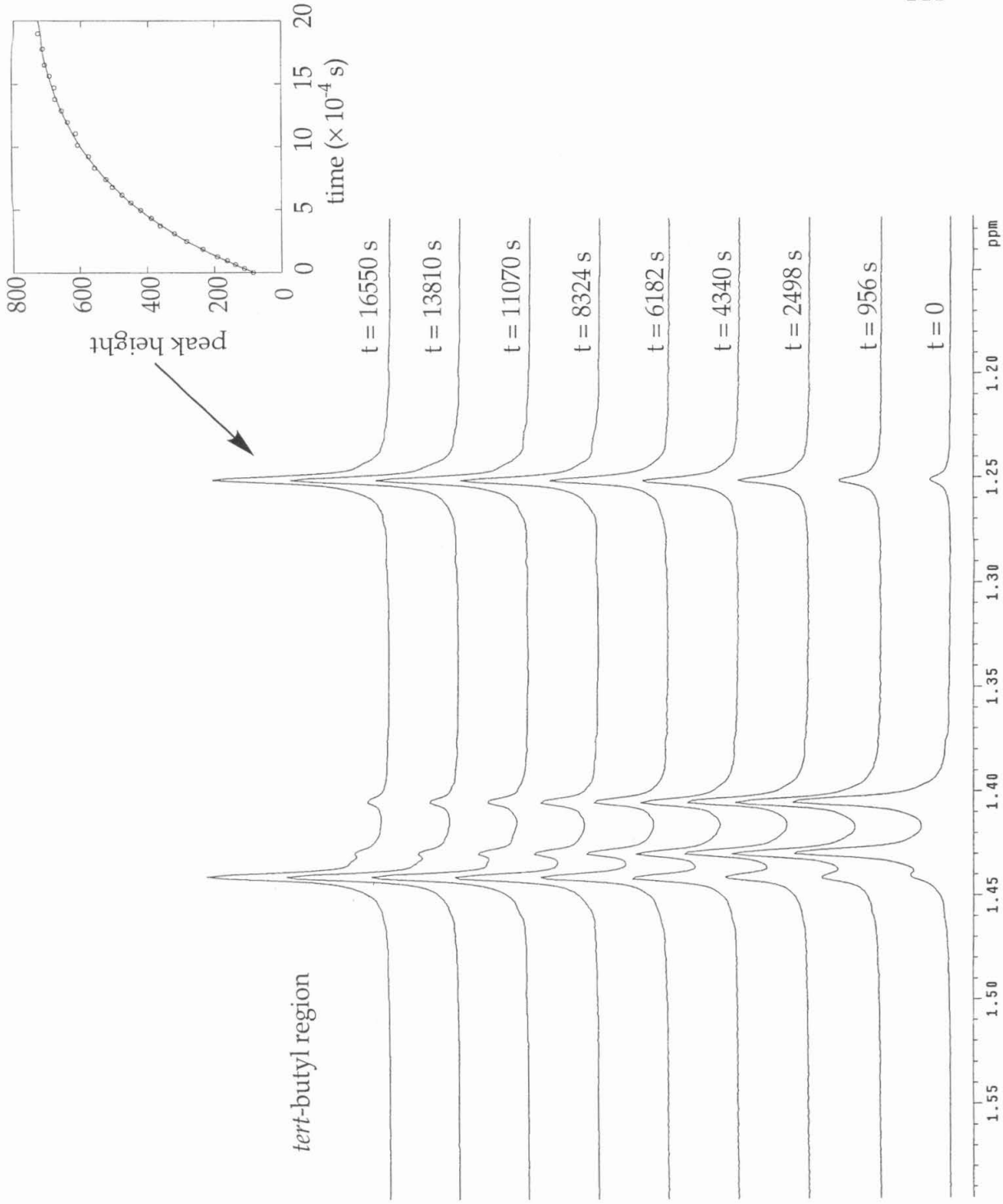

Figure 2. The *tert*-butyl region of the ^{1}H NMR spectra, showing changes for the reaction between benzene and **10b**. $[D_2O] = 2.72\ M$, $[C_6H_6] = 0.47\ M$, $[Pt] = 0.01\ M$. The inset shows an exponential curve fit of the peak height at 1.25 ppm versus time.

As previously found for **11b**,[11] the rates of benzene C–H bond activation are decreased by added water, and $1/k_{obs}$ is linear with respect to $[D_2O]/[C_6H_6]$ (Figure 3). The slope of the line (and, thus, k_{obs}) depends significantly on the ligand (Figure 4). The plot of k_{obs} vs $[C_6H_6]/[D_2O]$ deviates from linearity at very low water concentrations (Figure 5).

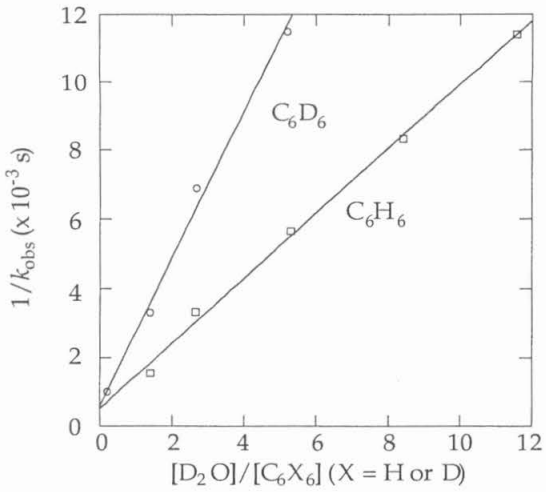

Figure 3. The inverse of observed rate constants in the reactions of **10a** with benzene varies linearly with the water:benzene concentration ratio.

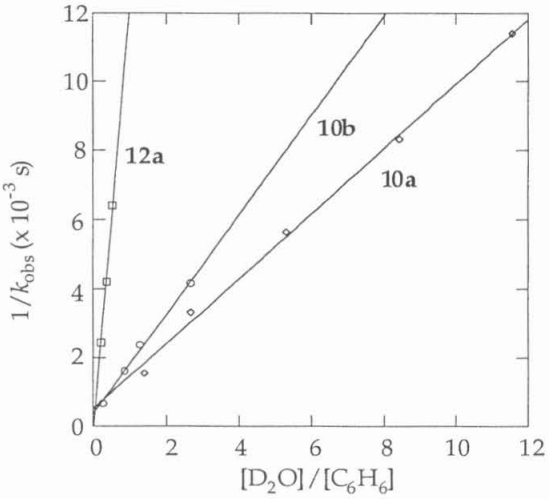

Complex	Slope (x 10^{-2})
10a	9.4
10b	14.4
12a	122

Figure 4. For the reactions of various Pt(II) methyl cations with benzene, the inverse of observed rate constants is linear with respect to water:benzene concentration ratio. The slopes of the lines vary greatly from cation to cation.

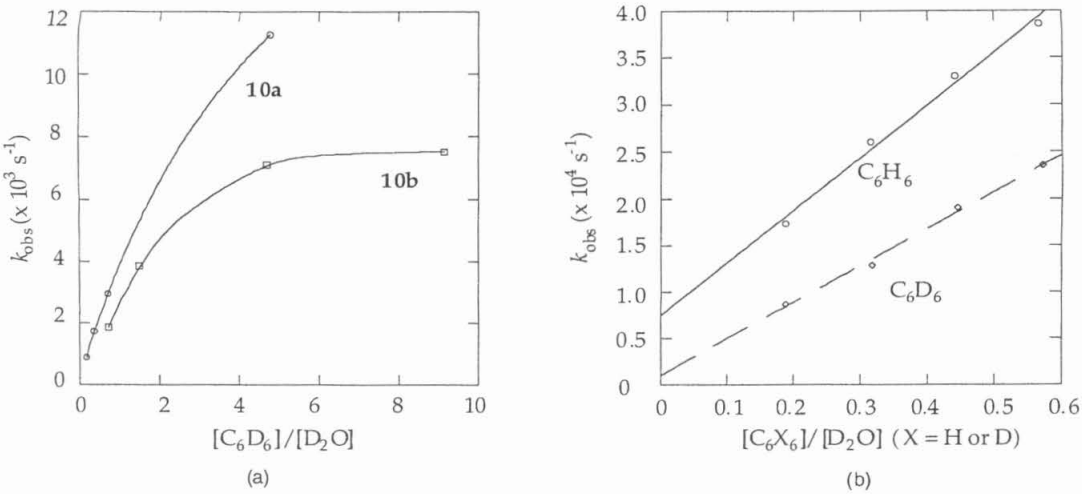

Figure 5. (a) A plot of k_{obs} vs. $[C_6D_6]/[D_2O]$ deviates from linearity at low water concentrations. ([Pt] = 0.01 *M*, $[C_6D_6]$ = 0.25 *M*). (b) For reactions of **10a** and benzene at high water concentrations, k_{obs} is linear with respect to $[C_6D_6]/[D_2O]$ ([Pt] = 0.01 *M*, $[D_2O]$ = 1.23 – 1.30 *M*).

The temperature dependence was studied over the range of 0 – 55 °C for the reaction between **10b** and C_6H_6, and over the range of 0 – 30 °C for the reaction between **10b** and C_6D_6. The water concentration was kept sufficiently high such that aquo adducts account for >90% of the Pt(II) species. The overall activation parameters were calculated from Eyring plots such as the one shown in Figure 6, and gives $\Delta H^{\ddagger}$ = 20 kcal·mol^{-1} , $\Delta S^{\ddagger}$ = 5 e.u. for C_6H_6 activation and $\Delta H^{\ddagger}$ = 20.5 kcal·mol^{-1}, $\Delta S^{\ddagger}$ = 6 e.u. for C_6D_6 activation. The entropy of activation may be contrasted to that found for **11b**, for which a $\Delta S^{\ddagger}$ of -16 e.u. was measured.[11]

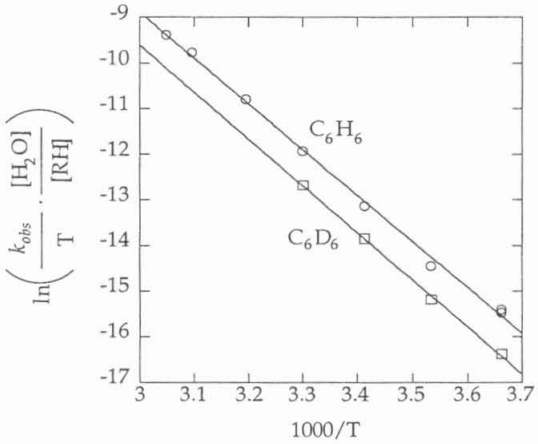

Figure 6. Eyring plot for the reactions of **10b** with C_6H_6 and C_6D_6.

Deuterium Scrambling. Earlier studies on **11b**[11] found that (a) <5% deuterium incorporation was observed in the methane generated in the reactions with C_6H_6 in TFE-*d*$_3$; and (b) nearly complete statistical scrambling of isotopes takes place in the reaction with either C_6D_6 or *1,3,5*-$C_6H_3D_3$. For complexes **10**, again, there is no incorporation of label from solvent, but in contrast there is only partial scrambling of protium and deuterium among the methyl group and deuterobenzenes. For example, when **10b** reacts with C_6D_6, the methane evolved consisted mostly of CH_3D (~ 60%) and CH_2D_2 (~ 30%). Even less scrambling has been observed for complexes **12**. For example, when **12a** reacts with C_6D_6, CH_2D_2 and higher isotopomers accounted for < 10% of the liberated methane. ^{1}H NMR shows that label is also incorporated into the methyl group of unreacted starting material, up to ~ 20% of [Pt–CH_2D]. For **11a** and **11c** the results are very similar to those of **11b**: reactions with C_6D_6 produced CH_2D_2 and CHD_3 as the major methane isotopomers, although deuterium incorporation into the unreacted platinum-methyl group is observed here as well.

Kinetic Deuterium Isotope Effects. KIEs were determined by three different methods: (1) in parallel reactions, separately determining the rate constants for reactions of C_6H_6 and C_6D_6 under the same conditions; (2) intermolecular competition, determining (by ^{1}H NMR) the isotopic composition of methane liberated in reaction with 1:1 C_6H_6 : C_6D_6, and (3) intramolecular competition, using *1,3,5*-$C_6H_3D_6$. The results are shown in Table 3. Note that the two competition methods give values[19] that are somewhat (but consistently) lower than those measured by parallel reactions (*vide infra*).

Table 3. *Kinetic* deuterium isotope effects for benzene C–L (L = H, D) bond activation reactions.

complex	T (°C)	method	k_H/k_D
10a	20	parallel	2.0
10b	20	parallel	2.2
10b	20	1,3,5-$C_6H_3D_3$	1.8
10b	20	1:1 C_6H_6:C_6D_6	1.9
10c	20	parallel	1.9
10c	20	1:1 C_6H_6:C_6D_6	1.6
10d	20	parallel	2.2
10d	20	1:1 C_6H_6:C_6D_6	2.0
10e	20	parallel	2.2
11a	35	parallel	1.1
11b	35	parallel	1.1
11c	35	parallel	1.1
12a	20	parallel	5.0
12b	20	parallel	3.6
12c	20	parallel	5.9

Reactions of 10b with Other Aromatic Hydrocarbons. The regioselectivity for the C–H bond activation for alkyl-substituted aromatic compounds appears to be affected by the steric bulk of both the substrates and

the ligand. Whereas **11b** reacts with *p*-xylene predominantly at the benzylic position (eq 8)[20], the reaction between **10b** and *p*-xylene results almost exclusively in aryl C–H bond activation (eq 9).

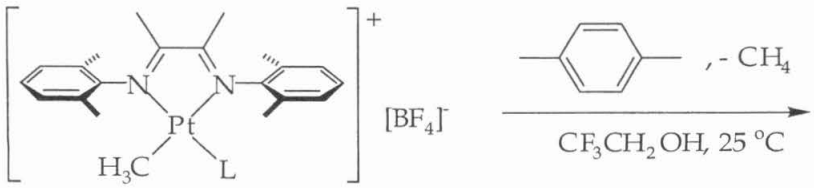

(L = TFE (*i*); H_2O (*ii*))

11b

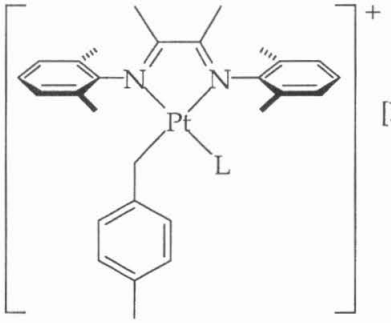

(8)

(L = TFE (*i*); H_2O (*ii*))

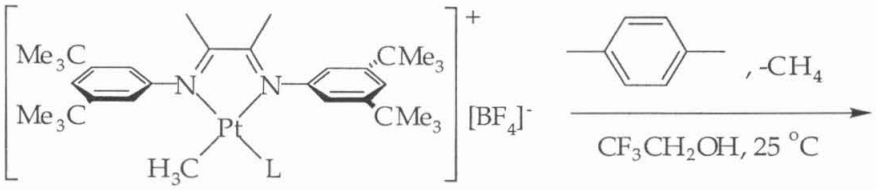

(L = TFE (*i*); H_2O (*ii*))

10b

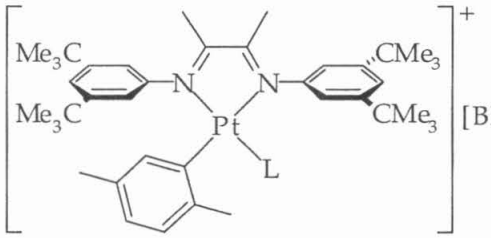

(9)

(L = TFE (*i*); H_2O (*ii*))

21b

In order to simplify the NMR, the mixture of **21b*i*** and **21b*ii*** was converted to the corresponding acetonitrile adduct; its ^1H NMR shows three *tert*-butyl resonances in the ratio of 2:1:1, which we interpret as resulting from hindered rotation of

one of the two ligand aryl groups, presumably the one attached to the N atom *cis* to the xylyl group. The aryl H resonances reflect the same reduced symmetry: five peaks in 1:1:1:1:2 ratio correspond to two non-equivalent ortho protons plus a para proton on one ring, and two equivalent ortho protons plus a para proton on the other (freely rotating) one.

In contrast, the reaction between mesitylene and **10b** proceeds mainly through benzylic C–H bond activation (Scheme 7).

Scheme 7

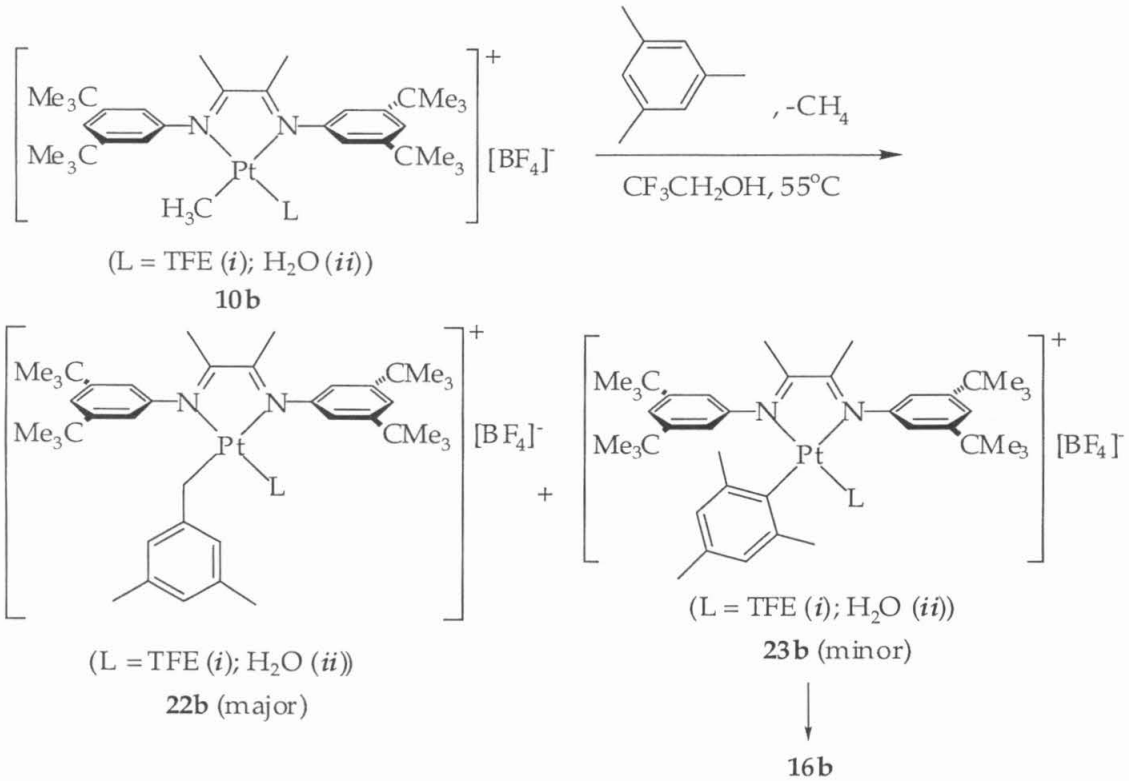

In the latter case, the selectivity for benzylic activation decreases at higher temperatures. At 25 °C, a ratio of 95:5 of benzylic activation product **22b** to aromatic activation product **23b** was observed, whereas at 55 °C, the selectivity dropped to 3:1. The product resulting from aromatic C–H bond activation appears to be much less stable than that from benzylic C–H activation: during the reaction between **10b** and mesitylene, the ^{1}H NMR resonances corresponding to **23b** initially grow in intensity and then disappear gradually, with formation of (μ-OH)$_2$ dimer **16b**. Compared to benzene C–H bond

activation, the reaction between **10b** and *p*-xylene is approximately 3 times slower, while that with mesitylene is approximately 10 times slower.

The kinetic deuterium isotope effects for reactions between **10b** and *p*-xylene and mesitylene were measured (parallel reactions method at 25 °C). These also appear to depend on steric bulk of the substrates: k_H/k_D = 2.2 for benzene (C_6X_6); 1.5 for *p*-xylene ($C_6X_3(CX_3)_2$); 1.2 for mesitylene ($C_6X_3(CX_3)_3$) (X = H, D).

Electron-deficient or extremely bulky aromatic compounds react sluggishly, or not at all, with **10b** at room temperature. For example, when 30 equivalents of *1,4*-di(*t*-butyl)benzene was added to a 0.01 M TFE-d_3 solution of **10b** ([H_2O] = 0.05 *M*), 85% of the starting material remained after 24 hours at room temperature. The ^1H NMR of the reaction mixture showed several broad, as yet unidentified new peaks. Similarly, **10b** showed little reactivity toward pentafluorotoluene or *1,4*-$(CF_3)_2C_6H_4$ after several hours at room temperature.

Acetonitrile Exchange Reactions. In order to shed some light on whether dissociative or associative substitution pathways operate in these systems, we briefly investigated the isotopic exchange between a Pt(II)-bound CH_3CN and free CD_3CN in several alcoholic solvents (Scheme 8), using ^1H NMR spectroscopy to follow the disappearance of bound acetonitrile and appearance of free CH_3CN.

Scheme 8

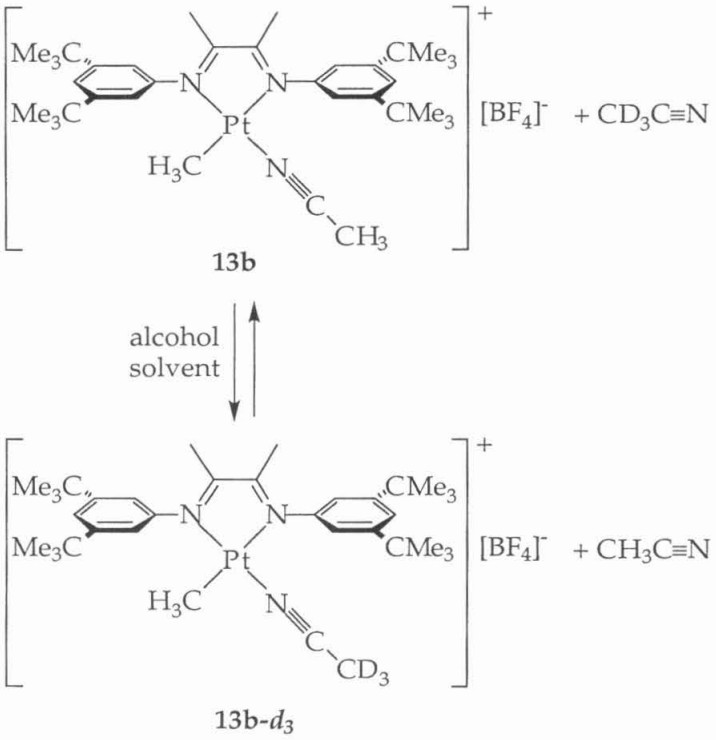

The rate constants for exchange of **13b** in CD_3OD, as a function of CD_3CN concentration and temperature, is shown in Figure 7. The shapes of the curves indicate a rate law of the form $k_{ex} = k_1 + k_2[CD_3CN]$, where the first term represents a dissociative or solvent-assisted pathway whose rate constant is determined from the intercept of the extrapolated linear part of the plot, and the second term a direct associative path whose rate is obtained from the slope of the latter. Eyring plots between 20 – 40 °C have been constructed for k_s (= $k_1/[CD_3OD]$) and k_2 (Figure 8); both lead to calculated negative entropies of activation, although the precision of the data and small range of temperatures limits our confidence in these values.

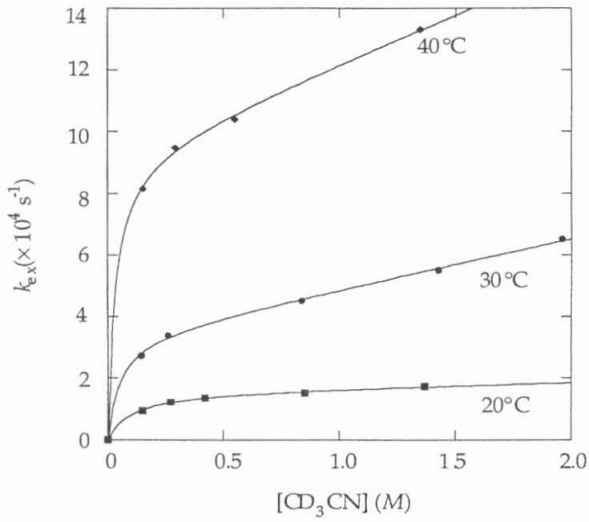

Figure 7. Plot of observed rate constants for exchange of free and bound acetonitrile versus free [acetonitrile] for **13b** at various temperatures.

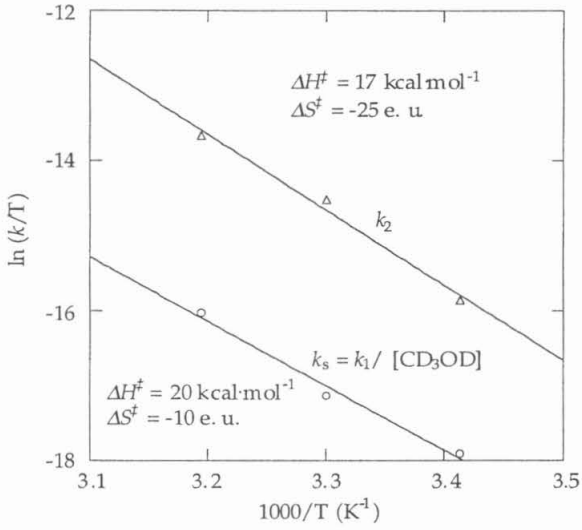

Figure 8. Eyring plots for second order acetonitrile exchange rate constants for both solvent-assisted pathway (k_S) and direct exchange pathway (k_2) for **13b**.

The exchange reactions in different solvents at 40 °C were also investigated, with the results shown in Figure 9. Rate constants were calculated in the same manner, and are displayed in Table 4. We also briefly examined the dependence of the exchange rates on the ligands. Under similar conditions ([CD_3CN] = 1.3 *M* , T= 40 °C, solvent = TFE-d_3), the exchange between bound

and free acetonitrile for **13d** (Ar = *3*-OMe-*5*-CF_3-C_6H_3) was *ca.* 6 – 7 times faster than for **13b** (Ar = *3,5*-Me_2-C_6H_3); and that for **14c** (Ar=*2,6*-Me_2-4-Br-C_6H_2) is *ca.* 3.5 times faster than for **14b** (Ar=*2,6*-Me_2-C_6H_3). In contrast, the rates of exchange were approximately the same for **13b** and **14b** (Table 5).

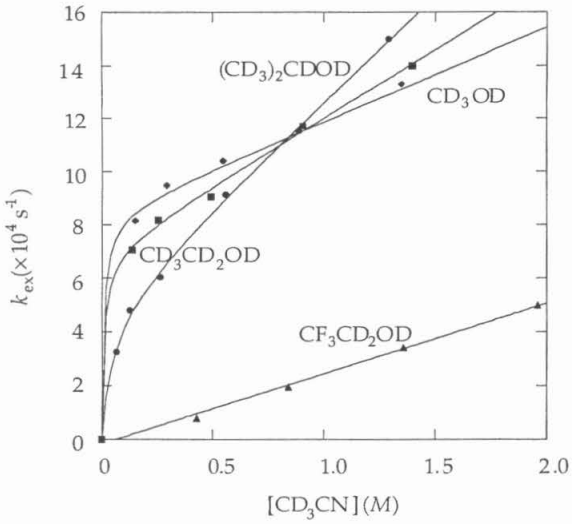

Figure 9. A plot of observed rate constants versus free acetonitrile concentrations for isotopic exchange of bound (**13b**) and free acetonitrile in different solvents at 40 °C.

Table 4. Second order rate constants for the acetonitrile exchange reactions for **13b** in various alcohol solvents at 40 °C.

solvent	$10^4 \cdot k_1$ (s^{-1})	$10^4 \cdot k_s$ ($M^{-1} \cdot s^{-1}$)	$10^4 \cdot k_2$ ($M^{-1} \cdot s^{-1}$)
methanol	8.4 ± 0.3	0.34 ± 0.01	3.6 ± 0.1
ethanol	6.7 ± 0.4	0.39 ± 0.02	5.2 ± 0.2
2-propanol	4.0 ± 0.3	0.31 ± 0.01	8.6 ± 0.2
TFE	< 0.01	< 0.01	2.6 ± 0.1

Table 5. Second order rate constants for the acetonitrile exchange reactions of various Pt(II) methyl cations in methanol (30 °C) and TFE (40 °C).

complex	solvent	T (°C)	$10^4 \cdot k_1$ (s^{-1})	$10^4 \cdot k_s$ ($M^{-1} \cdot s^{-1}$)	$10^4 \cdot k_2$ ($M^{-1} \cdot s^{-1}$)
13b	methanol	30	2.7 ± 0.3	0.11 ± 0.01	1.5 ± 0.1
13d	methanol	30	9.9 ± 0.4	0.4 ± 0.02	7.9 ± 0.3
14b	methanol	30	2.6 ± 0.2	0.11 ± 0.01	1.8 ± 0.2
14c	methanol	30	6.3 ± 0.3	0.26 ± 0.02	4.4 ± 0.3
13b	TFE	40	< 0.1	< 0.1	2.6 ± 0.1
13d	TFE	40	...[a]	...[a]	...[a]
14b	TFE	40	< 0.01	< 0.01	2.8 ± 0.1
14c	TFE	40	< 0.01	< 0.01	10.2 ± 0.1

[a] Acetonitrile exchange is too fast ($k_{ex} > 50 \times 10^{-4}$ s^{-1}) to measure rates.

In deuterated alcohols other than TFE-d_3, competing deuteration of the backbone methyl groups is observed. The rate of deuteration not only depends on solvent and ligand, but is also regioselective: the deuteration of the two non-equivalent backbone methyl groups occurs at different rates in each case, with the higher field NMR signal exhibiting more rapid deuteration. For example, for **13b** in CD_3OD at 30 °C, <5% deuteration occurred after 1.5 h; whereas for **13d**, the higher field backbone methyl resonance is completely deuterated within 15 min, while <5% deuteration is observed for the low field one. For **13b** at 40 °C, less than < 10% deuteration occurred after 1 h in CD_3OD, but in $(CD_3)_2CDOD$ the high field resonance is more than 80% deuterated after 15 min, and the low field one ~40% deuterated after 1 h. Deuterium exchange is even faster for carbonyl cations; in **7e**, backbone deuteration occurred even in TFE-d_3 at room temperature, whereas no observable deuteration occurred for **7a–7d** under these conditions.

Discussion

Synthesis and Characterization of Platinum Complexes. The procedures for ligand synthesis, formation of dimethylplatinum complexes, and protonolysis to monomethylplatinum cations all appear to be quite general for a wide array of substituted diaryldiimine ligands, thus making systematic examination of the effects of ligand electronic and steric properties possible. The only exception is in the synthesis of **6c**, where it appeared necessary to periodically purge and remove free SMe_2, which can compete with the diimine ligand **3c** for the coordination to the Pt(II) center. It is particularly convenient that cationic Pt(II)-methyl complexes are not readily protonolyzed,[9c] which permits their clean generation without requiring rigorous control of stoichiometry in adding an equivalent of acid.

All complexes prepared are characterized straightforwardly by ^{1}H NMR. The only important structural variable is the orientation of the aryl rings with respect to the coordination plane. Structural characterizations by Ruffo and co-workers on cationic Pt-methyl-olefin complexes with Ar =*2,6*-diethylphenyl revealed a near-orthogonal orientation between the aryl rings and the Pt coordination plane.[21] NMR studies by the same authors suggest there is hindered rotation around the N–C^{ipso} bond as well.[22] Similar conclusions have also been reached by Eisenberg and co-workers, where they were readily able to isolate the meso- and rac-isomers of a neutral (diimine)$PtMe_2$ complex with Ar = *2*-OMe-*4,6*-(*t*-Bu)$_2$-C_6H_2.[23] In comparison, few X-ray structures have been obtained for complexes containing diimine ligands with *3,5*-disubstituted aryl substituents. Recently the crystal structure of a related pyrrolyl-imine complex (**24**) found the phenyl ring at 58° to the N–Pt–N plane.[24]

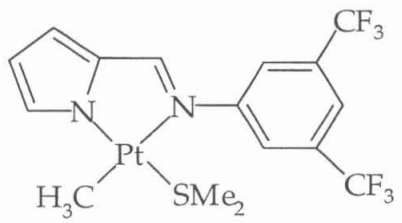

24

The latter finding is consistent with AM1 level calculations on **4e**, which predict that the phenyl rings are *ca.* 60° tilted out of the N–Pt–N plane.[25] On the other

hand, the X-ray structure of **16b** ($R^3 = R^5 = CMe_3$, $R^4 = H$) showed the phenyl rings are *ca.* 80° to the N–Pt–N planes.[18] However, the bimetallic structure of **16b**, and the relatively short Pt–O bridges could cause the phenyl rings to rotate further out of the plane to avoid steric congestion. ^1H NMR signals of the complexes with *3,5*-disubstituted aryldiimines are also consistent with rapid rotation around N–C^{ipso} bonds. For example, only one set of ligand and [Pt–CH_3] NMR peaks is observed for **7d** (which has asymmetrically substituted aryl groups) down to -40 °C, implying rotation about the C-N bond is fast on the NMR timescale. We expect this is the case for all *3,5*-disubstituted aryls.

The ^{195}Pt satellites are useful NMR features, not only in facilitating assignments but also as qualitative probes of electronic effect transmission. In particular, for the methyl carbonyl cations the downfield signals for the backbone methyl (**7**) exhibit larger $^4J_{Pt-H}$ values than the upfield signals. We tentatively assign the downfield resonances to the methyl trans to CO; the large *trans* influence of methyl bonded to platinum would be expected to elongate the opposite Pt–N bond, and reduce the corresponding coupling constant. Similarly, for **9**, the upfield signals for the backbone H exhibit $^3J_{Pt-H}$ values (~74 Hz) nearly twice as large as those for the downfield ones (~ 38 Hz), and are consequently assigned to the H trans to CO. Such effects have chemical as well as spectroscopic consequences, as manifested by the differential rates of deuteration of backbone methyls for complexes **13** in deuterated alcohols. We will not consider these effects in any detail here, except to note that they are consistent with the substantial perturbations of C–H bond activation by variation of diimine ligand electronic character, to be discussed below.

CO Stretching Frequencies as a Measure of Electronic Character. In order to examine electronic effects on C-H bond activation, we sought an empirical measure of actual electronic density at cationic Pt(II) as preferable to a semi-empirical prediction of expected ligand properties. As ν_{CO} is a well-established probe of electron density at a metal center, we prepared the platinum methyl carbonyl cations with the various diimine ligands. The ν_{CO} values are shown in Table 1, and plotted against the Hammett substituent constants ($\sigma = \sigma_p + \sigma_m$)[26] in Figure 10. All three series, **7a–f**, **8a–c** and **9a–c**, give fairly good linear correlations; however, the lines are well displaced from one another. In other words, for the same aryl σ values, the cations **8** show a higher CO stretching frequency — are comparatively electron-poor — relative to **7**. For

example, ν_{CO} for **7f** (Ar = *3,5*-$Me_2C_6H_3$) is 2105.7 cm^{-1} vs. 2109.6 cm^{-1} for **8b** (Ar = *2,6*-$Me_2C_6H_3$), though one might expect that they should be reasonably electronically similar (both having dimethylaryl groups) and exhibit similar CO stretching frequencies. Why don't they?

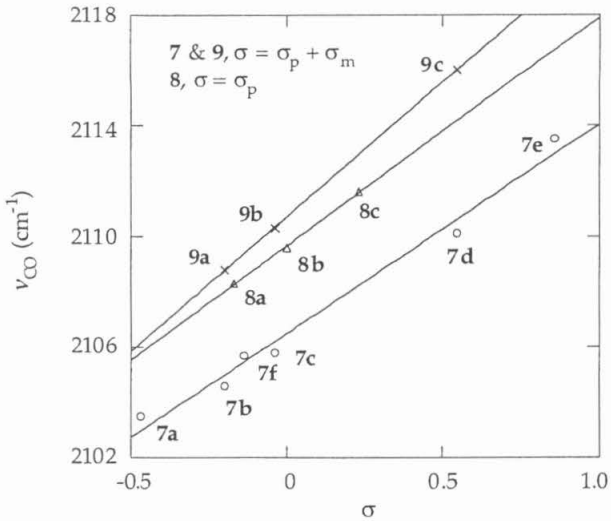

Figure 10. Plot of CO stretching frequencies for platinum (II) methyl/carbonyl cations **7, 8** and **9** vs. the sigma values of the aryl substituents.

Of course, as defined above the σ values for complexes **8** do *not* take account of the ortho methyl groups, as ortho substituent constants are considered unreliable owing to steric complications. But this cannot be the explanation, as σ for methyl is negative (electron-releasing relative to hydrogen); hence including a contribution for the ortho substituents would move the correlation line for **8** to the left, *further* from that for **7**. We believe that the difference lies in steric factors: the *2,6*-methyl groups in **8** cause the aryl groups to be oriented perpendicular to the coordination plane, minimizing crowding, whereas the less bulky aryls of **7** are rotated more parallel to the plane, in at least partial conjugation with the unsaturated [N=C(Me)–C(Me)=N] group. This would be expected to result in more effective transmission of the substituent effects from the aryl group, via the diimine, to the metal center. AM1 semi-empirical calculations[25] support this: free ligand **2b** is predicted to have the aryl ring locked perpendicular to the [N–Pt–N] plane, with consequently little π-donation from the phenyl ring to the nitrogen atoms, while in **1f** the dihedral angle between the aryl ring and the diimine backbone is predicted to be

approximately 60°, and the calculated electron density at nitrogen in **1f** is higher than in **2b**.

Methyl substitution at backbone positions of the diimine ligands is also electron releasing, as can be seen by comparing **7b–d** and **9a–c**, for which the aryl groups are identical: the CO stretching frequencies of the former (with backbone methyls) are red-shifted by about 4 – 6 cm^{-1}.

Ligand Electronic Effects on the Aquo/Solvento Equilibrium. All cations **10–12** generated by protonolysis of the corresponding dimethyl complexes with aqueous acid in TFE are formed as a mixture of solvento (*i*) and aquo (*ii*) adducts in rapid equilibrium (eq 5). In all cases measured, the equilibrium substantially favors the aquo adduct (Table 2). Furthermore, correlation of K_{eq} with ν_{CO} of the corresponding carbonyl cation shows that the preference for water over TFE increases as the metal center is made more electron-poor (Figure 11). This trend presumably reflects the greater electron donating ability of water, relative to TFE, toward cationic Pt(II) centers. Similarly, the phenyl cations **17** and **18** are more selective toward water binding than the corresponding methyl cations **10** and **11**. Methyl groups are extremely good σ-donors to metal centers, whereas phenyl groups are more electronegative (sp^2- *vs.* sp^3 -hybridized carbon) and thus less electron donating, rendering the platinum center more electron deficient.

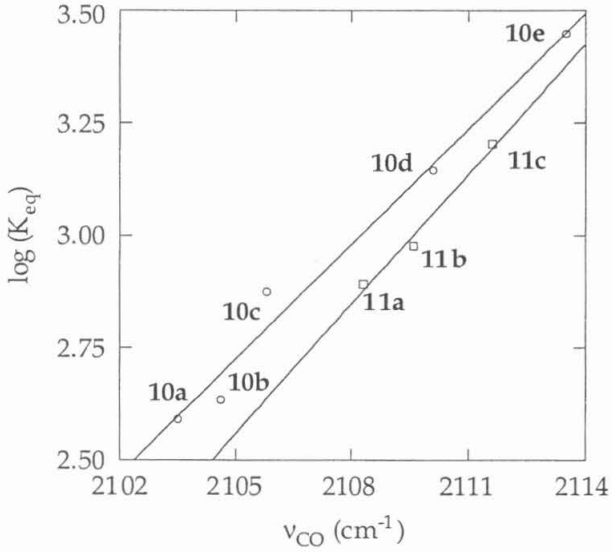

Figure 11. log(K_{eq}) of **10** and **11** versus the CO stretching frequencies of the corresponding methyl/carbonyl cations **7** and **8**.

Ligand Electronic Effects on Backbone Methyl Deuteration. In some cases deuterium is incorporated into the backbone methyls of Pt(II) methyl acetonitrile adducts in $(CD_3)_2CDOD$, CD_3CD_2OD and CD_3OD. This probably occurs via Lewis acid catalyzed imine-enamine tautomerization (Scheme 9), whose rate will depend on both the basicity of the solvent and the acidity of the imine α-methyl proton. The basicity of alcohols decreases in the order Me_2CHOH > EtOH > MeOH >> TFE, consistent with the observation that deuteration occurs fastest in deuterated isopropanol and slowest in TFE-d_3. Electron-withdrawing groups will increase the acidity of α-methyl protons, so the more electron-withdrawing diimine ligands should lead to a higher rate for deuterium incorporation into the methyl backbone. The more rapid exchange for **13d** than for **13b** is thus consistent with the higher ν_{CO} for **7d** than **7b**. The observation of exchange for **7e** even in TFE-d_3 at room temperature reflects the greater electron-withdrawing power of CO relative to acetonitrile.

Scheme 9

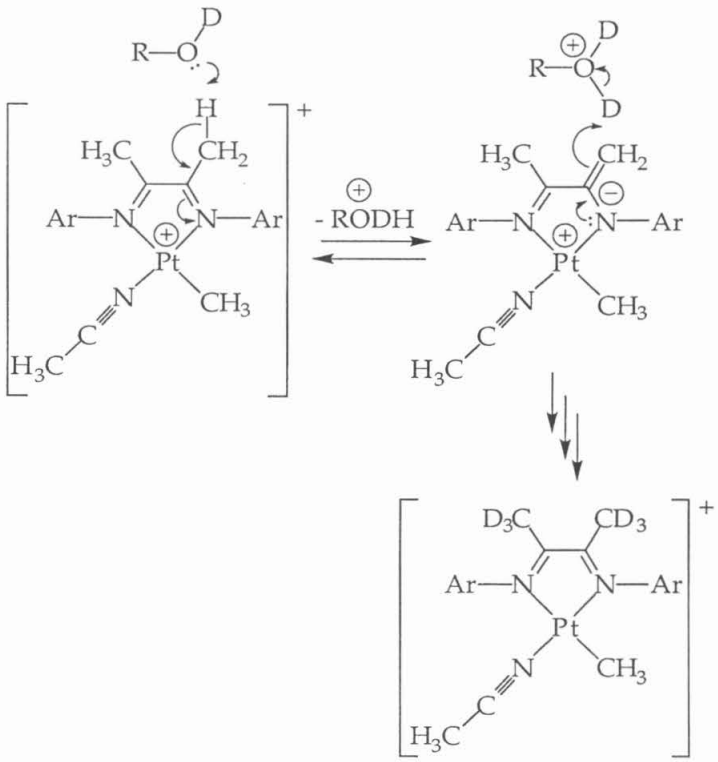

The differential deuteration rates observed for the two backbone methyl groups in the same molecule may be attributed to the differing *trans*-influence of methyl vs. MeCN. Thus a Pt–N bond *trans* to MeCN is expected to be shorter, resulting in stronger donation to platinum, making the nitrogen more electropositive and accelerating exchange at the attached methyl group.

Ligand Effects on Overall Reaction Rates of Arene C-H Bond Activation. Pt(II) methyl cations **10–12** react cleanly with benzene to give the corresponding phenyl cations **17–19**, accompanied by liberation of methane. The kinetics are conveniently followed by ^{1}H NMR, and exhibit clean first order behavior in [Pt]. At sufficiently high water concentrations, where the Pt(II) aquo adducts account for > 90% of the total platinum species, the dependence on concentrations of benzene and water satisfy the apparent rate law: rate = k_{obs}[benzene]/[water]. A series of comparative experiments were performed to determine and distinguish ligand electronic and steric effects on k_{obs}.

The reaction rates of C_6D_6 with cations **10** were measured at 20 °C under two sets of conditions. At the lower water concentration ([H_2O] = 0.05 *M*, [TFE-d_3] = 14.1 *M* and [C_6D_6] = 0.25 *M*), both the aquo and the solvento complexes are observed in the reaction mixtures; and at the higher water concentration ([H_2O] = 0.70 *M*, [TFE-d_3] = 12.3 *M* and [C_6D_6] = 1.31 *M*), the aquo complexes are the only observable species. The logarithms of the observed rate constants are plotted against the IR CO stretching frequencies of the corresponding carbonyl complexes (**7**) in Figure 12. Under either set of reaction conditions, a good linear correlation is obtained, demonstrating that the more electron-rich Pt(II) cations are *more* reactive toward C_6D_6. The slope of the linear correlation does depend on conditions, however. A similar correlation is found for cations **11** reacting with C_6D_6 at 35 °C (Figure 13a) and for cations **12** at 20 °C (Figure 13b). On the other hand, while the **10b** reacted 3.5 times faster with C_6D_6 than **10d** (at 20 °C), the corresponding methyl actonitrile complexes **13b** and **13d** showed similar reactivities (the difference in rates < 25%) in the reaction with C_6D_6 (at 80 °C).

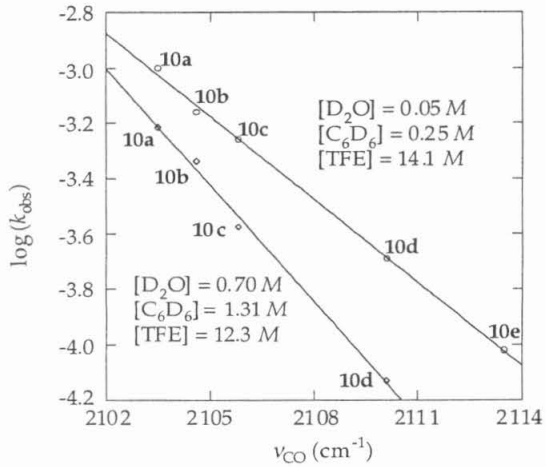

Figure 12. A plot of the logarithms of the observed rate constants in reactions of methyl cations **10** with C_6D_6 as a function of ν_{CO} of the corresponding methyl/carbonyl cations **7**.

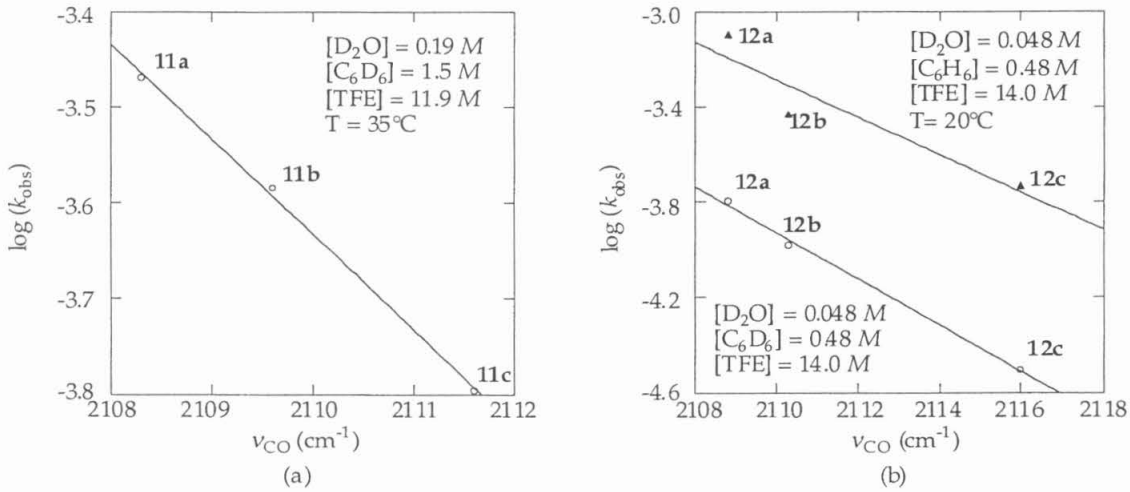

Figure 13. (a) A plot of the logarithms of the observed rate constants for reactions of cations **11** with C_6D_6 as a function of ν_{CO} for the corresponding methyl/carbonyl cations **8**. (b) A plot of the logarithms of the observed rate constants for reactions of cations **12** with C_6D_6/C_6H_6 as a function of ν_{CO} for the corresponding methyl/carbonyl cations **9**.

The steric effects of the diimine ligands have a profound effect on the reactivity of the metal center. For example, **8a** has a CO stretching frequency of 2108 cm^{-1}, indicating that the corresponding **11a** is somewhat more electron rich than **10d**, whose corresponding methyl-carbonyl cation **7d** has an IR stretching

frequency of 2110 cm^{-1}. However, under the same reaction conditions, **10d** reacts an order of magnitude faster with C_6D_6 than **11a** (Figure 14a). In general reactions of benzene with complexes containing *2,6*-dimethyl-substituted aryls (**11**) are considerably slower than those with no such substitution (**10**), indicating a substantial slowing effect of increasing steric bulk. On the other hand Figure 14a indicates that the reactions of complexes **12** are considerably slower than those of **10** with similar electron density, in spite of the fact that **12** should be if anything *less* crowded than **10**. We do not currently have a fully satisfying explanation for this apparent anomaly (*vide infra*).

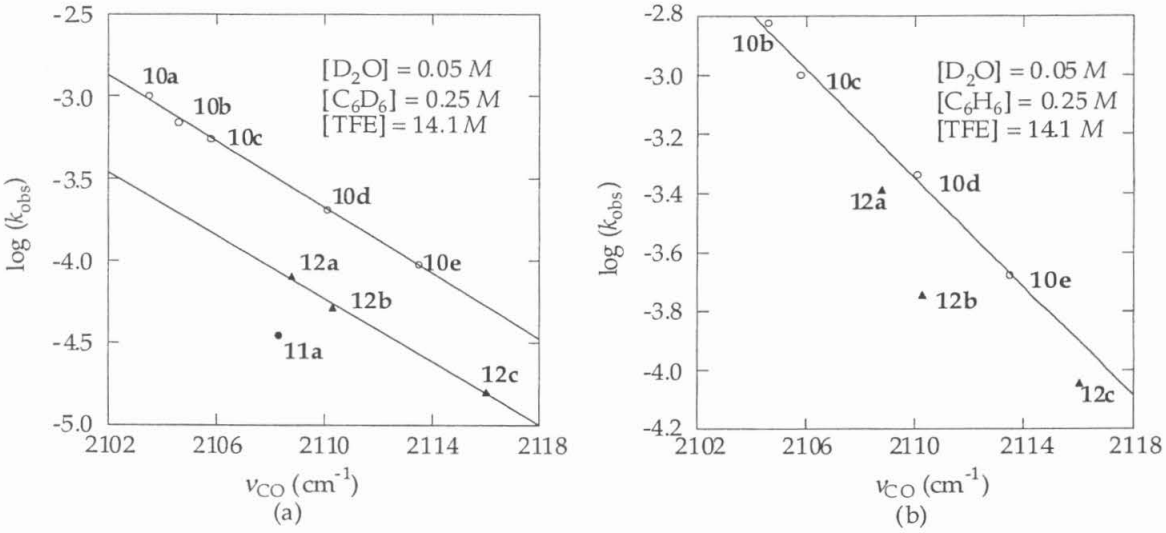

Figure 14. (a) A plot of the logarithms of the observed rate constants in reactions of Pt(II) cations of variable steric bulk with C_6D_6 as a function of ν_{CO}. (b) A plot of the logarithms of the observed rate constants in reactions of Pt(II) cations of variable steric bulk with C_6H_6 as a function of ν_{CO}.

Scheme 10

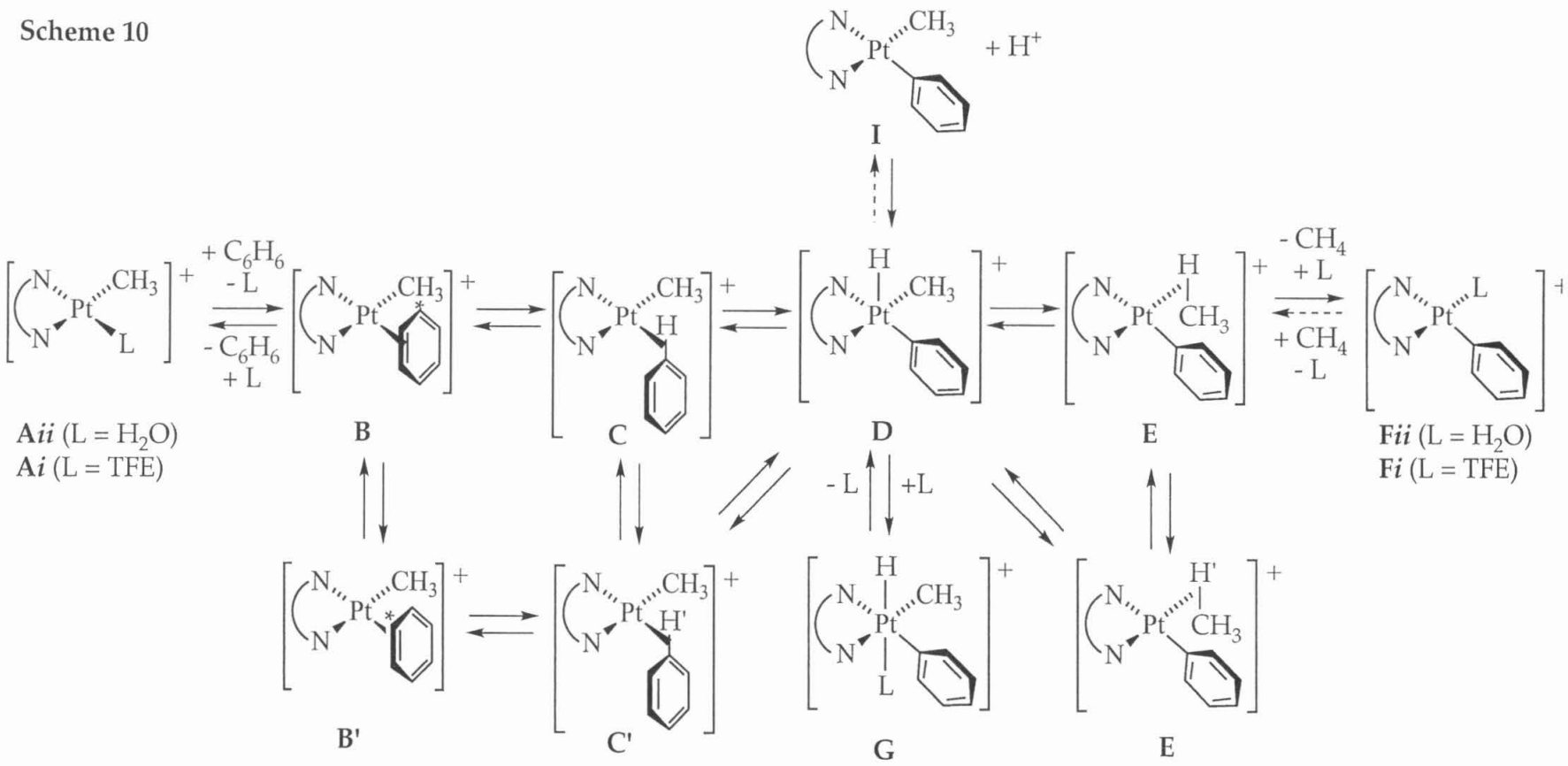
+ H+
I
+ C6H6
- L
- C6H6
+ L
Aii (L = H2O)
Ai (L = TFE)
B
C
D
E
- CH4
+ L
+ CH4
- L
Fii (L = H2O)
Fi (L = TFE)
- L
+L
B'
C'
G
E'

Details of the Mechanism of Benzene C-H Bond Activation. The mechanism proposed previously to account for the reaction of benzene with **11b** is shown in Scheme 10. The observed rate law, particularly the inverse dependence on water concentration, can be interpreted in terms of either a dissociative or solvent-assisted associative pathway, but several considerations (to be discussed later) lead to a strong preference for the latter, so we will use Scheme 11 as the framework for our discussion.

Scheme 11

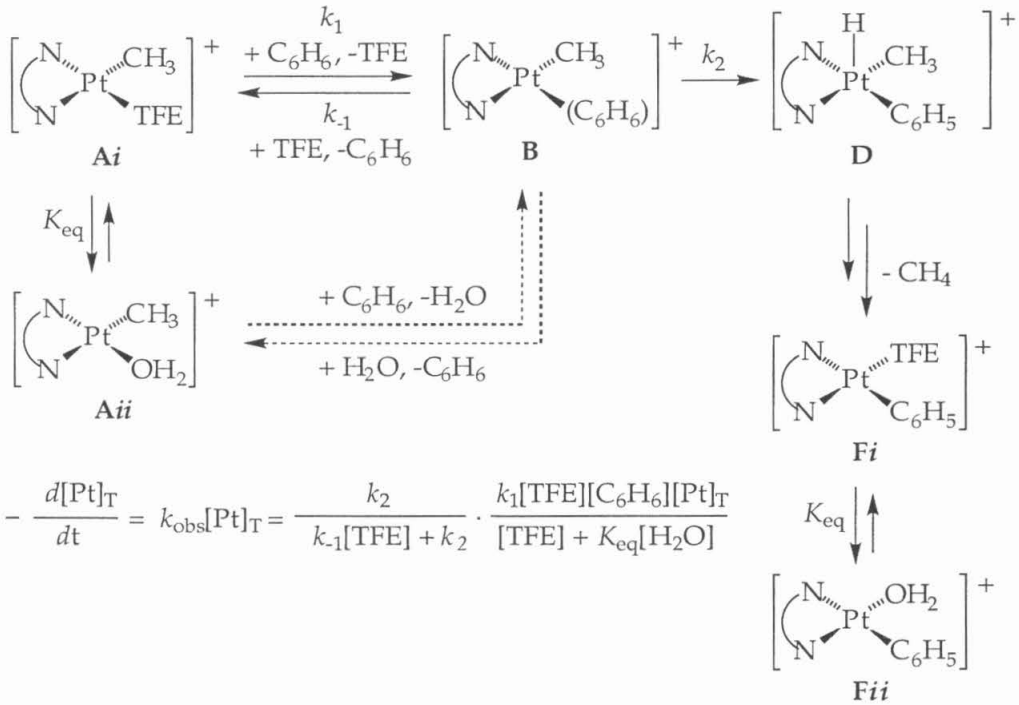

$$-\frac{d[\mathrm{Pt}]_T}{dt} = k_{obs}[\mathrm{Pt}]_T = \frac{k_2}{k_{-1}[\mathrm{TFE}] + k_2} \cdot \frac{k_1[\mathrm{TFE}][C_6H_6][\mathrm{Pt}]_T}{[\mathrm{TFE}] + K_{eq}[H_2O]}$$

In this scheme the aquo (**A*ii***) and solvento (**A*i***) complexes are in rapid equilibrium, with benzene displacing the more weakly bound solvent ligand; direct attack of benzene on **A*ii*** to displace water is assumed to be negligible. π-Benzene complex **B** then undergoes C-H bond cleavage (probably via a σ-complex **C**). Limiting cases for the rate-determining step would be formation of **B** ($k_2 > k_{-1}[\mathrm{TFE}]$), or C–H cleavage ($k_2 < k_{-1}[\mathrm{TFE}]$). In either case, the deduced rate law predicts that a plot of $1/k_{obs}$ versus $[H_2O]/[C_6H_6]$ will be linear. At high water concentrations ($K_{eq}[H_2O] >> [\mathrm{TFE}]$), the water complex **A*ii*** is the major species in solution, and a plot of k_{obs} versus $[C_6H_6]/[H_2O]$ is expected to be linear, as long as benzene and water are not present in high enough

concentrations to significantly alter the solvent properties. This expectation is born out by the experimental results. At low water concentrations ($K_{eq}[H_2O] \sim [TFE]$) concentrations of **A** and **B** will both be significant, so a plot of k_{obs} versus $[C_6H_6]/[H_2O]$ would be expected to deviate from linearity, as observed.

For **11b**, formation of π-benzene adduct **B** was inferred to be the rate-determining step, based primarily on the first-order dependence on benzene concentration coupled with the low KIE (~ 1) and the virtually complete isotopic scrambling observed.[11] It is of interest here to compare the behavior of cations **10** (which lack *2,6*-dimethyl substituents on the aryl groups) with that previously found for **11b** (as well as the new findings for **11a** and **11c**). While the two series appear quite similar in some regards, particularly with respect to one major trend — the dependence of reactivity on electronic character — other phenomena appear quite different. In the next few sections we will try to account for and reconcile both the differences and similarities within the basic framework of Scheme 10.

Isotopic Exchange and Kinetic Deuterium Isotope Effects. It should first be noted that no discernible amount of deuterium is detected in the methane liberated from the reaction between any complex and C_6H_6 in TFE-d_3. This means that reversible deprotonation of intermediate **D** (to give **I**) in Scheme 10 is much slower than all other reactions, since otherwise deuterium from solvent would exchange into the complex and thence into the methyl group. Furthermore, the fact that no H/D exchange occurs in the present system explains the observation that when cations **10** are generated by protonolysis of **7** in TFE-d_3, only [Pt–CH_2D] and [Pt–CH_3] complexes are formed, with corresponding amounts of CH_4 and CH_3D; no multiple deuteration is detectable. As shown in Scheme 12, addition of D^+ (from aqueous DBF_4) to the platinum dimethyl complexes gives a Pt(IV)–D species **a**, which undergoes C–D bond formation to form **b**, which may either directly release CH_3D to afford **c**, or rearrange and cleave a C-H bond to yield **a'**.

Scheme 12

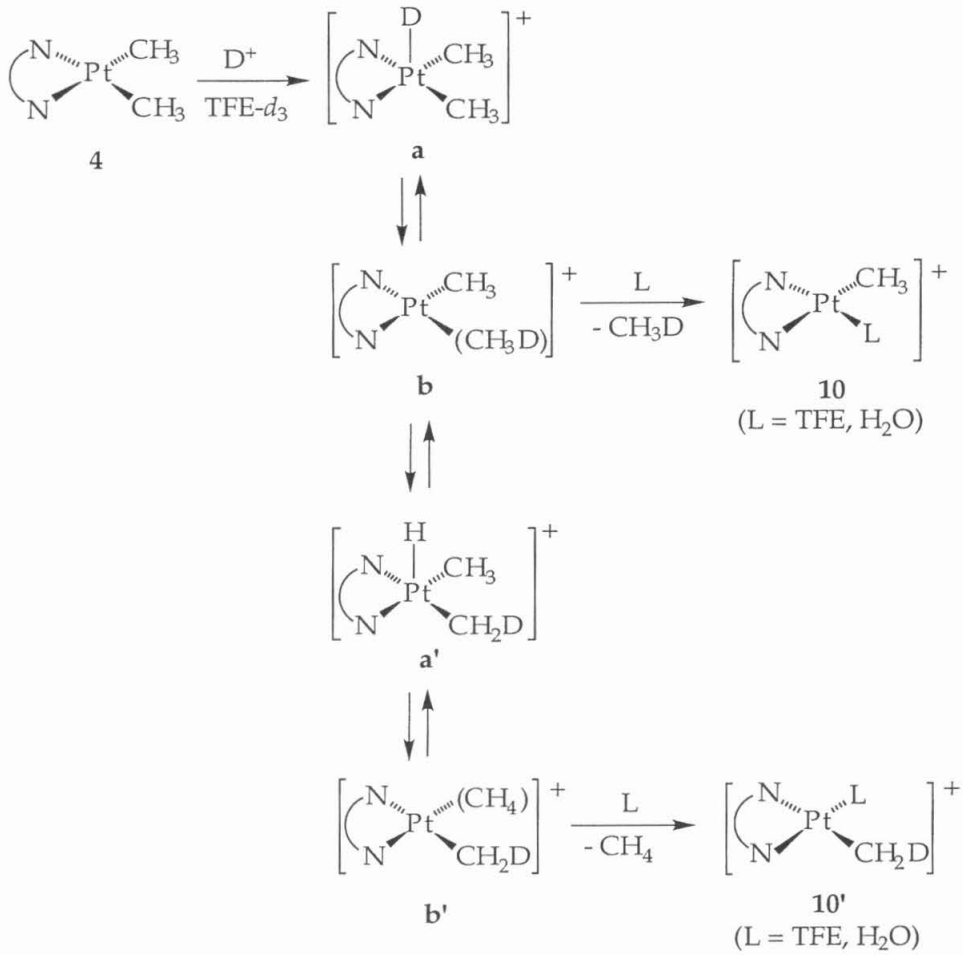

Because there is no H/D exchange between the solvent and Pt(IV) hydrido intermediates, only one deuterium atom is involved for each molecule of methane released. This deuterium atom is either incorporated into the liberated methane as CH_3D or left behind as [Pt-CH_2D]. This stands in contrast to previous protonolysis studies of Pt(II) alkyl complexes in CD_3OD, where substantial deuterium incorporation into the Pt alkyl group was observed.[5] The difference may reflect the reduced basicity of TFE compared to methanol.

If the rate of the scrambling process in Scheme 10 is fast relative to the loss of methane, a statistical mixture of CH_3D and CH_4 (4:3) will be obtained (assuming negligible KIE for C-H vs. C-D activation and methane dissociation); if the reverse, only CH_3D will be produced. As Figure 1 above shows, for **4b** the ratio of CH_3D to CH_4 increases with increasing acetonitrile concentration,

implying that elimination of methane is associative. Similar observations for **4e** and **5b** have been reported recently by Tilset and co-workers.[27]

When cations **10** are reacted with C_6D_6, the liberated methane includes isotopomers with more than one deuterium atom. This is consistent with the mechanism of Scheme 10, if reversible interconversions among intermediates **C-F** and the accompanying rearrangements to **C'** and **F'** occur at a rate at least comparable to those of dissociation of methane from **F** and **C**. However, in contrast to **11b**, where isotope scrambling between the methane and platinum-phenyl groups is essentially statistical,[11] for **10** a much smaller degree of scrambling is found. The ratio of approximately 2:1 CH_3D: CH_2D_2 for **10b** indicates that **F** loses methane on the order of twice as fast as it reverts to **C**.

Up to 20% of the unreacted starting material becomes deuterated, giving [Pt-CH_2D], during reactions between **10** and C_6D_6, which implies that some of the time intermediate **F**, which will have coordinated CH_3D after a single C–H activation/cleavage sequence, reverts all the way back to starting materials. The relatively low levels of deuterium incorporation into the platinum methyl group are consistent with the previous finding, based on protonolysis of a mixed [Pt(Me)(Ph)] complex, that the rate for benzene elimination is ~ 4 to 5 times slower than that of methane elimination, which translates to a $\Delta\Delta G^{\ddagger}$ of ~ 0.8 – 0.9 kcal·mol^{-1} at room temperature.[11] This observation also implies that some of the evolved methane will come from complexes that have interacted with more than one molecule of C_6D_6, which may have consequences for KIE measurements (*vide infra*).

Kinetic deuterium isotope effects (KIEs) were measured for all complexes **10–12** by comparing the rates of disappearance of starting material in the presence of C_6H_6 vs. those with C_6D_6 under otherwise identical conditions. The most striking observation in Table 3 is the difference in behavior between complexes **10** and **11**: the former have KIE values around 2, while the latter are close to unity. For several examples of **10**, we also measured the KIEs by intermolecular (1:1 C_6H_6:C_6D_6) and intramolecular (*1,3,5*-$C_6H_3D_3$) competition reactions; this approach would be much more complicated (by intermolecular competition) or impossible (by intramolecular competition) for **11**, because of the near-statistical isotope scrambling. We find that the KIE' s measured from the competition reactions are slightly, but consistently, smaller than those measured by parallel reactions. This observation may be accounted for by the fact that more than one molecule of benzene may be involved in the reaction (*vide supra*)

(Scheme 10). Thus, for example, in an intermolecular competition reaction of **10** with C_6D_6 or C_6H_6, initial C_6D_6 activation followed by complete reversion to starting material accompanied by deuterium incorporation into [Pt–CH_3] happens occasionally; the subsequent conversion to **17** will give deuterated methane even if it involves C_6H_6. In the parallel method, such a sequence (participation of more than one benzene molecule) will have no consequences, since only rates and not degrees of deuteration are measured. Thus the competitive method overestimates the apparent relative frequency of C_6D_6 activation.

The differences between **10** and **11** in behavior for both isotope exchange and KIE are explicable in terms of Figure 15, analogous to Scheme 10 but with the assumption of a change in rate-determining step. For **10**, to account for a significant KIE, the rate-determining step must involve the C–H (C–D) bond: either the actual C–H cleavage step, **D** → **E**, or (less likely) the coordination of the C–H bond, **C** → **D**. But that would also explain the relatively low level of isotopic exchange, as the barrier to dissociation of benzene from **B** (and, by extension, that of methane from **E**) must be lower than at least one barrier within the manifold of reactions that effect such exchange. This case is represented by the free energy profile for **10** in Figure 15. The highest point on the energy surface is transition state **Z**‡.

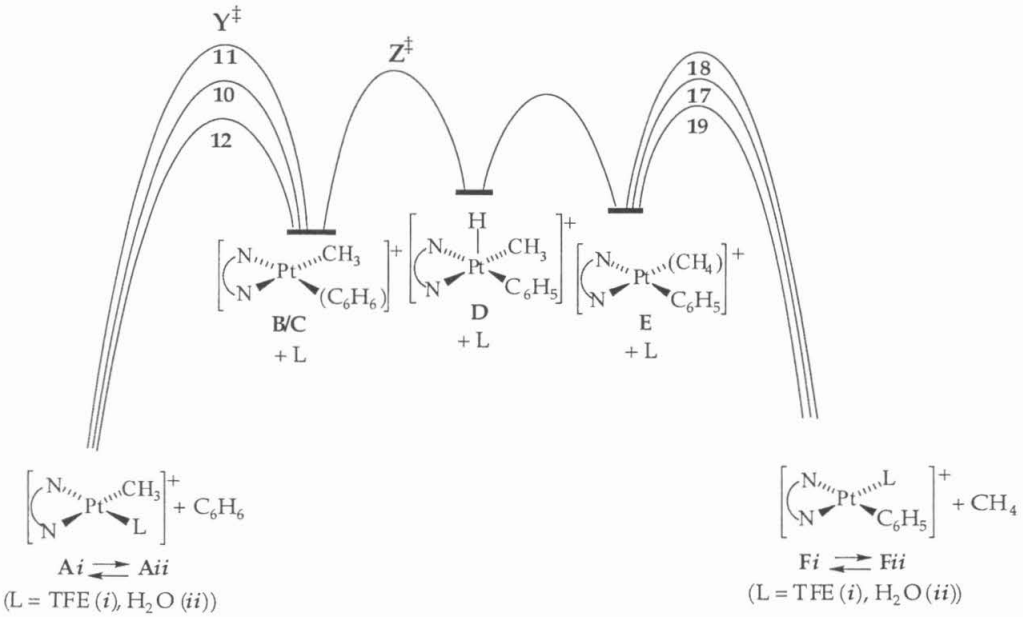

Figure 15. Reaction coordinate for reactions between **10, 11, 12** and benzene.

In contrast, for **11** the highest point on the surface must be transition state **Y‡**, which governs the initial coordination of benzene. Since this coordination involves a π-bond of benzene, no primary KIE at all would be anticipated. Furthermore, the complete statistical isotope exchange implies that once the manifold of intermediates **C–E** has been entered, loss of benzene or methane is much slower than interconversions among those intermediates. The differences in entropy of activation — strongly negative for **11b**, very small for **10b** — also seem consistent with the former, but not the latter, involving rate-determining associative (*vide infra*) substitution.

Why should this rate-determining step switch operate? A steric explanation appears the most probable. Coordination of benzene in η^2-C,C mode places the benzene molecule right in the coordination plane, subject to steric interactions with the other ligands. For **11**, with *2,6*-dimethyl-substituted aryl groups, these interactions can be expected to be more significant than for **10**, which has no substituents in the *2,6* positions. Hence in **11** there will be relative destabilization of both intermediate **B** itself and, presumably, the transition state (**Y‡**) leading thereto, compared to **10**.

The KIE for **12** is considerably larger than those for **10** (3.6 – 5.9 vs. ~ 2). One might argue that **12** are even less sterically crowded than **10**, by virtue of the missing backbone methyl groups, which would lower transition state **Y‡** still further (Figure 15). This might suggest that **12** gives a better measure of the inherent KIE for rate-determining C–H bond activation, whereas for **10** the energies of **Y‡** and **Z‡** are sufficiently close that C–H activation is not *completely* rate-determining, and the measured KIE values are hybrids. However, the rates of the reactions of **12** with benzene are also anomalous, so this conclusion must remain tentative for the present.

Electronic Effects on Rates. Within each series **10-12** the changes in substituents (in the *3,5*-positions for **10** and **12** and in the 4-positions for **11**) should be far enough removed from the metal center that steric parameters should change little, and thus the observed trend within each series should reflect a purely electronic effect. For both series, it was observed that as the Pt(II) centers become more electron-rich (as measured by lower CO stretching frequencies in the analogous carbonyl cations), benzene C-H bond activation becomes faster. In principle, this trend could be explained in a number of ways.

For cations **10** and **12**, for example, one might argue that 1) C-H activation is the rate-determining step; 2) the intermediates **D** thus formed are formally Pt(IV), more electron-deficient than the Pt(II) cations; 3) the transition state **Z**‡ leading to that intermediate should have at least partial higher oxidation state character. Hence more strongly electron-donating ligands can better stabilize the higher oxidation state intermediates/transition states and accelerate the reaction.

On the other hand, a closely parallel trend is observed also for cations **11**, for which C–H bond activation does *not* appear to be rate-determining, but rather replacement of TFE solvent by benzene. While it is conceivable that replacement might follow the same order — that is, that transition state **Y**‡ is also stabilized by electron-donating ligands — it is far from clear why that should be so, and it seems at odds with the fact that acetonitrile self-exchange rates follow the opposite trend: faster at more electron-deficient metal centers (*vide infra*). And, of course, it would be much more satisfying to find a single explanation that accounts simultaneously for both series.

Since the transition states for the two series appear to be quite different, the simplest explanation for common behavior is that we are dealing primarily with a ground state effect. That is, the most important effect of changing the electronic properties of the diimine ligand is upon the stability of the aquo complexes $[(ArN{=}CR{-}CRN{=}Ar)Pt(Me)(H_2O)]^+$ (R = Me or H, **A*ii*** in Scheme 10). If there is comparatively little change in the energies of either transition state **Y**‡ or **Z**‡ as the diimine ligand is changed, then the rates of benzene activation by series **10**/**12** and **11** will exhibit the same trend even though they have different rate-determining steps (Figure 16).

If we further postulate that the energy of solvento complex **A*i*** is also relatively insensitive to ligand, then the equilibrium constant between **A*ii*** and **A*i*** would be expected to vary with ligand in much the same way as the rate constant. This is in fact the case, as shown in Figure 17: the plot of $\log(k_{obs})$ vs. $\log(K_{eq})$ gives reasonably straight lines, with slope close to unity, for the three sets of data.

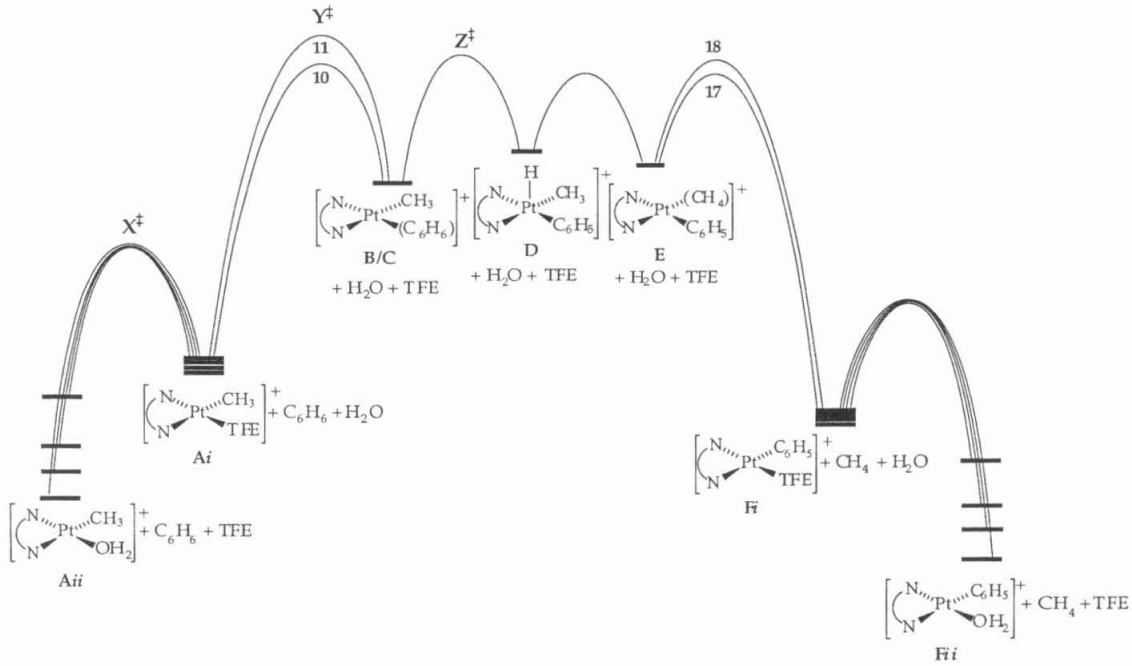

Figure 16. Reaction coordinate for reactions between **10** and **11** and benzene, showing that the differences in rate within a series, regardless of the rate determining step, arises from ground state energy differences for the aquo/methyl cations (**A*ii***).

While this interpretation is consistent with the most prominent features of the ligand-reactivity relationship, it is far from conclusive, and some observations remain unexplained, particularly the low reactivity of **12**. Figure 14 shows that both **12b** and **11a** are less reactive than **10d**, though all have comparable electron density. The difference between **11a** and **10d** can be explained on steric grounds — the former has *2,6*-dimethyl-substituted aryl groups — but **12b** should be if anything less crowded than **10d**. Apparently the replacement of backbone methyl groups with hydrogens has an effect here, as well as on the KIEs (*vide supra*). One possibly relevant observation is that **12** tend to have larger K_{eq}'s than predicated by their ν_{CO} values. For example, although **7d** and **9b** have comparable ν_{CO} values, the aquo-solvento equilibrium constant for **10d** is significantly smaller than that for **12b**. This might account, at least in part, for lower reaction rates for **12** compared to **10** of comparable electronic properties, but the reason for the higher K_{eq}'s for **12** remain unclear.

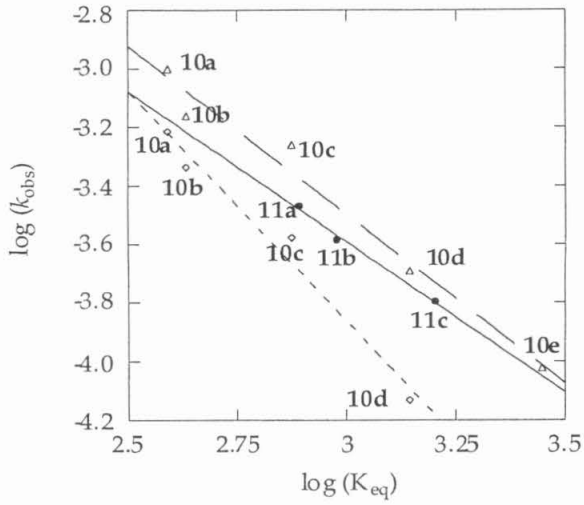

Symbol	Complex	Temp. (°C)	[C_6D_6] (*M*)	[D_2O] (*M*)	[TFE-d_3] (*M*)
—△—	10	20	0.25	0.05	14.1
—•—	11	35	1.50	0.19	11.9
---◇---	10	20	1.30	0.70	12.3

Figure 17. A log-log plot of the observed rate constants between C_6D_6 and methyl cations **10** and **11** versus the aquo/solvento equilibrium constants for the corresponding methyl solvento $\rightleftarrows$ aquo cations: **10*i*** $\rightleftarrows$ **10*ii*** and **11*i*** $\rightleftarrows$ **11*ii***.

Acetonitrile Exchange. A rate expression of $k_{ex} = k_1 + k_2[CD_3CN]$ has been obtained for acetonitrile isotopic exchange reactions. The k_1 term could represent either a unimolecular dissociative pathway or a solvent-assisted associative pathway. The highly negative entropy of activation for the k_1 term seems inconsistent with a dissociative pathway and indicative of a solvent-assisted pathway, though this is not definitive: solvation of the cations can play an important role. However, both terms exhibit similar entropies of activation, suggesting that both pathways operate by the same mechanism. That is, the isotopic acetonitrile exchange consists of both a solvent-assisted associative pathway and a direct attack associative pathway.

Although the k_1 values vary considerably as the solvent is changed from methanol to ethanol to isopropanol, when divided by bulk solvent concentrations the resulting k_s values are all about the same (Table 3).

Apparently the solvent term is not very sensitive to the steric bulk of the solvent. On the other hand, k_1 for TFE is essentially zero, presumably reflecting the very low basicity of that solvent. The second-order rate constants for direct acetonitrile attack (k_2) do vary across the entire set of alcohols, probably due to differences in solvation energies of the cations.[28]

Table 5 shows that the more electron-poor complexes (**13d** vs. **13b**, **14c** vs. **14b**) exhibit higher exchange rate constants for both the solvent-assisted (k_s) and direct (k_2) terms. This is the opposite trend from that found for benzene activation, and probably indicates stabilization of a five-coordinate transition state in the associative substitution. The most closely corresponding species in Figure 16 would be the transition state for substitution of water by TFE (**X**‡); but note that the energy of that species has *no consequence whatsoever* for the rate of benzene activation, if the arguments represented by that energy diagram are correct. Hence there is no inconsistency between the two opposing trends. Comparison of acetonitrile exchange for **14b** and **13d** (whose corresponding carbonyl cations have very similar ν_{CO} values) reveals a moderate steric effect as well, around a factor of 4, not quite so large as the steric retardation that appears to operate in benzene activation.

Reactions of Alkylaromatics. Our results combined with those of Tilset[20] suggest an inherent reactivity preference for aromatic over benzylic C–H activation, which can however be readily overridden by steric effects. Thus the relatively uncrowded **10b** reacts with *p*-xylene to give **20b**, the product of reaction at an aryl C–H, whereas more crowded **11b** gives primarily benzylic activation. With mesitylene, still more sterically encumbered, **10b** gives a mixture of products, somewhat favoring benzylic activation (**21b**); and the aromatic activation product **22b** appears, from its accelerated decomposition to $(\mu\text{-OH})_2$ dimer **16b**, to be significantly destabilized. The substrate-derived crowding in these two cases may also cause a shift to rate-determining (or partially so) substrate coordination, as the KIEs decrease significantly with steric bulk.

The C–H activation chemistry of purely aliphatic hydrocarbons will be reported later.[29]

Conclusions

The results reported here, combined with some earlier findings, support three main conclusions:

1) For the reaction of benzene with cationic Pt(II) complexes bearing *3,5*-disubstituted aryl diimine ligands (**10**), the rate determining step is C-H bond activation; whereas for the more sterically crowded analogs with *2,6*-dimethyl-substituted aryl groups (**11**), benzene coordination becomes rate-determining. This switch is manifested in distinctly different isotope scrambling and KIE patterns.

2) The more electron rich the ligand, as assayed by the CO stretching frequency of the corresponding carbonyl cationic complex, the faster the rate of C–H bond activation. This at first sight appears to be at odds with the common description of this class of reaction as electrophilic. However, the fact that the same trend is observed for the two different series of complexes, which have different rate-determining steps, suggest that this finding does not reflect the actual C–H bond activation process, but rather reflects only the relative ease of benzene displacing a ligand to initiate the reaction, which in turn appears to be mostly a ground state effect. It is hence not possible to say much, if anything, about the "inherent" nature of C–H activation based on these results.

3) Several lines of evidence suggest that associative substitution pathways operate here to get the hydrocarbon substrate into, and out of, the coordination sphere. While associative substitution does predominate in the chemistry of square-planar Pt(II), there are situations where dissociative mechanisms become preferred;[30] and one might think that the present cases, involving (presumably) very weakly bonded arenes and alkanes, would fall into that category. However, acetonitrile exchange seems to be clearly associative. More to the point, the fact that addition of acetonitrile, a better nucleophile than solvent TFE, suppresses isotopic scrambling between benzene and methyl groups strongly implies that the replacement of coordinated methane is associative. Analogous behavior has recently been observed for the displacement of coordinated arenes.[20] From the principle of microscopic reversibility, we infer that the displacement of solvent (water, acetonitrile) by hydrocarbon also proceeds associatively.

The implications of these findings with respect to the ultimate goal — the development of a practical, selective alkane functionalization catalyst — remain the subject of ongoing research in our labs.

Experimental Section

General Considerations. All moisture-sensitive compounds were manipulated using standard vacuum line, Schlenk or cannula techniques or in a drybox under a nitrogen atmopshere. Argon and dinitrogen gases were purified by passage over columns of MnO on vermiculite and activated molecular sieves. Trifluoroethanol was purchased from Aldrich, purified and dried over a mixture of $CaSO_4/NaHCO_3$, then either vacuum distilled or distilled under argon, and stored over activated molecular sieves under vacuum. Trifluoroethanol-d_3 was purchased from Aldrich, stored over activated molecular sieves and a small amount of $NaHCO_3$ under vacuum, and vacuum distilled into oven-dried J-Young NMR tubes for kinetic studies. Benzene and benzene-d_6 were vacuum distilled from sodium benzophenone ketyl shortly before kinetic runs, and stored over activated molecular sieves. Toluene was vacuum distilled from sodium benzophenone ketyl. Triethylamine was distilled from CaH_2 and stored under Ar. *3,5*-di-*tert*-butyl-*4*-methoxyaniline and the corresponding diimine ligand **1a** were synthesized by Dr. Joseph Sadighi. Bis(dimethyl(μ-dimethylsulfide)platinum(II was prepared according to literature procedure.[17] All other solvents and reagents were used as received without further purification.

NMR spectra were recorded on a GE QE300 (^{1}H, 300.1 MHz), a Varian INOVA 500 (^{1}H, 499.852 MHz, ^{13}C, 125.701 MHz) or a Varian Mercury 300 (^{1}H, 299.8 MHz, ^{19}F, 282.081 MHz, ^{13}C, 75.4626 MHz) spectrometer. IR spectra were recorded on a Perkin-Elmer 1600 series FTIR spectrometer. Mass spectra were measured on a Micromass LCT instrument with a Z-spray source at University of California Irvine, using electrospray orthogonal acceleration time-of-flight technique. Under the analytical conditions, protonolysis occurs at the platinum center in the platinum dimethyl complexes **4–6**, which were consequently detected as the cationic species $[(N–N)Pt(Me)(NCMe)]^+$ (NCMe was the solvent used in the analysis). Elemental analyses were performed at Midwest MicroLab LLC. A number of samples gave analytical results lower than the expected

values (these were generally very small samples that may have been contaminated with either a small amount of silica (from the filtration frit on which they were isolated) or TFE solvent), but all analyzed correctly in the electrospray mass spectrum.

1,4-*Bis*(3,5-di-*tert*-butylphenyl)-2,3-dimethyl-1,4-diaza-1,3-butadiene ($^{tBu_2Ar}DAB^{Me}$, 1b). 3,5-di-*tert*-butylaniline (0.9732 g, 4.74 mmol) and 2,3-butanedione (0.204 g, 2.36 mmol) were dissolved in 15 ml MeOH. To this yellow solution, 2 drops of formic acid were added, and a very pale yellow precipitate formed within 15 minutes. The mixture was stirred at room temperature for 14 hours, cooled, filtered, washed with cold methanol (2 × 5 ml) and dried over aspirator for 3 hours. **1b** was isolated as an extremely pale yellow powder (0.95 g, 87%). ^{1}H NMR (500 MHz, C_6D_6): δ = 1.32 (s, 36H, C(CH_3)$_3$), 2.33 (s, 6H N=C–CH_3), 6.90 (d, $^4J_{H-H}$ = 1.8Hz, 4H, Ar-*H*), 7.35 (t, $^4J_{H-H}$ = 1.8Hz, 2H, Ar-*H*). ^{13}C {^{1}H} NMR (125 MHz, C_6D_6): δ = 15.78 (N=C–CH_3), 31.97 (C(CH_3)$_3$), 35.40 (C(CH_3)$_3$), 114.27 (*o*-Ar-C), 118.19 (*p*-Ar-C),151.860, 152.24 (Ar–C), 168.57 (N=C–CH_3). ESMS: Calcd for $C_{32}H_{48}N_2H$ ([M+H]$^+$): 461.3896. Found: 461.3906.

1,4-*Bis*(3,4,5-trimethoxyphenyl)-2,3-dimethyl-1,4-diaza-1,3-butadiene ($^{OMe_3Ar}DAB^{Me}$, 1c). 3,4,5-trimethoxyaniline (0.9875 g, 5.39 mmol) and 2,3-butanedione (0.225 g, 2.61 mmol) were dissolved in 30 ml MeOH. To this yellow solution, several drops of formic acid were added, and a bright yellow precipitate formed overnight. The mixture was stirred at room temperature for 14 hours, cooled, filtered, washed with cold methanol (2 × 5 ml) and dried over aspirator for 3 hours. **1c** was isolated as a bright yellow powder (0.757 g, 70%). ^{1}H NMR (500 MHz, C_6D_6): δ = 2.32 (s, 6H, N=C–CH_3), 3.40 (s, 12H, OCH_3), 3.90 (s, 6H, OCH_3), 6.19 (s, 4H, Ar-*H*). ^{13}C {^{1}H} NMR (125 MHz, C_6D_6): δ = 15.91 (N=C–CH_3), 56.15 (OCH_3), 61.06 (OCH_3), 97.46 (*o*-Ar-C), 136.26, 147.90, 155.06 (Aryl C's), 169.04 (N=C–CH_3). ESMS: Calcd for $C_{22}H_{28}N_2O_6Na$ ([M+Na]$^+$): 439.1845. Found: 439.1848.

1,4-*Bis*(3-methoxy-5-(trifluoromethyl)phenyl)-2,3-dimethyl-1,4-diaza-1,3-butadiene ($^{OMeCF_3Ar}DAB^{Me}$, 1d). 3-methoxy-5-(trifluoromethyl)aniline (1.27 g, 6.65 mmol) and 2,3-butanedione (0.286 g, 3.32 mmol) were dissolved in 30 ml MeOH. To this yellow solution, several drops of formic acid were added, and the mixture was stirred at room temperature for 2 days without forming any

precipitation. The volatiles were then removed on a rotavap, and 6.8 gram of activated 5Å molecular sieves were added to a toluene solution of the above residues. The mixture was heated at 80–90 °C for two nights. The molecular sieves were then filtered away and washed with methylene chloride (4 × 10 ml). The volatiles were evaporated, and 20 ml of methanol was added to the residue. After stirring at room temperature for an hour, the insolubles were collected, washed with cold methanol (2 ×5 ml) and dried over aspirator for 3 hours. **1d** was isolated as an off-white powder (0.75 g, 52%). ^{1}H NMR (500 MHz, C_6D_6): δ = 1.90 (s, 6H, N=C–C*H*$_3$), 3.13 (s, 6H, OC*H*$_3$), 6.43 (m, 2H, Ar-*H*), 6.72 (m, 2H, Ar-*H*), 6.90 (m, 2H, Ar-*H*). ^{13}C {^{1}H} NMR (125 MHz, C_6D_6): δ = 15.52 (N=C–CH_3), 55.33 (OCH_3), 106.38 ($^3J_{C-F}$ = 3.8 Hz, Ar-C), 108.67 ($^3J_{C-F}$ = 3.67 Hz, Ar-C),108.79 ($^4J_{C-F}$ = 0.98 Hz, Ar-C), 125.63 ($^1J_{C-F}$ = 270.35 Hz, CF_3), 133.17 ($^2J_{C-F}$ = 32.3 Hz, Ar-C),153.56, 161.52 (Ar–C), 169.34 (N=C–CH_3). ^{19}F NMR (282 MHz, C_6D_6) δ = -64.81. ESMS: Calcd for $C_{20}H_{18}N_2O_2F_6H$ ([M+H]$^+$): 433.1351. Found: 433.1357.

1,4-*Bis*(2,4,6-trimethylphenyl)-2,3-dimethyl-1,4-diaza-1,3-butadiene (^{Me_3Ar}DAB^{Me}, 2a). 2,4,6-trimethylaniline (13.521 g, 100 mmol) and 2,3-butanedione (4.307 g, 50 mmol) were dissolved in 50 ml MeOH. To this yellow solution, several drops of formic acid were added, and a bright yellow precipitate formed overnight. The mixture was stirred at room temperature for 24 hours, filtered, washed with methanol (2 × 5 ml) and dried over aspirator for 4 hours. **2a** was isolated as a bright yellow powder (14.78 g, 92%). ^{1}H NMR (500 MHz, C_6D_6): δ = 2.00 (s, 12H, *o*-C*H*$_3$) 2.07 (s, 6H, *p*-C*H*$_3$), 2.22 (s, 6H, N=C–C*H*$_3$), 6.85 (s, 4H, Ar-*H*). ^{13}C {^{1}H} NMR (125 MHz, C_6D_6): δ = 16.08 (N=C–CH_3), 18.24 (*o*-CH_3), 21.21 (*p*-CH_3), 124.91 (*o*-Ar-C), 129.44 (*m*-Ar-C), 132.70 (*p*-Ar-C), 147.09 (ipso-Ar-C), 168.76 (N=C–CH_3). ESMS: Calcd for $C_{22}H_{28}N_2H$ ([M+H]$^+$): 321.2331. Found: 321.2323.

1,4-*Bis*(2,6-dimethyl-4-bromo-phenyl)-2,3-dimethyl-1,4-diaza-1,3-butadiene (^{Me_2BrAr}DAB^{Me}, 2c). 100 ml methanol was added to a mixture of 2,6-dimethyl-4-bromoaniline (5.103 g, 25.5 mmol) and 2,3-butanedione (1.078 g, 12.52 mmol). The aniline was not very soluble in methanol. To this yellow solution, several drops of formic acid were added. The mixture was stirred at room temperature for 48 hours, filtered, washed with methanol (5 × 5 ml). The filtrate was concentrated to ~ 30 ml, filtered, and washed. The insolubles were combined and dried over aspirator for 4 hours. **2c** was isolated as a pale yellow

powder (4.84 g, 86%). ^{1}H NMR (500 MHz, C_6D_6): δ = 1.71 (s, 12H, *o*-C*H*$_3$), 1.82 (s, 6H, N=C–C*H*$_3$), 7.14 (s, 4H, Ar-*H*). ^{13}C {^{1}H} NMR (125 MHz, C_6D_6): δ = 16.02 (N=C–CH$_3$), 17.78 (*o*-CH$_3$),116.725 (Br-Ar-*C*), 127.33 (*o*-Ar-*C*), 131.449(*m*-Ar-*C*), 148.11 (ipso-Ar-C), 168.84(N=C–CH$_3$). ESMS: Calcd for $C_{20}H_{22}N_2Br_2H$ ([M+H]$^+$): 449.0228 (^{79}Br), 451.0209 (^{81}Br). Found: 449.0231, 451.0222.

1,4-*Bis*(3,5-di-*tert*-butylphenyl)-1,4-diaza-1,3-butadiene (^{tBu_2Ar}DAB^H, 3a). Br_2 (0.25 ml, 4.85mmol) was added to a 30ml CH_2Cl_2 solution of PPh_3 (1.30g, 4.96 mmol) at 0 °C under Ar. After the red color disappeared, the solvent was removed by rotavap, leaving behind a white powder. A toluene solution of 3,5-di-*tert*-butylaniline (1.00 g, 4.87mmol) was added to the above white powder under Ar to form an orange solution with white precipitate. Triethylamine (2 ml, 14.4 mmol) was added to the mixture, and the solution turned light yellow with more white precipitate appearing. The mixture was heated to 80 – 90 °C under argon and the reaction was allowed to proceed overnight. After 14 hours, the reaction flask was cooled to room temperature, and the mixture was filtered to remove NEt_3HBr, and the insolubles were washed with petroleum ether (3 x 20 ml). The filtrate was then concentrated, and dry heptane was added to the oily residues. The iminophosphorane (1.4 g, 62%) was isolated by recrystallization from heptane. ^{1}H NMR (300 MHz, C_6D_6): δ = 1.31 (s, 18H, C(C*H*$_3$)$_3$), 6.9 – 7.1 (overlapping peaks, 12H, Ar-*H*), 7.80 (m, 6H, Ar–H). Dry THF was added to the iminophosphorane (1.05 g, 2.26mmol), glyoxal trimer (77 mg, 0.37 mmol) and 1 g 4 Å molecular sieves under Ar, and the mixture was refluxed overnight. After cooling to room temperature., THF was removed, and the residue was dissolved in 10 ml CH_2Cl_2. The yellow solution was filtered through a pad of silica gel and celite to remove triphenylphosphine oxide. The silica gel was washed with additional CH_2Cl_2. All CH_2Cl_2 solution was combined, and the solvent was removed. MeOH was added to the residue, and the yellow insolubles were collected (350 mg, 72%). ^{1}H NMR (500 MHz, C_6D_6): δ = 1.27 (s, 37H, C(C*H*$_3$)$_3$), 7.35 (d, $^4J_{H-H}$ = 1.5Hz, 4H, Ar-*H*), 7.48 (t, $^4J_{H-H}$ = 1.5Hz, 2H, Ar-*H*), 8.67(s, 2H, N=C–*H*). ^{13}C {^{1}H} NMR (125 MHz, C_6D_6): δ = 31.84 (C(CH$_3$)$_3$), 35.38 (*C*(CH$_3$)$_3$), 116.38 (*o*-Ar-C), 122.188 (*p*-Ar-C), 151.60 (*ipso*-Ar-C), 152.622 (*m*-Ar–C), 160.18 (N=C–H). ESMS: Calcd for $C_{30}H_{44}N_2H$ ([M+H]$^+$): 433.3583. Found: 433.3584.

1,4-*Bis*(3,4,5-trimethoxyphenyl)-1,4-diaza-1,3-butadienene (^{OMe_3Ar}DAB^H, 3b). The iminophosphorane was synthesized similarly starting

with 3,4,5-trimethoxyaniline (2 g, 0.0109 mol), PPh_3Br_2 (4.61g, 0.0109 mol) and NEt_3 (4ml, 0.0287 mol) in 10 ml toluene. 2:1 heptane : toluene solution was added to the oily residue to afford 3.81 g of the desired product (79%). ^{1}H NMR (300 MHz, C_6D_6): δ = 3.53 (s, 6H, *m*-OC*H*$_3$), 3.61 (s, 3H, *p*-OC*H*$_3$), 5.92 (s, 2H, Ar-*H*), 7.45 – 7.60 (overlapping peaks, 9H, phosphine *o*- and *p*-Ar-*H*), 7.70 – 7.80 (m, 6H, Ar–H). **3b** was prepared similarly to **3a** with 3.8 g iminophosphorane, 330 mg glyoxyal trimer and 1 g 4 Å molecular sieves in refluxing THF overnight. A substantial amount of iminophosphorane was recovered and 300 mg of product was isolated (20%). The ligands isolated contained 5% phosphine-containing complex. ^{1}H NMR (300 MHz, CD_2Cl_2): δ = 3.80 (s, 6H, *p*-OC*H*$_3$), 3.87 (s, 12H, *m*-OC*H*$_3$), 6.604 (s, 4H, Ar-*H*), 8.40 (s, 2H, N=C–*H*). ESMS: Calcd for $C_{20}H_{24}N_2O_6H$ ([M+H]$^+$): 389.1713. Found: 389.1723.

1,4-*Bis*(3-methoxy-5-(trifluoromethyl)phenyl)-1,4-diaza-1,3-butadienene ($^{OMeCF_3Ar}DAB^H$, 3c). The iminophosphorane was synthesized similarly starting with 3-methoxy-5-trifluoromethyl-aniline (1.25g, 0.00654 mol), PPh_3Br_2 (2.76g, 0.00654 mol) and NEt_3 (2ml, 0.0143 mol). After removing NEt_3HBr and solvent, 100 ml of 4:1 petroleum ether : toluene mixture was added to the oily residue to yield 2.25 g (70% after correcting for toluene content) light tan solid. The product contains ~ 8 wt% toluene. ^{1}H NMR (300 MHz, C_6D_6): δ = 3.18(s, 3H, OC*H*$_3$), 6.69 (br s, 1H), 6.84 (br s, 1H), 6.9 – 7.2 (overlapping peaks, 9H, phosphine *o,p*-Ar-*H*), 7.22(br s, 1H, Ar-*H*), 7.70 (ddd, 6H, J = 1.5 Hz, 7.5 Hz, 12Hz , phosphine *m*-Ar–*H*). Iminophosphorane (1.16g, 2.56 mmol), glyoxal trimer (90mg, 0.428 mmol) and 2 g activated molecular sieves were added to a reaction flask containing dry THF. The mixture was heated at ~ 80 °C overnight. After 17 hours, examination of an aliquot of the mixture indicated little progress in reaction. Another 100 mg of glyoxal trimer was added to the mixture, and the reaction flask was closed off and the reaction temperature was raised to ~100 °C. After 14 hours, the reaction mixture was cooled and another aliquot of the mixture was taken. The conversion was ~ 57%, but the ^{1}H NMR also indicated the existence of a third species (~ 5% of the total product) besides the starting iminophosphorane and the diimine. Since it was not clear whether this species was merely a side-product or the decomposition product of the diimine, the reaction mixture was worked up immediately. 200 mg yellow solids collected (38.5%, contains ~ 5% starting iminophosphoranes). ^{1}H NMR (300 MHz, C_6D_6): δ = 3.06 (s, 6H, OC*H*$_3$),

6.76 (brs, 2H, Ar-*H*), 6.98 (brs, 2H, Ar-*H*), 7.09 (brs, 2H, Ar-*H*), 7.99 (s, 2H, N=C–*H*). ESMS: Calcd for $C_{18}H_{14}N_2O_2F_6H$ ([M+H]$^+$): 405.1038. Found: 405.1051.

($^{tBu}{}_2{}^{OMeAr}$DAB^{Me})PtMe$_2$ (4a). **1a** (200 mg, 0.384 mmol) and bis(dimethyl(μ-dimethylsulfide)platinum(II)) (109.9 mg, 0.191 mmol) were added to a receiving flask equipped with a 180° valve. The flask was cooled to -78 °C and evacuated, and 10 ml toluene was vacuum transferred onto the solids. The dry ice bath was then removed, and the reaction mixture was allowed to warm gradually to room temperature, and was left stirring at room temperature for 3 nights (NB: The reaction was probably done after 10 hours). The solution turned quickly from pale yellow to deep purple upon warming to room temperature. At the end of the reaction, there was a considerable amount of purple solid suspended in the purple solution. Toluene was removed in vacuo, and 15 ml petroleum ether was added to the purple solid residues. The insolubles were collected, washed with petroleum ether (4 ×5 ml), and dried over aspirator for several hours. **4a** was collected as a purple-red solid (265 mg, 92.5%). ^{1}H NMR (500 MHz, CD_2Cl_2): δ = 0.93 (s, 6H, $^2J_{Pt\text{-}H}$ = 86.7 Hz, Pt–C*H*$_3$), 1.452 (s, 36H, C(C*H*$_3$)$_3$), 1.48 (s, 6H, N=C–C*H*$_3$), 3.73 (s, 6H, OC*H*$_3$), 6.865 (s, 4H, Ar-*H*). ^{13}C {^{1}H} NMR (125 MHz, CD_2Cl_2): δ = -13.21 ($^1J_{Pt\text{-}C}$ = 789 Hz, Pt–CH$_3$), 21.30 (N=C–CH$_3$), 32.37 (C(CH$_3$)$_3$), 36.45 (*C*(CH$_3$)$_3$), 64.91 (OCH$_3$), 120.68 (*o*-Ar-*C*), 142.96, 144.46, 157.87 (Ar–*C*), 171.08 (N=*C*–CH$_3$). The compound slowly decomposes in methylene chloride. ESMS: Calcd for $C_{35}H_{55}N_2O_2PtCH_3CN$ ([M-Me+NCMe]$^+$): 770.4156 (^{194}Pt), 771.4180 (^{195}Pt), 772.4192 (^{196}Pt). Found: 770.4173, 771.4180, 772.4189. Anal. Calcd for $C_{36}H_{58}N_2O_2Pt$ (Found): C 57.97 (52.2/53.53); H, 7.84 (7.00/7.24), N, 3.76 (3.33/3.34).

($^{tBu}{}_2{}^{Ar}$DAB^{Me})PtMe$_2$ (4b). **4b** was synthesized similarly from **1b** (160 mg, 0.348 mmol) and bis(dimethyl(μ-dimethylsulfide)platinum(II)) (100 mg, 0.174 mmol). **4b** was collected as a purple-red solid (220 mg, 92%). ^{1}H NMR (500 MHz, CD_2Cl_2): δ = 0.90 (s, 6H, $^2J_{Pt\text{-}H}$ = 85.3 Hz, Pt–C*H*$_3$), 1.36 (s, 36H, C(C*H*$_3$)$_3$), 1.48 (s, 6H, N=C–C*H*$_3$), 6.83 (d, $^3J_{H\text{-}H}$ = 1.5 Hz, 4H, *o*-Ar-*H*), 7.32 (t, $^3J_{H\text{-}H}$ = 1.5 Hz, 4H, *p*-Ar-*H*). ^{13}C {^{1}H} NMR (125 MHz, CD_2Cl_2): δ = -13.13 (Pt-CH$_3$), 21.24(N=C–CH$_3$), 31.69 (C(CH$_3$)$_3$), 35.49 (*C*(CH$_3$)$_3$), 116.76 (*o*-Ar-*C*), 120.18 (*p*-Ar-*C*), 147.68, 151.98 (Ar–*C*), 171.03 (N=*C*–CH$_3$). The compound slowly decomposes in methylene chloride. ESMS: Calcd for $C_{33}H_{51}N_2PtCH_3CN$ ([M-Me+NCMe]$^+$): 710.3945 (^{194}Pt), 711.3969 (^{195}Pt), 712.3980 (^{196}Pt). Found: 710.3945, 711.3951,

712.3969. Anal. Calcd for $C_{34}H_{54}N_2Pt$ (Found): C, 59.54 (58.29/58.95); H, 7.94 (7.76/7.86); N, 4.08 (4.07/4.01).

($^{OMe_3Ar}DAB^{Me}$)PtMe$_2$ (4c). **4c** was synthesized similarly from **1c** (200 mg, 0.48 mmol) and bis(dimethyl(μ-dimethylsulfide)platinum(II)) (138 mg, 0.24 mmol). **4c** was collected as a purple-red solid (278 mg, 90%). ^{1}H NMR (500 MHz, CD_2Cl_2): δ = 1.05 (s, 6H, $^2J_{Pt-H}$ = 85.2Hz, Pt–C*H*$_3$), 1.48 (s, 6H, N=C–C*H*$_3$), 3.82 (s, 6H, OC*H*$_3$), 3.84 (s, 12H, OC*H*$_3$), 6.24 (s, 4H, Ar-*H*). ^{13}C {^{1}H} NMR (125 MHz, CD_2Cl_2): δ = -13.29 ($^1J_{Pt-C}$ = 798 Hz, Pt-CH$_3$), 21.40 (N=C–CH$_3$), 56.72 (OCH$_3$), 61.17 (OCH$_3$), 99.77 (*o*-Ar-C), 136.46, 144.12, 154.02(Ar–C), 171.67 (N=C–CH$_3$). The compound slowly decomposes in methylene chloride. ESMS: Calcd for $C_{23}H_{31}N_2O_6PtCH_3CN$ ([M-Me+NCMe]$^+$): 666.2075 (^{194}Pt), 667.2098 (^{195}Pt), 668.2107 (^{196}Pt). Found: 666.2085, ^{194}Pt), 667.2090, 668.2101. Anal. Calcd for $C_{24}H_{34}N_2O_6Pt$ (Found): C, 44.93 (44.02); H, 5.34 (5.22); N, 4.37 (4.16).

($^{OMeCF_3Ar}DAB^{Me}$)PtMe$_2$ (4d). **4d** was synthesized similarly from **1d** (100 mg, 0.23 mmol) and bis(dimethyl(μ-dimethylsulfide)platinum(II)) (66.5 mg, 0.116 mmol). **4d** was collected as a purple-red solid (130 mg, 85.4%). ^{1}H NMR (500 MHz, CD_2Cl_2): δ = 1.07 (s, 6H, $^2J_{Pt-H}$ = 87.2Hz, Pt–C*H*$_3$), 1.41 (s, 6H, N=C–C*H*$_3$), 3.900(s, 6H, OC*H*$_3$), 6.78 (m, 2H, Ar-*H*), 6.89 (m, 2H, Ar-*H*), 7.10 (m, 2H, Ar-*H*). ^{13}C {^{1}H} NMR (125 MHz, CD_2Cl_2): δ = -12.91 (Pt–CH$_3$), 21.60 (N=C–CH$_3$), 56..51 (OCH$_3$), 109.58 ($^3J_{C-F}$ = 3 Hz, Ar-C), 111.36 ($^3J_{C-F}$ = 3 Hz, Ar-C), 111.55, 124.30 ($^1J_{C-F}$ = 275 Hz, CF$_3$), 132.64 ($^2J_{C-F}$ = 32.7 Hz, CF$_3$–C), 149.74, 161.01 (Ar–C), 171.869(N=C–CH$_3$). ^{19}F NMR (C6D6) δ = -63.70. The compound slowly decomposes in methylene chloride. ESMS: Calcd for $C_{21}H_{21}N_2O_2F_6PtCH_3CN$ ([M-Me+NCMe]$^+$): 682.1400 (^{194}Pt), 683.1423 (^{195}Pt), 684.1431 (^{196}Pt). Found: 682.1382, 683.1411, 684.1393. Anal. Calcd for $C_{22}H_{24}N_2O_2F_6Pt$ (Found): C, 40.19 (38.65/38.88); H, 3.68 (3.53/3.53); N, 4.26 (3.95/4.04).

($^{Me_3Ar}DAB^{Me}$)PtMe$_2$ (5a). **5a** was synthesized similarly from **2a** (111.6 mg, 0.348 mmol) and bis(dimethyl(μ-dimethylsulfide)platinum(II)) (100 mg, 0.174 mmol). **5a** was collected as a purple-red solid (160 mg, 84%). ^{1}H NMR (500 MHz, CD_2Cl_2): δ = 0.79 (s, 6H, $^2J_{Pt-H}$ = 85.7 Hz, Pt–C*H*$_3$), 1.24 (s, 6H, N=C–C*H*$_3$), 2.11 (s, 12H, *o*-C*H*$_3$), 2.37 (s, 6H, *p*-C*H*$_3$), 7.01 (s, 4H, Ar-*H*). ^{13}C {^{1}H} NMR (125 MHz, CD_2Cl_2): δ = -14.92 ($^1J_{Pt-C}$ = 797 Hz, Pt–CH$_3$), 17.48 (*o*-CH$_3$), 20.18 (N=C–CH$_3$), 21.14 (*p*-CH$_3$), 128.84 (*m*-Ar-C), 128.87 (*o*-Ar-C), 135.77 (*p*-Ar-C), 143.77 (*ipso*-Ar–C), 170.79 (N=C–CH$_3$). The compound slowly decomposes in

methylene chloride. ESMS: Calcd for $C_{23}H_{31}N_2PtCH_3CN$ ([M-Me+NCMe]$^+$): 570.2380 (^{194}Pt), 571.2403 (^{195}Pt), 572.2412 (^{196}Pt). Found: 570.2391, 571.2369, 572.2413. Anal. Calcd for $C_{24}H_{34}N_2Pt$ (Found): C, 52.83 (40.75/50.99); H, 6.28 (4.79/6.17); 5.13 (3.89/4.88).

(^{Me_2BrAr}DAB^{Me})PtMe$_2$ (5c). 5c was synthesized similarly from **2c** (78.4 mg, 0.174 mmol) and bis(dimethyl(*μ*-dimethylsulfide)platinum(II)) (50 mg, 0.087 mmol). **5c** was collected as a purple-red solid (100mg, 85%). ^{1}H NMR (500 MHz, CD_2Cl_2): δ = 0.89 (s, 6H, $^2J_{Pt-H}$ = 86 Hz, Pt–C*H*$_3$), 1.20 (s, 6H, N=C–C*H*$_3$), 2.13 (s, 12H, *o*-C*H*$_3$), 7.37 (s, 4H, Ar-*H*). ^{13}C {^{1}H} NMR (125 MHz, CD_2Cl_2): δ = -14.46 ($^1J_{Pt-C}$ = 800 Hz, Pt-CH$_3$), 17.44 (*o*-CH$_3$), 20.45 (N=C–CH$_3$), 119.21 (Br-Ar-C), 131.01 (*m*-Ar-C), 131.55 (*o*-Ar-C), 145.23 (*ipso*-Ar-C), 170.96 (N=C–CH$_3$). The compound slowly decomposes in methylene chloride. ESMS: Calcd for $C_{21}H_{25}N_2Br_2PtCH_3CN$ ([M-Me+NCMe]$^+$): 699.0300 (^{79}Br^{79}Br^{195}Pt), 700.0275 (^{79}Br^{81}Br^{194}Pt), 702.0276 (^{81}Br^{81}Br^{194}Pt), 703.0278 (^{81}Br^{81}Br^{195}Pt), 704.0283 (^{81}Br^{81}Br^{196}Pt). Found: 699.0306, 700.0275, 702.0278, 703.0297, 704.0309. Anal. Calcd for $C_{22}H_{28}N_2Br_2Pt$ (Found): C, 39.13 (38.24/38.03); H, 4.18 (4.07/4.01); 4.15 (3.93/3.88).

(^{tBu_2Ar}DAB^{H})PtMe$_2$ (6a). **6a** was synthesized similarly from **3a** (150 mg, 0.347 mmol) and bis(dimethyl(*μ*-dimethylsulfide)platinum(II)) (100 mg, 0.174 mmol). **6a** was collected as a dark green/tan black solid (187 mg, 82%). ^{1}H NMR (500 MHz, CD_2Cl_2): δ = 1.39 (s, 36H, C(C*H*$_3$)$_3$), 1.65 (s, 6H, $^2J_{Pt-H}$ = 85.4 Hz, Pt–C*H*$_3$), 7.27(d, $^3J_{H-H}$ = 1.5 Hz, 4H, *o*-Ar-*H*), 7.50 (t, $^3J_{H-H}$ = 1.5 Hz, 4H, *p*-Ar-*H*), 9.41 (s, 2H, $^3J_{Pt-H}$ = 24.1 Hz). ^{13}C {^{1}H} NMR (125 MHz, CD_2Cl_2): δ = -11.12 (Pt–CH$_3$), 31.69 (C(CH$_3$)$_3$), 35.53 (C(CH$_3$)$_3$), 118.12 (*o*-Ar-C), 122.90 (*p*-Ar-C), 149.91 (*ipso*-Ar-C), 152.30 (*m*-Ar–C), 161.87 (N=C–H). ESMS: Calcd for $C_{31}H_{47}N_2PtCH_3CN$ ([M-Me+NCMe]$^+$): 682.3632 (^{194}Pt), 683.3655 (^{195}Pt), 684.3666 (^{196}Pt). Found: 682.3641, 683.3646, 684.3667. Anal. Calcd for $C_{32}H_{50}N_2Pt$ (Found): C, 58.43 (56.16/56.16); H, 7.66 (7.85/7.37); N, 4.26 (3.99/4.00).

(^{OMe_3ArH}DAB)PtMe$_2$ (6b). **6b** was synthesized similarly from **3b** (95 mg, 0.245 mmol) and bis(dimethyl(*μ*-dimethylsulfide)platinum(II)) (70 mg, 0.122 mmol). The petroleum ether insolubles were collected, washed with benzene/methylene chloride (to remove triphenylphosphine oxide contained in **3b**), diethylether (20ml) and petroleum ether (4 × 20 ml), and dried over

aspirator for several hours. **6b** was collected as a dark green/tan solid (100mg, 67%). ^{1}H NMR (500 MHz, CD_2Cl_2): δ = 1.88 (s, 6H, $^2J_{Pt-H}$ = 86Hz, Pt–C*H*$_3$), 3.96 (s, 6H, *p*-OC*H*$_3$), 4.01 (s, 12H, *m*-OC*H*$_3$), 6.82 (s, 4H, Ar-*H*), 9.52 (s, 2H, $^3J_{Pt-H}$ = 27 Hz). ^{13}C {^{1}H} NMR (125 MHz, CD_2Cl_2): δ = -11.41 (Pt-CH_3), 54.07 (*m*-OCH_3), 56.45 (*p*-OCH_3), 101.08(*o*-Ar-C), 128.51 (*p*-Ar–C), 145.80 (*ipso*-Ar-C), 153.62 (*m*-Ar–C), 161.21 (N=C–H). ESMS: Calcd for $C_{21}H_{27}N_2O_6PtCH_3CN$ ([M-Me+NCMe]$^+$): 638.1761 (^{194}Pt), 639.1785 (^{195}Pt), 640.1793 (^{196}Pt). Found: 638.1774, 639.1793, 640.1801.

(^{OMeCF_3Ar}DAB^H)PtMe$_2$ (6c). **3c** (80 mg, 0.198 mmol) and bis(dimethyl(μ-dimethylsulfide)platinum(II)) (containing some $(SMe_2)_2PtMe_2$ monomer, 61 mg, ~0.1 mmol) were added to a reaction flask equipped with a 180° valve. Methylene chloride (5 ml) was added to the mixture in air. The solution turned quickly from pale yellow to green. The volatiles were partially removed after half an hour at -20 °C to remove SMe_2. The flask was then back-filled with Ar and 2 ml more methylene chloride was added to the reaction mixture. The mixture was then stirred at room temperature for another half hour to an hour. The solvent was then removed at -20 °C. Methylene chloride (0.5 ml) and petroleum ether (5 ml) were added to the dark solid residue, and the insolubles were collected and washed with petroleum ether (3 x 2 ml). **6c**, the dark green/black solid, was dried over aspirator for 2 hours (104 mg, 84%). **NB:** This reaction did not work in toluene; the green color initially formed faded after 4 hours at room temperature and an intracble mixture was left behind. ^{1}H NMR (500 MHz, CD_2Cl_2): δ = 1.91 (s, 6H, $^2J_{Pt-H}$ = 87 Hz, Pt–C*H*$_3$), 3.94 (s, 6H, OC*H*$_3$), 7.21 (s, 2H, Ar-*H*), 7.24 (s, 2H, Ar-*H*), 7.26 (s, 2H, Ar-*H*), 9.64 (s, 2H, $^3J_{Pt-H}$ = 27Hz). ^{13}C {^{1}H} NMR (125 MHz, CD_2Cl_2): δ = -11.00 (Pt–CH_3), 56..27 (OCH_3), 111.36 ($^3J_{C-F}$ = 3.8 Hz, Ar-C), 112.11 ($^3J_{C-F}$ = 3.6 Hz, Ar-C),112.42, 123.81 ($^1J_{C-F}$ = 272 Hz, CF_3), 132.49 ($^2J_{C-F}$ = 33.5 Hz, CF_3–C), 151.58, 160.57 (Ar–C), 162.52(N=C–H). ESMS: Calcd for $C_{19}H_{17}N_2O_2F_6PtCH_3CN$ ([M-Me+NCMe]$^+$): 654.1086 (^{194}Pt), 655.1110 (^{195}Pt), 656.1118 (^{196}Pt). Found: 654.1078, 655.1118 , 656.1111.

[(^{tBu_2OMeAr}DAB^{Me})PtMe(CO)]$^+$[BF$_4$]$^-$ (7a). To a suspension of **4a** (11.4 mg, 0.015 mmol) in ~ 2 ml trifluoroethanol (TFE), an aqueous solution of HBF_4 (2 μl, 0.015 mmol) was added. After stirring at room temperature for a few minutes, a homogenous orange solution was obtained. The reaction flask was degassed, and backfilled with 1 atm of CO. The color of the solution changed to

bright yellow almost instantaneously. The mixture was stirred under 1 atm of CO for 24 hours. TFE was then removed at -20 – 0 °C in *vacuo*, and a small amount of petroleum ether was added to the oily residue to effect solidification (scratching the reaction flask helps). PE was then removed on the vacuum line, and the resulting yellow solid (7 mg, 54%) was dried for 30 minutes.. The product contained a small amount of TFE, which was hard to remove. ^{1}H NMR (300 MHz, CD_2Cl_2): δ = 0.72 (s, 3H, $^2J_{Pt\text{-}H}$ = 66 Hz, Pt–C*H*$_3$), 1.45, 1.46 (s, 18H each, C(C*H*$_3$)$_3$), 2.36, 244 (s, 3H each, N=C–C*H*$_3$), 3.73, 3.73 (s, 3H each, OC*H*$_3$), 6.95, 7.18 (s, 2H each, Ar-*H*). ^{13}C {^{1}H} NMR (75 MHz, CD_2Cl_2): δ = .-10.45 (Pt–CH$_3$), 20.63, 22.32 (N=C–CH$_3$), 31.90, 31.96 (C(CH$_3$)$_3$), 36.48, 36.52 (*C*(CH$_3$)$_3$), 64.91, 64.99 (OCH$_3$), 119.90, 120.40, 137.49, 142.12, 145.82, 146.04, 159.17, 159.88 (Ar-*C*), 155.52, 175.98, 189.08. IR (CH_2Cl_2): ν(CO) = 2103.5 cm^{-1}. The compound decomposes in methylene chloride. Anal. Calcd for $C_{36}H_{55}N_2O_3PtBF_4$ (Found): C, 51.13 (42.25); H, 6.56 (5.27).

[(*t*Bu$_2$^{Ar}DAB^{Me})PtMe(CO)]$^+$[BF$_4$]$^-$ (7b). **7b** was synthesized similarly from **4b** (15.7 mg, 0.023 mmol) and an aqueous solution of HBF_4 (3 μl, 0.023 mmol) in 3 ml TFE. The yellow product contained a small amount of TFE, which was hard to remove. ^{1}H NMR (300 MHz, CD_2Cl_2): δ = 0.69 (s, 3H, $^2J_{Pt\text{-}H}$ = 69 Hz, Pt–C*H*$_3$), 1.36, 1.37 (s, 18H each, C(C*H*$_3$)$_3$), 2.35, 2.45 (s, 3H each, N=C–C*H*$_3$), 6.91 (d, $^4J_{H\text{-}H}$ = 1.8 Hz, 2H, Ar–*H*), 7.13 (d, $^4J_{H\text{-}H}$ = 1.8 Hz, 2H, Ar–*H*), 7.45, 7.46 (overlapping t, 2H total, Ar–*H*). ^{13}C {^{1}H} NMR (75 MHz, CD_2Cl_2): δ = -10.42 (Pt-CH$_3$), 20.57, 22.34 (N=C–CH$_3$), 31.32(overlapping C(CH$_3$)$_3$), 35.48, 35.54 (*C*(CH$_3$)$_3$), 115.49, 116.32, 122.37, 123.0, 153.15, 153.40 (Ar-*C*), 189.16; resonances for two Ar–C and N=*C*–CH$_3$ were not located. IR (CH_2Cl_2): ν(CO) = 2104.6 cm^{-1}. The compound decomposes in methylene chloride. Anal. Calcd for $C_{34}H_{51}N_2PtBF_4$ (Found): C, 51.98 (49.04/48.84); H, 6.54 (6.18, 6.21); 3.57 (3.35/3.32).

[(OMe$_3$^{Ar}DAB^{Me})PtMe(CO)]$^+$[BF$_4$]$^-$ (7c). **7c** was synthesized similarly from **4c** (14.7 mg, 0.023 mmol) and an aqueous solution of HBF_4 (3 μl, 0.023 mmol) in 3 ml TFE. 13 mg orange powder was obtained (80%). The product contained a small amount of TFE, which was hard to remove. ^{1}H NMR (300 MHz, CD_2Cl_2): δ = 0.84 (s, 3H, $^2J_{Pt\text{-}H}$ = 66 Hz, Pt–C*H*$_3$), 2.34, 2.47 (s, 3H each, N=C–C*H*$_3$), 3.82, 3.86, 3.88 (s, 6H each, OC*H*$_3$), 6..37, 6.54 (s, 2H each, Ar-*H*). ^{13}C {^{1}H} NMR (75 MHz, CD_2Cl_2): δ = .-10.35 (Pt-CH$_3$), 20.66 (overlapping N=C–CH$_3$),

56.56, 56.86, 61.10, 61.20 (OCH_3), 98.25, 98.64, 99.42, 99.75, 138.41, 143.02, 154.31, 154.42(Ar–C), *163.53*, 177.29, 191.04. IR (CH_2Cl_2): ν(CO) = 2105.8 cm^{-1}. The compound slowly decomposes in methylene chloride. Anal. Calcd for $C_{24}H_{31}N_2O_7PtBF_4$ (Found): C, 38.88 (36.64/36.70); H, 4.21 (4.00/3.99); 3.78 (3.34/3.26).

[($^{OMeCF_3Ar}DAB^{Me}$)PtMe(CO)]$^+$[BF_4]$^-$ (7d). **7d** was synthesized similarly from **4d** (15.1 mg, 0.023 mmol) and an aqueous solution of HBF_4 (3 μl, 0.023 mmol) in 3 ml TFE. 10 mg yellow/orange powder collected (62%). The product contained a small amount of TFE, which was hard to remove. ^1H NMR (300 MHz, CD_2Cl_2): δ = 0.77 (s, 3H, $^2J_{Pt-H}$ = 68 Hz, Pt–C*H*$_3$), 2.33, 2.47 (s, 3H each, N=C–C*H*$_3$), 3.93, 3.92 (s, 3H each, OC*H*$_3$), 6.93, 7.09, 7.20, 7.22 (overlapping broad m, 6H total, Ar-*H*). ^1H NMR (300 MHz, TFE-*d*$_3$): δ = 0.83 (s, 3H, $^2J_{Pt-H}$ = 66 Hz, Pt–C*H*$_3$), 2.27, 2.42 (s, 3H each, N=C–C*H*$_3$), 3.90, 3.91 (s, 6H total, OC*H*$_3$), 6.82, 6.91, 6.97, 7.08 (broad s, 1H each, Ar-*H*), 7.27, 7.29 (broad s, 2H total, Ar-*H*). $^{13}C\{^1H\}$ NMR (75 MHz, TFE-*d*$_3$): δ = -10.50 (Pt-CH_3), 20.68, 22.56(N=C–CH_3), 56.92, 56.95 (OCH_3), 110.68 (q, $^3J_{C-F}$~3Hz, *o*-Ar–C), 111.18 (*o*-Ar–C), 112.01(q, $^3J_{C-F}$~3 Hz, *o*-Ar–C), 112.68(*o*-Ar–C), 113.15 (overlapping q, $^3J_{C-F}$ ~ 3 Hz, *p*-Ar–C), 135.90 (q, $^2J_{C-F}$ ~ 23 Hz, C–CF_3), 136.35 (q, $^2J_{C-F}$ ~ 23 Hz, C–CF_3), 145.15, 149.641, 163.11, 163.30 (Ar–C), 179.03, 191.28, unable to find CF_3 resonances, which are probably buried under CF_3CD_2OD resonances. IR (CH_2Cl_2): ν(CO) = 2110.1 cm^{-1}. The compound decomposes quickly in methylene chloride and slowly in the solid state.

[($^{CF_3Ar}DAB^{Me}$)PtMe(CO)]$^+$[BF_4]$^-$ (7e). **7e** was synthesized similarly from **4e** (11.2 mg, 0.015 mmol) and an aqueous solution of HBF_4 (2 μl, 0.015 mmol) in 2 ml TFE The product contained a significant amount of TFE, which was hard to remove. ^1H NMR (300 MHz, TFE-*d*$_3$): δ = 0.77 (s, 3H, $^2J_{Pt-H}$ = 66 Hz, Pt–C*H*$_3$), 2.31, 2.45 (s, 3H each, N=C–C*H*$_3$, the peaks were completely deuterated within an hour at RT), 7.65 (d, $^4J_{H-H}$ = 1.5 Hz, 2H, *o*-Ar–*H*), 7.80 (d, $^4J_{H-H}$ = 1.5 Hz, 2H, *o*-Ar–*H*), 8.05 (t, $^4J_{H-H}$ = 1.5 Hz, 1H, *p*-Ar–*H*), 8.08 (t, $^4J_{H-H}$ = 1.5 Hz, 1H, *p*-Ar–*H*). $^{13}C\{^1H\}$ NMR (75 MHz, TFE-*d*$_3$): δ = -10.09 (Pt-CH_3), 123.01 (q, $^3J_{C-F}$~3Hz), 124.86 (q, $^3J_{C-F}$~3Hz), 127.6 (q, $^1J_{C-F}$~273Hz), 135.84 (q, $^2J_{C-F}$~21Hz, C–CF_3), 136.30 (q, $^2J_{C-F}$~3Hz, C–CF_3), 144.67, 148.99 (Ar–C), 180.43, 192.41, unable to find one set of CF_3 resonances and several Ar–C resonances, which are probably buried under CF_3CD_2OD resonances; unable to find resonances corresponding

to diimine methyl backbone, which were completely deuterated within an hour at room temperature in TFE-d_3. This significantly reduces the intensity of the ^{13}C signals. IR (CH_2Cl_2): ν(CO) = 2113.5 cm^{-1}. The compound decomposes quickly in methylene chloride and in the solid state.

[($^{35Me}{}_2{}^{Ar}DAB^{Me}$)PtMe(CO)]$^+$[$BF_4$]$^-$ (7f). **7f** was synthesized similarly from **4f** (19.8 mg, 0.038 mmol) and an aqueous solution of HBF_4 (5 μl, 0.038 mmol) in 8 ml TFE. 10 mg brown solid was obtained (43%). The product contained a small amount of TFE, which was hard to remove. ^1H NMR (300 MHz, CD_2Cl_2): δ = 0.72 (s, 3H, $^2J_{Pt\text{-}H}$ = 68 Hz, Pt–CH_3), 2.30, 2.42 (s, 3H each, N=C–CH_3), 2.38 (s, 12H, *m*-CH_3), 6.70 (br, 2H, *m*-Ar–*H*), 6.89 (br, 2H, *o*-Ar–*H*), 7.04 (br, 1H, *p*-Ar–*H*), 7.06 (br, 1H, *p*-Ar–*H*). IR (CH_2Cl_2): ν(CO) = 2105.7 cm^{-1}.

[($^{Me}{}_3{}^{Ar}DAB^{Me}$)PtMe(CO)]$^+$[BF_4]$^-$ (8a). **8a** was synthesized similarly from **5a** (16.7 mg, 0.031 mmol) and an aqueous solution of HBF_4 (4 μl, 0.031 mmol) in 5ml TFE. 7 mg yellow powder was obtained (35%). The product contained a small amount of TFE, which was hard to remove. ^1H NMR (300 MHz, CD_2Cl_2): δ = 0.58 (s, 3H, $^2J_{Pt\text{-}H}$ = 66 Hz, Pt–CH_3), 2.16, 2.31 (s, 6H each, *o*-Ar–CH_3), 2.21, 2.41 (s, 3H each, N=C–CH_3), 2.36 (overlapping s, 6H total, *p*-Ar–CH_3), 7.06, 7.07 (s, 4H total, Ar-*H*). ^{13}C {^1H} NMR (75 MHz, CD_2Cl_2): δ = -10.40 (Pt-CH_3), 18.04, 18.07 (*o*-Ar–CH_3), 19.84, 21.22, 21.28, 21.45 (*p*-Ar–*C* & N=C–CH_3), 127.72, 129.61, 129.85, 129.96, 137.63, 138.77, 139.28, 143.23 (Ar–*C*), 179.25, 191.39. IR (CH_2Cl_2): ν(CO) = 2108.3 cm^{-1}. The compound decomposes in methylene chloride, giving methane and Pt black. Anal. Calcd for $C_{24}H_{31}N_2OPtBF_4$ (Found): C, 44.66 (34.36/34.14); H, 4.84 (3.74/3.67); 4.34 (3.08/3.12). The sample appeared to contain silica from the frit; although the C:H:N are all low, they are in the correct ratio.

[($^{Me}{}_2{}^{Ar}DAB^{Me}$)PtMe(CO)]$^+$[BF_4]$^-$ (8b). **8b** was synthesized similarly from **5b** (19.8 mg, 0.038 mmol) and an aqueous solution of HBF_4 (5 μl, 0.038 mmol) in 5 ml TFE. 16 mg yellow powder was obtained (76%). The product contained a small amount of TFE, which was hard to remove. ^1H NMR (300 MHz, CD_2Cl_2): δ = 0.57 (s, 3H, $^2J_{Pt\text{-}H}$ = 66Hz, Pt–CH_3), 2.22, 2.37 (s, 6H each, *o*-Ar–CH_3), 2.24, 2.44 (s, 3H each, N=C–CH_3), 7.20 – 7.40 (m, 6H total, Ar-*H*). ^{13}C {^1H} NMR (75 MHz, CD_2Cl_2): δ = -10.55 (Pt-CH_3), 18.12, 18.17 (*o*-Ar–CH_3), 19.88, 21.49 (N=C–CH_3), 128.09, 128.79, 129.27, 129.30, 129.44, 130.00, 140.42, 145.78(Ar–*C*), 162.69, 179.25, 190.39. IR (CH_2Cl_2): ν(CO) = 2109.6 cm^{-1}. ESMS: Calcd for

$C_{22}H_{27}N_2OPt$ ([M]$^+$): 529.1750 (^{194}Pt), 530.1774 (^{195}Pt), 531.1782 (^{196}Pt). Found: 529.1764, 530.1771, 531.1781. Anal. Calcd for $C_{22}H_{27}N_2OPtBF_4$ (Found): C, 42.80 (41.17/40.94); H, 4.41 (4.44/4.19); 4.54 (4.18/4.16). The compound decomposes in methylene chloride.

[(^{Me_2BrAr}DAB^{Me})PtMe(CO)]$^+$[BF$_4$]$^-$ (8c). **8c** was synthesized similarly from **5c** (25.8 mg, 0.038 mmol) and an aqueous solution of HBF_4 (5 μl, 0.038 mmol) in 5 ml TFE. 16 mg yellow powder was obtained (60%). The product contained a small amount of TFE, which was hard to remove. ^{1}H NMR (300 MHz, CD_2Cl_2): δ = 0.61 (s, 3H, $^2J_{Pt\text{-}H}$ = 69 Hz, Pt–C*H*$_3$), 2.20, 2.35 (s, 6H each, Ar–C*H*$_3$), 2.25, 2.45 (s, 3H each, N=C–C*H*$_3$), 7.43, 7.44 (s, 2H each, Ar-*H*). ^{13}C {^{1}H} NMR (75 MHz, CD_2Cl_2): δ = -10.22 (Pt-CH$_3$), 18.03, 18.07 (Ar–CH$_3$), 20.12, 21.73 (overlapping N=C–CH$_3$), 122.09, 122.66, 130.59, 132.08, 132.13, 132.19, 132.27, 132.41(Ar–*C*), 179.91, 191.04. IR (CH_2Cl_2): ν(CO) = 2111.6 cm^{-1}. The compound slowly decomposes in methylene chloride. ESMS: Calcd for $C_{22}H_{25}N_2Br_2OPt$ ([M]$^+$): 684.9958 (^{79}Br^{79}Br^{194}Pt), 685.9984 (^{79}Br^{79}Br^{195}Pt), 686.9958, 687.9968, 688.9960, 689.9961 (^{81}Br^{81}Br^{195}Pt), 690.9966 (^{79}Br^{79}Br^{195}Pt). Found: 684.9980 , 685.9995 , 686.9962 687.9972, 688.9959, 690.0007, 690.9974. Anal. Calcd for $C_{22}H_{25}Br_2N_2OPtBF_4$ (Found): C, 34.09 (33.30/33.29); H, 3.25 (3.42/3.32); 3.61 (3.44/3.40).

[(^{tBu_2ArH}DAB^H)PtMe(CO)]$^+$[BF$_4$]$^-$ (9a). **9a** was synthesized similarly from **6a** (10 mg, 0.015 mmol) and an aqueous solution of HBF_4 (2 μl, 0.015 mmol) in 3 ml TFE. 5.2 mg orange powder was obtained (47%). The product contained a small amount of TFE, which was hard to remove. ^{1}H NMR (500 MHz, CD_2Cl_2): δ = 1.14 (t, 3H, $^2J_{Pt\text{-}H}$ = 69 Hz, Pt–C*H*$_3$), 1.37, 1.39 (s, 18H each, C(C*H*$_3$)$_3$), 7.12 (d, $^4J_{H\text{-}H}$ = 1.5 Hz, 2H, *o*-Ar–*H*), 7.44 (d, $^4J_{H\text{-}H}$ = 1.5 Hz, 2H, *o*-Ar–*H*), 7.59 (t, $^4J_{H\text{-}H}$ = 1.5 Hz, 1H, *p*-Ar–*H*), 7.64 (t, $^4J_{H\text{-}H}$ = 1.5 Hz, 1H, *p*-Ar–*H*), 9.04 (t, $^3J_{Pt\text{-}H}$ = 74 Hz, N=C–*H*), 9.29 (t, $^3J_{Pt\text{-}H}$ = 38 Hz, N=C–*H*). ^{13}C {^{1}H} NMR (125 MHz, CD_2Cl_2): δ = -8.81 (Pt-CH$_3$), 31.10, 31.14 (C(CH$_3$)$_3$), 35.44, 35.45 (*C*(CH$_3$)$_3$), 117.20, 117.33, 124.80, 126.91, 153.20, 154.04, 163.40, 176.49 (Ar-*C*), could not find CO resonance and two ArC resonances. IR (CH_2Cl_2): ν(CO) = 2108.8 cm^{-1}. Anal. Calcd for $C_{32}H_{47}N_2OPtBF_4$ (Found): C, 50.73 (47.67/47.62); H, 6.25 (5.94/5.91); N, 3.70 (3.45/3.36).

[(^{OMe_3ArH}DAB^H)PtMe(CO)]$^+$[BF$_4$]$^-$ (9b). **9b** was synthesized similarly from **6b** (13.8 mg, 0.023 mmol) and an aqueous solution of HBF_4 (3 μl, 0.023

mmol) in 3ml TFE. 5.2 mg deep reddish purple powder was obtained (33%). The product contained a small amount of TFE, which was hard to remove. ^{1}H NMR (500 MHz, CD_2Cl_2): δ = 1.24 (t, 3H, $^2J_{Pt-H}$ = 66 Hz, Pt–C*H*$_3$), 3.84, 3.88 (s, 3H, *p*-, OC*H*$_3$), 3.89, 3.94 (s, 6H each, OC*H*$_3$), 6.56, 6.90 (s, 2H each, Ar-*H*), 8.98, 9.21 (s, 1H each, N=C–*H*). IR (CH_2Cl_2): ν(CO) = 2110.3 cm^{-1}. The compound slowly decomposes in methylene chloride. ESMS: Calcd for $C_{22}H_{27}N_2OPt$ ([M]$^+$): 625.1445 (^{194}Pt), 626.1469 (^{195}Pt), 627.1477 (^{196}Pt). Found: 625.1447, 626.1460, 627.1473.

[($^{OMe}CF_3{}^{ArH}$DAE)PtMe(CO)]$^+$[BF$_4$]$^-$ (9c) **9c** was synthesized similarly from **6c** (14.5 mg, 0.023 mmol) and an aqueous solution of HBF_4 (3 μl, 0.023 mmol) in 3ml TFE. 6.0 mg was obtained (37%). The product contained a small amount of TFE, which was hard to remove. ^{1}H NMR (CD_2Cl_2): δ = 1.17 (t, 3H, $^2J_{Pt-H}$ = 68 Hz, Pt–C*H*$_3$), 3.94, 3.97 (s, 3H each, OC*H*$_3$), 7.12, 7.17, 7.32, 7.35, 7.40, 7.43 (broad s, 1H each, Ar-*H*), 9.10 (t, 1H, $^3J_{Pt-H}$ = 71 Hz, N=C–*H*), 9.32 (t, 1H, $^3J_{Pt-H}$ = 39 Hz, N=C–*H*); IR (CH_2Cl_2): ν(CO) = 2116.0 cm^{-1}. The compound quickly decomposes in methylene chloride.

Synthesis and Characterization of Methyl Aquo/Solvento Cations (10 –12). The aquo/solvento adducts of **10 – 12** were prepared similarly to procedures described by Tilset and co-workers.[11] The isolated orange/brown solids inevitably contained 5 - 15% decomposition products (mostly the μ-OH dimer). The amount of the impurities can be minimized by strict control of the temperature at which TFE is removed. These impurities are inert under conditions where benzene was activated and are not expected to affect the outcome of intermolecular/intramolecular competition reactions. For most kinetic studies, cations **10–12** are generated in situ (*vide infra*), and the chemical shifts reported below are for solutions in TFE-*d*$_3$ (300 MHz and 500 MHz) in the absence of substrates unless otherwise stated. The Pt–C*H*$_2$D resonances are typically 0.01 – 0.02 ppm upfield of those of the corresponding Pt–C*H*$_3$ peaks. $^2J_{Pt-H}$ can only be observed on the 300 MHz NMR instrument. Addition of benzene can significantly change the chemical shifts for the backbone methyl or H resonances.

10a*i*: δ = 0.77 (s, 3H, $^2J_{Pt-H}$ = 66 Hz, Pt–C*H*$_3$), 1.465, 1.48 (s, 18H each, C(C*H*$_3$)$_3$), 1.88, 2.03 (s, 3H each, N=C–C*H*$_3$), 3.75, 3.76 (s, 3H each, OC*H*$_3$), 6.92, 7.10 (s, 2H each, Ar-*H*).

10a*ii*: δ = 0.765 (s, 3H, $^2J_{Pt-H}$ = 66Hz, Pt–C*H*$_3$), 1.465, 1.49 (s, 18H each, C(C*H*$_3$)$_3$), 1.79, 2.01 (s, 3H each, N=C–C*H*$_3$), 3.75, 3.78 (s, 3H each, OC*H*$_3$), 6.91, 7.15 (s, 2H each, Ar-*H*)

10b*i*: δ = 0.733 (s, 3H, $^2J_{Pt-H}$ = 69Hz, Pt–C*H*$_3$), 1.35, 1.36 (s, 18H each, C(C*H*$_3$)$_3$), 1.85, 2.01 (s, 3H each, N=C–C*H*$_3$), 6.84 (d, $^4J_{H-H}$ = 1.5Hz, 2H, *o*-Ar–*H*), 7.03 (d, $^4J_{H-H}$ = 1.5Hz, 2H, *o*-Ar–*H*), 7.53, 7.61 (t, 1H each, *p*-Ar–*H*).

10bii : δ = 0.723 (s, 3H, $^2J_{Pt-H}$ = 69Hz, Pt–C*H*$_3$), 1.35, 1.37 (s, 18H each, C(C*H*$_3$)$_3$), 1.77, 1.99 (s, 3H each, N=C–C*H*$_3$), 6.83 (d, $^4J_{H-H}$ = 1.5Hz, 2H, *o*-Ar–*H*), 7.07 (d, $^4J_{H-H}$ = 1.5Hz, 2H, *o*-Ar–*H*), 7.52, 7.59 (t, 1H each, *p*-Ar–*H*).

10c*i*: δ = 0.93(s, 3H, $^2J_{Pt-H}$ = Hz, Pt–C*H*$_3$), 1.97, 2.075 (s, 3H each, N=C–C*H*$_3$), 3.90–3.92 (OC*H*$_3$, cannot be identified with certainty because of overlapping with solvent peaks), 6.37, 6.50 (s, 2H each, Ar-*H*).

10c*ii*: δ = 0.91(s, 3H, $^2J_{Pt-H}$ = Hz, Pt–C*H*$_3$), 1.86, 2.08 (s, 3H each, N=C–C*H*$_3$), 3.90–3.92 (OC*H*$_3$, cannot be identified with certainty due to overlapping solvent peaks), 6.36, 6.52 (s, 2H each, Ar-*H*).

10d*i*: δ = 0.875 (s, 3H, $^2J_{Pt-H}$ = Hz, Pt–C*H*$_3$), 1.95, 2.08 (s, 3H each, N=C–C*H*$_3$), 3.89–3.94 (cannot be identified with certainty due to overlapping solvent peaks, OC*H*$_3$), 6.82, 6.95, 7.08, 7.28 (overlapping with **10dii**).

10d*ii*: δ = 0.860 (s, 3H, $^2J_{Pt-H}$ = Hz, Pt–C*H*$_3$), 1.825, 2.05 (s, 3H each, N=C–C*H*$_3$), 3.93, 3.94 (s, 3H each, OC*H*$_3$), 6.82, 6.93, 6.97, 7.08 (broad s, 1H, Ar-*H*), 7.26 (broad s, 2H total, Ar-*H*, split into two peaks in the presence of benzene).

11a*i*: δ = 0.66 (s, 3H, $^2J_{Pt-H}$ = 72Hz, Pt–C*H*$_3$), *1.74, 1.89* (s, 3H each, N=C–C*H*$_3$), 2.15, 2.29 (s, 6H each, *o*-Ar–C*H*$_3$), 2.34(overlapping s, 6H total, *p*-Ar–C*H*$_3$), 7.06, 7.11 (s, 4H total, Ar-*H*). (In the presence of 100μl C_6D_6): δ = 0.74 (s, 3H, $^2J_{Pt-H}$ = 72Hz, Pt–C*H*$_3$), *1.58, 1.73* (s, 3H each, N=C–C*H*$_3$), 2.16, 2.27 (s, 6H each, *o*-Ar–C*H*$_3$), 2.36, 2.38 (s, 3H each, *p*-Ar–C*H*$_3$), 7.05, 7.10 (s, 4H total, Ar-*H*).

11a*ii*: δ = 0.64 (s, 3H, $^2J_{Pt-H}$ = 72Hz, Pt–C*H*$_3$), 0.63(s, Pt–C*H*$_2$D), *1.63, 1.81* (s, 3H each, N=C–C*H*$_3$), 2.15, 2.26 (s, 6H each, *o*-Ar–C*H*$_3$), 2.34(overlapping s, 6H total, *p*-Ar–C*H*$_3$), 7.06, 7.10 (s, 4H total, Ar-*H*). (In the presence of 100μl C_6D_6): δ = 0.73 (s, 3H, $^2J_{Pt-H}$ = 72Hz, Pt–C*H*$_3$), 0.72(s, Pt–C*H*$_2$D), *1.48, 1.66* (s, 3H each, N=C–

CH_3), 2.16, 2.27 (s, 6H each, *o*-Ar–CH_3), 2.36, 2.38 (s, 3H each, *p*-Ar–CH_3), 7.05, 7.10 (s, 4H total, Ar-*H*).

11b*i*: δ = 0.66 (s, 3H, $^2J_{Pt\text{-}H}$ = 72Hz, Pt–CH_3), *1.77, 1.92* (s, 3H each, N=C–CH_3), 2.21, 2.35 (s, 6H each, *o*-Ar–CH_3), 7.24–7.28(m, 6H total, Ar-*H*).

11b*ii*: δ = 0.64 (s, 3H, $^2J_{Pt\text{-}H}$ = 72Hz, Pt–CH_3), 0.62(s, Pt–CH_2D), *1.65, 1.83* (s, 3H each, N=C–CH_3), 2.21, 2.32 (s, 6H each, *o*-Ar–CH_3), 7.24–7.28(m, 6H total, Ar-*H*).

11c*i*: δ = 0.70 (s, 3H, $^2J_{Pt\text{-}H}$ = 72Hz, Pt–CH_3), *1.78, 1.91*(s, 3H each, N=C–CH_3), 2.18, 2.30 (s, 6H each, *o*-Ar–CH_3), 7.46 (s, 4H total, Ar-*H*).

11c*ii*: δ = 0.69 (s, 3H, $^2J_{Pt\text{-}H}$ = 72Hz, Pt–CH_3), 0.67(s, Pt–CH_2D), *1.65, 1.84* (s, 3H each, N=C–CH_3), 2.18, 2.27 (s, 6H each, *o*-Ar–CH_3), 7.43 (s, 4H total, Ar-*H*). (In the presence of 100μl C_6D_6): δ = 0.73 (s, 3H, $^2J_{Pt\text{-}H}$ = 72Hz, Pt–CH_3), *1.46, 1.66* (s, 3H each, N=C–CH_3), 2.13, 2.24 (s, 6H each, *o*-Ar–CH_3), 7.42 (s, 4H total, Ar-*H*).

12a*i*: δ = 1.25 (br s, 3H, Pt–CH_3), 1.38, 1.40 (s, 18H each, $C(CH_3)_3$), 7.13 (d, $^4J_{H\text{-}H}$ = 1.5Hz, 2H, *o*-Ar–*H*), 7.34 (d, $^4J_{H\text{-}H}$ = 1.5Hz, 2H, *o*-Ar–*H*), 7.66 (t, $^4J_{H\text{-}H}$ = 1.5Hz, 1H, *p*-Ar–*H*), 7.77 (t, $^4J_{H\text{-}H}$ = 1.5Hz, 1H, *p*-Ar–*H*), 8.69 (s, 1H, N=C–*H*), 8.71 (s, 1H, N=C–*H*). (In the presence of 30 μl C_6D_6): δ = 1.29 (br s, 3H, Pt–CH_3), 1.42, 1.44 (s, 18H each, $C(CH_3)_3$), 7.16 (d, $^4J_{H\text{-}H}$ = 1.5Hz, 2H, *o*-Ar–*H*), 7.53 (d, $^4J_{H\text{-}H}$ = 1.5Hz, 2H, *o*-Ar–*H*), 7.70 (t, $^4J_{H\text{-}H}$ = 1.5Hz, 1H, *p*-Ar–*H*), 7.83 (t, $^4J_{H\text{-}H}$ = 1.5Hz, 1H, *p*-Ar–*H*), 8.39 (s, 1H, N=C–*H*), 8.43 (s, 1H, N=C–*H*).

12a*ii*: δ = 1.24 (br s, 3H, Pt–CH_3), 1.38, 1.41 (s, 18H each, $C(CH_3)_3$), 7.13 (d, $^4J_{H\text{-}H}$ = 1.5Hz, 2H, *o*-Ar–*H*), 7.51 (d, $^4J_{H\text{-}H}$ = 1.5Hz, 2H, *o*-Ar–*H*), 7.65 (t, $^4J_{H\text{-}H}$ = 1.5Hz, 1H, *p*-Ar–*H*), 7.77 (t, $^4J_{H\text{-}H}$ = 1.5Hz, 1H, *p*-Ar–*H*), 8.80 (br s, 1H, N=C–*H*), 8.85 (s, 1H, N=C–*H*). (In the presence of 30 μl C_6D_6): δ = 1.27 (br s, 3H, Pt–CH_3), 1.42, 1.44 (s, 18H each, $C(CH_3)_3$), 7.12 (d, $^4J_{H\text{-}H}$ = 1.5Hz, 2H, *o*-Ar–*H*), 7.49 (d, $^4J_{H\text{-}H}$ = 1.5Hz, 2H, *o*-Ar–*H*), 7.68 (t, $^4J_{H\text{-}H}$ = 1.5Hz, 1H, *p*-Ar–*H*), 7.81 (t, $^4J_{H\text{-}H}$ = 1.5Hz, 1H, *p*-Ar–*H*), 8.53(br s, 1H, N=C–*H*), 8.55 (s, 1H, N=C–*H*).

12b*ii*: (in the presence of 30 μl C_6D_6): δ = 1.40 (br s, 3H, Pt–CH_3), 1.38 (s, Pt–CH_2D), 3.88, 3.94 (s, 3H each, *p*-OCH_3), 3.90, 3.96 (s, 6H each, *o*-OCH_3), 6.59, 6.97 (s, 2H each, Ar-*H*), 8.71, 8.80 (s, 1H each, N=C–*H*).

12c*ii*:δ = 1.34(br s, 3H, Pt–CH_3), 1.33 (s, Pt–CH_2D), 3.91, 3.94 (s, 3H each, OCH_3), 7.03, 7.15, 7.31, 7.35, 7.38, 7.48 (broad s, 1H each, Ar-*H*), *8.96, 9.07* (s, 1H each, N=C–*H*). (In the presence of 30 μl C_6D_6):δ = 1.37(br s, 3H, Pt–CH_3), 1.36 (s, Pt–CH_2D), 3.94, 3.97 (s, 3H each, OCH_3), 7.03, 7.15, 7.31, 7.35, 7.38, 7.48 (broad s, 1H each, Ar-*H*), *8.75, 8.84* (s, 1H each, N=C–*H*).

Syntheses of Methyl-Acetonitrile Cations (13 –15). Acetonitrile adducts **13 –15** were synthesized according to procedures reported in reference 11. Without added acetonitrile, **13 -15** are in equilibrium with solvento adducts in CD_3OD, CD_3CD_2OD and $(CD_3)_2CDOD$. ^{1}H NMR data:

13b (TFE-d_3): δ = 0.682 (s, 3H, $^2J_{Pt\text{-}H}$ = 72 Hz, Pt–CH_3), 1.36, 1.39 (s, 18H each, C(CH_3)$_3$), 1.92 (s, 3H, NC–CH_3), 1.99, 2.02 (s, 3H each, N=C–CH_3), 6.84 (d, $^4J_{H\text{-}H}$ = 1.5Hz, 2H, *o*-Ar–*H*), 6.97 (d, $^4J_{H\text{-}H}$ = 1.5Hz, 2H, *o*-Ar–*H*), 7.56, 7.60 (t, 1H each, *p*-Ar–*H*).

13b (CD_3OD): δ = 0.55 (s, 3H, $^2J_{Pt\text{-}H}$ = 73 Hz, Pt–CH_3), 1.37, 1.41 (s, 18H each, C(CH_3)$_3$), 2.05, 2.08 (s, 3H each, N=C–CH_3), 2.14 (s, 3H, NC–CH_3), 6.91 (d, $^4J_{H\text{-}H}$ = 1.5Hz, 2H, *o*-Ar–*H*), 7.05 (d, $^4J_{H\text{-}H}$ = 1.5Hz, 2H, *o*-Ar–*H*), 7.47, 7.52 (t, 1H each, *p*-Ar–*H*).

13b (CD_3CD_2OD): δ = 0.56 (s, 3H, $^2J_{Pt\text{-}H}$ = 75 Hz, Pt–CH_3), 1.37, 1.41 (s, 18H each, C(CH_3)$_3$), 2.09, 2.12 (s, 3H each, N=C–CH_3), 2.17 (s, 3H, NC–CH_3), 6.93 (d, $^4J_{H\text{-}H}$ = 1.5Hz, 2H, *o*-Ar–*H*), 7.06 (d, $^4J_{H\text{-}H}$ = 1.5Hz, 2H, *o*-Ar–*H*), 7.44, 7.49 (t, 1H each, *p*-Ar–*H*).

13b ($(CD_3)_2CDOD$): δ = 0.59 (s, 3H, $^2J_{Pt\text{-}H}$ = 75 Hz, Pt–CH_3), 1.37, 1.41 (s, 18H each, C(CH_3)$_3$), 2.12, 2.15 (s, 3H each, N=C–CH_3), 2.19 (s, 3H, NC–CH_3), 6.94 (d, $^4J_{H\text{-}H}$ = 1.5Hz, 2H, *o*-Ar–*H*), 7.08 (d, $^4J_{H\text{-}H}$ = 1.5Hz, 2H, *o*-Ar–*H*), 7.42, 7.46 (t, 1H each, *p*-Ar–*H*).

13d (TFE-d_3)**:** δ = 0.76 (t, 3H, $^2J_{Pt\text{-}H}$ = 67 Hz, Pt–CH_3), 2.01, 2.09 (s, 3H each, N=C–CH_3), 2.07 (s, 3H, NC–CH_3), 3.90, 3.92 (s, 3H each, OCH_3), 6.78, 6.88, 6.89, 7.05, 7.24, 7.26 (broad s, 1H each, Ar-*H*).

13d (CD_3OD): δ = 0.61 (t, 3H, $^2J_{Pt\text{-}H}$ = 67 Hz, Pt–CH_3), 2.09, 2.15 (s, 3H each, N=C–CH_3), 2.27 (s, 3H, NC–CH_3), 3.94, 3.97 (s, 3H each, OCH_3), 6.95, 7.00, 7.07, 7.15, 7.27, 7.31 (broad s, 1H each, Ar-*H*).

14b (CD_3OD): δ = 0.44 (s, 3H, $^2J_{Pt-H}$ = 75Hz, Pt–C*H*$_3$), 2.01, 2.05 (s, 3H each, N=C–C*H*$_3$), 2.06 (s, 3H, NC–C*H*$_3$), 2.23, 2.34(s, 6H each, Ar–C*H*$_3$), 7.25–7.34 (m, 6H total, Ar-*H*).

14c (TFE-*d*$_3$): δ = 0.62(s, 3H, $^2J_{Pt-H}$ = 75Hz, Pt–C*H*$_3$), 1.88, 1.94 (s, 3H each, N=C–C*H*$_3$), 1.97 (s, 3H, NC–C*H*$_3$), 2.15, 2.26 (s, 6H each, Ar–C*H*$_3$), 7.42, 7.47 (s, 2H each, Ar-*H*).

14c (CD_3OD): δ = 0.48 (s, 3H, $^2J_{Pt-H}$ = 75Hz, Pt–C*H*$_3$), 2.03, 2.06(s, 3H each, N=C–C*H*$_3$), 2.19 (s, 3H, NC–C*H*$_3$), 2.21, 2.33 (s, 6H each, Ar–C*H*$_3$), 7.48, 7.53 (s, 2H each, Ar-*H*).

NMR data for (μ-OH)$_2$ dimer 16b: ^{1}H NMR (TFE-*d*$_3$) : 1.24(s, 36H, C(C*H*$_3$)$_3$), 1.91 (s, 6H each, N=C–C*H*$_3$), 5.30 (brs, O–*H*), 7.03 (d, $^4J_{H-H}$ = 1.5Hz, 4H, *o*-Ar-*H*), 7.60 (t, $^4J_{H-H}$ = 1.5Hz, 4H, *p*-Ar–*H*). ^{19}F NMR (TFE-*d*$_3$): -152.0 (BF_4^-).

Measurement of Kinetics for C-H Bond Activation of Aromatic Substrates. Dry TFE-*d*$_3$ was vacuum transferred into an oven-dried 5 mm thin-walled NMR tube with J-Young valve. Approximately 0.0076 mmol of (N–N)PtMe$_2$ (**4** – **6**), 1 μL of aqueous HBF_4 (48 wt%, .00765 mmol) and a predetermined amount of D_2O were then added to the tube. The mixture was shaken to form a clear solution. ^{1}H NMR spectra were then taken of the mixture to ensure clean conversion to aquo/solvento adducts **10** – **12**. A predetermined amount of substrate was then added to the NMR tube, and after allowing the mixture to equilibrate to the preset temperature in the probe, disappearance of the starting material (and appearance of the products **17** – **19**) was monitored. Probe temperatures were calibrated with methanol thermometer and were maintained at ± 0.2 °C throughout data acquisition. The observed rate constants are calculated by curve fitting to the expression $A_t = A_f + (A_0 - A_f) \times \exp(-k_{obs} \times t)$, where A_t is the area under the peak (or the peak height). The area under the peak is found by multiplying the peak height by the full-width-at-half-maximum. The volume of the reaction mixture is determined as V(mL) = 0.01384 H - 0.006754, where H is the solvent height in millimeters. The water concentration is calculated as follows : $[H_2O] = [(1\mu L \times 1.4\ g{\cdot}mL^{-1} \times 52\% + y\ \mu l \times 1 g{\cdot}mL^{-1})/18\ g{\cdot}mol^{-1} - 0.00765 \times n/(n+1)]/V(mL)$, where 1.4 $g{\cdot}mL^{-1}$ is the density of the aqueous HBF_4 solution, 52% is the wt% of water in this aqueous solution, y is the amount of extra water added, 1 $g{\cdot}mL^{-1}$ is the density of water, and n is the ratio

of aquo:solvento adducts. The chemical shifts for the phenyl complexes **17-19** reported below were measured in TFE in the presence of benzene. Addition of a small amount of benzene (e.g., 15 μL) to TFE-d_3 shifts the resonances for the diimine backbone methyls or protons by as much as 0.3 ppm, and can significantly affect shimming.

17a*i*: δ = 1.34, 1.51 (s, 18H each, C(CH_3)$_3$), 1.94, 2.12 (s, 3H each, N=C–CH_3), 3.57, 3.77 (s, 3H each, OCH_3), 7.19, 7.75 (s, 2H each, Ar-*H*), resonances for Ph-H's cannot be identified with certainty.

17a*ii*: δ = 1.33, 1.51 (s, 18H each, C(CH_3)$_3$), 1.88, 2.14 (s, 3H each, N=C–CH_3), 3.59, 3.80 (s, 3H each, OCH_3), 6.71, 7.25(s, 2H each, Ar-*H*), 6.73 (m, 1H, Ph-H_p), 6.79(t, 7.4Hz, 2H, Ph–H_o), 6.87 (m, 2H, Ph–H_m).

17b*i*: δ = 1.23, 1.40 (s, 18H each, C(CH_3)$_3$), 1.90, 2.10 (s, 3H each, N=C–CH_3), 6.61(d, $^4J_{H\text{-}H}$ = 1.5Hz, 2H, *o*-Ar–*H*), 7.14 (d, $^4J_{H\text{-}H}$ = 1.5Hz, 2H, *o*-Ar–*H*), 7.23, 7.68 (t, 1H each, *p*-Ar–*H*), resonances for Ph-H's cannot be identified with certainty.

17b*ii* : δ = 1.22, 1.41 (s, 18H each, C(CH_3)$_3$), 1.85, 2.14 (s, 3H each, N=C–CH_3), 6.61 (d, $^4J_{H\text{-}H}$ = 1.5Hz, 2H, *o*-Ar–*H*), 7.18 (d, $^4J_{H\text{-}H}$ = 1.5Hz, 2H, *o*-Ar–*H*), 7.26, 7.65 (t, 1H each, *p*-Ar–*H*), 6.68 (m, 1H, Ph-H_p), 6.73(m, 2H, Ph–H_o), 6.82 (m, 2H, Ph–H_m).

17c*i*: δ = 2.04, 2.19 (s, 3H each, N=C–CH_3), 3.68, 3.89 (s, 3H each, *p*-OCH_3), 3.72, 3.922(s, 6H each, *o*-OCH_3), 6.09, 6.55 (s, 2H each, Ar-*H*), resonances for Ph-H's cannot be identified with certainty.

17c*ii*: δ =1.97, 2.19 (s, 3H each, N=C–CH_3), 3.71, 3.90 (s, 3H each, *p*-OCH_3), 3.70, 3.915(s, 6H each, *o*-OCH_3), 6.08, 6.67 (s, 2H each, Ar-*H*), 6.80 (m, 1H, Ph–H_p), 6.86 (tt, 8Hz, 1.8Hz, 2H, Ph–H_o), 6.94 (m, 2H, Ph–H_m).

17d*i*: δ = 2.00, 2.16 (s, 3H each, N=C–CH_3), 3.70, 3.92(s, 3H each, OCH_3), 6.48, 6.67, 6.90, 7.00, 7.30, 7.37 (broad s, 1H, Ar-*H*), resonances for Ph-H's cannot be identified with certainty.

17d*ii*: δ = 1.90, 2.15 (s, 3H each, N=C–CH_3), 3.67, 3.92 (s, 3H each, OCH_3), 6.46, 6.70, 6.91, 7.02, 7.28, 7.37(broad s, 1H, Ar-*H*), 6.74 (m, 1H, Ph–H_p), 6.79 (t, 9Hz, 2H, Ph–H_o), 6.85(m, 2H, Ph–H_m).

18a*i* : δ = 1.69, 1.87 (s, 3H each, N=C–C*H*$_3$), 2.13, 2.35 (s, 6H each, *o*-Ar–C*H*$_3$), 2.15, 2.37 (s, 3H each, *p*-Ar–C*H*$_3$), 6.69, 7.14 (s, 4H total, Ar-*H*), 6.69–6.84 (m, 5H, Ph–H's).

18a*ii*: δ = 1.61, 1.81 (s, 3H each, N=C–C*H*$_3$), 2.11, 2.35 (s, 6H each, *o*-Ar–C*H*$_3$), 2.17, 2.39 (s, 3H each, *p*-Ar–C*H*$_3$), 6.72, 7.13(s, 4H total, Ar-*H*), 6.69–6.84 (m, 5H, Ph–H's).

18b*i* : δ = 1.75, 1.96 (s, 3H each, N=C–C*H*$_3$), 2.20, 2.42 (s, 6H each, *o*-Ar–C*H*$_3$), aryl peaks cannot be identified with certainty (many overlapping peaks).

18b*ii* : δ = 1.67, 1.89 (s, 3H each, N=C–C*H*$_3$), 2.18, 2.40 (s, 6H each, *o*-Ar–C*H*$_3$), 6.91, 7.30 (s, 2H each, *o*-Ar-*H*), 6.93, 7.29 (s, 1H each, *p*-Ar-*H*), 6.72–7.00 (m, 5H, Ph–H's).

18c*i* : δ = 1.77, 1.95 (s, 3H each, N=C–C*H*$_3$), 2.14, 2.36 (s, 6H each, *o*-Ar–C*H*$_3$), 7.03, 7.48(s, 4H total, Ar-*H*), 6.69–6.84 (m, 5H, Ph–H's)

18c*ii* : δ = 1.67, 1.89 (s, 3H each, N=C–C*H*$_3$), 2.12, 2.34 (s, 6H each, *o*-Ar–C*H*$_3$), 7.06, 7.46 (s, 2H each, Ar-*H*), 6.69–6.90 (m, 5H, Ph–H's).

19a*ii*: δ = 1.23, 1.46(s, 18H each, C(C*H*$_3$)$_3$), 6.810 (d, $^4J_{H-H}$ = 1.5Hz, 2H, *o*-Ar–*H*), 7.52 (d, $^4J_{H-H}$ = 1.5Hz, 2H, *o*-Ar–*H*), 7.45 (t, $^4J_{H-H}$ = 1.5Hz, 1H, *p*-Ar–*H*), 7.84 (t, $^4J_{H-H}$ = 1.5Hz, 1H, *p*-Ar–*H*), 8.46 (br s, 1H, N=C–*H*), 8.53 (s, 1H, N=C–*H*), 6.84(m, 2H, Ph-H$_o$) The other three Ph–H peaks are probably hidden by free benzene peaks.

19b*ii* δ = 3.78, 3.95 (s, 3H each, *p*-OC*H*$_3$), 3.65, 3.97 (s, 6H each, *o*-OC*H*$_3$), 6.29, 6.99(s, 2H each, Ar-*H*), 8.66, 8.79 (s, 1H each, N=C–*H*), 7.06–7.14 (m, PhH's).

19c*ii* (in the presence of 30μl C_6H_6):δ = 3.61, 3.94 (s, 3H each, OC*H*$_3$), 6.62, 6.87, 7.08, 7.35, 7.44, 7.48 (broad s, 1H each, Ar-*H*), *8.68, 6.82* (s, 1H each, N=C–*H*), cannot be identified with certainty. (In the presence of 60μl C_6D_6):δ = 3.60, 3.93 (s, 3H each, OC*H*$_3$), 6.62, 6.87, 7.08, 7.35, 7.44, 7.48 (broad s, 1H each, Ar-*H*), *8.53, 8.66* (s, 1H each, N=C–*H*), cannot be identified with certainty.

20b (in the presence of 50 μl C_6D_6): δ = 1.25, 1.43 (s, 18H each, C(C*H*$_3$)$_3$), 1.66, 1.97, 2.04 (s, 3H each, N=C–C*H*$_3$ or C*H*$_3$–CN), 6.60 (d, $^4J_{H-H}$ = 1.6 Hz, 2H, *o*-Ar–

H), 7.04 (d, $^4J_{H-H}$ = 1.6 Hz, 2H, *o*-Ar–*H*), 7.31, 7.65 (t, $^4J_{H-H}$ = 1.6 Hz, 1H each, *p*-Ar–*H*), 6.72 (m, 2H, Ph–H_o), 6.74 (m, 1H, Ph-H_p), 6.80 (m, 2H, Ph–H_m).

20d (in the presence of 50 μl C_6D_6): δ = 1.78, 2.02, 2.13 (s, 3H each, N=C–CH_3 or CH_3–CN), 3.65, 3.92 (s, 3H each, OCH_3), 6.40, 6.60, 6.92, 6.93, 7.11, 7.30 (broad s, 1H, Ar-*H*), 6.73 (m, 1H, Ph–H_p), 6.79 (m, 2H, Ph–H_o), 6.83 (m, 2H, Ph–H_m).

21b*ii*: δ = 1.16, 1.24 (s, 9H each, $C(CH_3)_3$), 1.39 (s, 18H, $C(CH_3)_3$), 1.74, 2.08 (s, 3H each, N=C–CH_3), 1.99, 2.51 (s, 3H each, *p*-xylene-Me), 6.55(t, $^4J_{H-H}$ = 1.8Hz, 1H, *o*-Ar–*H*), 6.64 (t, $^4J_{H-H}$ = 1.8Hz, 1H, *o*-Ar–*H*), 7.19 (d, 2H, *o*-Ar–*H*), 7.23, 7.64 (t, $^4J_{H-H}$ = 1.8Hz, 1H each, *p*-Ar–*H*), 6.43 (m, 1H, *p*-xylene-H), 6.55(m, 2H, *p*-xylene-H).

21b*i*: δ = 1.20, 1.21 (s, 9H each, $C(CH_3)_3$), 1.39 (s, 18H, $C(CH_3)_3$), 1.86, 1.98 (s, 3H each, N=C–CH_3), 2.13, 2.38 (s, 3H each, *p*-xylene-Me), 6.67(m, 2H, *o*-Ar–*H*), 7.05 (d, $^4J_{H-H}$ = 1.5 Hz, 2H, *o*-Ar–*H*), 7.23, 7.56 (t, $^4J_{H-H}$ = 1.8Hz, 1H each, *p*-Ar–*H*), 6.25(m, 1H, *p*-xylene-H), 6.60(m, 2H, *p*-xylene-H).

21b (MeCN adduct in CD_3NO_2): δ = 1.16, 1.28 (s, 9H each, $C(CH_3)_3$), 1.43 (s, 18H, $C(CH_3)_3$), 1.95 (s, 3H, N=C–CH_3), 2.02 (s, 3H, CH_3CN), 2.17, 2.27, 2.40 (s, 3H each, N=C–CH_3 or *p*-xylene-Me), 6.36 (m, 1H, *p*-xylene-H), 6.50 (m, 2H, *p*-xylene-H), 6.36 (t, $^4J_{H-H}$ = 1.8Hz, 1H, *o*-Ar–*H*), 6.77 (t, $^4J_{H-H}$ = 1.5 Hz, 1H, *o*-Ar–*H*), 7.16 (d, 2H, *o*-Ar–*H*), 7.24 (t, $^4J_{H-H}$ = 1.5Hz, 1H, *p*-Ar–*H*), 7.63 (t, $^4J_{H-H}$ = 1.8Hz, 1H, *p*-Ar–*H*).

22b (MeCN adduct in CD_3NO_2): δ = 1.34, 1.38(s, 18 H each, $C(CH_3)_3$), 1.75 (t, $^3J_{H-H}$ = 27Hz, 3H, CH_3CN), 2.081, 2.135 (s, 3H, N=C–CH_3), 2.15 (s, 6H, mesitylene-Me), 2.80 (t, $^2J_{H-H}$ = 103 Hz, 2H, Pt–CH_2Ar), 6.51 (m, 2H, mesitylene-H), 6.59 (m, 1H, mesitylene-H), 6.93, 6.97 (d, $^4J_{H-H}$ = 1.5Hz, 2H each, *o*-Ar–*H*), 7.40, 7.48(t, $^4J_{H-H}$ = 1.5Hz, 1H each, *p*-Ar–*H*).

22b*ii* (aquo adduct in TFE-d_3) : δ = 1.38, 1.42 (s, 18 H each, $C(CH_3)_3$), 1.78, 1.92 (s, 3H, N=C–CH_3), 2.53 (s, 6H, mesitylene-Me), 5.93 (br s, 2H, *o*-mesitylene-H (*substantial H incorporation into this position when mesitylene-d_{12} is used*), 6.47, 7.06 (d, $^4J_{H-H}$ = 1.5Hz, 2H each, *o*-Ar–*H*), 7.56, 7.60 (t, $^4J_{H-H}$ = 1.5Hz, 1H each, *p*-Ar–*H*), several peaks cannot be identified with certainty; they are probably buried under free mesitylene peaks.

23b*ii*: most peaks cannot be identified with certainty, except: 1.23 (s, $C(CH_3)_3$), and 1.70, 2.07 (s, N=C–CH_3).

Measurement of Equilibrium Constants. Dry TFE-d_3 was vacuum transferred into an oven-dried J-Young tube. Approximately 0.0076 mmol of (N–N)$PtMe_2$ (**4** - **6**) and 1 μl of aqueous HBF_4 (48 wt%, 0.00765 mmol) were then added to the tube. After allowing the mixture to equilibrate to 20 °C, the ratio of the aquo to solvento adducts, n, was then determined by integration. The water concentration was determined as follows: $[(1\mu l \times 1.4\ g{\cdot}mL^{-1} \times (1 - 0.48) / 18\ g{\cdot}mol^{-1}) - 0.0076\ mmol \times n/(1 + n)]/V(mL)$. Volume was determined as described above. The TFE-d_3 concentration was taken as 14.07 *M*.

Acetonitrile Exchange Reactions: 3.5 mg of the appropriate acetonitrile adduct **13-15** (2.5 mg in $(CD_3)_2CDOD$ because of limited solubility) was added to an oven-dried NMR tube. About 0.7 mL of the deuterated solvent was then added, and a ^1H NMR spectrum was recorded before addition of a predetermined amount of CD_3CN. Under these conditions, the acetonitrile adducts were the only observable species in solution. After allowing the mixture to equilibrate to a preset temperature (~ 5 min.), the disappearance of coordinated CH_3CN and appearance of free CH_3CN were monitored, and observed rate of exchange was determined from the expression: $A_t = A_f + (A_0 - A_f) \times \exp(-k_{ex} \times t)$, where A_t is the area under the peak (or the peak height). The volume of the solution is determined as described above.

Measurement of KIE via Inter- or Intramolecular Competition Reactions: Dry TFE-d_3 was added to an oven-dried NMR tube containing pre-formed aquo/solvento adducts **10**. A mixture of 1:1 C_6H_6 : C_6D_6 or $C_6D_3H_3$ was then added to the tube. After reaction was complete, the integration ratio of CH_nD_{4-n} to CH_4 was then taken to give the KIE.

Measurement of the Ratio of CH_3D : CH_4 as a Function of Added Acetonitrile in the Protonolysis of 4b. To a suspension of 0.0076 mol of **4b** over dry TFE-d_3 in oven-dried NMR tube, a predetermined amount of CD_3CN was added. To this mixture, 5 μl of a stock solution of 1 μl aqueous HBF_4 (48 wt%) in 24 μl TFE-d_3 was added. The tube was shaken, and after a clear orange solution was formed, the ratio of CH_3D : CH_4 was measured by integration. To account for the percentage of protonolysis by H^+ (rather than D^+), the H^+ concentration

was measured by integrating the [O*H*] resonance against the aromatic protons of **4b**. H^+ typically accounts for 1–3% of the total H^+/D^+ source. This percentage was subtracted from the percentage of liberated CH_4. The adjusted ratio of CH_3D : CH_4 was then plotted against the acetonitrile concentrations to yield Figure 1.

References and Notes

1. (a) Arndtsen, B. A.; Bergman, R. G.; Mobley, T. A.; Peterson, T. H. *Acc. Chem. Res.* **1995**, *28*, 154. (b) *Selective Hydrocarbon Activation*; Davies, J. A.; Watson, P. L.; Liebman, J. F. and Greenberg, A., Eds.; VCH: New York, 1990. (c) *Activation and Functionalization of Alkanes*; Hill, C. L., Ed.; John Wiley & Sons: New York, 1989. (d) Shilov, A. E. and Shul'pin, G. B. *Activation and Catalytic Reactions of Saturated Hydrocarbons in the Presence of Metal Complexes.* Kluwer Academic Publishers: Dordrecht, 2000.

2. For some examples, see (a) Periana, R. A.; Taube, D. J.; Gamble, S.; Taube, H.; Satoh, T.; Fujii, H. *Science* **1998**, *280*, 560–564. (b)Periana, R. A.; Taube, D. J.; Evitt, E. R.; Loffler, D. G.; Wentrcek, P. R.; Voss, G.; Masuda, T. *Science.* **1993**, *259*, 340–343. (c)Waltz, K. M.; Hartwig, J. F. *J. Am. Chem. Soc.* **2000**, *122*, 11358–11369. (d)Waltz, K. M.; Muhoro, C. N.; Hartwig, J. F. *Organometallics* **1999**, *18*, 3383–3393. (e)Waltz, K. M.; Hartwig, J. F. *Science.***1997**, *277*, 211–213. (f)Sen, A.; Benvenuto, M. A.; Lin, M.; Hutson, A. C.; Basickes, N. *J. Am. Chem. Soc.* **1994**, *116*, 998–1003.

3. Stahl, S.; Labinger, J. A.; Bercaw, J. E. *Angew. Chem., Int. Ed.* **1998**, *37*, 2181–2192.

4. Gol'dshleger, N. F.; Es'kova, V. V.; Shilov, A. E.; Shteinman, A. A. *Zh. Fiz. Khim.* **1972**, *46*, 1353–1354 (English translation **1972**, *46*, 785–786).

5. Labinger, J. A.; Herring, A. M.; Lyon, D. K.; Luinstra, G. A.; Bercaw, J. E.; Horvath, I. T.; Eller, K. *Organometallics* **1993**, *12*, 895–905.

6. (a)Luinstra, G. A.; Wang, L.; Stahl, S. S.; Labinger, J. A.; Bercaw, J. E. *Organometallics* **1994**, *13*, 755-756. (b)Luinstra, G. A.; Labinger, J. A.;

Bercaw, J. E. *J. Am. Chem. Soc.* **1993**, *115*, 3004-3005. (c) Luinstra, G. A.; Wang, L.; Stahl, S. S.; Labinger, J. A.; Bercaw, J. E. *J. Organomet. Chem.* **1995**, *504*, 75.

7 (a)Kushch, L. A.; Lavrushko, V. V.; Misharin, Y. S.; Moravskii, A. P.; Shilov, A. E. *Nouv. J. Chim.* **1983**, *7*, 729-733. (b)Hutson, A. C.; Lin, M.; Basickes, N.; Sen, A. *J. Organomet. Chem.* **1995**, *504*, 69-74. (c)Horvath, I. T.; Cook, R. A.; Millar, J. M.; Kiss, G. *Organometallics* **1993**, *12*, 8-10.

8. (a)Stahl, S. S.; Labinger, J. A.; Bercaw, J. E. *J. Am. Chem. Soc.* **1996**, *118*, 5961–5976. (b)Stahl, S. S.; Labinger, J. A.; Bercaw, J. E. *J. Am. Chem. Soc.* **1995**, *117*, 9371–9372.

9. (a)Holtcamp, M. W.; Henling, L. M.; Day, M. W.; Labinger, J. A.; Bercaw, J. E. *Inorg. Chim. Acta* **1998**, *270*, 467–478. (b)Holtcamp, M. W.; Labinger, J. A.; Bercaw, J. E. *J. Am. Chem. Soc.* **1997**, *119*, 848–849. (c) Holtcamp, M. W.; Labinger, J. A.; Bercaw, J. E. *Inorg. Chim. Acta* **1997**, *265*, 117–125.

10. Johansson, L.; Ryan, O. B.; Tilset, M. *J. Am. Chem. Soc.* **1999**, *121*, 1974–1975.

11. Johansson, L.; Tilset, M.; Labinger, J. A.; Bercaw, J. E. *J. Am. Chem. Soc.* **2000**, *122*, 10846–10855.

12. (a)Tellers, D. M.; Skoog, S. J.; Bergman, R. G.; Gunnoe, T. B.; Harman, W. D. *Organometallics* **2000**, *19*, 2428–2432. (b)Tellers, D. M.; Bergman, R. G. *J. Am. Chem. Soc.* **2000**, *122*, 954–955.

13. Westheimer, F. H.; Taguchi, K. *J. Org. Chem.* **1971**, *36*, 1570–1572.

14. Kliegman, J. M.; Barnes, R. K. *J. Org. Chem.* **1970**, *35*, 3140–3143. *2,6*-dimethylaniline and its derivatives *do* react fairly cleanly with glyoxal (40% aq.) to yield the corresponding diimines.

15. (a)Saito, T.; Ohkubo, T.; Kuboki, H.; Maeda, M.; Tsuda, K.; Karakasa, T.; Satsumabayashi, S. *J. Chem. Soc., Perkin Trans. 1* **1998**, 3065–3080. (b)Nitta, M.; Soeda, H.; Iino, Y. *Bull. Chem. Soc. Jpn.* **1990**, *63*, 932–934. (c)Hartmann, R. W.; Vom Orde, H. D.; Heindl, A.; Schoenenberger, H. *Arch. Pharm.*

(Weinheim, Ger.) **1988**, *321*, 497–501. (d)Soloshonok, V. A.; Gerus, I. I.; Yagupol'skii, Y. L.; Kukhar, V. P. *Zh. Org. Khim.* **1987**, *23*, 2308–2313.

16. Iminophosphoranes containing extremely electron-withdrawing substituents (e.g, Ar = *3,5*-$(CF_3)_2$-C_6H_3) do not react with gloxyal trimer in refluxing THF. The corresponding diimines can only be prepared by reacting the iminophosphoranes with glyoxal monomer at room temperature in methylene chloride. For preparation of glyoxal monomer, see : Wang, Y.; Arif, A. M.; Gladysz, J. A. *Organometallics* **1994**, *13*, 2164–2169.

17. Hill, G. S.; Irwin, M. J.; Levy, C. J.; Rendina, L. M.; Puddephatt, R. J. *Inorg. Synth.* **1998**, *32*, 149–153.

18. Rostovtsev, V. V.; Labinger, J. A.; Bercaw, J. E. unpublished results.

19. The estimated uncertainties are ~ 5% for the parallel reactions, and ~ 10% for the inter- and intramolecular competition reactions.

20. Johansson, L. thesis: *Department of Chemistry, Faculty of Mathematics and Natural Sciences*; University of Oslo: Oslo, Norway, 2000; p 117–145.

21. (a) Ganis, P.; Orabona, I.; Ruffo, F.; Vitagliano, A. *Organometallics* **1998**, *17*, 2646–2650. (b) Fusto, M.; Giordano, F.; Orabona, I.; Ruffo, F. *Organometallics* **1997**, *16*, 5981–5987.

22. Zuccaccia, C.; Macchioni, A.; Orabona, I.; Ruffo, F. *Organometallics* **1999**, *18*, 4367–4372.

23. Yang, K.; Lachicotte, R. J.; Eisenberg, R. *Organometallics* **1998**, *17*, 5102–5113.

24. Scollard, J.D; Labinger, J. A.; Bercaw, J. E. manuscript in preparation.

25. Brandow, C. G.; Zhong, H. A., unpublished results.

26. *The Chemist's Companion: a Handbook of Practical Data, Techniques, and References*; Gordon, A. J., Ford, R. A., Eds.; John Wiley & Sons: New York, 1972.

27. Johansson, L.; Tilset, M. *J. Am. Chem. Soc.* **2001**, *123*, 739-740.

28. Romeo, R.; Minniti, D.; Lanza, S. *Inorg. Chem.* **1980**, *19*, 3663–3668.

29. Zhong, H. A.; Labinger, J. A.; Bercaw, J. E. unpublished results.

30. Romeo, R. *Comments Inorg. Chem.* **1990**, *11*, 21–57.

Appendix A

Alkane C–H Bond Activation by Cationic Platinum(II) Complexes and Reaction of a Cationic Platinum(II) Hydride Complex with *tert*-Butylacetylene

Introduction

In recent years, considerable effort has been directed toward identifying new catalysts for alkane functionalization. The first step of such a transformation will inevitably involve C–H activation. In Chapter 4, it was discussed how ligands affect the reactivities and regioselectivities of arene C–H activation by cationic platinum(II). In this section, we will briefly describe the reactions between an α-aryldiimine ligated cationic platinum(II) complex (**1**) with alkanes.

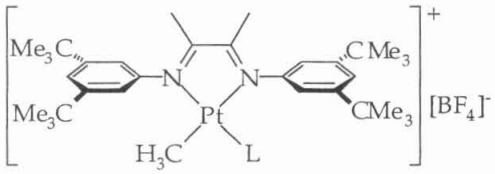

(L = TFE (*i*); H_2O (*ii*))

1

Results and Discussion

Alkane C–H Activation by 1. Cationic platinum(II) complex **1** reacts with methane and β-H containing alkanes. For example, when a mixture of 0.01 *M* **1**, 0.05 *M* H_2O and ~ 0.1 *M* $^{13}CH_4$ in TFE-d_3 was heated at 45 °C for 4 hours, a doublet ($^1J_{C-H}$ = 127 Hz) centered at the same chemical shift as [Pt–CH_3] (0.74 ppm for TFE adduct and 0.75 ppm for H_2O adduct), was observed in the ^{1}H NMR spectrum. This is consistent with the formation of a Pt–$^{13}CH_3$ bond (Scheme 1). In the ^{13}C NMR spectrum, the Pt–$^{13}CH_3$ peaks at -7.76 ppm (TFE adduct) and -9.13 ppm (H_2O adduct) also grew gradually in intensity. The ratio of [Pt–CH_3] to [Pt–^{13}CH_3] was approximately 1:1 after 4 hours at 45 °C. These reaction conditions also led to substantial decomposition of the starting material (**1**) to give a (μ-OH)$_2$ dimer and other unidentifiable compounds. However, no discernible amount of Pt black was observed. The rate of decomposition was approximately the same as the rate of reaction between **1** and $^{13}CH_4$ under these conditions.

Scheme 1

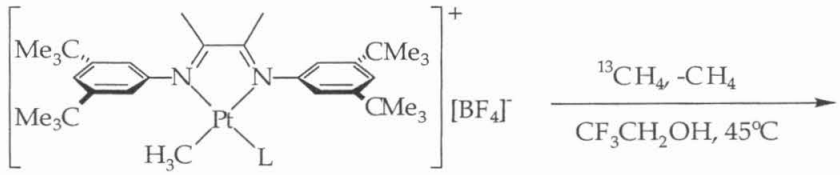

(L = TFE (*i*); H_2O (*ii*))

1

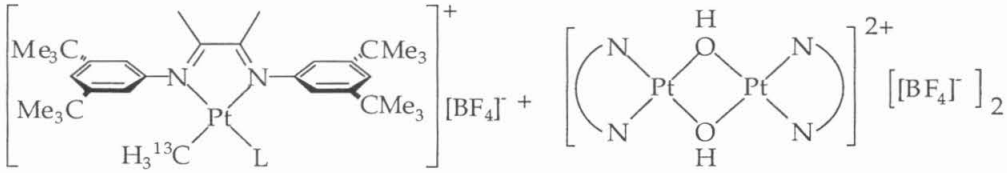

(L = TFE (*i*); H_2O (*ii*))

1-$^{13}CH_3$

+ other decomposition products

2

	1	**1**-$^{13}CH_3$	**2** + other decomp. products
t = 0	100%	0%	0%
t = 4 hrs	30%	30%	40%

In contrast, **1** reacted with cyclohexane at room temperature to afford [(N-N)Pt(cyclohexene)(H)][BF_4] (**3**, >90% purity by ^{1}H NMR) (Scheme 2).

Scheme 2

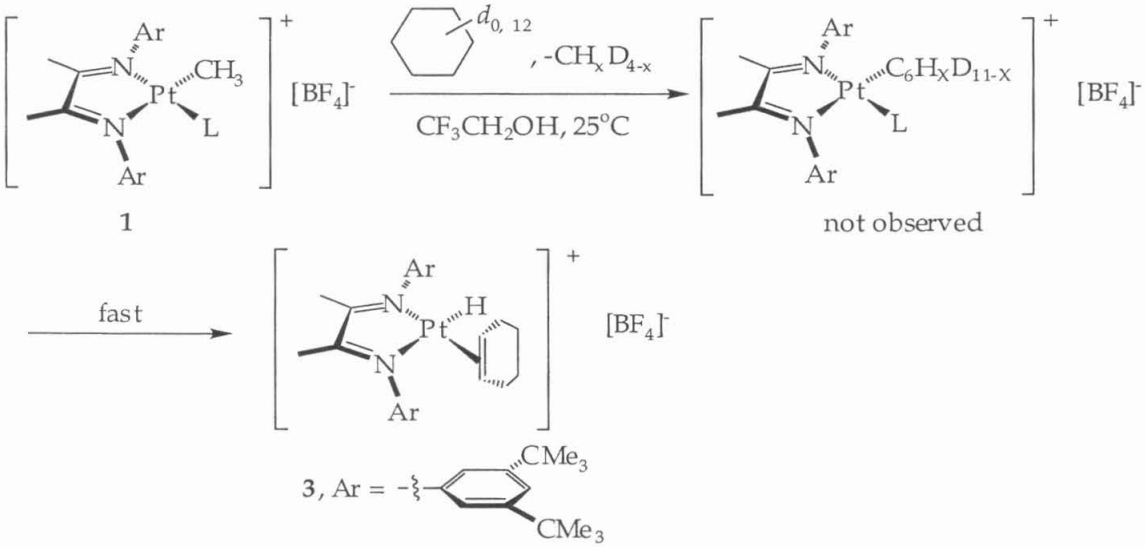

1

3, Ar = -

^{1}H NMR spectroscopy showed that as reaction progressed, a peak at -22 ppm ($^1J_{Pt-H}$ = 1270 Hz) grew in intensity, with concomitant appearance of a broad peak at 4.95 ppm. The peak upfield at -22 ppm is assigned as the Pt–H resonance, while the peak at 4.95 ppm is assigned as the vinylic protons of the coordinated cyclohexene. The resonance for the coordinated cyclohexene remained broad even at -50 °C (in methylene chloride-d_2), implying rapid rotation of the bound olefin. A spectrum of the reaction product is shown in Figure 1.

To confirm the presence of coordinated cyclohexene in the product, excess acetonitrile or *tert*-butylacetylene was added to either a methylene chloride-d_2 or TFE-d_3 solution of **3**. Resonances corresponding to free cyclohexene (verified by comparing to the spectrum of an authentic sample) appeared almost instantaneously at room temperature. The intensity of the free cyclohexene peak (the vinylic protons were integrated against the aromatic protons of the diimine ligands; and the alkyl protons were integrated against Me backbone of the ligands) established a 1:1 ratio of cyclohexene to Pt. Complex **3** represents one of the few examples of a stable hydrido Pt(II) olefin complex with nitrogen-chelates.[1]

Complex **3** is presumably formed by a two step reaction, in which a Pt-cyclohexyl complex is initially formed, followed by β-hydride elimination to afford the final product. The kinetics of the reaction between **1** and cyclohexane ([**1**] = 0.01 *M*, [C_6H_{12}] = 0.56 *M*, [H_2O] = 0.05 *M*, $k_{obs} = 1.2 \times 10^{-4}$ s^{-1}) were followed by monitoring the appearance and disappearance of peaks in the aryl region of the ^{1}H NMR spectrum (Figure 2). The intermediate, [Pt–cyclohexyl] complex, could not be detected, implying that formation of the Pt–cyclohexyl complex is much slower than the subsequent β-hydride elimination to form **3**. Complex **1** reacts with cyclohexane ~ 55 times slower than with benzene under comparable conditions. Because of this reduced reactivity, an appreciable amount of the bis(μ-hydroxy)-bridged dimer (**2**) was observed at later stage of the reaction. A KIE of 2.4 has been measured for the reaction between **1** and cyclohexane. In contrast to the reaction between **1** and benzene-d_6, where CH_3D accounted for 60% of the liberated methane, methane isotopomers, CH_3D : CH_2D_2 : CHD_3 (the amount of CD_4 was not determined), generated from the reaction between **1** and cyclohexane-d_{12} were present in a 1.3 : 2.4 : 1 ratio. As a result of this substantial deuterium scrambling, weak signals could be detected at -22 and 4.95 ppm in the ^{1}H NMR spectrum. Attempts to isolate **3** in pure form

have so far been unsuccessful. The isolated products usually contained 5 – 10% of the $(\mu\text{–OH})_2$ dimer (**2**).

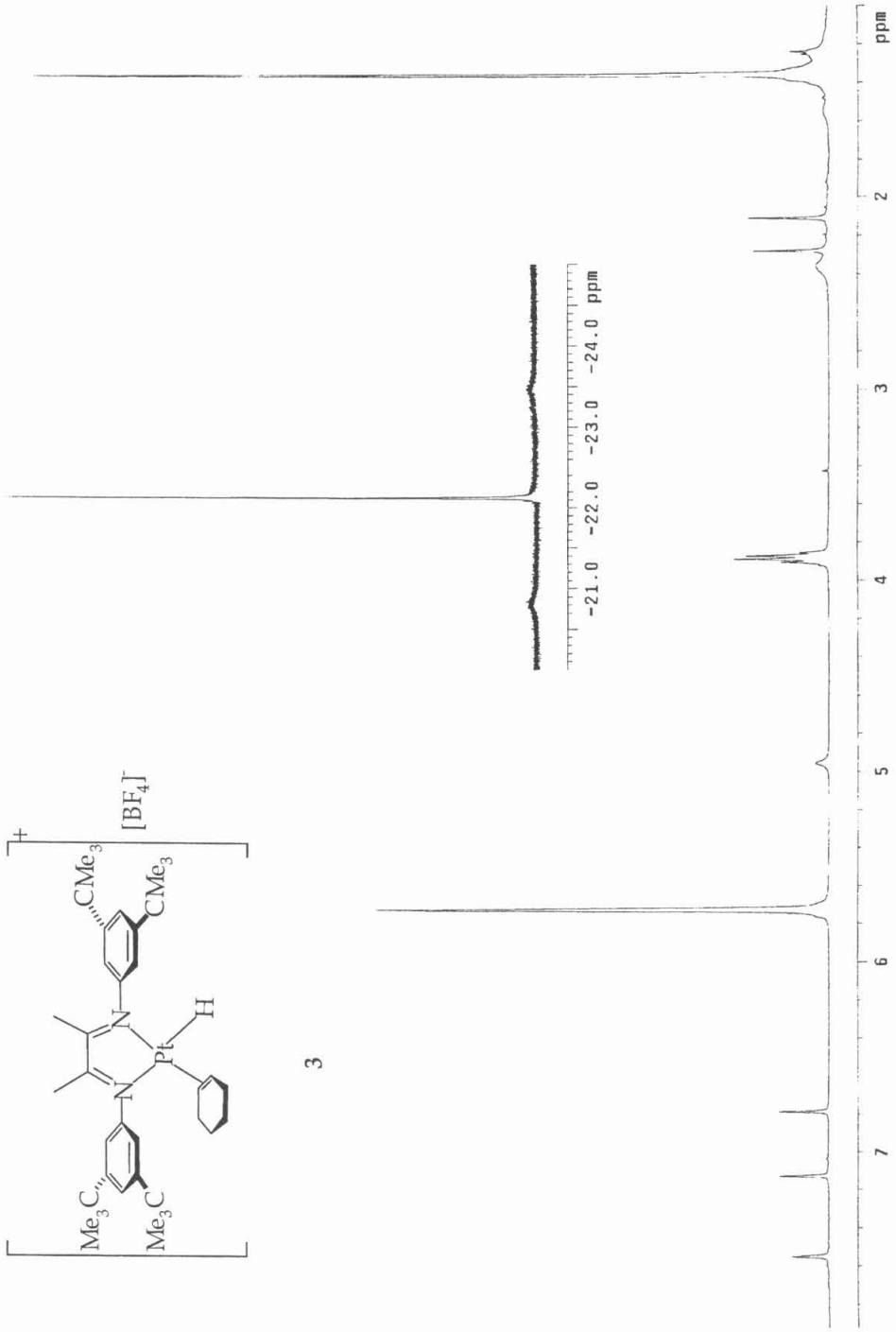

Figure 1. ^{1}H NMR spectrum of **3** in TFE-d_3.

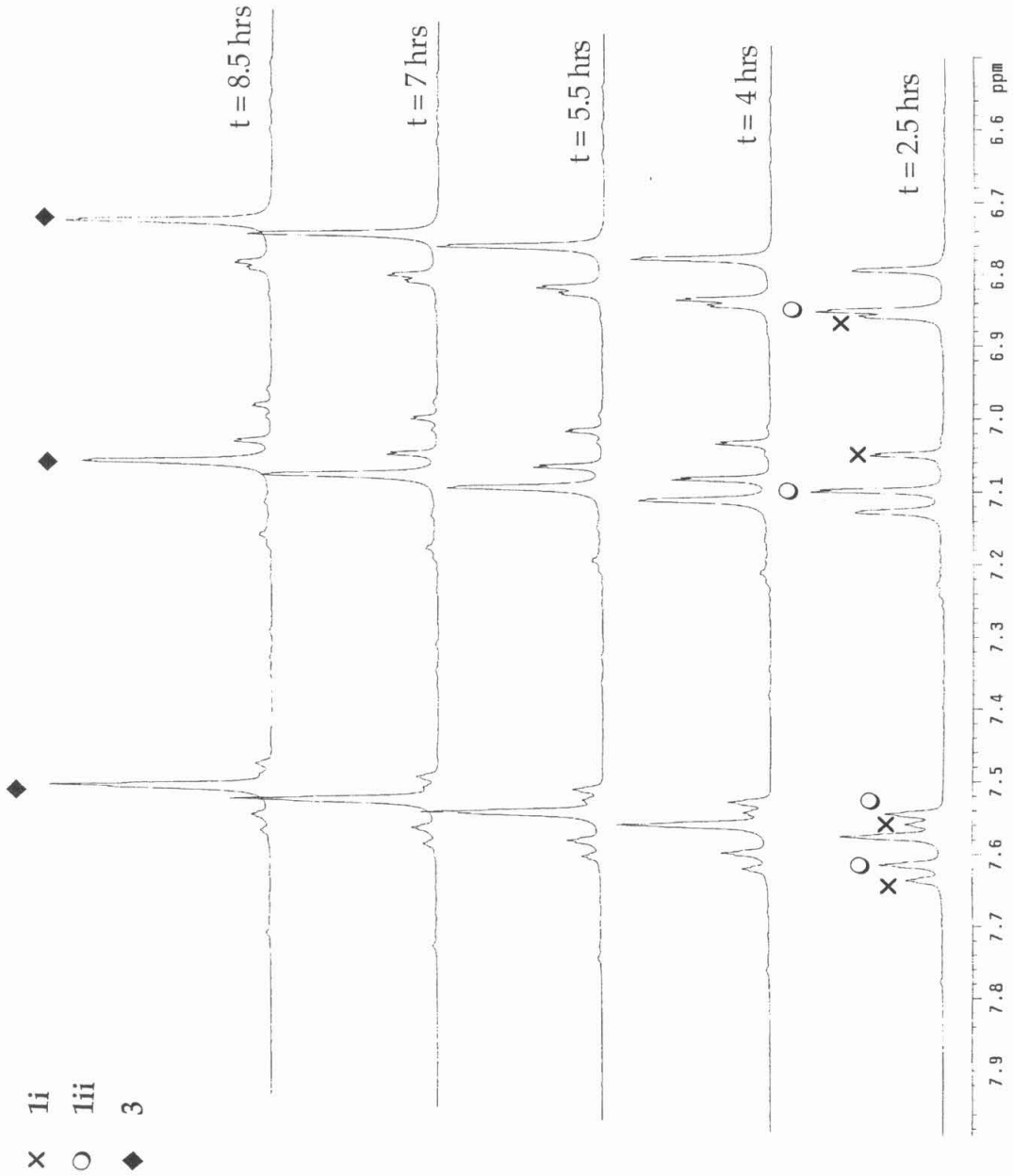

Figure 2. Aryl Region of the ^{1}H NMR spectra of the reaction between **1** and cyclohexane.

Reactions of **1** with *n*-pentane or *n*-butane generated two Pt–H complexes in a ~ 2:1 ratio. In the reaction between **1** and *n*-pentane, acetonitrile was added to the product mixture to displace the bound olefin adducts. Comparison of ^{1}H NMR spectra of the displaced olefin to those of authentic samples of 1-pentene, cis-2-pentene and a mixture of *cis/trans*-2-pentene indicated that the bound olefins are *cis*- and *trans*-2-pentene (1:2 *cis* : *trans*). The observed product mixture is most likely a thermodynamic product mixture (eq 1). The facile isomerization of bound 1-pentene to 2-pentenes is not surprising in light of the fast rearrangement observed in the reaction of **3** with tert-butylacetylene (*vide infra*). Considering the structural similarities between *n*-butane and *n*-pentane, the product mixture observed for the reaction between **1** and *n*-butane likely consisted of only bound internal olefins.

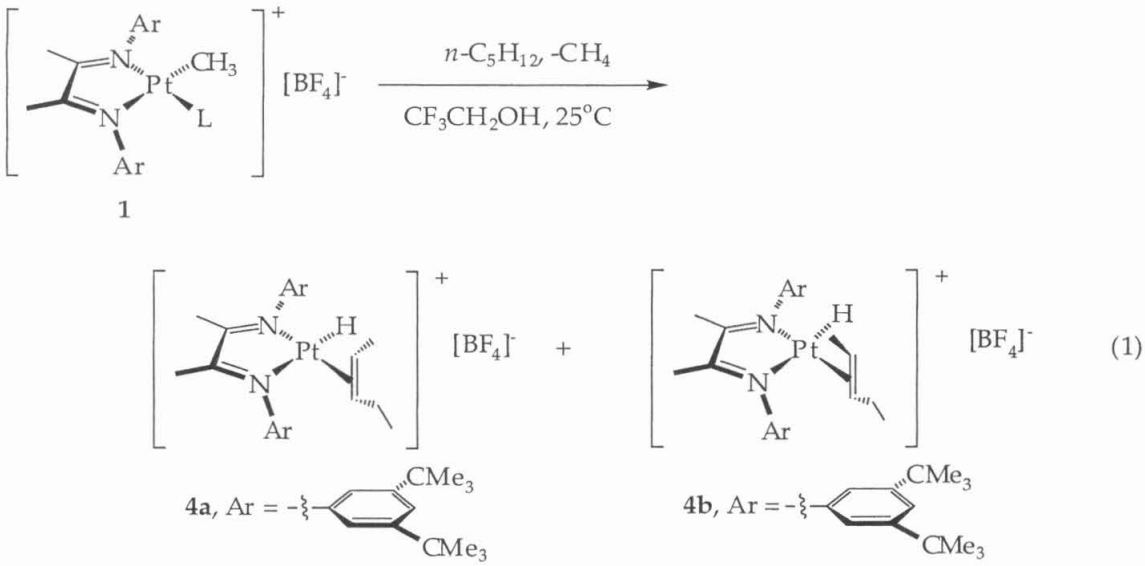

Complex **1** also reacts with 2,3-dimethylbutane. A single resonance was detected in the Pt–H region of the ^{1}H NMR spectrum. Signals were also present at 3.45 and 3.51 ppm in a 1:1 ratio, which are indicative of a bound terminal olefin. Consequently, **5** is tentatively assigned as the major product from the reaction between **1** and 2,3-dimethylbutane (eq 2). The absence of bound internal olefin is probably a consequence of steric hindrance prohibiting the activation of, or β-hydride elimination from a 3° carbon center. The ^{1}H NMR spectrum of the product **5** also shows three *tert*-butyl resonances in a ratio of ~2:1:1, which results from hindered rotation of one of the two ligand aryl

groups, presumably the one attached to the N atom *cis* to the bound olefin group. The aryl H resonances confirm the reduced symmetry: five peaks present in a 1:1:1:1:2 ratio correspond to two non-equivalent ortho protons plus a para proton on one ring, and two equivalent ortho protons plus a para proton on the other (freely rotating) one.

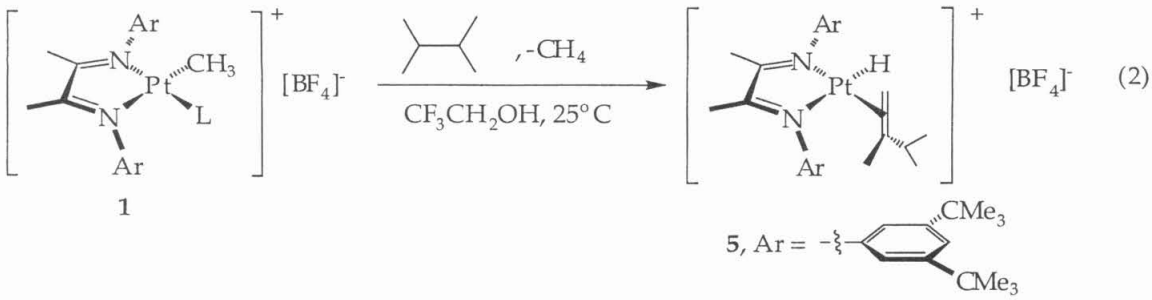

Addition of neopentane to a TFE solution of **1** did not lead to products that can be attributed to neopentane C–H activation. Instead, rapid formation of the $(\mu\text{-OH})_2$ dimer (**2**) and other unidentifiable decomposition products were observed. The decomposition pathway was not determined.

Reactions of Platinum (II) Hydride 3 with *tert*-Butylacetylene. A rather unexpected reaction occurred between **3** and excess *tert*-butylacetylene at room temperature. When excess tert-butylacetylene was added to a yellow solution of **3** at room temperature, a red color appeared almost instantaneously. The red color started to fade within five minutes, and the final product consisted of four resonances in the vinylic and allylic region of the ^{1}H NMR spectrum, all of which showed well resolved ^{195}Pt satellites. An allylic proton (d, $J_{H\text{-}H}$ = 2.0 Hz, $J_{Pt\text{-}H}$ = 40 Hz) resonated at 2.72 ppm, and coupled with a vinylic proton, which resonated at 6.07 ppm (d, $J_{H\text{-}H}$ = 2.0 Hz, $J_{Pt\text{-}H}$ = 10 Hz). The other two signals, both singlets, were present at 4.23 ($J_{Pt\text{-}H}$ = 22 Hz) and 5.29 ($J_{Pt\text{-}H}$ = 92 Hz) ppm respectively. The number of resonances supported the incorporation of three *tert*-butylacetylene molecules into the Pt–H bond, but the coupling pattern suggested that rearrangement had occurred. The connectivity of the incorporated alkynes was, however, not obvious from the spectral data.

A recent report by Brookhart and co-workers on the reactions of cationic palladium(II) methyl complexes with alkynes,[2] demonstrated that complexes of

the type [(N-N)PdMe(NCMe)]$^+$ react with three equivalents of acetylene to give a 5-ethylidene-2-cylopentene-1-yl palladium(II) complex (**4**) (eq 3).

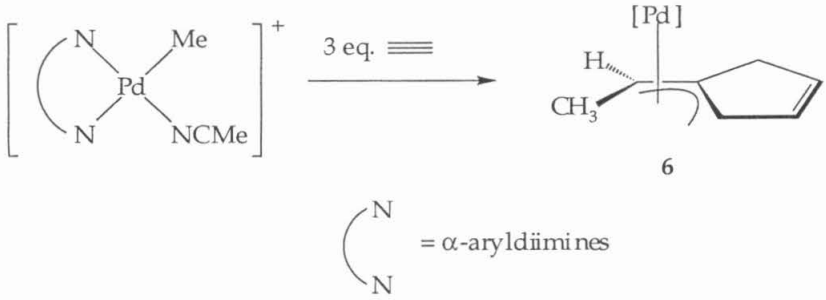

(3)

An analogous rearrangement product, **9**, is proposed for the reaction between **3** and *tert*-butylacetylene (Scheme 3). Initially tert-butylacetylene displaces bound cyclohexene to form a transient [(N-N)Pt(H)(HC≡CCMe$_3$)]$^+$ species that undergoes facile insertion into the Pt–H bond to form a cationic platinum vinyl complex (**7**). Since [(N-N)Pt(H)(HC≡CCMe$_3$)]$^+$ was not observed, we suggest that insertion into Pt–H bond is fast relative to coordination of *tert*-butylacetylene to the platinum center. The insertion regiochemistry was suggested by the coupling between vinylic protons. The large H–H coupling constant (~16 Hz) is typical of coupling between *trans*-vinylic protons. At slightly higher temperatures, insertion of a second equivalent of *tert*-butylacetylene into the [Pt–vinyl] bond occurred to afford **8**. The coupling between the *trans*-vinylic protons (~10 Hz) is slightly smaller in complex **8** than that observed for **7**. Although sequential formation of **7** and **8** could be observed by low temperature NMR spectroscopy (Figure 3), no intermediates could be detected on the reaction pathway from **8** to **9**.

Scheme 3

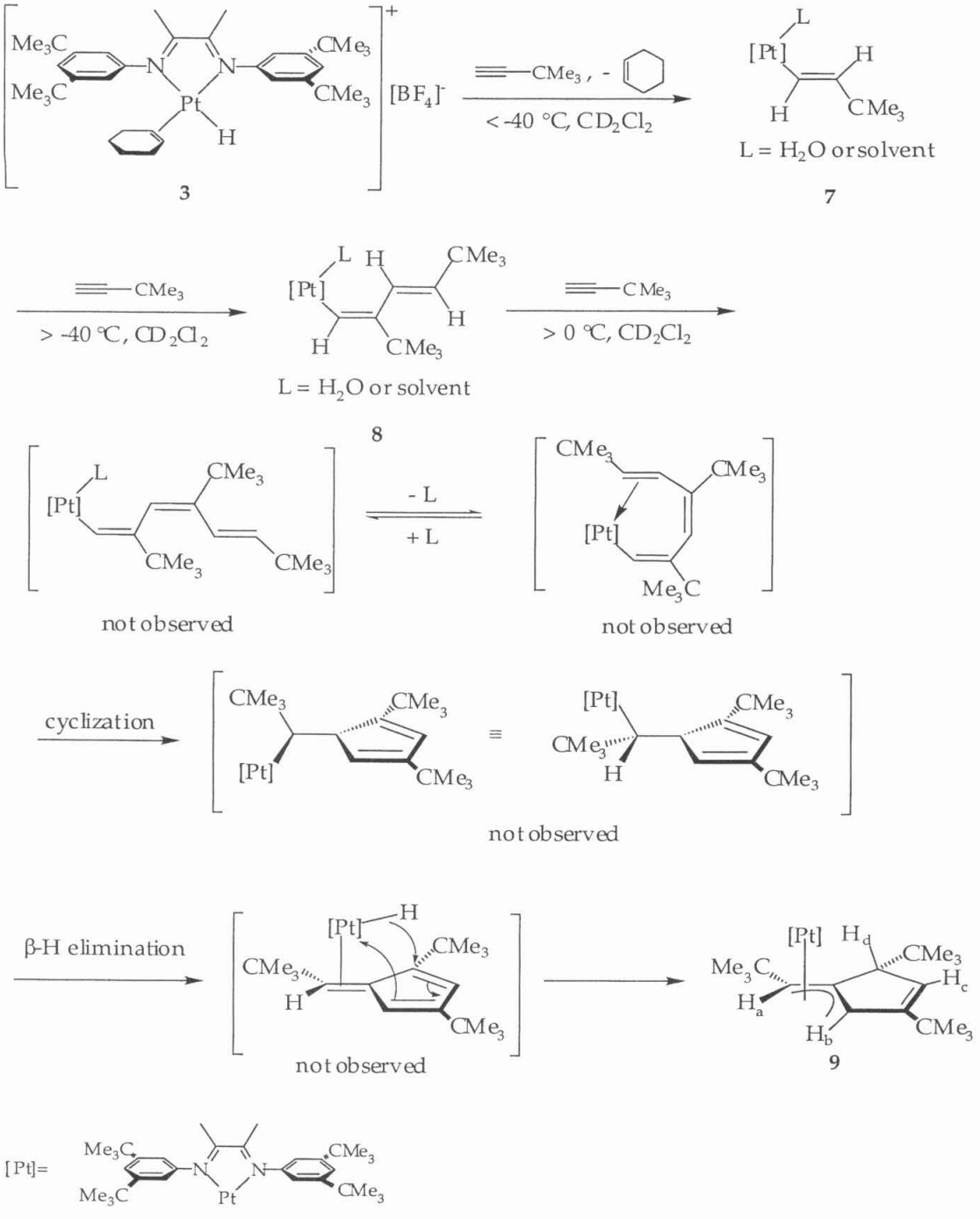
Me3C
Me3C
CMe3
CMe3
[BF4]-
3
CMe3 , -
< -40 °C, CD2Cl2
[Pt]
L
H
H
CMe3
L = H2O or solvent
7
CMe3
> -40 °C, CD2Cl2
L = H2O or solvent
8
> 0 °C, CD2Cl2
- L
+ L
not observed
not observed
cyclization
not observed
β-H elimination
not observed
9
[Pt]=

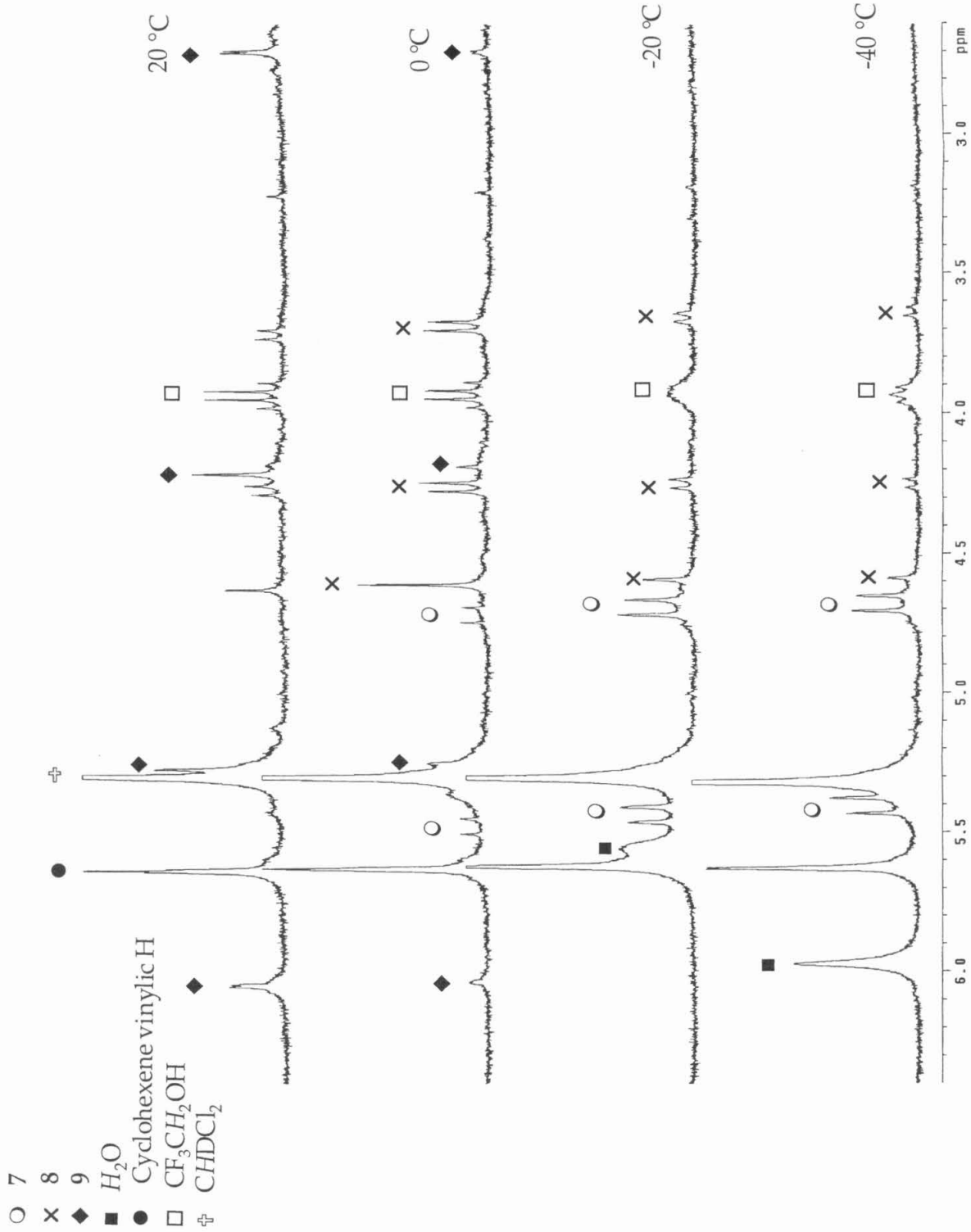

Figure 3. Allyl and Vinyl region of the ^{1}H NMR spectra for the reaction between **3** and *tert*-butylacetylene.

One possible mechanism for the formation of **9** is shown in Scheme 3. After insertion of a third equivalent of *tert*-butylacetylene, intramolecular migratory insertion/cyclization with subsequent β-hydride insertion gives a platinum(II) fulvene complexes, which can undergo rapid rearrangement to form the final product **9**. The alternative rearrangement product, **9'**, is not formed, presumably for steric reasons (eq 4). The fact that none of the above intermediates could be detected implies that insertion of the third equivalent of *tert*-butylacetylene was rate-determining in the above transformation, and that β-H elimination, rearrangement and hydride re-insertion was relatively fast at room temperatures. Complex **9** is apparently inert to further insertion - since higher insertion products could not be observed after one week at room temperature in the presence of excess *tert*-butylacetylene.

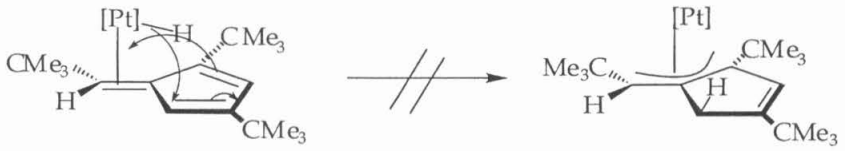

(4)

9'

Conclusions

Complex **1** activated C–H bonds in methane and several β-H containing cyclic and acyclic alkanes. These reactions took place at or near room temperatures (22 – 45 °C). The products from the reactions of **1** and β-H containing alkanes are a thermodynamic mixture of platinum(II) hydrido olefins, with no intermediate Pt-alkyl complexes being observed. These results suggested that β-H elimination, rearrangement and insertion into Pt–H bonds took place at faster rates in these cationic platinum(II) complexes than activation of aliphatic C–H bonds.

The bound olefins in these platinum(II) complexes appeared to undergo both rapid rotation. *tert*-Butylacetylene could easily displace these coordinated olefins and insert into the Pt–H bond. Incorporation of two additional equivalents of tert-butylacetylene molecules, followed by rapid rearrangement, afforded a [Pt-allyl] complex **9** as the final product. It appeared that for insertion into a Pt–H bond, acetylene coordination was rate-determining, but for the

formation of **9**, insertion of *tert*-butylacetylene into the Pt–vinyl bond in **8** was the slow step.

Experimental Section

General Considerations. All moisture-sensitive compounds were manipulated using standard vacuum line, Schlenk line or cannula techniques or in a dry box under a nitrogen atmosphere. Argon and dinitrogen gases were purified by passage over columns of MnO on vermiculite and activated molecular sieves. Trifluoroethanol was purchased from Aldrich, purified and dried over a mixture of $CaSO_4/NaHCO_3$, then either vacuum distilled or distilled under argon, and stored over activated molecular sieves under vacuum. Trifluoroethanol-d_3 was purchased from Aldrich, stored over activated molecular sieves and a small amount of $NaHCO_3$ under vacuum, and vacuum distilled into oven-dried J-Young NMR tubes for kinetic studies. All other solvents and reagents were used as received without further purification.

NMR spectra were recorded on a GE QE300 (^{1}H, 300.1 MHz), a varian INOVA 500 (^{1}H, 499.852 MHz, ^{13}C, 125.701 MHz) or a varian Mercury 300 (^{1}H, 299.8 MHz, ^{19}F, 282.081 MHz, ^{13}C, 75.4626 MHz) spectrometer.

Reactions Between 1 and $^{13}CH_4$. **1** (0.008 *M*) was generated in-situ in a J-Young NMR tube as described in Chapter 4. The NMR tube was evacuated and $^{13}CH_4$ was added to the tube via a calibrated gas bulb. The $^{13}CH_4$ concentration was determined by integration against [Pt–CH_3] peaks. The tube was then heated in a 45 °C - oil bath and the progress of the reaction was monitored periodically by NMR spectroscopy. ^{1}H NMR (300 MHz, TFE-d_3): δ = 0.74 (d, $J_{13C\text{-}H}$ = 127 Hz, Pt–CH_3, aquo adduct), δ = 0.75 (d, $J_{13C\text{-}H}$ = 127 Hz, Pt–CH_3, solvento adduct). ^{13}C NMR (75 MHz, TFE-d_3) : δ = 7.76 (Pt–$^{13}CH_3$, solvento adduct) and 9.07 (Pt–$^{13}CH_3$, aquo adduct).

Reactions Between 1 and Cyclohexane. Dry TFE (~ 5 ml) was vacuum transferred onto a mixture of 31.5 mg (N-N)$PtMe_2$ (0.046 mmol) (N-N = Ar=N–C(Me)–C(Me)–N=Ar, Ar=*3,5*-$(CMe_3)_2$-C_6H_3) and 6 μl HBF_4 (aq, 48 wt%, 0.046 mmol) in a round bottom flask. The mixture was allowed to stir for 5 minutes to obtain a clear orange solution. Dry cyclohexane was added to the mixture via a cannula. Two layers were observed. The mixture was left to stir for 27 hours.

The volatiles were then removed at -20 °C under high vacuum. Petroleum ether was added to the oily residue with stirring and the volatiles were removed after 10 minutes. Orange/light brown solid was collected (20 mg, > 90% purity and contains some residue TFE and (μ-OH)$_2$ dimer). ^{1}H NMR (300 MHz, TFE-d_3): δ = -22.14 (t, 1H, $^1J_{Pt-H}$ = 1309 Hz, Pt–*H*), 1.36 (s, 36H, C(C*H*$_3$)$_3$), 2.14 (s, 3H, N=C–C*H*$_3$), 2.28 (s, 3H, N=C–C*H*$_3$), 2.36 (brs, 4H, Cyclohexene), 5.01 (br, J_{Pt-H} = 70 Hz, 2H, vinylic H), 6.79 (s, 2H, H$_o$), 7.12 (s, 2H, H$_o$), 7.56 (s, 2H, H$_p$), unable to find the second set of methylene H's of cyclohexene moiety, but could be the broad shoulder next to the CMe$_3$ resonances. In methylene-chloride-d_2, the para-H's split into two resonances at 7.37 and 7.35 ppm (1:1).

Reactions Between 1 and *n*-Butane. **1** (0.009 *M*) was generated in-situ in a J-Young NMR tube as described in Chapter 4. The NMR tube was evacuated and ~ 40 – 50 equivalents of *n*-butane was added to the J-Young tube. Two Pt–H (~ 2:1) signals could be observed by ^{1}H NMR after 1.5 hrs at room temperature. The tube was left at room temperature over night, and the progress of the reaction was checked again after 17 hours. The starting platinum (II) methyl complex had mostly disappeared at this stage. ^{1}H NMR (300 MHz, TFE-d_3): CMe$_3$ resonances are buried under the signals for *n*-butane, and the methyl backbone region has more resonances than expected. Peaks that can be identified with certainty are as follows:

major species: δ = -22.01 (t, 1H, $^1J_{Pt-H}$ = 1251 Hz, Pt–*H*), 4.33 (br, J_{Pt-H} = 66 Hz, 2H, vinylic H), 6.76 (s, 1H, H$_o$), 6.78 (s, 1H, H$_o$), 7.06 (s, 2H, H$_o$), 7.56 (s, 2H, H$_p$).

minor species: δ = -23.09 (t, 1H, $^1J_{Pt-H}$ = 1395 Hz, Pt–*H*), 4.46 (br, 2H, vinylic H), 6.71 (s, 1H, H$_o$), 6.84 (s, 1H, H$_o$), 7.01 (s, 2H, H$_o$), 7.60 (s, 2H, H$_p$).

Reactions Between 1 and *n*-Pentane. (N-N)PtMe$_2$ (N-N = Ar=N–C(Me)–C(Me)–N=Ar, Ar=3,5-(CMe$_3$)$_2$-C$_6$H$_3$) (15 mg, 0.022 mmol) and HBF$_4$ (aq, 48 wt%, 3 μl, 0.023 mmol) was mixed in 1 ml TFE to generate a clear solution. *n*-Pentane was added to the mixture till two layers were formed, and the mixture was left to stir over night. After 24 hours, the volatiles were removed on high vacuum line, and the residue was dissolved in a 6:1 mixture of C$_6$D$_6$: CD$_2$Cl$_2$. Peaks are not well resolved in C$_6$D$_6$: CD$_2$Cl$_2$. ^{1}H NMR (500 MHz, C$_6$D$_6$/CD$_2$Cl$_2$):

major species: δ = -22.41 (t, $^1J_{Pt-H}$ = 1251 Hz, Pt–*H*), 3.99, 4.00 (br, 1H each J_{Pt-H} > 30 Hz, vinylic H).

minor species: δ = -22.99 (t, $^1J_{Pt-H}$ = 1399 Hz, Pt–*H*), 4.24, 4.30 (br, 1H each, vinylic H).

Reactions Between 1 and 2,3-Dimethylbutane. TFE (~ 5 ml) was added to a mixture of (N-N)$PtMe_2$ (26.3 mg, 0.038 mmol) (N-N = Ar=N–C(Me)–C(Me)–N=Ar, Ar=*3,5*-$(CMe_3)_2$-C_6H_3) and HBF_4 (aq, 48 wt%, 5 μl, 0.038 mmol) in a round bottom flask. The mixture was allowed to stir for 5 minutes to obtain a clear orange solution. 2,3-dimethylbutane was added to the mixture till two layers formed. The mixture was left to stir over night. The volatiles were then removed at -20 °C under high vacuum. Petroleum ether was added to the oily residue with stirring and the volatiles were removed after 10 minutes. 26 mg brown solids collected (> 80% purity and contains some residue TFE and μ-OH dimer). ^{1}H NMR (500 MHz, TFE-d_3): δ = -22.58 (t, 1H, $^1J_{Pt-H}$ = 1198 Hz, Pt–*H*), 0.93 (d, $^3J_{H-H}$ = 5.9 Hz, 3H, CH(CH_3)$_2$), 1.14 (d, $^3J_{Pt-H}$ = 5.9 Hz, 3H, CH(CH_3)$_2$),1.35 (s, ~18H, C(CH_3)$_3$), 1.36, 1.37 (s, ~ 9H each, C(CH_3)$_3$), 1.95 (s, 3H, C=C–CH_3), 2.16 (s, 3H, N=C-CH_3), 2.19 (s, 3H, N=C-CH_3), 3.45 (t, J_{Pt-H} = 44 Hz, 1H, *H*C=C), 3.51 (t, J_{Pt-H} = 44 Hz, 1H, *H*C=C), 6.84, 6.86 (s, 1H each, H_o), 7.06 (s, 2H, H_o), 7.55, 7.57 (s, 1H each, H_p).

References and Notes

(1) Albano, V. G.; Castellari, C.; Ferrara, M. L.; Panunzi, A.; Ruffo, F. *J. Organomet. Chem.* **1994**, *469*, 237–244.

(2) LaPointe, A. M.; Brookhart, M. *Organometallics* **1998**, *17*, 1530–1537.

Appendix B

Arene C–H Bond Activation and Acetonitrile Exchange Kinetic Data

In all cases, [Pt] is kept at 0.01 – 0.011 *M*; the observed rate constants have an uncertainty between 5 - 10% of the reported values except the last two entries in Table S12 where the uncertainty is >20%.

Tables 1 – 12. Summary of arene C–H bond activation kinetic data.

Table 1. Observed rate constants for reactions between complexes **10** and C_6L_6 (L = H or D) at 20 °C ([C_6L_6] = 0.24 – 0.25 *M*, [H_2O] = 0.05 *M*).

Pt Complex	Substrate	T (°C)	[substrate](*M*)	[H_2O] (*M*)	k_{obs} ($\times 10^4$)
10a	C_6D_6	20	0.247	0.052	10
10b	C_6D_6	20	0.242	0.051	7.0
10c	C_6D_6	20	0.242	0.049	5.5
10c	C_6H_6	20	0.242	0.050	10
10d	C_6D_6	20	0.249	0.05	2.1
10d	C_6H_6	20	0.245	0.05	4.6
10e	C_6D_6	20	0.247	0.049	0.94
10e	C_6H_6	20	0.242	0.048	2.1

Table 2. Observed rate constants for reactions between complexes **10** and C_6D_6 at 20 °C ([C_6D_6] = 1.31 *M*, [H_2O] = 0.70 *M*).

Pt Complex	Substrate	T (°C)	[substrate](*M*)	[H_2O] (*M*)	k_{obs} ($\times 10^4$)
10a	C_6D_6	20	1.31	0.70	6.1
10b	C_6D_6	20	1.31	0.70	4.55
10c	C_6D_6	20	1.31	0.70	2.2
10d	C_6D_6	20	1.31	0.70	0.74

Table 3. Observed rate constants for reactions between complexes **11** and C_6L_6 (L = H or D) at 35 °C ([C_6L_6] = 1.50 *M*, [H_2O] = 0.19 *M*).

Pt Complex	Substrate	T (°C)	[substrate](*M*)	[H_2O] (*M*)	k_{obs} ($\times 10^4$)
11a	C_6D_6	35	1.50	0.194	3.4
11a	C_6H_6	35	1.50	0.194	3.8
11b	C_6D_6	35	1.43	0.183	2.6
11b	C_6H_6	35	1.51	0.195	2.75
11c	C_6D_6	35	1.51	0.194	1.6
11c	C_6H_6	35	1.51	0.194	1.8

Table 4. Observed rate constants for reactions between complexes **12** and C_6L_6 (L = H or D) at 20 °C.

Pt Complex	Substrate	T (°C)	[substrate](*M*)	[H_2O] (*M*)	k_{obs} ($\times 10^4$)
12a[a]	C_6D_6	20	0.484	0.0475	1.6
12a	C_6H_6	20	0.481	0.0475	8.0
12a	C_6H_6	20	0.255	0.051	4.1
12b[a]	C_6D_6	20	0.484	0.0475	1.04
12b	C_6H_6	20	0.48	0.047	3.7
12b	C_6H_6	20	0.245	0.049	1.8
12c[b]	C_6D_6	20	0.93	0.045	0.63
12c	C_6H_6	20	0.48	0.047	1.84

a) k_{obs}'s halved to obtain the points for **12a** and **b** in Figure 14a; b) k_{obs} quartered to obtain the point for **12c** in Figure 14a, and halved to get the point in Figure 13b.

Table 5. Observed rate constants for reactions between **10a** and C_6L_6 (L = H or D) at 20 °C at variable substrate concentrations.

Pt Complex	Substrate	T (°C)	[substrate](*M*)	[H_2O] (*M*)	k_{obs} ($\times 10^4$)
10a	C_6D_6	20	0.247	1.31	1.78
10a	C_6D_6	20	0.40	1.27	2.6
10a	C_6D_6	20	0.555	1.26	3.3
10a	C_6D_6	20	0.70	1.233	3.86
10a	C_6H_6	20	0.252	1.33	0.87
10a	C_6H_6	20	0.395	1.245	1.29
10a	C_6H_6	20	0.559	1.257	1.9
10a	C_6H_6	20	0.706	1.233	2.35

Table 6. Observed rate constants for reactions between **10a** and C_6L_6 (L = H or D) at 20 °C at variable water concentrations.

Pt Complex	Substrate	T (°C)	[substrate](*M*)	[H_2O] (*M*)	k_{obs} ($\times 10^4$)
10a	C_6D_6	20	0.247	0.052	10
10a	C_6D_6	20	0.252	0.35	2.95
10a	C_6D_6	20	0.252	0.68	1.73
10a	C_6D_6	20	0.252	1.33	0.87
10a	C_6H_6	20	0.25	0.35	6.45
10a	C_6H_6	20	0.254	0.68	3.0
10a	C_6H_6	20	0.247	1.31	1.78
10a	C_6H_6	20	0.23	1.94	1.2
10a	C_6H_6	20	0.23	2.66	0.88

Table 7. Observed rate constants for reactions between **10b** and C_6L_6 (L = H or D) at 20 °C with variable water concentrations.

Pt Complex	Substrate	T (°C)	[substrate](*M*)	[H_2O] (*M*)	k_{obs} ($\times 10^4$)
10b	C_6D_6	20	0.247	0.027	7.5
10b	C_6D_6	20	0.242	0.051	7.0
10b	C_6D_6	20	0.247	0.164	3.85
10b	C_6D_6	20	0.263	0.361	1.86
10b	C_6H_6	20	0.27	0.072	15.0
10b	C_6H_6	20	0.255	0.22	6.2
10b	C_6H_6	20	0.240	0.365	3.95
10b	C_6H_6	20	0.255	0.683	2.4

Table 8. Observed rate constants for reactions between **12a** and C_6H_6 (L = H or D) at 20 °C at variable water concentrations.

Pt Complex	Substrate	T (°C)	[substrate](*M*)	[H_2O] (*M*)	k_{obs} ($\times 10^4$)
12a	C_6H_6	20	0.255	0.051	4.1
12a	C_6H_6	20	0.255	0.094	1.56
12a	C_6H_6	20	0.261	0.134	2.37

Table 9. Observed rate constants for reactions between **10b** and arenes at 25 °C at various substrate concentrations.

Pt Complex	Substrate	T (°C)	[substrate](*M*)	[H_2O] (*M*)	k_{obs} ($\times 10^4$)
10b	C_9D_{12}	25	0.31	0.05	3.2
10b	C_9D_{12}	25	0.305	0.13	1.7
10b	C_9D_{12}	25	0.31	0.21	1.1
10b	C_9H_{12}	25	0.31	0.05	4.3
10b	C_9H_{12}	25	0.31	0.13	2.04
10b	C_9H_{12}	25	0.315	0.21	1.4
10b	C_8D_{10}	25	0.304	0.214	4.6
10b	C_8H_{10}	25	0.29	0.207	6.9
10b	C_6D_6	25	0.25	0.05	13.9

* C_9D_{12} = (mesitylene-d_{12}), C_9H_{12} = (mesitylene-d_0),C_8D_{10} = (*p*-xylene-d_{10}), C_8H_{10} = (*p*-xylene-d_0)

Table 10. Observed rate constants for reactions between **10b** and C_6H_6 at variable temperatures.

Pt Complex	Substrate	T (°C)	[substrate](*M*)	[H_2O] (*M*)	k_{obs} ($\times 10^4$)
10b	C_6H_6	0	0.735	0.372	1.1
10b	C_6H_6	0	0.735	0.212	1.8
10b	C_6H_6	10	0.706	0.358	2.95
10b	C_6H_6	20	0.247	0.315	4.5
10b	C_6H_6	30	0.240	0.642	7.5
10b	C_6H_6	40	0.238	2.014	7.6
10b	C_6H_6	50	0.160	4.0	7.4
10b	C_6H_6	55	0.156	3.93	11.0

Table 11. Observed rate constants for reactions between **10b** and C_6D_6 at variable temperatures.

Pt Complex	Substrate	T (°C)	[substrate](*M*)	[H_2O] (*M*)	k_{obs} ($\times 10^4$)
10b	C_6D_6	0	0.734	0.369	0.42
10b	C_6D_6	10	0.713	0.358	1.44
10b	C_6D_6	20	0.263	0.361	1.86
10b	C_6D_6	30	0.247	0.372	6.3

Table 12. Observed rate constants for reactions between **10b** and C_6H_6 at [OTf^-] concentrations.

Pt Complex	RH	T (°C)	[RH] (*M*)	[OTf^-] (*M*)	[H_2O] (*M*)	k_{obs} ($\times 10^4$)
10b	C_6H_6	20	0.24	0	0.366	3.95
10b	C_6H_6	20	0.244	0.0672	0.372	3.83
10b	C_6H_6	20	0.238	0.113	0.362	3.66
10b	C_6H_6	20	0.240	0.190	0.365	5.2
10b	C_6H_6	20	0.240	0.190	0.365	3.9

Tables 13 – 21. Summary of acetonitrile exchange kinetic data.

Table 13. Observed exchange rate constants for **13** in TFE-d_3.

Pt Complex	Solvent	T (°C)	[CD_3CN] (*M*)	k_{ex} ($\times 10^4$)
13b	TFE-d_3	40	0.43	0.79
13b	TFE-d_3	40	0.84	1.94
13b	TFE-d_3	40	1.36	3.42
13b	TFE-d_3	40	1.96	4.99
13d	TFE-d_3	30	0.41	3.4

Table 14. Observed exchange rate constants for **13b** in CD_3OD at 40 °C at variable acetonitrile concentrations.

Pt Complex	Solvent	T (°C)	[CD_3CN] (*M*)	k_{ex} ($\times 10^4$)
13b	CD_3OD	40	0.15	8.2
13b	CD_3OD	40	0.29	9.5
13b	CD_3OD	40	0.55	10.4
13b	CD_3OD	40	1.35	13.3

Table 15. Observed exchange rate constants for **13b** in CD_3OD at 30 °C at variable acetonitrile concentrations.

Pt Complex	Solvent	T (°C)	[CD_3CN] (*M*)	k_{ex} ($\times 10^4$)
13b	CD_3OD	30	0.15	2.7
13b	CD_3OD	30	0.26	3.4
13b	CD_3OD	30	0.84	4.5
13b	CD_3OD	30	1.43	5.5
13b	CD_3OD	30	1.96	6.5
13d	CD_3OD	30	0.26	1.2
13d	CD_3OD	30	0.58	1.4
13d	CD_3OD	30	0.82	1.64

Table 16. Observed exchange rate constants for **13b** in CD_3OD at 20 °C at variable acetonitrile concentrations.

Pt Complex	Solvent	T (°C)	[CD_3CN] (*M*)	k_{ex} ($\times 10^4$)
13b	CD_3OD	20	0.15	0.95
13b	CD_3OD	20	0.27	1.22
13b	CD_3OD	20	0.42	1.35
13b	CD_3OD	20	0.85	1.51
13b	CD_3OD	20	1.37	1.71

Table 17. Observed exchange rate constants for **13b** in $(CD_3)_2CDOD$ at 40 °C at variable acetonitrile concentrations.

Pt Complex	Solvent	T (°C)	$[CD_3CN]$ (*M*)	k_{ex} ($\times 10^4$)
13b	$(CD_3)_2CDOD$	40	0.067	3.3
13b	$(CD_3)_2CDOD$	40	0.127	4.8
13b	$(CD_3)_2CDOD$	40	0.26	6.04
13b	$(CD_3)_2CDOD$	40	0.56	9.1
13b	$(CD_3)_2CDOD$	40	0.89	11.5
13b	$(CD_3)_2CDOD$	40	1.29	15.0

Table 18. Observed exchange rate constants for **13b** in CD_3CD_2OD at 40 °C at variable acetonitrile concentrations.

Pt Complex	Solvent	T (°C)	$[CD_3CN]$ (*M*)	k_{ex} ($\times 10^4$)
13b	CD_3CD_2OD	40	0.137	7.05
13b	CD_3CD_2OD	40	0.254	8.2
13b	CD_3CD_2OD	40	0.494	9.04
13b	CD_3CD_2OD	40	0.905	11.7
13b	CD_3CD_2OD	40	1.40	14.0

Table 19. Observed exchange rate constants for **13b** in CD_3CD_2OD at 30 °C at variable acetonitrile concentrations.

Pt Complex	Solvent	T (°C)	[CD_3CN] (*M*)	k_{ex} ($\times 10^4$)
13b	CD_3CD_2OD	30	0.15	2.8
13b	CD_3CD_2OD	30	0.29	3.1
13b	CD_3CD_2OD	30	0.81	4.4
13b	CD_3CD_2OD	30	1.34	5.5
13b	CD_3CD_2OD	30	1.90	6.6

Table 20. Observed exchange rate constants for **14** in TFE-d_3 at 40 °C at variable acetonitrile concentrations.

Pt Complex	Solvent	T (°C)	[CD_3CN] (*M*)	k_{ex} ($\times 10^4$)
14b	TFE-d_3	40	0.41	0.88
14b	TFE-d_3	40	0.834	2.1
14b	TFE-d_3	40	1.36	3.5
14c	TFE-d_3	40	0.40	2.74
14c	TFE-d_3	40	0.76	6.2
14c	TFE-d_3	40	1.27	11.6

Table 21. Observed exchange rate constants for **14** in CD_3OD at 30 °C at variable acetonitrile concentrations.

Pt Complex	Solvent	T (°C)	[CD_3CN] (*M*)	k_{ex} ($\times 10^4$)
14b	CD_3OD	30	0.263	3.1
14b	CD_3OD	30	0.775	4.1
14b	CD_3OD	30	1.29	4.9
14c	CD_3OD	30	0.27	7.44
14c	CD_3OD	30	0.775	9.85
14c	CD_3OD	30	1.27	12.0

Appendix C

X-Ray Crystallographic Data for (Thp-Cy5)$ZrCl_2$ (1c, Chapter 2)

Table 1. *Crystal* data and structure refinement for **AHZ6** (**1c**, Chapter 2, CCDC 162494).

Empirical formula	$C_{25}H_{38}Cl_2Si_2Zr$
Formula weight	556.85
Crystallization Solvent	Toluene/hexanes
Crystal Habit	Lozenge
Crystal size	0.30 x 0.27 x 0.20 mm^3
Crystal color	Colorless

Data Collection

Preliminary Photos	Rotation
Type of diffractometer	Bruker SMART 1000 CCD area detector
Wavelength	0.71073 Å MoKa
Data Collection Temperature	98(2) K
θ range for 25750 reflections used in lattice determination	2.41 to 28.27°
Unit cell dimensions	a = 9.7646(5) Å b = 16.8335(8) Å b= 92.5530(10)° c = 15.7839(8) Å
Volume	2591.9(2) $Å^3$
Z	4
Crystal system	Monoclinic
Space group	$P2_1/n$
Density (calculated)	1.427 Mg/m^3
F(000)	1160
Data collection program	Bruker SMART
q range for data collection	1.77 to 28.38°
Completeness to q = 28.38°	95.4 %
Index ranges	$-12 \leq h \leq 12$, $-22 \leq k \leq 22$, $-21 \leq l \leq 20$
Data collection scan type	ω scans at 7 ϕ settings
Data reduction program	Bruker SAINT v6.2
Reflections collected	52487
Independent reflections	6180 [R_{int}= 0.0528]
Absorption coefficient	0.734 mm^{-1}
Max. and min. transmission (calculated)	0.8695 and 0.8120

Table 1 (cont.)

Structure solution and Refinement

Structure solution program	SHELXS-97 (Sheldrick, 1990)
Primary solution method	Direct methods
Secondary solution method	Direct methods
Hydrogen placement	Difference Fourier map
Structure refinement program	SHELXL-97 (Sheldrick, 1997)
Refinement method	Full matrix least-squares on F^2
Data / restraints / parameters	6180 / 0 / 423
Treatment of hydrogen atoms	Unrestrained
Goodness-of-fit on F^2	1.894
Final R indices [I>2s(I), 5206 reflections]	R1 = 0.0297, *w*R2 = 0.0517
R indices (all data)	R1 = 0.0370, *w*R2 = 0.0523
Type of weighting scheme used	Sigma
Weighting scheme used	$w=1/\sigma^2(Fo^2)$
Max shift/error	0.004
Average shift/error	0.000
Largest diff. peak and hole	0.707 and -0.520 e.Å^{-3}

Special Refinement Details

Refinement of F^2 against ALL reflections. The weighted R-factor (*w*R) and goodness of fit (S) are based on F^2, conventional R-factors (R) are based on F, with F set to zero for negative F^2. The threshold expression of $F^2 > 2\sigma(F^2)$ is used only for calculating R-factors(gt), etc., and is not relevant to the choice of reflections for refinement. R-factors based on F^2 are statistically about twice as large as those based on F, and R-factors based on ALL data will be even larger.

All esds (except the esd in the dihedral angle between two l.s. planes) are estimated using the full covariance matrix. The cell esds are taken into account individually in the estimation of esds in distances, angles and torsion angles; correlations between esds in cell parameters are only used when they are defined by crystal symmetry. An approximate (isotropic) treatment of cell esds is used for estimating esds involving l.s. planes.

Table 2. Atomic coordinates (x 10^4) and equivalent isotropic displacement parameters ($Å^2$x 10^3) for **AHZ6** (CCDC 162494). U(eq) is defined as the trace of the orthogonalized U^{ij} tensor.

	x	y	z	U_{eq}
Zr	9000(1)	1639(1)	2436(1)	10(1)
Cl(1)	10431(1)	1515(1)	3728(1)	18(1)
Cl(2)	10723(1)	1418(1)	1392(1)	16(1)
Si(1)	6108(1)	2009(1)	3277(1)	14(1)
Si(2)	6492(1)	1914(1)	1094(1)	14(1)
C(1)	6790(2)	1094(1)	2750(1)	11(1)
C(2)	6928(2)	1052(1)	1823(1)	11(1)
C(3)	7861(2)	415(1)	1673(1)	12(1)
C(4)	8329(2)	108(1)	2463(1)	12(1)
C(5)	7657(2)	489(1)	3122(1)	12(1)
C(6)	7309(2)	2671(1)	2706(1)	13(1)
C(7)	7469(2)	2634(1)	1800(1)	13(1)
C(8)	8791(2)	2945(1)	1651(1)	13(1)
C(9)	9463(2)	3167(1)	2421(1)	13(1)
C(10)	8544(2)	2994(1)	3062(1)	14(1)
C(11)	8226(2)	83(1)	822(1)	14(1)
C(12)	6938(2)	-229(1)	346(1)	19(1)
C(13)	9308(2)	-566(1)	908(1)	19(1)
C(14)	7780(2)	246(1)	4043(1)	14(1)
C(15)	6386(2)	-20(1)	4342(1)	20(1)
C(16)	8831(2)	-408(1)	4208(1)	18(1)
C(17)	6527(2)	2091(1)	4431(1)	20(1)
C(18)	4240(2)	2193(2)	3102(2)	24(1)
C(19)	4646(2)	2128(2)	875(2)	24(1)
C(20)	7333(2)	1889(1)	62(1)	19(1)
C(21)	10844(2)	3556(1)	2557(1)	15(1)
C(22)	11694(2)	3627(1)	1772(1)	21(1)
C(23)	12737(2)	4267(1)	2017(2)	28(1)
C(24)	11935(3)	4865(2)	2505(3)	49(1)
C(25)	10749(2)	4421(1)	2878(2)	21(1)

Table 3. Selected bond lengths [Å] and angles [°] for **AHZ6** (CCDC 162494).

Zr-Pln(1)	2.2094(8)	Pln(1)-Zr-Pln(2)	108.16(6)
Zr-Pln(2)	2.1917(8)		
Zr-Cent(1)	2.233	Cent(1)-Zr-Cent(2)	121.6
Zr-Cent(2)	2.201		
Zr-Cl(1)	2.4291(5)	Zr-Cl(2)	2.4348(5)
Zr-C(1)	2.4173(17)	Zr-C(6)	2.4467(17)
Zr-C(2)	2.4149(17)	Zr-C(7)	2.4313(17)
Zr-C(3)	2.6107(17)	Zr-C(8)	2.5268(18)
Zr-C(4)	2.6614(18)	Zr-C(9)	2.6107(17)
Zr-C(5)	2.6009(17)	Zr-C(10)	2.5328(18)
Cl(1)-Zr-Cl(2)	99.536(17)		

Table 4. Bond lengths [Å] and angles [°] for **AHZ6** (CCDC 162494).

Zr-Pln(1)	2.2094(8)	C(14)-H(14)	0.919(17)
Zr-Pln(2)	2.1917(8)	C(15)-H(15A)	0.944(19)
Zr-Cent(1)	2.233	C(15)-H(15B)	0.97(2)
Zr-Cent(2)	2.201	C(15)-H(15C)	0.97(2)
Zr-C(2)	2.4149(17)	C(16)-H(16A)	0.949(19)
Zr-C(1)	2.4173(17)	C(16)-H(16B)	1.003(19)
Zr-Cl(1)	2.4291(5)	C(16)-H(16C)	0.94(2)
Zr-C(7)	2.4313(17)	C(17)-H(17A)	0.94(2)
Zr-Cl(2)	2.4348(5)	C(17)-H(17B)	0.92(2)
Zr-C(6)	2.4467(17)	C(17)-H(17C)	0.96(2)
Zr-C(8)	2.5268(18)	C(18)-H(18A)	0.96(3)
Zr-C(10)	2.5328(18)	C(18)-H(18B)	0.80(3)
Zr-C(5)	2.6009(17)	C(18)-H(18C)	0.91(3)
Zr-C(3)	2.6107(17)	C(19)-H(19A)	0.87(3)
Zr-C(9)	2.6107(17)	C(19)-H(19B)	0.84(3)
Zr-C(4)	2.6614(18)	C(19)-H(19C)	0.84(3)
Si(1)-C(17)	1.855(2)	C(20)-H(20A)	0.94(2)
Si(1)-C(18)	1.859(2)	C(20)-H(20B)	0.94(2)
Si(1)-C(6)	1.8768(18)	C(20)-H(20C)	0.92(2)
Si(1)-C(1)	1.8854(18)	C(21)-C(22)	1.526(3)
Si(2)-C(19)	1.856(2)	C(21)-C(25)	1.546(3)
Si(2)-C(20)	1.856(2)	C(21)-H(21)	0.931(17)
Si(2)-C(7)	1.8768(19)	C(22)-C(23)	1.521(3)
Si(2)-C(2)	1.8879(18)	C(22)-H(22A)	0.920(18)
C(1)-C(5)	1.433(2)	C(22)-H(22B)	0.982(19)
C(1)-C(2)	1.477(2)	C(23)-C(24)	1.508(4)
C(2)-C(3)	1.434(2)	C(23)-H(23A)	0.91(2)
C(3)-C(4)	1.408(2)	C(23)-H(23B)	0.92(2)
C(3)-C(11)	1.511(2)	C(24)-C(25)	1.519(3)
C(4)-C(5)	1.409(2)	C(24)-H(24A)	0.90(3)
C(4)-H(4)	0.914(17)	C(24)-H(24B)	0.87(3)
C(5)-C(14)	1.511(2)	C(25)-H(25A)	0.94(2)
C(6)-C(10)	1.416(2)	C(25)-H(25B)	0.88(2)
C(6)-C(7)	1.448(2)		
C(7)-C(8)	1.423(2)	Pln(1)-Zr-Pln(2)	108.16(6)
C(8)-C(9)	1.406(3)	Cent(1)-Zr-Cent(2)	121.6
C(8)-H(8)	0.912(17)	C(2)-Zr-C(1)	35.59(6)
C(9)-C(10)	1.412(2)	C(2)-Zr-Cl(1)	137.85(4)
C(9)-C(21)	1.505(2)	C(1)-Zr-Cl(1)	106.31(4)
C(10)-H(10)	0.892(17)	C(2)-Zr-C(7)	68.11(6)
C(11)-C(13)	1.522(3)	C(1)-Zr-C(7)	78.92(6)
C(11)-C(12)	1.529(3)	Cl(1)-Zr-C(7)	136.57(4)
C(11)-H(11)	0.981(16)	C(2)-Zr-Cl(2)	104.96(4)
C(12)-H(12A)	0.935(19)	C(1)-Zr-Cl(2)	136.92(4)
C(12)-H(12B)	0.939(19)	Cl(1)-Zr-Cl(2)	99.536(17)
C(12)-H(12C)	0.975(19)	C(7)-Zr-Cl(2)	104.89(4)
C(13)-H(13A)	0.966(19)	C(2)-Zr-C(6)	78.48(6)
C(13)-H(13B)	0.932(19)	C(1)-Zr-C(6)	67.56(6)
C(13)-H(13C)	0.945(19)	Cl(1)-Zr-C(6)	106.39(4)
C(14)-C(16)	1.520(3)	C(7)-Zr-C(6)	34.52(6)
C(14)-C(15)	1.528(3)	Cl(2)-Zr-C(6)	135.95(4)

C(2)-Zr-C(8)	96.41(6)	C(17)-Si(1)-C(1)	115.34(9)
C(1)-Zr-C(8)	112.19(6)	C(18)-Si(1)-C(1)	115.75(10)
Cl(1)-Zr-C(8)	121.15(5)	C(6)-Si(1)-C(1)	91.92(8)
C(7)-Zr-C(8)	33.28(6)	C(17)-Si(1)-Zr	105.04(7)
Cl(2)-Zr-C(8)	81.08(4)	C(18)-Si(1)-Zr	147.20(9)
C(6)-Zr-C(8)	55.09(6)	C(6)-Si(1)-Zr	48.83(5)
C(2)-Zr-C(10)	111.47(6)	C(1)-Si(1)-Zr	47.95(5)
C(1)-Zr-C(10)	95.06(6)	C(19)-Si(2)-C(20)	107.74(11)
Cl(1)-Zr-C(10)	81.64(5)	C(19)-Si(2)-C(7)	116.65(10)
C(7)-Zr-C(10)	54.96(6)	C(20)-Si(2)-C(7)	107.59(9)
Cl(2)-Zr-C(10)	122.73(4)	C(19)-Si(2)-C(2)	116.98(10)
C(6)-Zr-C(10)	32.99(6)	C(20)-Si(2)-C(2)	114.89(9)
C(8)-Zr-C(10)	52.86(6)	C(7)-Si(2)-C(2)	92.26(8)
C(2)-Zr-C(5)	55.47(6)	C(19)-Si(2)-Zr	149.33(9)
C(1)-Zr-C(5)	32.92(5)	C(20)-Si(2)-Zr	102.83(7)
Cl(1)-Zr-C(5)	82.44(4)	C(7)-Si(2)-Zr	49.21(5)
C(7)-Zr-C(5)	111.83(6)	C(2)-Si(2)-Zr	48.74(5)
Cl(2)-Zr-C(5)	122.94(4)	C(5)-C(1)-C(2)	107.10(15)
C(6)-Zr-C(5)	95.68(6)	C(5)-C(1)-Si(1)	127.81(13)
C(8)-Zr-C(5)	145.10(6)	C(2)-C(1)-Si(1)	121.67(13)
C(10)-Zr-C(5)	114.03(6)	C(5)-C(1)-Zr	80.61(10)
C(2)-Zr-C(3)	32.86(5)	C(2)-C(1)-Zr	72.12(9)
C(1)-Zr-C(3)	55.15(6)	Si(1)-C(1)-Zr	96.65(7)
Cl(1)-Zr-C(3)	122.46(4)	C(3)-C(2)-C(1)	106.62(15)
C(7)-Zr-C(3)	96.38(6)	C(3)-C(2)-Si(2)	126.97(13)
Cl(2)-Zr-C(3)	81.94(4)	C(1)-C(2)-Si(2)	122.65(13)
C(6)-Zr-C(3)	111.32(6)	C(3)-C(2)-Zr	81.10(10)
C(8)-Zr-C(3)	115.91(6)	C(1)-C(2)-Zr	72.29(9)
C(10)-Zr-C(3)	144.30(6)	Si(2)-C(2)-Zr	95.27(7)
C(5)-Zr-C(3)	52.57(5)	C(4)-C(3)-C(2)	108.18(15)
C(2)-Zr-C(9)	122.80(6)	C(4)-C(3)-C(11)	124.81(16)
C(1)-Zr-C(9)	122.18(6)	C(2)-C(3)-C(11)	126.89(16)
Cl(1)-Zr-C(9)	89.94(4)	C(4)-C(3)-Zr	76.51(10)
C(7)-Zr-C(9)	54.69(6)	C(2)-C(3)-Zr	66.04(9)
Cl(2)-Zr-C(9)	91.14(4)	C(11)-C(3)-Zr	126.10(11)
C(6)-Zr-C(9)	54.63(6)	C(3)-C(4)-C(5)	110.04(16)
C(8)-Zr-C(9)	31.71(6)	C(3)-C(4)-Zr	72.54(10)
C(10)-Zr-C(9)	31.81(6)	C(5)-C(4)-Zr	72.12(10)
C(5)-Zr-C(9)	145.82(6)	C(3)-C(4)-H(4)	126.6(10)
C(3)-Zr-C(9)	147.52(6)	C(5)-C(4)-H(4)	123.3(10)
C(2)-Zr-C(4)	53.66(6)	Zr-C(4)-H(4)	124.5(11)
C(1)-Zr-C(4)	53.54(6)	C(4)-C(5)-C(1)	107.92(16)
Cl(1)-Zr-C(4)	92.06(4)	C(4)-C(5)-C(14)	124.55(16)
C(7)-Zr-C(4)	121.74(6)	C(1)-C(5)-C(14)	127.39(16)
Cl(2)-Zr-C(4)	92.31(4)	C(4)-C(5)-Zr	76.85(10)
C(6)-Zr-C(4)	121.07(6)	C(1)-C(5)-Zr	66.48(9)
C(8)-Zr-C(4)	146.73(6)	C(14)-C(5)-Zr	125.62(12)
C(10)-Zr-C(4)	144.93(6)	C(10)-C(6)-C(7)	106.34(15)
C(5)-Zr-C(4)	31.03(5)	C(10)-C(6)-Si(1)	125.26(14)
C(3)-Zr-C(4)	30.96(5)	C(7)-C(6)-Si(1)	123.06(13)
C(9)-Zr-C(4)	175.67(6)	C(10)-C(6)-Zr	76.85(10)
C(17)-Si(1)-C(18)	107.73(11)	C(7)-C(6)-Zr	72.16(10)
C(17)-Si(1)-C(6)	108.17(9)	Si(1)-C(6)-Zr	95.91(7)
C(18)-Si(1)-C(6)	117.36(10)	C(8)-C(7)-C(6)	106.58(16)

C(8)-C(7)-Si(2)	125.52(14)	C(14)-C(16)-H(16B)	111.7(10)
C(6)-C(7)-Si(2)	122.71(13)	H(16A)-C(16)-H(16B)	106.4(15)
C(8)-C(7)-Zr	77.05(10)	C(14)-C(16)-H(16C)	110.8(12)
C(6)-C(7)-Zr	73.32(10)	H(16A)-C(16)-H(16C)	110.0(16)
Si(2)-C(7)-Zr	95.03(7)	H(16B)-C(16)-H(16C)	107.2(15)
C(9)-C(8)-C(7)	110.33(17)	Si(1)-C(17)-H(17A)	113.2(12)
C(9)-C(8)-Zr	77.44(10)	Si(1)-C(17)-H(17B)	112.5(13)
C(7)-C(8)-Zr	69.67(10)	H(17A)-C(17)-H(17B)	107.7(18)
C(9)-C(8)-H(8)	125.5(11)	Si(1)-C(17)-H(17C)	109.6(13)
C(7)-C(8)-H(8)	124.2(11)	H(17A)-C(17)-H(17C)	105.9(17)
Zr-C(8)-H(8)	119.2(11)	H(17B)-C(17)-H(17C)	107.6(17)
C(8)-C(9)-C(10)	106.13(16)	Si(1)-C(18)-H(18A)	105.9(15)
C(8)-C(9)-C(21)	128.25(17)	Si(1)-C(18)-H(18B)	115.1(19)
C(10)-C(9)-C(21)	125.53(17)	H(18A)-C(18)-H(18B)	97(2)
C(8)-C(9)-Zr	70.86(10)	Si(1)-C(18)-H(18C)	107.3(18)
C(10)-C(9)-Zr	71.05(10)	H(18A)-C(18)-H(18C)	109(2)
C(21)-C(9)-Zr	125.54(12)	H(18B)-C(18)-H(18C)	121(3)
C(9)-C(10)-C(6)	110.63(17)	Si(2)-C(19)-H(19A)	113(2)
C(9)-C(10)-Zr	77.14(10)	Si(2)-C(19)-H(19B)	111(2)
C(6)-C(10)-Zr	70.16(10)	H(19A)-C(19)-H(19B)	113(3)
C(9)-C(10)-H(10)	124.8(11)	Si(2)-C(19)-H(19C)	112(2)
C(6)-C(10)-H(10)	124.6(11)	H(19A)-C(19)-H(19C)	92(3)
Zr-C(10)-H(10)	118.7(11)	H(19B)-C(19)-H(19C)	115(3)
C(3)-C(11)-C(13)	112.16(16)	Si(2)-C(20)-H(20A)	114.8(13)
C(3)-C(11)-C(12)	110.01(15)	Si(2)-C(20)-H(20B)	114.3(11)
C(13)-C(11)-C(12)	110.47(17)	H(20A)-C(20)-H(20B)	103.9(17)
C(3)-C(11)-H(11)	108.0(10)	Si(2)-C(20)-H(20C)	105.1(13)
C(13)-C(11)-H(11)	107.3(10)	H(20A)-C(20)-H(20C)	108.1(18)
C(12)-C(11)-H(11)	108.8(10)	H(20B)-C(20)-H(20C)	110.6(17)
C(11)-C(12)-H(12A)	111.4(11)	C(9)-C(21)-C(22)	115.76(16)
C(11)-C(12)-H(12B)	111.4(11)	C(9)-C(21)-C(25)	112.97(16)
H(12A)-C(12)-H(12B)	106.4(16)	C(22)-C(21)-C(25)	103.54(16)
C(11)-C(12)-H(12C)	112.2(11)	C(9)-C(21)-H(21)	107.7(10)
H(12A)-C(12)-H(12C)	107.1(15)	C(22)-C(21)-H(21)	108.4(10)
H(12B)-C(12)-H(12C)	108.1(16)	C(25)-C(21)-H(21)	108.2(10)
C(11)-C(13)-H(13A)	112.3(11)	C(23)-C(22)-C(21)	103.40(17)
C(11)-C(13)-H(13B)	111.7(12)	C(23)-C(22)-H(22A)	115.6(12)
H(13A)-C(13)-H(13B)	109.1(15)	C(21)-C(22)-H(22A)	111.8(11)
C(11)-C(13)-H(13C)	110.0(11)	C(23)-C(22)-H(22B)	107.0(11)
H(13A)-C(13)-H(13C)	107.6(15)	C(21)-C(22)-H(22B)	108.8(11)
H(13B)-C(13)-H(13C)	105.8(16)	H(22A)-C(22)-H(22B)	109.8(16)
C(5)-C(14)-C(16)	112.65(16)	C(24)-C(23)-C(22)	104.25(19)
C(5)-C(14)-C(15)	110.04(16)	C(24)-C(23)-H(23A)	112.4(14)
C(16)-C(14)-C(15)	109.79(17)	C(22)-C(23)-H(23A)	109.3(14)
C(5)-C(14)-H(14)	108.4(11)	C(24)-C(23)-H(23B)	108.8(14)
C(16)-C(14)-H(14)	108.8(11)	C(22)-C(23)-H(23B)	108.2(14)
C(15)-C(14)-H(14)	107.1(11)	H(23A)-C(23)-H(23B)	113.4(19)
C(14)-C(15)-H(15A)	113.6(11)	C(23)-C(24)-C(25)	106.9(2)
C(14)-C(15)-H(15B)	110.2(11)	C(23)-C(24)-H(24A)	111.3(17)
H(15A)-C(15)-H(15B)	105.6(16)	C(25)-C(24)-H(24A)	112.5(18)
C(14)-C(15)-H(15C)	110.7(11)	C(23)-C(24)-H(24B)	109(2)
H(15A)-C(15)-H(15C)	107.5(16)	C(25)-C(24)-H(24B)	109(2)
H(15B)-C(15)-H(15C)	109.0(16)	H(24A)-C(24)-H(24B)	108(3)
C(14)-C(16)-H(16A)	110.6(11)	C(24)-C(25)-C(21)	106.24(18)

C(24)-C(25)-H(25A)	110.7(12)	C(21)-C(25)-H(25B)	112.1(13)
C(21)-C(25)-H(25A)	112.9(12)	H(25A)-C(25)-H(25B)	105.6(17)
C(24)-C(25)-H(25B)	109.3(13)		

Table 5. Anisotropic displacement parameters ($Å^2 x 10^4$) for **AHZ6** (CCDC 162494). The anisotropic displacement factor exponent takes the form: $-2p^2 [h^2 a^{*2} U^{11} + ... + 2 h k a^* b^* U^{12}]$.

	U^{11}	U^{22}	U^{33}	U^{23}	U^{13}	U^{12}
Zr	98(1)	106(1)	101(1)	1(1)	2(1)	1(1)
Cl(1)	187(2)	186(3)	149(2)	24(2)	-50(2)	-32(2)
Cl(2)	145(2)	160(2)	165(2)	-4(2)	43(2)	4(2)
Si(1)	129(3)	132(3)	150(3)	-11(2)	35(2)	2(2)
Si(2)	129(3)	140(3)	134(3)	11(2)	-16(2)	-1(2)
C(1)	100(9)	119(9)	117(9)	-12(7)	20(7)	-27(7)
C(2)	100(9)	126(10)	112(9)	-5(7)	2(7)	-27(7)
C(3)	101(9)	116(10)	131(10)	-5(7)	10(7)	-47(7)
C(4)	120(10)	90(10)	150(10)	7(8)	16(8)	-4(8)
C(5)	101(9)	112(9)	137(10)	-10(8)	0(7)	-50(7)
C(6)	131(10)	82(9)	182(10)	-2(8)	20(8)	22(7)
C(7)	127(10)	94(9)	156(10)	19(8)	-17(8)	25(7)
C(8)	149(10)	106(10)	146(10)	34(8)	23(8)	28(7)
C(9)	137(9)	76(9)	173(10)	1(7)	-2(8)	17(7)
C(10)	173(10)	100(10)	131(10)	-16(8)	2(8)	17(8)
C(11)	179(10)	130(10)	119(10)	-3(8)	27(8)	-32(8)
C(12)	237(12)	182(12)	150(11)	-10(9)	5(9)	-33(9)
C(13)	234(12)	190(11)	142(11)	-32(9)	52(9)	12(9)
C(14)	171(10)	135(10)	113(10)	-9(8)	11(8)	-40(8)
C(15)	200(11)	229(12)	167(11)	27(9)	46(9)	-21(9)
C(16)	198(12)	184(11)	158(11)	23(9)	-1(9)	-4(9)
C(17)	236(12)	178(12)	179(11)	-39(9)	43(9)	-4(9)
C(18)	145(11)	284(14)	289(14)	-37(11)	59(10)	20(10)
C(19)	157(12)	274(14)	275(14)	4(11)	-52(10)	21(10)
C(20)	225(12)	177(12)	171(11)	29(9)	-2(9)	11(9)
C(21)	142(10)	138(10)	174(10)	17(8)	-18(8)	1(8)
C(22)	142(11)	233(12)	252(12)	-9(10)	19(9)	-1(9)
C(23)	188(12)	316(14)	333(14)	36(11)	30(11)	-83(10)
C(24)	351(17)	333(16)	810(20)	-189(17)	199(16)	-181(13)
C(25)	181(12)	178(11)	253(12)	-39(9)	-13(9)	-22(9)

Table 6. Hydrogen coordinates (x 10^4) and isotropic displacement parameters ($Å^2$x 10^3) for **AHZ6** (CCDC 162494).

	x	y	z	U_{iso}
H(4)	8940(17)	-298(10)	2553(10)	7(5)
H(8)	9144(17)	2988(10)	1128(11)	9(5)
H(10)	8721(17)	3069(10)	3615(11)	7(5)
H(11)	8614(16)	516(10)	493(10)	6(4)
H(12A)	6556(18)	-656(11)	632(12)	16(5)
H(12B)	7135(19)	-416(11)	-195(12)	20(5)
H(12C)	6228(19)	177(11)	279(11)	16(5)
H(13A)	10150(20)	-378(11)	1183(11)	16(5)
H(13B)	9499(18)	-784(11)	383(12)	20(5)
H(13C)	8983(19)	-990(11)	1235(12)	20(5)
H(14)	8038(17)	683(10)	4360(11)	9(5)
H(15A)	5690(19)	365(12)	4259(11)	19(5)
H(15B)	6441(19)	-124(11)	4945(13)	24(6)
H(15C)	6081(19)	-500(12)	4045(12)	23(6)
H(16A)	8575(18)	-874(11)	3901(12)	18(5)
H(16B)	8900(18)	-564(11)	4821(12)	17(5)
H(16C)	9700(20)	-241(11)	4060(12)	23(6)
H(17A)	7460(20)	2026(11)	4572(12)	20(5)
H(17B)	6050(20)	1730(12)	4744(13)	31(6)
H(17C)	6290(20)	2613(13)	4625(13)	33(6)
H(18A)	3800(30)	1859(15)	3498(17)	60(8)
H(18B)	3900(30)	2001(16)	2677(18)	60(10)
H(18C)	4080(30)	2710(18)	3236(18)	82(10)
H(19A)	4340(30)	1961(19)	380(20)	98(12)
H(19B)	4480(30)	2610(20)	950(20)	93(12)
H(19C)	4130(30)	1814(18)	1129(19)	77(11)
H(20A)	7030(20)	1478(13)	-305(13)	35(6)
H(20B)	8290(20)	1822(11)	108(11)	19(5)
H(20C)	7110(20)	2364(13)	-193(13)	33(6)
H(21)	11342(17)	3261(10)	2964(11)	6(4)
H(22A)	12053(19)	3145(11)	1619(11)	14(5)
H(22B)	11111(19)	3840(11)	1302(12)	16(5)
H(23A)	13080(20)	4476(13)	1540(14)	36(7)
H(23B)	13400(20)	4044(13)	2378(14)	38(7)
H(24A)	12470(30)	5109(16)	2905(16)	61(9)
H(24B)	11620(40)	5230(20)	2160(20)	119(17)
H(25A)	10790(20)	4458(12)	3470(13)	26(6)
H(25B)	9970(20)	4650(12)	2710(12)	24(6)

Appendix D

X-Ray Crystallographic Data for (Thp-Ph)$ZrCl_2$ (1e, Chapter 2)

AHZ2 (THP-ϕ)$ZrCl_2$

Solution and Refinement:

A sphere of data was collected with 1.0° ω-scans. Reflections which did not agree well in a preliminary merging were recollected. No decay correction was needed. Individual backgrounds were replaced with a background function of 2θ derived from the backgrounds of reflections with $I < 8\sigma(I)$. Lorentz and polarization factors were applied and the multiples were merged in point group $\bar{1}$. No absorption correction was made. The ψ-scan reflections showed several anomalies and all 224 ψ-scan reflections were deleted. This problem with extremely high χ angles did not affect the rest of the data. CRYM programs were used for data processing.

The structure was solved with SHELXS-86.

With the exception of the minor component of the disordered solvent molecule, all non-hydrogen atoms were refined anisotropically and all hydrogen atoms were refined isotropically. For the minor component of the benzene, the carbon atoms were refined isotropically and the hydrogens placed at calculated positions. Refinement was full-matrix least-squares using CRYM programs.

Weights w are calculated as $1/\sigma^2(F_o^2)$; variances ($\sigma^2(F_o^2)$) were derived from counting statistics plus an additional term, $(0.014I)^2$; variances of the merged data were obtained by propagation of error plus another additional term, $(0.014\bar{I})^2$.

Definitions:

$$R = \frac{\Sigma|F_o - F_c|}{\Sigma F_o} \text{ for } F_o > 0; \quad R_w = \left\{ \frac{\Sigma w(F_o^2 - F_c^2)^2}{\Sigma w(F_o^2)^2} \right\}^{\frac{1}{2}}$$

$$S = \left\{ \frac{\Sigma w(F_o^2 - F_c^2)^2}{n - p} \right\}^{\frac{1}{2}}$$

where n = number of data,

p = number of parameters refined.

Comment:

There are two half-molecules of benzene in the asymmetric unit. Each benzene sits on a center of symmetry which generates the other half of the molecule. One of the benzene molecules is disordered. It was modelled with two benzene molecules in an 85:15 ratio with the two rings rotated about 30° with respect to each other. The displacement ellipsoids of the major component show considerable in-plane rotation.

The molecules are arranged in layers separated by sheets of benzene. The benzene molecules at the other symmetry sites lie between the phenyl groups of the ligand. The Cp rings form a 73.0° angle. The phenyl group is rotated 13.5° with respect to the cyclopentadienyl ring to which it is bonded and 38.4° with respect to the $ZrCl_2$ plane. Despite the disordered solvent molecule, this is an excellent structure.

References

The CRYM Crystallographic Computing System

Duchamp, D. J. (1964). Am. Crystallogr. Assoc. Meet., Bozeman, Montana, Paper B14, p. 29-30.

SHELXS-86

Sheldrick, G. M. (1990). *Acta Cryst.* **A46**, 467-473.

ORTEP

Johnson, C. K. (1976). *ORTEP*II. Report ORNL-5138. Oak Ridge National Laboratory, Oak Ridge, Tennessee, USA.

Table 1. Crystal and Intensity Collection Data for AHZ2 (THP-ϕ)$ZrCl_2$

Formula: $C_{32}H_{34}D_6Cl_2Si_2Zr$	Formula weight: 649.01
Crystal color: Colorless	Habit: Plate
Crystal size: $0.11 \times 0.22 \times 0.33$ mm	$\rho_{calc} = 1.396$ g cm^{-3}
Crystal system: Triclinic	Space group: $P\bar{1}$ (#2)
$a = 9.203(2)$Å	$\alpha = 87.05(2)°$
$b = 9.870(3)$Å	$\beta = 81.52(2)°$
$c = 19.305(5)$Å	$\gamma = 62.92(2)°$
V = 1544.0(7)Å^3	$Z = 2$
Lattice parameters: 25 reflections,	$12° \leq \theta \leq 16°$
$\mu = 6.26$ cm^{-1} ($\mu r_{max} = 0.13$)	Absorption correction: None
CAD-4 diffractometer	ω scan
MoKα, $\lambda = 0.7107$Å	Graphite monochromator
2θ range: 3°–55°	$-11 \leq h \leq 11, -12 \leq k \leq 12, -25 \leq l \leq 25$
T = 85K	$F_{000} = 668$
Number of reflections measured: 14372	Number of independent reflections: 7051
Number with $F_o^2 > 0$: 6843	Number with $F_o^2 > 3\sigma(F_o^2)$: 6085
Standard reflections: 3 every 75 min	Variation: Within counting statistics
GOF_{merge} : 0.99 for 6788 multiples	R_{merge} : 0.018 for 6360 duplicates
Number used in refinement: 7051	Criterion: All reflections used

Final $R(F_o)$: 0.024 for 6085 reflections with $F_o^2 > 3\sigma(F_o^2)$

Final $R(F_o)$: 0.029 for 6843 reflections with $F_o^2 > 0$

Final weighted $R(F_o^2)$: 0.056 for 7051 reflections

Final goodness of fit: 1.46 for 507 parameters and 7051 reflections

$(\Delta/\sigma)_{max}$ in final least squares cycle: 0.02

$\Delta\rho_{max}$: 0.52 eÅ^{-3}, $\Delta\rho_{min}$: -0.49 eÅ^{-3} in final difference map

Table 2. Final Heavy Atom Parameters for

AHZ2 (THP-ϕ)$ZrCl_2$

x, y, z and U^a_{eq} or U_{iso}

Atom	x	y	z	U_{eq} or U_{iso}
Zr	−0.01423(2)	0.36789(2)	0.78611(1)	0.00720(4)
Cl1	−0.01935(5)	0.12402(4)	0.79887(2)	0.01474(8)
Cl2	−0.30636(5)	0.54333(4)	0.81134(2)	0.01254(10)
Si1	0.11021(5)	0.62381(5)	0.75829(2)	0.00920(8)
Si2	0.37779(5)	0.23395(5)	0.74665(2)	0.01061(9)
C1	0.1269(2)	0.4919(2)	0.83342(8)	0.0100(3)
C2	0.2382(2)	0.3300(2)	0.82876(8)	0.0105(3)
C3	0.1716(2)	0.2595(2)	0.88122(8)	0.0109(3)
C4	0.0226(2)	0.3705(2)	0.91811(8)	0.0100(3)
C5	−0.0024(2)	0.5128(2)	0.88835(8)	0.0096(3)
C6	0.0929(2)	0.4909(2)	0.69639(8)	0.0092(3)
C7	0.2053(2)	0.3259(2)	0.69151(8)	0.0090(3)
C8	0.1245(2)	0.2557(2)	0.65975(8)	0.0103(3)
C9	−0.0323(2)	0.3697(2)	0.64826(8)	0.0098(3)
C10	−0.0507(2)	0.5135(2)	0.66749(8)	0.0093(3)
C11	−0.0839(2)	0.8016(2)	0.78079(10)	0.0137(4)
C12	0.2819(2)	0.6737(2)	0.73031(10)	0.0157(3)
C13	0.5581(2)	0.2719(2)	0.71967(11)	0.0194(5)
C14	0.4540(2)	0.0248(2)	0.75609(10)	0.0165(4)
C15	−0.0833(2)	0.3428(2)	0.97648(8)	0.0105(3)
C16	−0.0251(2)	0.2032(2)	1.01050(9)	0.0136(3)
C17	−0.1236(2)	0.1772(2)	1.06599(9)	0.0152(3)

Table 2. (Cont.)

Atom	x	y	z	U_{eq} or U_{iso}
C18	−0.2807(2)	0.2900(2)	1.08842(9)	0.0155(3)
C19	−0.3397(2)	0.4293(2)	1.05530(9)	0.0151(4)
C20	−0.2423(2)	0.4557(2)	0.99987(9)	0.0131(3)
C21	−0.1924(2)	0.6644(2)	0.65357(9)	0.0113(3)
C22	−0.1296(2)	0.7531(2)	0.60038(10)	0.0190(4)
C23	−0.3319(2)	0.6458(2)	0.62827(10)	0.0172(4)
C24	0.1978(2)	0.0916(2)	0.63528(9)	0.0126(4)
C25	0.3394(2)	0.0622(2)	0.57568(9)	0.0174(4)
C26	0.0712(3)	0.0512(2)	0.61135(11)	0.0192(4)
C27	0.5455(3)	−0.1048(2)	0.94618(11)	0.0250(5)
C28	0.5945(2)	0.0093(2)	0.93872(11)	0.0245(5)
C29	0.4516(3)	−0.1150(2)	1.00712(11)	0.0240(4)
C30†	−0.5433(18)	0.6415(7)	0.4711(4)	0.042(1)
C31†	−0.3842(15)	0.5268(16)	0.4566(2)	0.041(1)
C32†	−0.3405(5)	0.3859(12)	0.4852(5)	0.041(1)
C33‡	−0.459(5)	0.591(5)	0.454(1)	0.019(5)*
C34‡	−0.351(3)	0.447(5)	0.468(2)	0.018(5)*
C35‡	−0.393(5)	0.362(3)	0.512(2)	0.022(5)*

[a] $U_{eq} = \frac{1}{3}\sum_i \sum_j [U_{ij}(a_i^* a_j^*)(\vec{a}_i \cdot \vec{a}_j)]$

* Isotropic displacement parameter, U_{iso}

† Population: 0.85(2)

‡ Population: 0.15(2)

***Table 3.* Selected Distances and Angles for**

AHZ2 (THP-ϕ)$ZrCl_2$

	Distance(Å)		Distance(Å)
Zr –Cp1	2.208	C7 –C8	1.434(2)
Zr –Cp2	2.244	C8 –C9	1.410(2)
Zr –Cl1	2.4280(5)	C8 –C24	1.515(3)
Zr –Cl2	2.4343(4)	C9 –C10	1.413(2)
Si1 –C1	1.874(2)	C10 –C21	1.512(2)
Si1 –C6	1.892(2)	C15 –C16	1.398(3)
Si1 –C11	1.859(2)	C15 –C20	1.400(3)
Si1 –C12	1.859(2)	C16 –C17	1.390(3)
Si2 –C2	1.873(2)	C17 –C18	1.384(3)
Si2 –C7	1.888(2)	C18 –C19	1.388(3)
Si2 –C13	1.859(2)	C19 –C20	1.385(3)
Si2 –C14	1.862(2)	C21 –C22	1.532(3)
C1 –C2	1.452(2)	C21 –C23	1.526(3)
C1 –C5	1.417(2)	C24 –C25	1.534(3)
C2 –C3	1.420(2)	C24 –C26	1.527(3)
C3 –C4	1.418(2)		
C4 –C5	1.420(2)		
C4 –C15	1.478(2)		
C6 –C7	1.478(2)		
C6 –C10	1.429(2)		

Table 3. **(Cont.)**

	Angle(°)		Angle(°)
Cp1 –Zr –Cp2	121.8	C5 –C1 –C2	106.8(1)
Cp1 –Zr –Cl1	108.4	C1 –C2 –Si2	122.8(1)
Cp1 –Zr –Cl2	108.3	C3 –C2 –Si2	125.2(1)
Cp2 –Zr –Cl1	107.6	C3 –C2 –C1	106.8(1)
Cp2 –Zr –Cl2	107.6	C4 –C3 –C2	110.0(2)
Cl1 –Zr –Cl2	101.24(2)	C5 –C4 –C3	106.3(2)
C6 –Si1 –C1	92.0(1)	C15 –C4 –C3	126.5(2)
C11 –Si1 –C1	107.0(1)	C15 –C4 –C5	127.2(2)
C12 –Si1 –C1	118.9(1)	C4 –C5 –C1	110.1(2)
C11 –Si1 –C6	114.0(1)	C7 –C6 –Si1	122.7(1)
C12 –Si1 –C6	115.1(1)	C10 –C6 –Si1	127.0(1)
C12 –Si1 –C11	109.0(1)	C10 –C6 –C7	106.9(1)
C7 –Si2 –C2	92.4(1)	C6 –C7 –Si2	121.8(1)
C13 –Si2 –C2	117.6(1)	C8 –C7 –Si2	128.0(1)
C14 –Si2 –C2	108.2(1)	C8 –C7 –C6	106.8(1)
C13 –Si2 –C7	115.4(1)	C9 –C8 –C7	108.2(1)
C14 –Si2 –C7	114.0(1)	C24 –C8 –C7	127.0(2)
C14 –Si2 –C13	108.4(1)	C24 –C8 –C9	124.6(2)
C2 –C1 –Si1	123.3(1)	C10 –C9 –C8	109.7(2)
C5 –C1 –Si1	124.9(1)	C9 –C10 –C6	108.3(1)

Table 3. (Cont.)

	Angle(°)
C21 –C10 –C6	126.6(2)
C21 –C10 –C9	124.9(2)
C16 –C15 –C4	120.4(2)
C20 –C15 –C4	121.1(2)
C20 –C15 –C16	118.5(2)
C17 –C16 –C15	120.6(2)
C18 –C17 –C16	120.2(2)
C19 –C18 –C17	119.8(2)
C20 –C19 –C18	120.3(2)
C19 –C20 –C15	120.6(2)
C22 –C21 –C10	109.7(2)
C23 –C21 –C10	112.4(2)
C23 –C21 –C22	110.6(2)
C25 –C24 –C8	108.6(1)
C26 –C24 –C8	112.9(2)
C26 –C24 –C25	110.4(2)

Table 4. Final Refined and Assigned Hydrogen Parameters for AHZ2 (THP-ϕ)$ZrCl_2$

Atom	x	y	z	U_{iso}
	x, y, z and U_{iso}			
H3	0.218(2)	0.156(2)	0.8886(10)	0.020(5)
H5	−0.087(2)	0.604(2)	0.9021(10)	0.015(5)
H9	−0.113(2)	0.354(2)	0.6301(9)	0.011(5)
H11a	−0.069(3)	0.848(3)	0.8191(12)	0.029(6)
H11b	−0.109(3)	0.869(3)	0.7418(11)	0.027(6)
H11c	−0.177(3)	0.781(2)	0.7958(10)	0.020(5)
H12a	0.248(3)	0.776(3)	0.7446(12)	0.038(7)
H12b	0.374(3)	0.616(3)	0.7516(12)	0.038(7)
H12c	0.306(3)	0.668(2)	0.6799(12)	0.029(6)
H13a	0.629(3)	0.201(3)	0.6836(13)	0.042(7)
H13b	0.526(3)	0.370(3)	0.6990(13)	0.045(7)
H13c	0.618(3)	0.259(3)	0.7549(14)	0.050(8)
H14a	0.530(3)	−0.007(2)	0.7887(11)	0.023(5)
H14b	0.367(3)	−0.004(2)	0.7714(11)	0.028(6)
H14c	0.507(3)	−0.029(2)	0.7127(11)	0.026(6)
H16	0.086(2)	0.127(2)	0.9969(9)	0.013(5)
H17	−0.078(3)	0.080(2)	1.0879(10)	0.021(5)
H18	−0.348(2)	0.271(2)	1.1260(10)	0.018(5)
H19	−0.443(3)	0.508(2)	1.0711(10)	0.020(5)
H20	−0.285(2)	0.551(2)	0.9748(10)	0.015(5)
H21	−0.234(2)	0.720(2)	0.6942(9)	0.007(4)
H22a	−0.038(3)	0.767(2)	0.6166(11)	0.023(5)
H22b	−0.083(3)	0.697(2)	0.5547(11)	0.024(6)
H22c	−0.221(3)	0.850(3)	0.5915(11)	0.028(6)
H23a	−0.369(2)	0.589(2)	0.6626(10)	0.017(5)
H23b	−0.423(3)	0.745(3)	0.6232(11)	0.023(5)
H23c	−0.299(2)	0.603(2)	0.5831(10)	0.010(5)
H24	0.240(2)	0.029(2)	0.6723(10)	0.017(5)
H25a	0.427(3)	0.079(2)	0.5938(10)	0.021(5)
H25b	0.389(3)	−0.041(3)	0.5580(11)	0.030(6)
H25c	0.297(2)	0.134(2)	0.5371(10)	0.018(5)
H26a	−0.013(3)	0.067(2)	0.6469(12)	0.026(6)
H26b	0.030(2)	0.106(2)	0.5701(11)	0.019(5)
H26c	0.122(3)	−0.054(3)	0.5958(11)	0.026(6)
H27	0.573(3)	−0.173(2)	0.9096(11)	0.023(5)
H28	0.660(3)	0.018(2)	0.8954(11)	0.026(6)
H29	0.414(2)	−0.191(2)	1.0130(10)	0.014(5)
H30†	−0.571(4)	0.737(4)	0.4527(18)	0.068(12)
H31†	−0.313(4)	0.543(4)	0.4298(18)	0.057(11)

Table 4. (Cont.)

Atom	x	y	z	U_{iso}
H32†	−0.237(5)	0.312(4)	0.4768(17)	0.057(11)
H33‡	−0.428	0.653	0.4223	0.023
H34‡	−0.241	0.407	0.4447	0.022
H35‡	−0.312	0.261	0.5190	0.026

† Population: 0.85(2)
‡ Population: 0.15(2)

Table 5. Anisotropic Displacement Parameters for AHZ2 (THP-ϕ)$ZrCl_2$

Atom	U_{11}	U_{22}	U_{33}	U_{12}	U_{13}	U_{23}
Zr	0.0065(1)	0.0063(1)	0.0092(1)	−0.0031(1)	−0.0016(1)	0.0001(1)
Cl1	0.0213(2)	0.0104(2)	0.0165(2)	−0.0102(2)	−0.0049(2)	0.0028(1)
Cl2	0.0071(2)	0.0144(2)	0.0143(2)	−0.0033(2)	−0.0010(1)	−0.0012(1)
Si1	0.0089(2)	0.0086(2)	0.0116(2)	−0.0052(2)	−0.0016(2)	0.0000(2)
Si2	0.0065(2)	0.0111(2)	0.0120(2)	−0.0019(2)	−0.0017(2)	−0.0002(2)
C1	0.0087(8)	0.0109(8)	0.0121(8)	−0.0051(6)	−0.0040(6)	−0.0016(6)
C2	0.0078(8)	0.0115(8)	0.0126(8)	−0.0038(6)	−0.0042(6)	−0.0009(6)
C3	0.0110(8)	0.0097(8)	0.0119(8)	−0.0035(7)	−0.0059(6)	0.0013(6)
C4	0.0102(8)	0.0110(8)	0.0099(7)	−0.0047(6)	−0.0049(6)	−0.0004(6)
C5	0.0084(8)	0.0085(8)	0.0116(8)	−0.0028(6)	−0.0035(6)	−0.0018(6)
C6	0.0093(8)	0.0087(7)	0.0098(7)	−0.0046(6)	−0.0002(6)	0.0011(6)
C7	0.0076(7)	0.0095(7)	0.0088(7)	−0.0032(6)	0.0000(6)	0.0003(6)
C8	0.0108(8)	0.0105(8)	0.0092(7)	−0.0047(7)	−0.0002(6)	−0.0002(6)
C9	0.0097(8)	0.0110(8)	0.0093(7)	−0.0049(7)	−0.0026(6)	0.0004(6)
C10	0.0096(8)	0.0105(8)	0.0081(7)	−0.0053(6)	0.0000(6)	0.0012(6)
C11	0.0140(9)	0.0111(8)	0.0167(9)	−0.0061(7)	−0.0029(7)	−0.0004(7)
C12	0.0156(9)	0.0188(9)	0.0174(9)	−0.0119(8)	−0.0028(7)	0.0012(7)
C13	0.0106(9)	0.0254(10)	0.0214(10)	−0.0076(8)	−0.0013(7)	−0.0009(8)
C14	0.0129(9)	0.0136(9)	0.0182(9)	−0.0012(7)	−0.0043(7)	−0.0009(7)
C15	0.0118(8)	0.0129(8)	0.0095(7)	−0.0073(7)	−0.0035(6)	−0.0003(6)
C16	0.0144(9)	0.0124(8)	0.0141(8)	−0.0058(7)	−0.0033(7)	−0.0005(6)
C17	0.0220(9)	0.0147(8)	0.0132(8)	−0.0115(8)	−0.0055(7)	0.0034(7)
C18	0.0188(9)	0.0220(9)	0.0108(8)	−0.0138(8)	−0.0018(7)	0.0004(7)
C19	0.0108(8)	0.0197(9)	0.0140(8)	−0.0064(7)	−0.0004(7)	−0.0022(7)
C20	0.0128(8)	0.0141(8)	0.0122(8)	−0.0055(7)	−0.0035(6)	0.0005(6)
C21	0.0109(8)	0.0103(8)	0.0118(8)	−0.0036(7)	−0.0034(6)	0.0007(6)
C22	0.0191(10)	0.0157(9)	0.0219(10)	−0.0073(8)	−0.0067(8)	0.0080(7)
C23	0.0130(9)	0.0147(9)	0.0228(10)	−0.0036(7)	−0.0085(7)	0.0018(7)
C24	0.0146(8)	0.0089(8)	0.0127(8)	−0.0032(7)	−0.0036(7)	−0.0011(6)
C25	0.0172(9)	0.0142(9)	0.0147(9)	−0.0019(7)	−0.0008(7)	−0.0031(7)
C26	0.0223(10)	0.0129(9)	0.0241(10)	−0.0085(8)	−0.0046(8)	−0.0054(8)
C27	0.0227(10)	0.0193(10)	0.0246(10)	0.0007(8)	−0.0100(8)	−0.0105(8)
C28	0.0190(10)	0.0251(10)	0.0235(10)	−0.0032(8)	−0.0071(8)	−0.0041(8)
C29	0.0222(10)	0.0192(10)	0.0291(11)	−0.0049(8)	−0.0129(8)	−0.0031(8)
C30	0.0835(60)	0.0344(25)	0.0274(21)	−0.0402(35)	−0.0198(30)	0.0071(19)
C31	0.0628(45)	0.0709(56)	0.0159(15)	−0.0574(46)	0.0144(18)	−0.0118(20)
C32	0.0334(22)	0.0436(35)	0.0441(31)	−0.0131(24)	−0.0033(24)	−0.0252(27)

The form of the displacement factor is:

$$\exp -2\pi^2(U_{11}h^2a^{*^2} + U_{22}k^2b^{*^2} + U_{33}\ell^2c^{*^2} + 2U_{12}hka^*b^* + 2U_{13}h\ell a^*c^* + 2U_{23}k\ell b^*c^*)$$

Table 6. Complete Distances and Angles for

AHZ2 (THP-ϕ)$ZrCl_2$

	Distance(Å)		Distance(Å)
Zr –Cp1	2.208	C11 –H11a	0.95(2)
Zr –Cp2	2.244	C11 –H11b	0.96(2)
Zr –Cl1	2.4280(5)	C11 –H11c	0.97(2)
Zr –Cl2	2.4343(4)	C12 –H12a	0.95(3)
Zr –C1	2.435(2)	C12 –H12b	0.92(3)
Zr –C2	2.441(2)	C12 –H12c	0.96(2)
Zr –C3	2.549(2)	C13 –H13a	0.95(3)
Zr –C4	2.623(2)	C13 –H13b	0.96(3)
Zr –C5	2.539(2)	C13 –H13c	0.91(3)
Zr –C6	2.412(2)	C14 –H14a	0.94(2)
Zr –C7	2.412(2)	C14 –H14b	0.96(2)
Zr –C8	2.623(2)	C14 –H14c	0.95(2)
Zr –C9	2.689(2)	C15 –C16	1.398(3)
Zr –C10	2.621(2)	C15 –C20	1.400(3)
Si1 –C1	1.874(2)	C16 –C17	1.390(3)
Si1 –C6	1.892(2)	C16 –H16	0.96(2)
Si1 –C11	1.859(2)	C17 –C18	1.384(3)
Si1 –C12	1.859(2)	C17 –H17	0.96(2)
Si2 –C2	1.873(2)	C18 –C19	1.388(3)
Si2 –C7	1.888(2)	C18 –H18	0.95(2)
Si2 –C13	1.859(2)	C19 –C20	1.385(3)
Si2 –C14	1.862(2)	C19 –H19	0.93(2)
C1 –C2	1.452(2)	C20 –H20	0.97(2)
C1 –C5	1.417(2)	C21 –C22	1.532(3)
C2 –C3	1.420(2)	C21 –C23	1.526(3)
C3 –C4	1.418(2)	C21 –H21	0.91(2)
C3 –H3	0.92(2)	C22 –H22a	1.01(2)
C4 –C5	1.420(2)	C22 –H22b	1.00(2)
C4 –C15	1.478(2)	C22 –H22c	0.97(2)
C5 –H5	0.90(2)	C23 –H23a	0.97(2)
C6 –C7	1.478(2)	C23 –H23b	0.97(2)
C6 –C10	1.429(2)	C23 –H23c	0.94(2)
C7 –C8	1.434(2)	C24 –C25	1.534(3)
C8 –C9	1.410(2)	C24 –C26	1.527(3)
C8 –C24	1.515(3)	C24 –H24	0.93(2)
C9 –C10	1.413(2)	C25 –H25a	1.00(2)
C9 –H9	0.94(2)	C25 –H25b	0.96(2)
C10 –C21	1.512(2)	C25 –H25c	0.99(2)

Table 6. (Cont.)

	Distance(Å)		Angle(°)
C26 –H26a	0.92(2)	Cp1 –Zr –Cp2	121.8
C26 –H26b	0.96(2)	Cp1 –Zr –Cl1	108.4
C26 –H26c	0.97(2)	Cp1 –Zr –Cl2	108.3
C27 –C28	1.385(3)	Cp2 –Zr –Cl1	107.6
C27 –C29	1.381(3)	Cp2 –Zr –Cl2	107.6
C27 –H27	0.93(2)	Cl1 –Zr –Cl2	101.24(2)
C28 –H28	0.98(2)	C6 –Si1 –C1	92.0(1)
C28^{ii} –C29	1.393(3)	C11 –Si1 –C1	107.0(1)
C29 –H29	0.95(2)	C12 –Si1 –C1	118.9(1)
C30 –C31	1.380(15)	C11 –Si1 –C6	114.0(1)
C30 –H30	0.93(4)	C12 –Si1 –C6	115.1(1)
C30^{i} –C32	1.380(14)	C12 –Si1 –C11	109.0(1)
C31 –C32	1.370(14)	C7 –Si2 –C2	92.4(1)
C31 –H31	0.84(4)	C13 –Si2 –C2	117.6(1)
C32 –H32	0.89(4)	C14 –Si2 –C2	108.2(1)
C33 –C34	1.35(5)	C13 –Si2 –C7	115.4(1)
C33 –H33	0.95	C14 –Si2 –C7	114.0(1)
C33^{i} –C35	1.31(6)	C14 –Si2 –C13	108.4(1)
C34 –C35	1.31(5)	C2 –C1 –Si1	123.3(1)
C34 –H34	0.95	C5 –C1 –Si1	124.9(1)
C35 –H35	0.95	C5 –C1 –C2	106.8(1)
		C1 –C2 –Si2	122.8(1)
		C3 –C2 –Si2	125.2(1)
		C3 –C2 –C1	106.8(1)
		C4 –C3 –C2	110.0(2)
		H3 –C3 –C2	124.2(14)
		H3 –C3 –C4	125.7(14)
		C5 –C4 –C3	106.3(2)
		C15 –C4 –C3	126.5(2)
		C15 –C4 –C5	127.2(2)
		C4 –C5 –C1	110.1(2)
		H5 –C5 –C1	124.1(14)
		H5 –C5 –C4	125.8(14)
		C7 –C6 –Si1	122.7(1)
		C10 –C6 –Si1	127.0(1)
		C10 –C6 –C7	106.9(1)
		C6 –C7 –Si2	121.8(1)
		C8 –C7 –Si2	128.0(1)

Table 6. (Cont.)

			Angle(°)				Angle(°)
C8	–C7	–C6	106.8(1)	H16	–C16	–C15	119.4(12)
C9	–C8	–C7	108.2(1)	H16	–C16	–C17	120.0(12)
C24	–C8	–C7	127.0(2)	C18	–C17	–C16	120.2(2)
C24	–C8	–C9	124.6(2)	H17	–C17	–C16	117.7(13)
C10	–C9	–C8	109.7(2)	H17	–C17	–C18	122.1(13)
H9	–C9	–C8	125.9(12)	C19	–C18	–C17	119.8(2)
H9	–C9	–C10	124.4(12)	H18	–C18	–C17	119.9(13)
C9	–C10	–C6	108.3(1)	H18	–C18	–C19	120.3(13)
C21	–C10	–C6	126.6(2)	C20	–C19	–C18	120.3(2)
C21	–C10	–C9	124.9(2)	H19	–C19	–C18	120.8(13)
H11a	–C11	–Si1	106.8(14)	H19	–C19	–C20	118.9(13)
H11b	–C11	–Si1	111.6(14)	C19	–C20	–C15	120.6(2)
H11c	–C11	–Si1	111.7(13)	H20	–C20	–C15	118.6(12)
H11b	–C11	–H11a	110.8(20)	H20	–C20	–C19	120.7(12)
H11c	–C11	–H11a	107.7(19)	C22	–C21	–C10	109.7(2)
H11c	–C11	–H11b	108.2(19)	C23	–C21	–C10	112.4(2)
H12a	–C12	–Si1	108.8(16)	H21	–C21	–C10	108.7(12)
H12b	–C12	–Si1	113.1(16)	C23	–C21	–C22	110.6(2)
H12c	–C12	–Si1	109.2(14)	H21	–C21	–C22	107.6(12)
H12b	–C12	–H12a	105.1(22)	H21	–C21	–C23	107.7(12)
H12c	–C12	–H12a	108.0(21)	H22a	–C22	–C21	111.5(13)
H12c	–C12	–H12b	112.5(21)	H22b	–C22	–C21	110.5(13)
H13a	–C13	–Si2	108.3(16)	H22c	–C22	–C21	109.7(14)
H13b	–C13	–Si2	111.5(16)	H22b	–C22	–H22a	106.6(18)
H13c	–C13	–Si2	112.9(18)	H22c	–C22	–H22a	111.4(19)
H13b	–C13	–H13a	105.2(23)	H22c	–C22	–H22b	107.0(19)
H13c	–C13	–H13a	107.0(24)	H23a	–C23	–C21	109.3(13)
H13c	–C13	–H13b	111.6(24)	H23b	–C23	–C21	109.5(14)
H14a	–C14	–Si2	106.7(14)	H23c	–C23	–C21	110.8(12)
H14b	–C14	–Si2	113.4(14)	H23b	–C23	–H23a	109.1(18)
H14c	–C14	–Si2	111.9(14)	H23c	–C23	–H23a	113.6(18)
H14b	–C14	–H14a	110.4(20)	H23c	–C23	–H23b	104.5(18)
H14c	–C14	–H14a	109.9(20)	C25	–C24	–C8	108.6(1)
H14c	–C14	–H14b	104.6(20)	C26	–C24	–C8	112.9(2)
C16	–C15	–C4	120.4(2)	H24	–C24	–C8	108.5(13)
C20	–C15	–C4	121.1(2)	C26	–C24	–C25	110.4(2)
C20	–C15	–C16	118.5(2)	H24	–C24	–C25	108.8(13)
C17	–C16	–C15	120.6(2)	H24	–C24	–C26	107.7(13)

Table 6. (Cont.)

			Angle(°)				Angle(°)
H25a	–C25	–C24	109.2(13)	H35	–C35	–C34	118.9
H25b	–C25	–C24	111.3(14)				
H25c	–C25	–C24	109.6(12)				
H25b	–C25	–H25a	108.1(19)				
H25c	–C25	–H25a	108.9(18)				
H25c	–C25	–H25b	109.7(19)				
H26a	–C26	–C24	110.7(15)				
H26b	–C26	–C24	111.4(13)				
H26c	–C26	–C24	110.6(14)				
H26b	–C26	–H26a	111.4(20)				
H26c	–C26	–H26a	109.3(20)				
H26c	–C26	–H26b	103.2(19)				
C29	–C27	–C28	120.5(2)				
H27	–C27	–C28	120.0(14)				
H27	–C27	–C29	119.5(14)				
H28	–C28	–C27	120.7(14)				
C29	–C28^{ii}	–C27^{ii}	119.9(2)				
C29	–C28^{ii}	–H28^{ii}	119.4(14)				
C28^{ii}	–C29	–C27	119.6(2)				
H29	–C29	–C27	122.1(13)				
H29	–C29	–C28^{ii}	118.3(13)				
H30	–C30	–C31	120.1(26)				
C32	–C30^{i}	–C31^{i}	119.7(9)				
C32	–C30^{i}	–H30^{i}	120.2(26)				
C32	–C31	–C30	120.8(10)				
H31	–C31	–C30	120.1(27)				
H31	–C31	–C32	119.1(27)				
C31	–C32	–C30^{i}	119.6(9)				
H32	–C32	–C30^{i}	119.4(26)				
H32	–C32	–C31	120.9(26)				
H33	–C33	–C34	122.3				
C35	–C33^{i}	–C34^{i}	115.5(38)				
C35	–C33^{i}	–H33^{i}	122.3				
C35	–C34	–C33	122.3(37)				
H34	–C34	–C33	118.8				
H34	–C34	–C35	118.9				
C34	–C35	–C33^{i}	122.2(39)				
H35	–C35	–C33^{i}	118.9				

Symmetry code $(i) 1-x, 1-y, 1-z$ (ii) $1-x, -y, 2-z$

Appendix E

X-Ray Crystallographic Data for $SDpZrCl_2$ (3a, Chapter 2)

Table 1. Crystal data and structure refinement for **AHZ3** (**3a**, Chapter 2).

Empirical formula	$C_{22}H_{36}Cl_2Si_3Zr$
Formula weight	546.90
Crystallization Solvent	Cyclohexane/Toluene
Crystal Habit	Rhomboids
Crystal size	0.12 x 0.17 x 0.21 mm^3
Crystal color	Pale yellow

Data Collection

Preliminary Photos	None	
Type of diffractometer	CAD-4	
Wavelength	0.71073 Å MoKa	
Data Collection Temperature	85 K	
θ range for reflections used in lattice determination	12.4 to 15.3°	
Unit cell dimensions	a = 9.684(2) Å b = 10.441(3) Å c = 13.723(3) Å	a= 96.62(2)° b= 100.54(2)° g = 107.35(2)°
Volume	1280.6(5) $Å^3$	
Z	2	
Crystal system	Triclinic	
Space group	$P\bar{1}$	
Density (calculated)	1.418 Mg/m^3	
F(000)	568	
θ range for data collection	1.5 to 27.5°	
Completeness to θ = 27.5°	99.7 %	
Index ranges	$-12 \leq h \leq 12$, $-13 \leq k \leq 13$, $-17 \leq l \leq 17$	
Data collection scan type	ω scans	
Reflections collected	13849	
Independent reflections	5863 [R_{int}= 0.018; GOF_{merge}= 0.986]	
Absorption coefficient	0.786 mm^{-1}	
Absorption correction	None	
Number of standards	3 reflections measured every 75 min.	
Variation of standards	-0.27 %.	

Table 1 (cont.)

Structure solution and Refinement

Structure solution program	SHELXS-97 (Sheldrick, 1990)
Primary solution method	Direct methods
Secondary solution method	Difference Fourier map
Hydrogen placement	Difference Fourier map
Structure refinement program	SHELXL-97 (Sheldrick, 1997)
Refinement method	Full matrix least-squares on F^2
Data / restraints / parameters	5863 / 0 / 397
Treatment of hydrogen atoms	Unrestrained
Goodness-of-fit on F^2	1.334
Final R indices [I>2s(I)]	R1 = 0.0238, *w*R2 = 0.0499
R indices (all data)	R1 = 0.0302, *w*R2 = 0.0518
Type of weighting scheme used	Sigma
Weighting scheme used	$w=1/\sigma^2(Fo^2)$
Max shift/error	0.001
Average shift/error	0.000
Largest diff. peak and hole	0.422 and -0.255 e.Å^{-3}

Special Refinement Details

The variances [$\sigma^2(Fo^2)$] were derived from counting statistics plus an additional term, $(0.014I)^2$, and the variances of the merged data were obtained by propagation of error plus the addition of another term, $(0.014\langle I\rangle)^2$.

Refinement of F^2 against ALL reflections. The weighted R-factor (*w*R) and goodness of fit (S) are based on F^2, conventional R-factors (R) are based on F, with F set to zero for negative F^2. The threshold expression of $F^2 > 2\sigma(F^2)$ is used only for calculating R-factors(gt), etc., and is not relevant to the choice of reflections for refinement. R-factors based on F^2 are statistically about twice as large as those based on F, and R-factors based on ALL data will be even larger.

All esds (except the esd in the dihedral angle between two l.s. planes) are estimated using the full covariance matrix. The cell esds are taken into account individually in the estimation of esds in distances, angles and torsion angles; correlations between esds in cell parameters are only used when they are defined by crystal symmetry. An approximate (isotropic) treatment of cell esds is used for estimating esds involving l.s. planes.

Table 2. Atomic coordinates (x 10^4) and equivalent isotropic displacement parameters ($Å^2$x 10^3) for **AHZ3**. U(eq) is defined as the trace of the orthogonalized U^{ij} tensor.

	x	y	z	U_{eq}
Zr	1008(1)	3350(1)	3206(1)	9(1)
Cl(1)	-30(1)	4882(1)	2356(1)	17(1)
Cl(2)	-711(1)	2738(1)	4309(1)	17(1)
Si(1)	4300(1)	5273(1)	2302(1)	14(1)
Si(2)	2699(1)	3465(1)	1011(1)	11(1)
Si(3)	3758(1)	2037(1)	3318(1)	12(1)
C(1)	3632(2)	4866(2)	3466(1)	12(1)
C(2)	3667(2)	3700(2)	3930(1)	12(1)
C(3)	3001(2)	3781(2)	4768(1)	13(1)
C(4)	2575(2)	4968(2)	4841(1)	15(1)
C(5)	2973(2)	5635(2)	4055(1)	14(1)
C(6)	1427(2)	2253(2)	1653(1)	10(1)
C(7)	1844(2)	1538(2)	2466(1)	10(1)
C(8)	504(2)	781(2)	2718(1)	12(1)
C(9)	-699(2)	1009(2)	2089(1)	12(1)
C(10)	-173(2)	1850(2)	1416(1)	10(1)
C(11)	327(2)	-227(2)	3439(1)	15(1)
C(12)	739(3)	-1463(2)	3035(2)	23(1)
C(13)	-1238(2)	-726(2)	3615(2)	23(1)
C(14)	-1158(2)	2132(2)	537(1)	13(1)
C(15)	-2741(2)	1896(2)	668(2)	19(1)
C(16)	-1182(2)	1217(2)	-430(1)	18(1)
C(17)	6340(2)	5558(2)	2464(2)	22(1)
C(18)	3980(3)	6919(2)	2089(2)	23(1)
C(19)	1757(2)	4369(2)	138(2)	17(1)
C(20)	3563(2)	2515(2)	190(2)	19(1)
C(21)	5237(2)	2062(2)	2626(2)	19(1)
C(22)	4047(2)	1015(2)	4320(2)	20(1)

Table 3. Selected bond lengths [Å] and angles [°] for **AHZ3**.

Zr-Cent(1)	2.2086(8)	Zr-Pln(1)	2.2066(11)
Zr-Cent(2)	2.2315(7)	Zr-Pln(2)	2.2206(11)
Zr-Cl(1)	2.4280(7)		
Zr-Cl(2)	2.4446(7)		
Cent(1)-Zr-Cent(2)	126.34(2)	Pln(1)-Zr-Pln(2)	118.44(7)
Cl(1)-Zr-Cl(2)	99.26(2)		

Cent(1) is the centroid formed by C(1), C(2), C(3), C(4) and C(5).
Cent(2) is the centroid formed by C(6), C(7), C(8), C(9) and C(10).
Pln(1) is the plane formed by C(1), C(2), C(3), C(4) and C(5).
Pln(2) is the plane formed by C(6), C(7), C(8), C(9) and C(10).

Table 4. Bond lengths [Å] and angles [°] for **AHZ3**.

Zr-Cent(1)	2.2086(8)	C(13)-H(13B)	0.97(2)
Zr-Cent(2)	2.2315(7)	C(13)-H(13C)	0.97(2)
Zr-Pln(1)	2.2066(11)	C(14)-C(15)	1.526(2)
Zr-Pln(2)	2.2206(11)	C(14)-C(16)	1.537(2)
		C(14)-H(14)	0.945(19)
Zr-Cl(1)	2.4280(7)	C(15)-H(15A)	0.96(2)
Zr-Cl(2)	2.4446(7)	C(15)-H(15B)	0.95(2)
Zr-C(6)	2.4600(17)	C(15)-H(15C)	0.93(2)
Zr-C(7)	2.4575(17)	C(16)-H(16A)	0.95(2)
Zr-C(2)	2.4844(17)	C(16)-H(16B)	0.93(2)
Zr-C(1)	2.4963(18)	C(16)-H(16C)	0.96(2)
Zr-C(3)	2.5034(18)	C(17)-H(17A)	0.92(3)
Zr-C(5)	2.552(2)	C(17)-H(17B)	0.93(3)
Zr-C(4)	2.5573(19)	C(17)-H(17C)	0.99(3)
Zr-C(8)	2.5628(19)	C(18)-H(18A)	0.96(2)
Zr-C(10)	2.6103(18)	C(18)-H(18B)	0.93(3)
Zr-C(9)	2.6182(19)	C(18)-H(18C)	0.93(2)
Si(1)-C(1)	1.8750(18)	C(19)-H(19A)	0.94(2)
Si(1)-C(17)	1.875(2)	C(19)-H(19B)	0.96(2)
Si(1)-C(18)	1.880(2)	C(19)-H(19C)	0.91(2)
Si(1)-Si(2)	2.3630(11)	C(20)-H(20A)	0.92(2)
Si(2)-C(19)	1.8803(19)	C(20)-H(20B)	0.97(2)
Si(2)-C(20)	1.880(2)	C(20)-H(20C)	0.93(3)
Si(2)-C(6)	1.9022(18)	C(21)-H(21A)	0.92(2)
Si(3)-C(21)	1.854(2)	C(21)-H(21B)	0.97(2)
Si(3)-C(2)	1.8737(18)	C(21)-H(21C)	0.95(3)
Si(3)-C(22)	1.866(2)	C(22)-H(22B)	0.95(3)
Si(3)-C(7)	1.8878(18)	C(22)-H(22C)	0.93(2)
C(1)-C(5)	1.432(2)	C(22)-H(22C)	0.93(2)
C(1)-C(2)	1.444(2)		
C(2)-C(3)	1.424(2)		
C(3)-C(4)	1.417(2)	Cent(1)-Zr-Cent(2)	126.34(2)
C(3)-H(3)	0.925(19)	Pln(1)-Zr-Pln(2)	118.44(7)
C(4)-C(5)	1.400(3)		
C(4)-H(4)	0.91(2)	Cl(1)-Zr-Cl(2)	99.26(2)
C(5)-H(5)	0.94(2)	Cl(1)-Zr-C(6)	93.42(4)
C(6)-C(10)	1.442(2)	Cl(2)-Zr-C(6)	136.73(4)
C(6)-C(7)	1.474(2)	Cl(1)-Zr-C(7)	128.20(4)
C(7)-C(8)	1.429(2)	Cl(2)-Zr-C(7)	117.12(4)
C(8)-C(9)	1.416(2)	C(6)-Zr-C(7)	34.87(5)
C(8)-C(11)	1.521(2)	Cl(1)-Zr-C(2)	127.65(4)
C(9)-C(10)	1.406(2)	Cl(2)-Zr-C(2)	116.88(4)
C(9)-H(9)	0.88(2)	C(6)-Zr-C(2)	85.33(6)
C(10)-C(14)	1.510(2)	C(7)-Zr-C(2)	67.46(6)
C(11)-C(13)	1.524(3)	Cl(1)-Zr-C(1)	93.98(5)
C(11)-C(12)	1.534(3)	Cl(2)-Zr-C(1)	134.50(4)
C(11)-H(11)	0.954(19)	C(6)-Zr-C(1)	84.98(6)
C(12)-H(12A)	0.97(2)	C(7)-Zr-C(1)	85.93(6)
C(12)-H(12B)	0.96(2)	C(2)-Zr-C(1)	33.71(6)
C(12)-H(12C)	0.97(2)	Cl(1)-Zr-C(3)	131.62(5)
C(13)-H(13A)	0.96(2)	Cl(2)-Zr-C(3)	85.01(5)

C(6)-Zr-C(3)	116.09(6)	C(18)-Si(1)-Si(2)	110.01(8)
C(7)-Zr-C(3)	89.29(6)	C(19)-Si(2)-C(20)	104.32(9)
C(2)-Zr-C(3)	33.18(5)	C(19)-Si(2)-C(6)	115.14(8)
C(1)-Zr-C(3)	54.87(6)	C(20)-Si(2)-C(6)	110.74(9)
Cl(1)-Zr-C(5)	79.97(5)	C(19)-Si(2)-Si(1)	102.68(7)
Cl(2)-Zr-C(5)	107.58(5)	C(20)-Si(2)-Si(1)	118.03(7)
C(6)-Zr-C(5)	115.34(6)	C(6)-Si(2)-Si(1)	106.05(6)
C(7)-Zr-C(5)	118.01(6)	C(21)-Si(3)-C(2)	118.67(9)
C(2)-Zr-C(5)	54.58(6)	C(21)-Si(3)-C(22)	105.27(9)
C(1)-Zr-C(5)	32.95(6)	C(2)-Si(3)-C(22)	108.12(9)
C(3)-Zr-C(5)	53.42(6)	C(21)-Si(3)-C(7)	113.41(8)
Cl(1)-Zr-C(4)	100.28(5)	C(2)-Si(3)-C(7)	93.70(8)
Cl(2)-Zr-C(4)	80.33(5)	C(22)-Si(3)-C(7)	117.98(9)
C(6)-Zr-C(4)	137.65(6)	C(5)-C(1)-C(2)	106.85(15)
C(7)-Zr-C(4)	120.21(6)	C(5)-C(1)-Si(1)	126.84(13)
C(2)-Zr-C(4)	54.71(6)	C(2)-C(1)-Si(1)	126.30(13)
C(1)-Zr-C(4)	54.44(6)	C(5)-C(1)-Zr	75.66(10)
C(3)-Zr-C(4)	32.51(6)	C(2)-C(1)-Zr	72.69(9)
C(5)-Zr-C(4)	31.82(6)	Si(1)-C(1)-Zr	116.57(8)
Cl(1)-Zr-C(8)	130.67(4)	C(3)-C(2)-C(1)	106.87(15)
Cl(2)-Zr-C(8)	86.01(4)	C(3)-C(2)-Si(3)	121.25(13)
C(6)-Zr-C(8)	55.46(6)	C(1)-C(2)-Si(3)	127.20(13)
C(7)-Zr-C(8)	33.00(5)	C(3)-C(2)-Zr	74.14(9)
C(2)-Zr-C(8)	90.45(6)	C(1)-C(2)-Zr	73.60(9)
C(1)-Zr-C(8)	116.81(6)	Si(3)-C(2)-Zr	98.58(7)
C(3)-Zr-C(8)	97.62(6)	C(2)-C(3)-C(4)	109.31(16)
C(5)-Zr-C(8)	145.02(6)	C(2)-C(3)-Zr	72.68(9)
C(4)-Zr-C(8)	128.80(6)	C(4)-C(3)-Zr	75.84(10)
Cl(1)-Zr-C(10)	79.69(4)	C(2)-C(3)-H(3)	126.9(12)
Cl(2)-Zr-C(10)	109.68(4)	C(4)-C(3)-H(3)	123.8(12)
C(6)-Zr-C(10)	32.87(5)	Zr-C(3)-H(3)	117.5(12)
C(7)-Zr-C(10)	54.79(5)	C(5)-C(4)-C(3)	107.53(16)
C(2)-Zr-C(10)	117.37(6)	C(5)-C(4)-Zr	73.88(10)
C(1)-Zr-C(10)	115.48(6)	C(3)-C(4)-Zr	71.65(10)
C(3)-Zr-C(10)	144.08(6)	C(5)-C(4)-H(4)	126.3(13)
C(5)-Zr-C(10)	139.79(6)	C(3)-C(4)-H(4)	126.0(13)
C(4)-Zr-C(10)	169.92(5)	Zr-C(4)-H(4)	116.5(13)
C(8)-Zr-C(10)	53.03(6)	C(4)-C(5)-C(1)	109.42(16)
Cl(1)-Zr-C(9)	99.82(5)	C(4)-C(5)-Zr	74.31(10)
Cl(2)-Zr-C(9)	83.09(4)	C(1)-C(5)-Zr	71.40(10)
C(6)-Zr-C(9)	53.92(6)	C(4)-C(5)-H(5)	126.7(12)
C(7)-Zr-C(9)	53.81(6)	C(1)-C(5)-H(5)	123.7(12)
C(2)-Zr-C(9)	119.97(6)	Zr-C(5)-H(5)	117.1(12)
C(1)-Zr-C(9)	137.04(6)	C(10)-C(6)-C(7)	106.47(14)
C(3)-Zr-C(9)	128.43(6)	C(10)-C(6)-Si(2)	125.32(12)
C(5)-Zr-C(9)	169.26(5)	C(7)-C(6)-Si(2)	128.21(12)
C(4)-Zr-C(9)	155.71(6)	C(10)-C(6)-Zr	79.30(10)
C(8)-Zr-C(9)	31.69(5)	C(7)-C(6)-Zr	72.47(9)
C(10)-Zr-C(9)	31.20(5)	Si(2)-C(6)-Zr	114.43(8)
C(1)-Si(1)-C(17)	112.32(9)	C(8)-C(7)-C(6)	107.36(14)
C(1)-Si(1)-C(18)	106.15(9)	C(8)-C(7)-Si(3)	124.49(12)
C(17)-Si(1)-C(18)	107.60(10)	C(6)-C(7)-Si(3)	124.66(12)
C(1)-Si(1)-Si(2)	104.13(6)	C(8)-C(7)-Zr	77.55(10)
C(17)-Si(1)-Si(2)	116.20(8)	C(6)-C(7)-Zr	72.66(9)

Si(3)-C(7)-Zr	99.11(7)	C(14)-C(15)-H(15C)	113.4(14)
C(7)-C(8)-C(9)	107.98(15)	H(15A)-C(15)-H(15C)	105.4(19)
C(7)-C(8)-C(11)	127.60(15)	H(15B)-C(15)-H(15C)	108.4(18)
C(9)-C(8)-C(11)	124.09(15)	C(14)-C(16)-H(16A)	112.3(13)
C(7)-C(8)-Zr	69.45(9)	C(14)-C(16)-H(16B)	108.9(13)
C(9)-C(8)-Zr	76.31(10)	H(16A)-C(16)-H(16B)	108.1(19)
C(11)-C(8)-Zr	125.18(11)	C(14)-C(16)-H(16C)	110.6(13)
C(10)-C(9)-C(8)	109.87(15)	H(16A)-C(16)-H(16C)	107.4(18)
C(10)-C(9)-Zr	74.09(10)	H(16B)-C(16)-H(16C)	109.5(18)
C(8)-C(9)-Zr	72.00(10)	Si(1)-C(17)-H(17A)	111.3(15)
C(10)-C(9)-H(9)	124.6(14)	Si(1)-C(17)-H(17B)	107.4(15)
C(8)-C(9)-H(9)	125.5(14)	H(17A)-C(17)-H(17B)	107(2)
Zr-C(9)-H(9)	119.8(14)	Si(1)-C(17)-H(17C)	114.2(16)
C(9)-C(10)-C(6)	108.17(15)	H(17A)-C(17)-H(17C)	108(2)
C(9)-C(10)-C(14)	124.27(15)	H(17B)-C(17)-H(17C)	108(2)
C(6)-C(10)-C(14)	127.26(15)	Si(1)-C(18)-H(18A)	112.0(14)
C(9)-C(10)-Zr	74.71(10)	Si(1)-C(18)-H(18B)	108.8(15)
C(6)-C(10)-Zr	67.83(9)	H(18A)-C(18)-H(18B)	108(2)
C(14)-C(10)-Zr	128.07(11)	Si(1)-C(18)-H(18C)	109.2(15)
C(8)-C(11)-C(13)	113.28(16)	H(18A)-C(18)-H(18C)	110(2)
C(8)-C(11)-C(12)	109.80(15)	H(18B)-C(18)-H(18C)	108(2)
C(13)-C(11)-C(12)	108.91(16)	Si(2)-C(19)-H(19A)	112.0(12)
C(8)-C(11)-H(11)	110.0(11)	Si(2)-C(19)-H(19B)	113.6(13)
C(13)-C(11)-H(11)	106.7(11)	H(19A)-C(19)-H(19B)	108.3(17)
C(12)-C(11)-H(11)	108.0(11)	Si(2)-C(19)-H(19C)	105.5(14)
C(11)-C(12)-H(12A)	110.7(13)	H(19A)-C(19)-H(19C)	108.3(19)
C(11)-C(12)-H(12B)	111.6(14)	H(19B)-C(19)-H(19C)	108.9(19)
H(12A)-C(12)-H(12B)	109.5(18)	Si(2)-C(20)-H(20A)	113.2(14)
C(11)-C(12)-H(12C)	109.2(13)	Si(2)-C(20)-H(20B)	109.4(14)
H(12A)-C(12)-H(12C)	106.8(18)	H(20A)-C(20)-H(20B)	105.1(19)
H(12B)-C(12)-H(12C)	108.9(19)	Si(2)-C(20)-H(20C)	108.0(15)
C(11)-C(13)-H(13A)	109.6(13)	H(20A)-C(20)-H(20C)	112.2(19)
C(11)-C(13)-H(13B)	110.7(13)	H(20B)-C(20)-H(20C)	109(2)
H(13A)-C(13)-H(13B)	108.2(18)	Si(3)-C(21)-H(21A)	112.0(13)
C(11)-C(13)-H(13C)	111.9(14)	Si(3)-C(21)-H(21B)	105.6(14)
H(13A)-C(13)-H(13C)	108.8(18)	H(21A)-C(21)-H(21B)	110.7(19)
H(13B)-C(13)-H(13C)	107.7(18)	Si(3)-C(21)-H(21C)	111.0(15)
C(10)-C(14)-C(15)	112.77(15)	H(21A)-C(21)-H(21C)	108(2)
C(10)-C(14)-C(16)	108.74(14)	H(21B)-C(21)-H(21C)	109(2)
C(15)-C(14)-C(16)	109.83(15)	Si(3)-C(22)-H(22B)	104.7(15)
C(10)-C(14)-H(14)	108.6(12)	Si(3)-C(22)-H(22C)	115.7(14)
C(15)-C(14)-H(14)	107.7(11)	H(22B)-C(22)-H(22C)	109(2)
C(16)-C(14)-H(14)	109.1(12)	Si(3)-C(22)-H(22C)	110.9(14)
C(14)-C(15)-H(15A)	111.2(13)	H(22B)-C(22)-H(22C)	107(2)
C(14)-C(15)-H(15B)	110.3(13)	H(22C)-C(22)-H(22C)	109(2)
H(15A)-C(15)-H(15B)	107.8(18)		

Cent(1) is the centroid formed by C(1), C(2), C(3), C(4) and C(5).
Cent(2) is the centroid formed by C(6), C(7), C(8), C(9) and C(10).
Pln(1) is the plane formed by C(1), C(2), C(3), C(4) and C(5).
Pln(2) is the plane formed by C(6), C(7), C(8), C(9) and C(10).

Table 5. *Anisotropic displacement parameters* ($Å^2 x\ 10^4$) for **AHZ3**. The anisotropic displacement factor exponent takes the form: $-2p^2 [h^2 a^{*2} U^{11} + ... + 2 h k a^* b^* U^{12}]$.

	U^{11}	U^{22}	U^{33}	U^{23}	U^{13}	U^{12}
Zr	93(1)	102(1)	80(1)	11(1)	20(1)	49(1)
Cl(1)	215(2)	154(2)	165(2)	20(2)	-10(2)	116(2)
Cl(2)	158(2)	202(2)	150(2)	12(2)	83(2)	57(2)
Si(1)	134(2)	140(2)	130(2)	44(2)	28(2)	20(2)
Si(2)	109(2)	148(2)	98(2)	46(2)	35(2)	51(2)
Si(3)	129(2)	152(2)	100(2)	38(2)	25(2)	84(2)
C(1)	96(7)	132(8)	111(8)	14(6)	6(6)	22(6)
C(2)	88(7)	143(8)	103(8)	19(7)	-3(6)	36(6)
C(3)	116(8)	160(9)	93(8)	21(7)	1(6)	40(7)
C(4)	133(8)	169(9)	111(8)	-36(7)	-2(7)	51(7)
C(5)	137(8)	102(8)	154(9)	-8(7)	-2(7)	27(7)
C(6)	115(8)	101(8)	89(8)	10(6)	34(6)	48(6)
C(7)	148(8)	111(8)	80(8)	16(6)	40(6)	77(7)
C(8)	154(8)	97(8)	102(8)	-4(6)	45(6)	37(6)
C(9)	122(8)	120(8)	96(8)	-15(6)	30(6)	15(7)
C(10)	118(8)	110(8)	83(8)	-6(6)	22(6)	51(6)
C(11)	232(9)	120(9)	106(8)	33(7)	48(7)	39(7)
C(12)	394(12)	147(10)	185(10)	61(8)	104(9)	114(9)
C(13)	299(11)	163(10)	216(10)	81(8)	125(9)	22(8)
C(14)	116(8)	169(9)	99(8)	27(7)	21(6)	55(7)
C(15)	121(8)	303(11)	154(9)	49(8)	28(7)	93(8)
C(16)	192(9)	240(11)	110(9)	0(7)	22(7)	93(8)
C(17)	146(9)	295(12)	179(10)	32(9)	44(8)	1(8)
C(18)	320(11)	165(10)	204(10)	65(8)	63(9)	60(9)
C(19)	158(9)	214(10)	153(9)	94(8)	26(7)	69(8)
C(20)	180(9)	263(10)	160(9)	54(8)	86(8)	111(8)
C(21)	165(9)	281(11)	170(9)	30(8)	39(7)	129(8)
C(22)	244(10)	216(10)	171(10)	71(8)	18(8)	127(8)

Table 6. Hydrogen coordinates (x 10^4) and isotropic displacement parameters ($Å^2$x 10^3) for **AHZ3**.

	x	y	z	U_{iso}
H(3)	2850(20)	3170(20)	5203(15)	11(5)
H(4)	2070(20)	5210(20)	5287(15)	15(5)
H(5)	2780(20)	6430(20)	3893(15)	16(5)
H(9)	-1640(20)	690(20)	2118(16)	19(5)
H(11)	980(20)	191(19)	4082(15)	9(5)
H(12A)	720(20)	-2080(20)	3519(16)	22(6)
H(12B)	1700(30)	-1190(20)	2881(17)	29(6)
H(12C)	10(30)	-1980(20)	2429(18)	27(6)
H(13A)	-1280(20)	-1340(20)	4086(17)	23(6)
H(13B)	-1950(20)	-1210(20)	2991(18)	25(6)
H(13C)	-1550(20)	30(20)	3879(17)	29(6)
H(14)	-760(20)	3060(20)	480(14)	10(5)
H(15A)	-3220(20)	960(20)	714(16)	23(6)
H(15B)	-3320(20)	2100(20)	107(17)	22(6)
H(15C)	-2790(20)	2410(20)	1252(18)	26(6)
H(16A)	-1750(20)	1390(20)	-1014(17)	25(6)
H(16B)	-1600(20)	310(20)	-379(16)	21(6)
H(16C)	-190(20)	1370(20)	-526(16)	23(6)
H(17A)	6620(30)	5610(20)	1860(19)	33(7)
H(17B)	6840(30)	6400(30)	2887(19)	37(7)
H(17C)	6670(30)	4860(30)	2770(20)	54(8)
H(18A)	2950(30)	6850(20)	2009(18)	34(7)
H(18B)	4530(30)	7600(30)	2643(19)	33(7)
H(18C)	4320(30)	7170(20)	1520(19)	34(7)
H(19A)	1260(20)	4870(20)	465(15)	14(5)
H(19B)	1060(20)	3770(20)	-447(16)	20(5)
H(19C)	2500(30)	4970(20)	-63(17)	27(6)
H(20A)	3880(20)	1870(20)	488(17)	26(6)
H(20B)	2820(30)	2000(20)	-416(19)	34(7)
H(20C)	4330(30)	3150(20)	9(18)	37(7)
H(21A)	5240(20)	2600(20)	2147(17)	20(6)
H(21B)	5030(30)	1120(30)	2315(18)	34(7)
H(21C)	6190(30)	2380(30)	3071(19)	41(7)
H(22B)	5060(30)	1440(30)	4672(19)	39(7)
H(22C)	3440(30)	980(20)	4775(18)	31(6)
H(22C)	3960(20)	130(20)	4037(17)	29(6)

Appendix F

X-Ray Crystallographic Data for (tBu-Mp)$ZrCl_2$ (2b, Chapter 3)

Table 1. *Crystal* data and structure refinement for **AHZ7** (**2b**, Chapter 3, CCDC 162495).

Empirical formula	$2(C_{16}H_{22}Cl_2SiZr)$
Formula weight	809.09
Crystallization Solvent	Toluene/hexanes
Crystal Habit	Tablet
Crystal size	0.20 x 0.18 x 0.13 mm^3
Crystal color	Colorless

Data Collection

Preliminary Photos	Rotation
Type of diffractometer	CCD area detector
Wavelength	0.71073 Å MoKa
Data Collection Temperature	98(2) K
q range for 25460 reflections used in lattice determination	2.31 to 28.34°
Unit cell dimensions	a = 13.8301(7) Å b = 14.4666(7) Å b= 108.0630(10)° c = 18.5422(9) Å
Volume	3527.0(3) $Å^3$
Z	4
Crystal system	Monoclinic
Space group	$P2_1/c$
Density (calculated)	1.524 Mg/m^3
F(000)	1648
Data collection program	Bruker SMART
q range for data collection	1.55 to 28.44°
Completeness to q = 28.44°	94.3%
Index ranges	$-18 \leq h \leq 18$, $-19 \leq k \leq 18$, $-24 \leq l \leq 24$
Data collection scan type	ω scans at 6 ϕ settings
Data reduction program	Bruker SAINT v6.2
Reflections collected	60839
Independent reflections	8384 [R_{int}= 0.0598]
Absorption coefficient	0.983 mm^{-1}
Absorption correction	None
Max. and min. transmission	0.8870 and 0.8307

Table 1 (cont.)

Structure solution and Refinement

Structure solution program	SHELXS-97 (Sheldrick, 1990)
Primary solution method	Direct methods
Secondary solution method	Direct methods
Hydrogen placement	Difference Fourier map
Structure refinement program	SHELXL-97 (Sheldrick, 1997)
Refinement method	Full matrix least-squares on F^2
Data / restraints / parameters	8384 / 0 / 537
Treatment of hydrogen atoms	Unrestrained
Goodness-of-fit on F^2	1.574
Final R indices [I>2s(I), 6657 reflections]	R1 = 0.0317, *w*R2 = 0.0518
R indices (all data)	R1 = 0.0437, *w*R2 = 0.0532
Type of weighting scheme used	Sigma
Weighting scheme used	$w=1/\sigma^2(Fo^2)$
Max shift/error	0.002
Average shift/error	0.000
Largest diff. peak and hole	1.391 and -0.531 e.Å^{-3}

Special Refinement Details

The largest peak in the final difference Fourier, height 1.39 e$^-$/Å^3, is within 1Å of a zirconium atom. There are no other peaks with height greater than 1 e$^-$/Å^{-3}.

Refinement of F^2 against ALL reflections. The weighted R-factor (*w*R) and goodness of fit (S) are based on F^2, conventional R-factors (R) are based on F, with F set to zero for negative F^2. The threshold expression of $F^2 > 2\sigma(F^2)$ is used only for calculating R-factors(gt), etc., and is not relevant to the choice of reflections for refinement. R-factors based on F^2 are statistically about twice as large as those based on F, and R-factors based on ALL data will be even larger.

All esds (except the esd in the dihedral angle between two l.s. planes) are estimated using the full covariance matrix. The cell esds are taken into account individually in the estimation of esds in distances, angles and torsion angles; correlations between esds in cell parameters are only used when they are defined by crystal symmetry. An approximate (isotropic) treatment of cell esds is used for estimating esds involving l.s. planes.

Table 2. *Atomic* coordinates (x 10^4) and equivalent isotropic displacement parameters ($Å^2$x 10^3) for **AHZ7** (CCDC 162495). U(eq) is defined as the trace of the orthogonalized U^{ij} tensor.

	x	y	z	U_{eq}
Zr(1)	3460(1)	5753(1)	2795(1)	15(1)
Cl(1A)	4635(1)	6956(1)	2670(1)	24(1)
Cl(2A)	3236(1)	4832(1)	1652(1)	26(1)
SiA	2268(1)	5097(1)	4013(1)	17(1)
C(1A)	1949(2)	5944(1)	3217(1)	16(1)
C(2A)	2432(2)	6828(2)	3276(1)	18(1)
C(3A)	2294(2)	7179(2)	2545(1)	18(1)
C(4A)	1741(2)	6534(2)	2007(1)	16(1)
C(5A)	1552(2)	5772(2)	2423(1)	16(1)
C(6A)	3564(2)	4844(2)	3949(1)	17(1)
C(7A)	4391(2)	5480(2)	4151(1)	21(1)
C(8A)	5105(2)	5227(2)	3785(1)	24(1)
C(9A)	4732(2)	4460(2)	3334(1)	24(1)
C(10A)	3788(2)	4226(2)	3431(1)	22(1)
C(11A)	2345(2)	5660(2)	4924(2)	27(1)
C(12A)	1433(2)	4072(2)	3795(2)	26(1)
C(13A)	1322(2)	6719(2)	1158(1)	19(1)
C(14A)	741(2)	5873(2)	746(2)	26(1)
C(15A)	595(2)	7544(2)	1058(2)	24(1)
C(16A)	2164(2)	6980(2)	820(2)	25(1)
Zr(2)	7510(1)	5274(1)	1811(1)	15(1)
Cl(1B)	9075(1)	4408(1)	2005(1)	30(1)
Cl(2B)	7096(1)	4751(1)	2930(1)	23(1)
SiB	5974(1)	6733(1)	577(1)	18(1)
C(1B)	7142(2)	6893(1)	1410(1)	16(1)
C(2B)	8135(2)	6683(2)	1373(1)	18(1)
C(3B)	8807(2)	6595(2)	2114(1)	17(1)
C(4B)	8269(2)	6737(1)	2634(1)	16(1)
C(5B)	7235(2)	6892(2)	2194(1)	17(1)
C(6B)	6056(2)	5445(2)	624(1)	18(1)
C(7B)	6822(2)	4925(2)	443(1)	22(1)
C(8B)	6911(2)	4051(2)	789(1)	25(1)
C(9B)	6233(2)	4022(2)	1210(1)	23(1)
C(10B)	5713(2)	4872(2)	1112(1)	21(1)
C(11B)	6201(2)	7201(2)	-284(2)	25(1)
C(12B)	4811(2)	7184(2)	736(2)	26(1)
C(13B)	8746(2)	6837(2)	3487(1)	21(1)
C(14B)	7940(2)	6934(2)	3881(2)	27(1)
C(15B)	9388(3)	7726(2)	3604(2)	39(1)
C(16B)	9447(2)	6026(2)	3822(2)	26(1)

Table 3. Selected bond lengths [Å] and angles [°] for **AHZ7** (CCDC 162495).

Zr(1)-Pln(1A)	2.2118(10)	Zr(1)-Cent(1A)	2.220
Zr(1)-Pln(2A)	2.1994(10)	Zr(1)-Cent(2A)	2.202
Zr(1)-Cl(2A)	2.4411(6)	Zr(1)-Cl(1A)	2.4413(6)
Zr(1)-C(1A)	2.462(2)	Zr(1)-C(6A)	2.477(2)
Zr(1)-C(2A)	2.454(2)	Zr(1)-C(7A)	2.475(2)
Zr(1)-C(3A)	2.570(2)	Zr(1)-C(8A)	2.557(2)
Zr(1)-C(4A)	2.629(2)	Zr(1)-C(9A)	2.550(2)
Zr(1)-C(5A)	2.512(2)	Zr(1)-C(10A)	2.478(2)
Zr(2)-Pln(1B)	2.2087(10)	Zr(2)-Cent(1B)	2.217
Zr(2)-Pln(2B)	2.1981(10)	Zr(2)-Cent(2B)	2.199
Zr(2)-Cl(1B)	2.4294(6)	Zr(2)-Cl(2B)	2.4365(6)
Zr(2)-C(1B)	2.463(2)	Zr(2)-C(6B)	2.492(2)
Zr(2)-C(2B)	2.449(2)	Zr(2)-C(7B)	2.470(2)
Zr(2)-C(3B)	2.562(2)	Zr(2)-C(8B)	2.536(2)
Zr(2)-C(4B)	2.630(2)	Zr(2)-C(9B)	2.534(2)
Zr(2)-C(5B)	2.510(2)	Zr(2)-C(10B)	2.489(2)
Pln(1A)-Zr(1)-Pln(2A)	118.51(9)	Pln(1B)-Zr(2)-Pln(2B)	118.52(9)
Cent(1A)-Zr(1)-Cent(2A)	126.3	Cent(1B)-Zr(2)-Cent(2B)	125.3
Cl(1A)-Zr(1)-Cl(2A)	102.44(2)	Cl(1B)-Zr(2)-Cl(2B)	98.52(2)

Table 4. Bond lengths [Å] and angles [°] for **AHZ7** (CCDC 162495).

Zr(1)-Pln(1A)	2.2118(10)	C(15A)-H(15B)	0.93(2)
Zr(1)-Pln(2A)	2.1994(10)	C(15A)-H(15C)	0.94(2)
Zr(1)-Cent(1A)	2.220	C(16A)-H(16A)	1.01(2)
Zr(1)-Cent(2A)	2.202	C(16A)-H(16B)	0.98(2)
Zr(1)-Cl(2A)	2.4411(6)	C(16A)-H(16C)	0.96(2)
Zr(1)-Cl(1A)	2.4413(6)	Zr(2)-Pln(1B)	2.2087(10)
Zr(1)-C(2A)	2.454(2)	Zr(2)-Pln(2B)	2.1981(10)
Zr(1)-C(1A)	2.462(2)	Zr(2)-Cent(1B)	2.217
Zr(1)-C(7A)	2.475(2)	Zr(2)-Cent(2B)	2.199
Zr(1)-C(6A)	2.477(2)	Zr(2)-Cl(1B)	2.4294(6)
Zr(1)-C(10A)	2.478(2)	Zr(2)-Cl(2B)	2.4365(6)
Zr(1)-C(5A)	2.512(2)	Zr(2)-C(2B)	2.449(2)
Zr(1)-C(9A)	2.550(2)	Zr(2)-C(1B)	2.463(2)
Zr(1)-C(8A)	2.557(2)	Zr(2)-C(7B)	2.470(2)
Zr(1)-C(3A)	2.570(2)	Zr(2)-C(10B)	2.489(2)
Zr(1)-C(4A)	2.629(2)	Zr(2)-C(6B)	2.492(2)
SiA-C(12A)	1.845(3)	Zr(2)-C(5B)	2.510(2)
SiA-C(11A)	1.849(3)	Zr(2)-C(9B)	2.534(2)
SiA-C(1A)	1.864(2)	Zr(2)-C(8B)	2.536(2)
SiA-C(6A)	1.870(2)	Zr(2)-C(3B)	2.562(2)
C(1A)-C(5A)	1.424(3)	Zr(2)-C(4B)	2.630(2)
C(1A)-C(2A)	1.431(3)	SiB-C(12B)	1.842(3)
C(2A)-C(3A)	1.404(3)	SiB-C(11B)	1.848(3)
C(2A)-H(2A)	0.92(2)	SiB-C(6B)	1.868(2)
C(3A)-C(4A)	1.406(3)	SiB-C(1B)	1.872(2)
C(3A)-H(3A)	0.90(2)	C(1B)-C(5B)	1.420(3)
C(4A)-C(5A)	1.416(3)	C(1B)-C(2B)	1.428(3)
C(4A)-C(13A)	1.524(3)	C(2B)-C(3B)	1.406(3)
C(5A)-H(5A)	0.91(2)	C(2B)-H(2B)	0.963(19)
C(6A)-C(10A)	1.415(3)	C(3B)-C(4B)	1.403(3)
C(6A)-C(7A)	1.424(3)	C(3B)-H(3B)	0.94(2)
C(7A)-C(8A)	1.408(3)	C(4B)-C(5B)	1.427(3)
C(7A)-H(7A)	0.90(2)	C(4B)-C(13B)	1.520(3)
C(8A)-C(9A)	1.389(3)	C(5B)-H(5B)	0.91(2)
C(8A)-H(8A)	0.93(2)	C(6B)-C(10B)	1.413(3)
C(9A)-C(10A)	1.413(3)	C(6B)-C(7B)	1.421(3)
C(9A)-H(9A)	0.93(2)	C(7B)-C(8B)	1.406(3)
C(10A)-H(10A)	0.87(2)	C(7B)-H(7B)	0.92(2)
C(11A)-H(11A)	0.87(2)	C(8B)-C(9B)	1.393(3)
C(11A)-H(11B)	1.03(3)	C(8B)-H(8B)	0.88(2)
C(11A)-H(11C)	0.90(3)	C(9B)-C(10B)	1.407(3)
C(12A)-H(12A)	0.97(2)	C(9B)-H(9B)	0.88(2)
C(12A)-H(12B)	0.91(2)	C(10B)-H(10B)	0.894(19)
C(12A)-H(12C)	0.88(3)	C(11B)-H(11D)	0.95(3)
C(13A)-C(16A)	1.531(3)	C(11B)-H(11E)	0.99(2)
C(13A)-C(14A)	1.532(3)	C(11B)-H(11F)	0.91(2)
C(13A)-C(15A)	1.535(3)	C(12B)-H(12D)	0.94(3)
C(14A)-H(14A)	1.03(2)	C(12B)-H(12E)	0.90(3)
C(14A)-H(14B)	0.89(2)	C(12B)-H(12F)	0.94(3)
C(14A)-H(14C)	0.99(2)	C(13B)-C(14B)	1.518(3)
C(15A)-H(15A)	0.96(2)	C(13B)-C(16B)	1.526(3)

C(13B)-C(15B)	1.539(3)
C(14B)-H(14D)	1.00(2)
C(14B)-H(14E)	1.03(2)
C(14B)-H(14F)	0.97(2)
C(15B)-H(15D)	1.02(3)
C(15B)-H(15E)	1.05(3)
C(15B)-H(15F)	0.93(3)
C(16B)-H(16D)	0.97(2)
C(16B)-H(16E)	1.00(2)
C(16B)-H(16F)	0.92(2)
Pln(1A)-Zr(1)-Pln(2A)	118.51(9)
Cent(1A)-Zr(1)-Cent(2A)	126.3
Cl(2A)-Zr(1)-Cl(1A)	102.44(2)
Cl(2A)-Zr(1)-C(2A)	136.87(6)
Cl(1A)-Zr(1)-C(2A)	93.46(5)
Cl(2A)-Zr(1)-C(1A)	116.44(5)
Cl(1A)-Zr(1)-C(1A)	127.28(5)
C(2A)-Zr(1)-C(1A)	33.86(7)
Cl(2A)-Zr(1)-C(7A)	132.88(6)
Cl(1A)-Zr(1)-C(7A)	93.34(6)
C(2A)-Zr(1)-C(7A)	84.85(8)
C(1A)-Zr(1)-C(7A)	85.49(7)
Cl(2A)-Zr(1)-C(6A)	114.70(5)
Cl(1A)-Zr(1)-C(6A)	126.76(5)
C(2A)-Zr(1)-C(6A)	84.73(7)
C(1A)-Zr(1)-C(6A)	67.27(7)
C(7A)-Zr(1)-C(6A)	33.43(7)
Cl(2A)-Zr(1)-C(10A)	83.18(6)
Cl(1A)-Zr(1)-C(10A)	130.66(6)
C(2A)-Zr(1)-C(10A)	115.71(8)
C(1A)-Zr(1)-C(10A)	89.85(7)
C(7A)-Zr(1)-C(10A)	54.12(8)
C(6A)-Zr(1)-C(10A)	33.19(7)
Cl(2A)-Zr(1)-C(5A)	85.87(5)
Cl(1A)-Zr(1)-C(5A)	129.76(5)
C(2A)-Zr(1)-C(5A)	54.22(7)
C(1A)-Zr(1)-C(5A)	33.25(7)
C(7A)-Zr(1)-C(5A)	116.91(7)
C(6A)-Zr(1)-C(5A)	91.05(7)
C(10A)-Zr(1)-C(5A)	99.34(8)
Cl(2A)-Zr(1)-C(9A)	79.98(6)
Cl(1A)-Zr(1)-C(9A)	99.28(6)
C(2A)-Zr(1)-C(9A)	136.88(8)
C(1A)-Zr(1)-C(9A)	120.55(7)
C(7A)-Zr(1)-C(9A)	53.57(8)
C(6A)-Zr(1)-C(9A)	54.82(7)
C(10A)-Zr(1)-C(9A)	32.61(7)
C(5A)-Zr(1)-C(9A)	130.86(8)
Cl(2A)-Zr(1)-C(8A)	107.81(6)
Cl(1A)-Zr(1)-C(8A)	79.04(6)
C(2A)-Zr(1)-C(8A)	114.52(8)
C(1A)-Zr(1)-C(8A)	117.36(7)
C(7A)-Zr(1)-C(8A)	32.45(7)

C(6A)-Zr(1)-C(8A)	54.64(7)
C(10A)-Zr(1)-C(8A)	53.31(8)
C(5A)-Zr(1)-C(8A)	145.68(7)
C(9A)-Zr(1)-C(8A)	31.56(8)
Cl(2A)-Zr(1)-C(3A)	112.20(5)
Cl(1A)-Zr(1)-C(3A)	79.01(5)
C(2A)-Zr(1)-C(3A)	32.35(7)
C(1A)-Zr(1)-C(3A)	54.62(7)
C(7A)-Zr(1)-C(3A)	114.31(8)
C(6A)-Zr(1)-C(3A)	116.59(7)
C(10A)-Zr(1)-C(3A)	144.44(8)
C(5A)-Zr(1)-C(3A)	52.77(7)
C(9A)-Zr(1)-C(3A)	167.81(8)
C(8A)-Zr(1)-C(3A)	137.51(8)
Cl(2A)-Zr(1)-C(4A)	84.41(5)
Cl(1A)-Zr(1)-C(4A)	98.88(5)
C(2A)-Zr(1)-C(4A)	53.39(7)
C(1A)-Zr(1)-C(4A)	54.44(7)
C(7A)-Zr(1)-C(4A)	136.87(7)
C(6A)-Zr(1)-C(4A)	120.61(7)
C(10A)-Zr(1)-C(4A)	130.41(7)
C(5A)-Zr(1)-C(4A)	31.87(7)
C(9A)-Zr(1)-C(4A)	158.19(8)
C(8A)-Zr(1)-C(4A)	167.79(7)
C(3A)-Zr(1)-C(4A)	31.36(7)
C(12A)-SiA-C(11A)	114.20(13)
C(12A)-SiA-C(1A)	112.11(12)
C(11A)-SiA-C(1A)	111.52(12)
C(12A)-SiA-C(6A)	112.09(11)
C(11A)-SiA-C(6A)	111.07(11)
C(1A)-SiA-C(6A)	94.20(9)
C(5A)-C(1A)-C(2A)	104.89(19)
C(5A)-C(1A)-SiA	128.67(16)
C(2A)-C(1A)-SiA	122.48(16)
C(5A)-C(1A)-Zr(1)	75.33(12)
C(2A)-C(1A)-Zr(1)	72.76(12)
SiA-C(1A)-Zr(1)	99.36(9)
C(3A)-C(2A)-C(1A)	109.2(2)
C(3A)-C(2A)-Zr(1)	78.39(13)
C(1A)-C(2A)-Zr(1)	73.38(12)
C(3A)-C(2A)-H(2A)	127.1(13)
C(1A)-C(2A)-H(2A)	123.7(13)
Zr(1)-C(2A)-H(2A)	116.4(13)
C(2A)-C(3A)-C(4A)	109.0(2)
C(2A)-C(3A)-Zr(1)	69.26(12)
C(4A)-C(3A)-Zr(1)	76.62(13)
C(2A)-C(3A)-H(3A)	125.6(13)
C(4A)-C(3A)-H(3A)	125.3(13)
Zr(1)-C(3A)-H(3A)	119.0(13)
C(3A)-C(4A)-C(5A)	106.36(19)
C(3A)-C(4A)-C(13A)	124.5(2)
C(5A)-C(4A)-C(13A)	128.6(2)
C(3A)-C(4A)-Zr(1)	72.02(12)
C(5A)-C(4A)-Zr(1)	69.54(12)

C(13A)-C(4A)-Zr(1)	129.73(14)	C(14A)-C(13A)-C(15A)	109.8(2)
C(4A)-C(5A)-C(1A)	110.5(2)	C(13A)-C(14A)-H(14A)	112.0(13)
C(4A)-C(5A)-Zr(1)	78.59(12)	C(13A)-C(14A)-H(14B)	107.9(15)
C(1A)-C(5A)-Zr(1)	71.42(12)	H(14A)-C(14A)-H(14B)	106.5(19)
C(4A)-C(5A)-H(5A)	125.0(12)	C(13A)-C(14A)-H(14C)	111.2(13)
C(1A)-C(5A)-H(5A)	124.5(12)	H(14A)-C(14A)-H(14C)	112.0(18)
Zr(1)-C(5A)-H(5A)	117.1(12)	H(14B)-C(14A)-H(14C)	106.8(19)
C(10A)-C(6A)-C(7A)	105.0(2)	C(13A)-C(15A)-H(15A)	114.0(13)
C(10A)-C(6A)-SiA	125.63(17)	C(13A)-C(15A)-H(15B)	109.2(13)
C(7A)-C(6A)-SiA	124.40(17)	H(15A)-C(15A)-H(15B)	104.8(18)
C(10A)-C(6A)-Zr(1)	73.46(12)	C(13A)-C(15A)-H(15C)	112.8(13)
C(7A)-C(6A)-Zr(1)	73.22(12)	H(15A)-C(15A)-H(15C)	109.0(18)
SiA-C(6A)-Zr(1)	98.70(9)	H(15B)-C(15A)-H(15C)	106.4(18)
C(8A)-C(7A)-C(6A)	109.4(2)	C(13A)-C(16A)-H(16A)	111.0(12)
C(8A)-C(7A)-Zr(1)	76.96(13)	C(13A)-C(16A)-H(16B)	109.9(13)
C(6A)-C(7A)-Zr(1)	73.34(12)	H(16A)-C(16A)-H(16B)	108.7(18)
C(8A)-C(7A)-H(7A)	126.5(13)	C(13A)-C(16A)-H(16C)	114.6(14)
C(6A)-C(7A)-H(7A)	124.2(13)	H(16A)-C(16A)-H(16C)	105.1(19)
Zr(1)-C(7A)-H(7A)	115.3(13)	H(16B)-C(16A)-H(16C)	107.2(19)
C(9A)-C(8A)-C(7A)	108.2(2)	Pln(1B)-Zr(2)-Pln(2B)	118.52(9)
C(9A)-C(8A)-Zr(1)	73.96(13)	Cent(1B)-Zr(2)-Cent(2B)	125.3
C(7A)-C(8A)-Zr(1)	70.58(12)	Cl(1B)-Zr(2)-Cl(2B)	98.52(2)
C(9A)-C(8A)-H(8A)	123.9(13)	Cl(1B)-Zr(2)-C(2B)	95.08(5)
C(7A)-C(8A)-H(8A)	127.9(13)	Cl(2B)-Zr(2)-C(2B)	137.80(6)
Zr(1)-C(8A)-H(8A)	120.3(12)	Cl(1B)-Zr(2)-C(1B)	128.78(5)
C(8A)-C(9A)-C(10A)	107.5(2)	Cl(2B)-Zr(2)-C(1B)	118.11(5)
C(8A)-C(9A)-Zr(1)	74.48(13)	C(2B)-Zr(2)-C(1B)	33.81(7)
C(10A)-C(9A)-Zr(1)	70.89(13)	Cl(1B)-Zr(2)-C(7B)	95.07(6)
C(8A)-C(9A)-H(9A)	127.3(13)	Cl(2B)-Zr(2)-C(7B)	133.90(6)
C(10A)-C(9A)-H(9A)	125.1(13)	C(2B)-Zr(2)-C(7B)	83.84(8)
Zr(1)-C(9A)-H(9A)	121.6(13)	C(1B)-Zr(2)-C(7B)	84.62(7)
C(9A)-C(10A)-C(6A)	109.9(2)	Cl(1B)-Zr(2)-C(10B)	131.03(6)
C(9A)-C(10A)-Zr(1)	76.51(13)	Cl(2B)-Zr(2)-C(10B)	84.88(5)
C(6A)-C(10A)-Zr(1)	73.35(13)	C(2B)-Zr(2)-C(10B)	114.80(7)
C(9A)-C(10A)-H(10A)	126.1(14)	C(1B)-Zr(2)-C(10B)	89.15(7)
C(6A)-C(10A)-H(10A)	124.0(14)	C(7B)-Zr(2)-C(10B)	54.03(8)
Zr(1)-C(10A)-H(10A)	115.0(14)	Cl(1B)-Zr(2)-C(6B)	128.30(5)
SiA-C(11A)-H(11A)	109.5(16)	Cl(2B)-Zr(2)-C(6B)	116.40(5)
SiA-C(11A)-H(11B)	113.7(13)	C(2B)-Zr(2)-C(6B)	83.99(7)
H(11A)-C(11A)-H(11B)	106(2)	C(1B)-Zr(2)-C(6B)	66.67(7)
SiA-C(11A)-H(11C)	110.5(17)	C(7B)-Zr(2)-C(6B)	33.28(7)
H(11A)-C(11A)-H(11C)	111(2)	C(10B)-Zr(2)-C(6B)	32.97(7)
H(11B)-C(11A)-H(11C)	107(2)	Cl(1B)-Zr(2)-C(5B)	130.21(5)
SiA-C(12A)-H(12A)	116.0(14)	Cl(2B)-Zr(2)-C(5B)	87.26(5)
SiA-C(12A)-H(12B)	111.4(14)	C(2B)-Zr(2)-C(5B)	54.36(7)
H(12A)-C(12A)-H(12B)	105.0(19)	C(1B)-Zr(2)-C(5B)	33.17(7)
SiA-C(12A)-H(12C)	115.6(17)	C(7B)-Zr(2)-C(5B)	115.94(8)
H(12A)-C(12A)-H(12C)	104(2)	C(10B)-Zr(2)-C(5B)	98.67(8)
H(12B)-C(12A)-H(12C)	103(2)	C(6B)-Zr(2)-C(5B)	90.34(7)
C(4A)-C(13A)-C(16A)	111.81(18)	Cl(1B)-Zr(2)-C(9B)	99.45(6)
C(4A)-C(13A)-C(14A)	110.37(19)	Cl(2B)-Zr(2)-C(9B)	80.63(6)
C(16A)-C(13A)-C(14A)	109.9(2)	C(2B)-Zr(2)-C(9B)	135.92(8)
C(4A)-C(13A)-C(15A)	106.63(19)	C(1B)-Zr(2)-C(9B)	119.74(7)
C(16A)-C(13A)-C(15A)	108.2(2)	C(7B)-Zr(2)-C(9B)	53.69(8)

C(10B)-Zr(2)-C(9B)	32.52(7)	C(4B)-C(3B)-H(3B)	124.8(12)
C(6B)-Zr(2)-C(9B)	54.59(7)	C(2B)-C(3B)-H(3B)	126.1(12)
C(5B)-Zr(2)-C(9B)	130.17(8)	Zr(2)-C(3B)-H(3B)	118.1(12)
Cl(1B)-Zr(2)-C(8B)	79.67(6)	C(3B)-C(4B)-C(5B)	106.37(19)
Cl(2B)-Zr(2)-C(8B)	108.11(6)	C(3B)-C(4B)-C(13B)	125.22(19)
C(2B)-Zr(2)-C(8B)	113.58(8)	C(5B)-C(4B)-C(13B)	127.88(19)
C(1B)-Zr(2)-C(8B)	116.65(7)	C(3B)-C(4B)-Zr(2)	71.66(12)
C(7B)-Zr(2)-C(8B)	32.59(7)	C(5B)-C(4B)-Zr(2)	69.30(12)
C(10B)-Zr(2)-C(8B)	53.54(8)	C(13B)-C(4B)-Zr(2)	130.31(14)
C(6B)-Zr(2)-C(8B)	54.66(8)	C(1B)-C(5B)-C(4B)	109.97(19)
C(5B)-Zr(2)-C(8B)	144.98(8)	C(1B)-C(5B)-Zr(2)	71.62(12)
C(9B)-Zr(2)-C(8B)	31.90(8)	C(4B)-C(5B)-Zr(2)	78.56(12)
Cl(1B)-Zr(2)-C(3B)	79.69(5)	C(1B)-C(5B)-H(5B)	126.8(13)
Cl(2B)-Zr(2)-C(3B)	112.22(5)	C(4B)-C(5B)-H(5B)	123.2(13)
C(2B)-Zr(2)-C(3B)	32.50(7)	Zr(2)-C(5B)-H(5B)	117.2(13)
C(1B)-Zr(2)-C(3B)	54.67(7)	C(10B)-C(6B)-C(7B)	105.3(2)
C(7B)-Zr(2)-C(3B)	113.49(7)	C(10B)-C(6B)-SiB	125.97(18)
C(10B)-Zr(2)-C(3B)	143.76(8)	C(7B)-C(6B)-SiB	123.79(17)
C(6B)-Zr(2)-C(3B)	115.99(7)	C(10B)-C(6B)-Zr(2)	73.43(12)
C(5B)-Zr(2)-C(3B)	53.07(7)	C(7B)-C(6B)-Zr(2)	72.52(12)
C(9B)-Zr(2)-C(3B)	167.14(7)	SiB-C(6B)-Zr(2)	99.28(9)
C(8B)-Zr(2)-C(3B)	136.79(8)	C(8B)-C(7B)-C(6B)	109.5(2)
Cl(1B)-Zr(2)-C(4B)	98.75(5)	C(8B)-C(7B)-Zr(2)	76.28(13)
Cl(2B)-Zr(2)-C(4B)	85.00(5)	C(6B)-C(7B)-Zr(2)	74.20(12)
C(2B)-Zr(2)-C(4B)	53.41(7)	C(8B)-C(7B)-H(7B)	127.9(13)
C(1B)-Zr(2)-C(4B)	54.39(7)	C(6B)-C(7B)-H(7B)	122.5(13)
C(7B)-Zr(2)-C(4B)	135.87(7)	Zr(2)-C(7B)-H(7B)	118.5(13)
C(10B)-Zr(2)-C(4B)	130.14(7)	C(9B)-C(8B)-C(7B)	107.7(2)
C(6B)-Zr(2)-C(4B)	120.03(7)	C(9B)-C(8B)-Zr(2)	74.00(13)
C(5B)-Zr(2)-C(4B)	32.15(7)	C(7B)-C(8B)-Zr(2)	71.13(13)
C(9B)-Zr(2)-C(4B)	158.26(7)	C(9B)-C(8B)-H(8B)	125.9(15)
C(8B)-Zr(2)-C(4B)	166.89(7)	C(7B)-C(8B)-H(8B)	126.3(15)
C(3B)-Zr(2)-C(4B)	31.32(6)	Zr(2)-C(8B)-H(8B)	118.3(15)
C(12B)-SiB-C(11B)	113.55(13)	C(8B)-C(9B)-C(10B)	107.8(2)
C(12B)-SiB-C(6B)	112.92(12)	C(8B)-C(9B)-Zr(2)	74.10(13)
C(11B)-SiB-C(6B)	112.46(12)	C(10B)-C(9B)-Zr(2)	71.98(13)
C(12B)-SiB-C(1B)	113.37(11)	C(8B)-C(9B)-H(9B)	125.3(15)
C(11B)-SiB-C(1B)	109.45(11)	C(10B)-C(9B)-H(9B)	126.8(15)
C(6B)-SiB-C(1B)	93.46(9)	Zr(2)-C(9B)-H(9B)	118.2(15)
C(5B)-C(1B)-C(2B)	105.38(19)	C(9B)-C(10B)-C(6B)	109.6(2)
C(5B)-C(1B)-SiB	128.78(16)	C(9B)-C(10B)-Zr(2)	75.50(13)
C(2B)-C(1B)-SiB	122.06(16)	C(6B)-C(10B)-Zr(2)	73.60(12)
C(5B)-C(1B)-Zr(2)	75.21(12)	C(9B)-C(10B)-H(10B)	125.6(13)
C(2B)-C(1B)-Zr(2)	72.55(12)	C(6B)-C(10B)-H(10B)	124.8(13)
SiB-C(1B)-Zr(2)	100.16(9)	Zr(2)-C(10B)-H(10B)	116.4(12)
C(3B)-C(2B)-C(1B)	109.09(19)	SiB-C(11B)-H(11D)	111.1(15)
C(3B)-C(2B)-Zr(2)	78.16(13)	SiB-C(11B)-H(11E)	111.2(14)
C(1B)-C(2B)-Zr(2)	73.65(12)	H(11D)-C(11B)-H(11E)	108(2)
C(3B)-C(2B)-H(2B)	124.0(12)	SiB-C(11B)-H(11F)	106.7(14)
C(1B)-C(2B)-H(2B)	126.9(11)	H(11D)-C(11B)-H(11F)	111(2)
Zr(2)-C(2B)-H(2B)	114.6(12)	H(11E)-C(11B)-H(11F)	108.5(19)
C(4B)-C(3B)-C(2B)	109.1(2)	SiB-C(12B)-H(12D)	108.2(15)
C(4B)-C(3B)-Zr(2)	77.02(12)	SiB-C(12B)-H(12E)	112.3(16)
C(2B)-C(3B)-Zr(2)	69.34(12)	H(12D)-C(12B)-H(12E)	107(2)

SiB-C(12B)-H(12F)	109.9(15)	H(14E)-C(14B)-H(14F)	108.4(18)
H(12D)-C(12B)-H(12F)	112(2)	C(13B)-C(15B)-H(15D)	109.3(14)
H(12E)-C(12B)-H(12F)	108(2)	C(13B)-C(15B)-H(15E)	113.7(16)
C(14B)-C(13B)-C(4B)	111.30(19)	H(15D)-C(15B)-H(15E)	113(2)
C(14B)-C(13B)-C(16B)	110.1(2)	C(13B)-C(15B)-H(15F)	110.9(16)
C(4B)-C(13B)-C(16B)	111.53(19)	H(15D)-C(15B)-H(15F)	100(2)
C(14B)-C(13B)-C(15B)	109.4(2)	H(15E)-C(15B)-H(15F)	109(2)
C(4B)-C(13B)-C(15B)	105.78(19)	C(13B)-C(16B)-H(16D)	112.3(13)
C(16B)-C(13B)-C(15B)	108.6(2)	C(13B)-C(16B)-H(16E)	108.5(13)
C(13B)-C(14B)-H(14D)	112.5(14)	H(16D)-C(16B)-H(16E)	108.9(18)
C(13B)-C(14B)-H(14E)	109.5(12)	C(13B)-C(16B)-H(16F)	116.4(13)
H(14D)-C(14B)-H(14E)	106.0(18)	H(16D)-C(16B)-H(16F)	104.3(18)
C(13B)-C(14B)-H(14F)	115.9(13)	H(16E)-C(16B)-H(16F)	106.1(18)
H(14D)-C(14B)-H(14F)	104.0(19)		

Table 5. *Anisotropic* displacement parameters ($Å^2 x 10^4$) for **AHZ7** (CCDC 162495). The anisotropic displacement factor exponent takes the form: $-2p^2 [h^2 a^{*2} U^{11} + ... + 2 h k a^* b^* U^{12}]$.

	U^{11}	U^{22}	U^{33}	U^{23}	U^{13}	U^{12}
Zr(1)	138(1)	161(1)	144(1)	7(1)	37(1)	3(1)
Cl(1A)	206(3)	267(3)	254(3)	38(2)	76(2)	-49(2)
Cl(2A)	253(3)	305(4)	218(3)	-76(3)	53(2)	54(3)
SiA	175(3)	177(3)	160(3)	26(3)	54(3)	8(3)
C(1A)	138(11)	164(12)	173(12)	-7(9)	65(9)	33(9)
C(2A)	186(12)	148(12)	188(13)	-24(10)	43(10)	11(10)
C(3A)	170(12)	134(12)	229(13)	28(10)	69(10)	19(10)
C(4A)	126(11)	175(12)	182(12)	24(9)	52(9)	33(9)
C(5A)	119(11)	165(13)	187(12)	-11(10)	40(9)	-1(10)
C(6A)	180(11)	164(12)	160(12)	55(9)	39(9)	35(10)
C(7A)	202(13)	237(14)	164(12)	28(10)	7(10)	11(10)
C(8A)	131(12)	319(15)	231(13)	115(11)	-4(10)	11(11)
C(9A)	212(13)	241(14)	269(14)	87(11)	97(11)	114(11)
C(10A)	231(13)	160(13)	267(14)	66(11)	66(11)	13(11)
C(11A)	249(15)	347(17)	205(14)	28(12)	55(11)	50(13)
C(12A)	237(14)	240(15)	302(16)	60(13)	96(12)	-9(11)
C(13A)	181(12)	217(13)	159(12)	30(10)	42(9)	4(10)
C(14A)	257(14)	324(16)	163(14)	24(11)	27(11)	-2(12)
C(15A)	214(14)	298(16)	216(15)	86(12)	58(12)	52(12)
C(16A)	238(14)	310(16)	213(14)	55(12)	89(11)	20(12)
Zr(2)	154(1)	141(1)	144(1)	-3(1)	37(1)	-18(1)
Cl(1B)	209(3)	232(3)	452(4)	-55(3)	99(3)	24(3)
Cl(2B)	279(3)	242(3)	179(3)	8(2)	81(2)	-58(3)
SiB	165(3)	202(4)	153(3)	12(3)	29(3)	-17(3)
C(1B)	182(12)	112(12)	185(12)	11(9)	42(10)	-11(9)
C(2B)	197(12)	154(12)	185(12)	-1(10)	77(10)	-43(10)
C(3B)	142(12)	142(12)	224(12)	7(10)	54(10)	-35(9)
C(4B)	185(12)	97(11)	169(12)	-6(9)	33(9)	-24(9)
C(5B)	193(12)	110(12)	229(13)	-23(9)	95(10)	-11(9)
C(6B)	194(12)	221(13)	98(11)	-26(9)	-3(9)	-67(10)
C(7B)	276(13)	245(14)	126(12)	-43(10)	53(10)	-87(11)
C(8B)	334(15)	169(14)	199(13)	-60(10)	33(11)	-19(11)
C(9B)	279(14)	181(14)	176(13)	3(10)	-7(11)	-96(11)
C(10B)	178(12)	254(14)	163(12)	-23(10)	24(10)	-79(10)
C(11B)	240(14)	265(16)	220(14)	53(12)	35(12)	-40(12)
C(12B)	189(14)	347(18)	232(15)	-40(13)	34(12)	-8(12)
C(13B)	215(12)	214(13)	168(12)	-33(10)	35(10)	-24(10)
C(14B)	297(15)	319(16)	189(14)	-43(12)	64(12)	41(13)
C(15B)	510(20)	371(19)	206(16)	-83(13)	0(14)	-197(16)
C(16B)	191(13)	373(17)	167(14)	-1(12)	6(11)	9(12)

Table 6. Hydrogen coordinates (x 10^4) and isotropic displacement parameters ($Å^2$x 10^3) for **AHZ7** (CCDC 162495).

	x	y	z	U_{iso}
H(2A)	2754(15)	7114(14)	3729(12)	17(6)
H(3A)	2537(15)	7723(15)	2436(11)	16(6)
H(5A)	1221(15)	5247(14)	2215(11)	9(5)
H(7A)	4431(15)	5970(14)	4458(12)	13(6)
H(8A)	5721(16)	5517(14)	3818(11)	14(6)
H(9A)	5046(16)	4137(14)	3032(12)	16(6)
H(10A)	3386(15)	3787(14)	3199(11)	10(6)
H(11A)	1760(20)	5897(17)	4898(13)	35(8)
H(11B)	2853(18)	6199(17)	5061(13)	37(7)
H(11C)	2540(20)	5252(19)	5307(16)	48(9)
H(12A)	723(18)	4178(16)	3748(12)	29(7)
H(12B)	1644(17)	3631(16)	4160(13)	27(7)
H(12C)	1414(19)	3774(18)	3377(15)	40(8)
H(14A)	1211(17)	5310(16)	783(12)	30(7)
H(14B)	491(17)	6011(16)	255(14)	27(7)
H(14C)	153(16)	5728(15)	923(12)	21(6)
H(15A)	37(17)	7442(14)	1255(12)	19(6)
H(15B)	291(16)	7655(15)	543(13)	22(6)
H(15C)	931(16)	8096(16)	1266(12)	21(7)
H(16A)	2579(17)	7519(16)	1103(12)	24(6)
H(16B)	1866(17)	7152(16)	286(14)	32(7)
H(16C)	2649(18)	6501(17)	841(13)	33(7)
H(2B)	8331(14)	6606(13)	922(11)	9(5)
H(3B)	9501(15)	6443(13)	2247(11)	11(5)
H(5B)	6725(16)	6981(14)	2404(11)	16(6)
H(7B)	7165(15)	5146(14)	124(12)	16(6)
H(8B)	7341(16)	3609(15)	765(12)	21(7)
H(9B)	6163(17)	3554(16)	1497(12)	24(7)
H(10B)	5248(14)	5034(13)	1332(11)	6(5)
H(11D)	5620(20)	7125(17)	-715(15)	43(8)
H(11E)	6782(18)	6888(16)	-385(13)	33(7)
H(11F)	6358(16)	7807(16)	-192(12)	24(7)
H(12D)	4862(18)	7828(19)	770(14)	41(8)
H(12E)	4734(18)	6977(17)	1175(15)	39(8)
H(12F)	4240(20)	6994(18)	340(15)	48(8)
H(14D)	7487(18)	7478(17)	3695(13)	34(7)
H(14E)	8283(17)	7044(16)	4450(13)	33(7)
H(14F)	7473(17)	6418(16)	3822(12)	25(7)
H(15D)	8917(19)	8282(18)	3436(13)	37(8)
H(15E)	9980(20)	7700(20)	3354(16)	68(10)
H(15F)	9671(19)	7858(17)	4116(15)	42(8)
H(16D)	9778(17)	6094(15)	4363(13)	26(6)
H(16E)	9978(19)	5985(16)	3562(13)	34(7)
H(16F)	9147(15)	5452(15)	3775(11)	10(6)

Appendix G

X-Ray Crystallographic Data for $(iPr_2\text{-}Mp)ZrCl_2$ (3a, Chapter 3)

Table 1. Crystal data and structure refinement for **AHZ4** (**3a**, Chapter 3, CCDC 162496).

Empirical formula	$C_{18}H_{26}Cl_2SiZr$
Formula weight	432.60
Crystallization Solvent	Toluene/petroleum ether
Crystal Habit	Block
Crystal size	0.41 x 0.26 x 0.19 mm^3
Crystal color	Pale green

Data Collection

Preliminary Photos	Rotation
Type of diffractometer	CCD area detector
Wavelength	0.71073 Å MoKa
Data Collection Temperature	98(2) K
q range for 15807 reflections used in lattice determination	2.48 to 27.95°
Unit cell dimensions	a = 13.4997(6) Å b = 9.9070(4) Å b= 104.3300(10)° c = 14.9907(6) Å
Volume	1942.50(14) $Å^3$
Z	4
Crystal system	Monoclinic
Space group	$P2_1/c$
Density (calculated)	1.479 Mg/m^3
F(000)	888
Data collection program	Bruker SMART
q range for data collection	2.49 to 28.03°
Completeness to q = 28.03°	93.4 %
Index ranges	$-16 \leq h \leq 17$, $-12 \leq k \leq 12$, $-19 \leq l \leq 19$
Data collection scan type	ω scans at 5 ϕ settings
Data reduction program	Bruker SAINT v6.2
Reflections collected	20659
Independent reflections	4379 [R_{int}= 0.0401]
Absorption coefficient	0.898 mm^{-1}
Absorption correction	None
Max. and min. transmission	0.8515 and 0.7114

Table 1 (cont.)

Structure solution and Refinement

Structure solution program	SHELXS-97 (Sheldrick, 1990)
Primary solution method	Direct methods
Secondary solution method	Direct methods
Hydrogen placement	Difference Fourier map
Structure refinement program	SHELXL-97 (Sheldrick, 1997)
Refinement method	Full matrix least-squares on F^2
Data / restraints / parameters	4379 / 0 / 303
Treatment of hydrogen atoms	Unrestrained
Goodness-of-fit on F^2	2.054
Final R indices [I>2s(I), 4024 reflections]	R1 = 0.0207, *w*R2 = 0.0487
R indices (all data)	R1 = 0.0231, *w*R2 = 0.0490
Type of weighting scheme used	Sigma
Weighting scheme used	$w=1/\sigma^2(Fo^2)$
Max shift/error	0.000
Average shift/error	0.000
Largest diff. peak and hole	0.425 and -0.344 e.Å^{-3}

Special Refinement Details

Refinement of F^2 against ALL reflections. The weighted R-factor (*w*R) and goodness of fit (S) are based on F^2, conventional R-factors (R) are based on F, with F set to zero for negative F^2. The threshold expression of $F^2 > 2\sigma(F^2)$ is used only for calculating R-factors(gt), etc., and is not relevant to the choice of reflections for refinement. R-factors based on F^2 are statistically about twice as large as those based on F, and R-factors based on ALL data will be even larger.

All esds (except the esd in the dihedral angle between two l.s. planes) are estimated using the full covariance matrix. The cell esds are taken into account individually in the estimation of esds in distances, angles and torsion angles; correlations between esds in cell parameters are only used when they are defined by crystal symmetry. An approximate (isotropic) treatment of cell esds is used for estimating esds involving l.s. planes.

Table 2. Atomic coordinates (x 10^4) and equivalent isotropic displacement parameters ($Å^2$x 10^3) for **AHZ4** (CCDC 162496). U(eq) is defined as the trace of the orthogonalized U^{ij} tensor.

	x	y	z	U_{eq}
Zr	2585(1)	1019(1)	980(1)	13(1)
Cl(1)	1284(1)	1808(1)	-357(1)	26(1)
Cl(2)	3459(1)	3171(1)	1426(1)	23(1)
Si(3)	2738(1)	-2242(1)	1589(1)	15(1)
C(1)	2129(1)	-735(1)	1988(1)	14(1)
C(2)	2627(1)	320(1)	2597(1)	15(1)
C(3)	1977(1)	1466(2)	2443(1)	16(1)
C(4)	1090(1)	1176(1)	1752(1)	15(1)
C(5)	1194(1)	-168(1)	1464(1)	14(1)
C(6)	3374(1)	-1226(1)	838(1)	18(1)
C(7)	4189(1)	-281(2)	1150(1)	20(1)
C(8)	4208(1)	638(2)	436(1)	24(1)
C(9)	3402(1)	318(2)	-314(1)	24(1)
C(10)	2883(1)	-808(2)	-70(1)	20(1)
C(11)	1752(1)	-3372(2)	891(1)	20(1)
C(12)	3654(1)	-3209(2)	2490(1)	27(1)
C(13)	3586(1)	150(2)	3367(1)	21(1)
C(14)	4095(2)	1481(2)	3715(1)	34(1)
C(15)	3295(2)	-598(2)	4156(1)	43(1)
C(16)	158(1)	2063(2)	1440(1)	19(1)
C(17)	424(2)	3552(2)	1450(2)	35(1)
C(18)	-579(1)	1780(2)	2040(1)	28(1)

Table 3. Selected bond lengths [Å] and angles [°] for **z** (CCDC 162496).

Zr-Pln(1)	2.2054(6)	Zr-Cent(1)	2.209
Zr-Pln(2)	2.2072(6)	Zr-Cent(2)	2.209
Zr-Cl(1)	2.4433(4)	Zr-Cl(2)	2.4476(4)
Zr-C(1)	2.4783(13)	Zr-C(6)	2.4979(14)
Zr-C(2)	2.5074(13)	Zr-C(7)	2.4778(15)
Zr-C(3)	2.5632(14)	Zr-C(8)	2.5490(15)
Zr-C(4)	2.5668(14)	Zr-C(9)	2.5535(15)
Zr-C(5)	2.4721(14)	Zr-C(10)	2.4956(14)
Pln(1)-Zr-Pln(2)	120.34(6)	Cent(1)-Zr-Cent(2)	125.6
Cl(1)-Zr-Cl(2)	98.383(13)		

Table 4. Bond lengths [Å] and angles [°] for **AHZ4** (CCDC 162496).

Zr-Pln(1)	2.2054(6)	C(15)-H(15B)	0.97(2)
Zr-Pln(2)	2.2072(6)	C(15)-H(15C)	1.00(2)
Zr-Cent(1)	2.209	C(16)-C(17)	1.517(2)
Zr-Cent(2)	2.209	C(16)-C(18)	1.523(2)
Zr-Cl(1)	2.4433(4)	C(16)-H(16)	0.942(15)
Zr-Cl(2)	2.4476(4)	C(17)-H(17A)	0.902(19)
Zr-C(5)	2.4721(14)	C(17)-H(17B)	0.95(2)
Zr-C(7)	2.4778(15)	C(17)-H(17C)	0.90(2)
Zr-C(1)	2.4783(13)	C(18)-H(18A)	0.941(18)
Zr-C(10)	2.4956(14)	C(18)-H(18B)	0.949(19)
Zr-C(6)	2.4979(14)	C(18)-H(18C)	0.93(2)
Zr-C(2)	2.5074(13)		
Zr-C(8)	2.5490(15)	Pln(1)-Zr-Pln(2)	120.34(6)
Zr-C(9)	2.5535(15)	Cent(1)-Zr-Cent(2)	125.6
Zr-C(3)	2.5632(14)	Cl(1)-Zr-Cl(2)	98.383(13)
Zr-C(4)	2.5668(14)	Cl(1)-Zr-C(5)	87.07(3)
Si(3)-C(11)	1.8520(15)	Cl(2)-Zr-C(5)	133.14(3)
Si(3)-C(12)	1.8557(16)	Cl(1)-Zr-C(7)	133.09(4)
Si(3)-C(6)	1.8700(15)	Cl(2)-Zr-C(7)	94.30(4)
Si(3)-C(1)	1.8725(15)	C(5)-Zr-C(7)	115.48(5)
C(1)-C(5)	1.4262(19)	Cl(1)-Zr-C(1)	119.19(3)
C(1)-C(2)	1.4391(18)	Cl(2)-Zr-C(1)	128.26(3)
C(2)-C(3)	1.419(2)	C(5)-Zr-C(1)	33.49(4)
C(2)-C(13)	1.5155(19)	C(7)-Zr-C(1)	85.14(5)
C(3)-C(4)	1.4053(19)	Cl(1)-Zr-C(10)	84.85(4)
C(3)-H(3)	0.876(16)	Cl(2)-Zr-C(10)	131.44(4)
C(4)-C(5)	1.4170(19)	C(5)-Zr-C(10)	95.33(5)
C(4)-C(16)	1.5109(19)	C(7)-Zr-C(10)	54.16(5)
C(5)-H(5)	0.970(16)	C(1)-Zr-C(10)	88.82(5)
C(6)-C(10)	1.420(2)	Cl(1)-Zr-C(6)	116.74(3)
C(6)-C(7)	1.432(2)	Cl(2)-Zr-C(6)	127.72(4)
C(7)-C(8)	1.411(2)	C(5)-Zr-C(6)	88.41(5)
C(7)-H(7)	0.927(16)	C(7)-Zr-C(6)	33.44(5)
C(8)-C(9)	1.394(2)	C(1)-Zr-C(6)	66.62(5)
C(8)-H(8)	0.972(19)	C(10)-Zr-C(6)	33.04(5)
C(9)-C(10)	1.412(2)	Cl(1)-Zr-C(2)	136.13(3)
C(9)-H(9)	0.919(17)	Cl(2)-Zr-C(2)	94.72(3)
C(10)-H(10)	0.931(16)	C(5)-Zr-C(2)	54.69(4)
C(11)-H(11A)	0.89(2)	C(7)-Zr-C(2)	86.94(5)
C(11)-H(11B)	0.91(2)	C(1)-Zr-C(2)	33.55(4)
C(11)-H(11C)	0.921(19)	C(10)-Zr-C(2)	116.13(5)
C(12)-H(12A)	0.98(2)	C(6)-Zr-C(2)	85.88(5)
C(12)-H(12B)	0.932(18)	Cl(1)-Zr-C(8)	106.59(4)
C(12)-H(12C)	0.91(2)	Cl(2)-Zr-C(8)	79.76(4)
C(13)-C(14)	1.519(2)	C(5)-Zr-C(8)	143.05(5)
C(13)-C(15)	1.527(2)	C(7)-Zr-C(8)	32.55(5)
C(13)-H(13)	0.958(16)	C(1)-Zr-C(8)	117.01(5)
C(14)-H(14A)	0.93(2)	C(10)-Zr-C(8)	53.48(5)
C(14)-H(14B)	0.96(2)	C(6)-Zr-C(8)	54.69(5)
C(14)-H(14C)	1.00(2)	C(2)-Zr-C(8)	116.91(5)
C(15)-H(15A)	0.95(2)	Cl(1)-Zr-C(9)	79.75(4)

Cl(2)-Zr-C(9)	100.10(4)	C(3)-C(4)-C(16)	126.95(13)
C(5)-Zr-C(9)	126.56(5)	C(5)-C(4)-C(16)	126.15(12)
C(7)-Zr-C(9)	53.55(5)	C(3)-C(4)-Zr	73.96(8)
C(1)-Zr-C(9)	119.43(5)	C(5)-C(4)-Zr	70.03(8)
C(10)-Zr-C(9)	32.44(5)	C(16)-C(4)-Zr	125.65(9)
C(6)-Zr-C(9)	54.50(5)	C(4)-C(5)-C(1)	110.04(12)
C(2)-Zr-C(9)	138.42(5)	C(4)-C(5)-Zr	77.38(8)
C(8)-Zr-C(9)	31.71(5)	C(1)-C(5)-Zr	73.49(8)
Cl(1)-Zr-C(3)	109.21(3)	C(4)-C(5)-H(5)	124.9(10)
Cl(2)-Zr-C(3)	81.40(3)	C(1)-C(5)-H(5)	125.0(10)
C(5)-Zr-C(3)	53.38(4)	Zr-C(5)-H(5)	116.2(9)
C(7)-Zr-C(3)	117.30(5)	C(10)-C(6)-C(7)	105.12(13)
C(1)-Zr-C(3)	54.47(5)	C(10)-C(6)-Si(3)	124.00(11)
C(10)-Zr-C(3)	143.18(5)	C(7)-C(6)-Si(3)	125.83(11)
C(6)-Zr-C(3)	117.41(5)	C(10)-C(6)-Zr	73.39(8)
C(2)-Zr-C(3)	32.48(5)	C(7)-C(6)-Zr	72.51(8)
C(8)-Zr-C(3)	141.47(5)	Si(3)-C(6)-Zr	99.14(6)
C(9)-Zr-C(3)	170.70(5)	C(8)-C(7)-C(6)	109.34(13)
Cl(1)-Zr-C(4)	82.21(3)	C(8)-C(7)-Zr	76.50(9)
Cl(2)-Zr-C(4)	101.75(3)	C(6)-C(7)-Zr	74.05(8)
C(5)-Zr-C(4)	32.59(4)	C(8)-C(7)-H(7)	124.7(10)
C(7)-Zr-C(4)	138.54(5)	C(6)-C(7)-H(7)	125.9(11)
C(1)-Zr-C(4)	54.97(4)	Zr-C(7)-H(7)	117.4(10)
C(10)-Zr-C(4)	126.55(5)	C(9)-C(8)-C(7)	107.89(14)
C(6)-Zr-C(4)	119.44(5)	C(9)-C(8)-Zr	74.32(9)
C(2)-Zr-C(4)	54.10(4)	C(7)-C(8)-Zr	70.94(9)
C(8)-Zr-C(4)	170.85(5)	C(9)-C(8)-H(8)	129.8(10)
C(9)-Zr-C(4)	153.40(5)	C(7)-C(8)-H(8)	122.4(10)
C(3)-Zr-C(4)	31.80(4)	Zr-C(8)-H(8)	120.1(11)
C(11)-Si(3)-C(12)	110.82(8)	C(8)-C(9)-C(10)	108.02(14)
C(11)-Si(3)-C(6)	111.01(7)	C(8)-C(9)-Zr	73.96(9)
C(12)-Si(3)-C(6)	113.13(8)	C(10)-C(9)-Zr	71.52(8)
C(11)-Si(3)-C(1)	110.59(7)	C(8)-C(9)-H(9)	126.4(11)
C(12)-Si(3)-C(1)	116.45(7)	C(10)-C(9)-H(9)	125.6(11)
C(6)-Si(3)-C(1)	93.81(6)	Zr-C(9)-H(9)	121.8(11)
C(5)-C(1)-C(2)	105.94(12)	C(9)-C(10)-C(6)	109.58(14)
C(5)-C(1)-Si(3)	122.42(10)	C(9)-C(10)-Zr	76.03(9)
C(2)-C(1)-Si(3)	127.45(10)	C(6)-C(10)-Zr	73.57(8)
C(5)-C(1)-Zr	73.02(8)	C(9)-C(10)-H(10)	124.6(10)
C(2)-C(1)-Zr	74.33(7)	C(6)-C(10)-H(10)	125.8(10)
Si(3)-C(1)-Zr	99.75(6)	Zr-C(10)-H(10)	114.6(10)
C(3)-C(2)-C(1)	107.73(12)	Si(3)-C(11)-H(11A)	113.8(14)
C(3)-C(2)-C(13)	126.17(12)	Si(3)-C(11)-H(11B)	112.7(12)
C(1)-C(2)-C(13)	125.39(13)	H(11A)-C(11)-H(11B)	99.4(18)
C(3)-C(2)-Zr	75.92(8)	Si(3)-C(11)-H(11C)	112.1(12)
C(1)-C(2)-Zr	72.12(7)	H(11A)-C(11)-H(11C)	114.6(17)
C(13)-C(2)-Zr	125.32(10)	H(11B)-C(11)-H(11C)	103.1(17)
C(4)-C(3)-C(2)	109.62(12)	Si(3)-C(12)-H(12A)	110.2(11)
C(4)-C(3)-Zr	74.24(8)	Si(3)-C(12)-H(12B)	115.1(11)
C(2)-C(3)-Zr	71.60(8)	H(12A)-C(12)-H(12B)	106.0(15)
C(4)-C(3)-H(3)	127.3(10)	Si(3)-C(12)-H(12C)	102.9(12)
C(2)-C(3)-H(3)	123.1(10)	H(12A)-C(12)-H(12C)	116.0(17)
Zr-C(3)-H(3)	121.0(10)	H(12B)-C(12)-H(12C)	106.9(17)
C(3)-C(4)-C(5)	106.63(12)	C(2)-C(13)-C(14)	113.20(13)

C(2)-C(13)-C(15)	108.04(14)	C(4)-C(16)-C(18)	109.02(12)
C(14)-C(13)-C(15)	109.66(14)	C(17)-C(16)-C(18)	111.12(15)
C(2)-C(13)-H(13)	110.1(9)	C(4)-C(16)-H(16)	107.5(10)
C(14)-C(13)-H(13)	105.5(10)	C(17)-C(16)-H(16)	109.6(10)
C(15)-C(13)-H(13)	110.4(10)	C(18)-C(16)-H(16)	106.7(10)
C(13)-C(14)-H(14A)	113.8(13)	C(16)-C(17)-H(17A)	110.5(12)
C(13)-C(14)-H(14B)	110.5(12)	C(16)-C(17)-H(17B)	111.0(11)
H(14A)-C(14)-H(14B)	106.0(17)	H(17A)-C(17)-H(17B)	105.2(16)
C(13)-C(14)-H(14C)	111.1(13)	C(16)-C(17)-H(17C)	110.6(14)
H(14A)-C(14)-H(14C)	106.3(18)	H(17A)-C(17)-H(17C)	110.1(18)
H(14B)-C(14)-H(14C)	108.9(16)	H(17B)-C(17)-H(17C)	109.3(17)
C(13)-C(15)-H(15A)	109.5(13)	C(16)-C(18)-H(18A)	110.3(11)
C(13)-C(15)-H(15B)	109.7(13)	C(16)-C(18)-H(18B)	110.3(11)
H(15A)-C(15)-H(15B)	108.3(17)	H(18A)-C(18)-H(18B)	109.8(15)
C(13)-C(15)-H(15C)	113.6(11)	C(16)-C(18)-H(18C)	109.3(12)
H(15A)-C(15)-H(15C)	110.6(19)	H(18A)-C(18)-H(18C)	109.7(16)
H(15B)-C(15)-H(15C)	104.9(16)	H(18B)-C(18)-H(18C)	107.4(16)
C(4)-C(16)-C(17)	112.71(13)		

Table 5. *Anisotropic displacement parameters* ($Å^2 x 10^4$) for **AHZ4** (CCDC 162496). The anisotropic displacement factor exponent takes the form: $-2p^2 [h^2 a^{*2} U^{11} + ... + 2 h k a^* b^* U^{12}]$.

	U^{11}	U^{22}	U^{33}	U^{23}	U^{13}	U^{12}
Zr	132(1)	102(1)	145(1)	0(1)	33(1)	-9(1)
Cl(1)	207(2)	338(2)	207(2)	98(2)	3(2)	-8(2)
Cl(2)	242(2)	125(2)	319(2)	-24(1)	71(2)	-48(1)
Si(3)	156(2)	100(2)	189(2)	6(2)	35(2)	13(2)
C(1)	158(7)	118(7)	145(6)	22(5)	54(5)	-18(5)
C(2)	164(7)	162(7)	130(6)	1(5)	37(5)	-5(6)
C(3)	198(8)	133(7)	155(6)	-29(6)	65(6)	-12(6)
C(4)	150(7)	142(7)	172(6)	16(5)	68(6)	13(5)
C(5)	139(7)	136(7)	148(6)	5(5)	48(5)	-13(5)
C(6)	177(7)	127(7)	239(7)	-37(6)	87(6)	26(6)
C(7)	153(7)	171(8)	294(8)	-38(6)	78(6)	6(6)
C(8)	224(8)	186(8)	373(8)	-33(7)	192(7)	-17(7)
C(9)	342(9)	194(8)	227(7)	-17(6)	168(7)	-12(7)
C(10)	254(8)	166(7)	212(7)	-55(6)	98(6)	-17(6)
C(11)	214(8)	138(8)	255(8)	-5(6)	54(7)	-6(6)
C(12)	264(9)	181(8)	311(9)	9(7)	-10(8)	58(7)
C(13)	218(8)	199(8)	180(7)	-14(6)	-14(6)	32(6)
C(14)	319(10)	277(10)	311(9)	1(8)	-125(8)	-55(8)
C(15)	477(13)	481(13)	229(8)	139(9)	-91(9)	-127(11)
C(16)	177(8)	155(7)	213(7)	-19(6)	27(6)	37(6)
C(17)	279(10)	169(8)	568(12)	-15(8)	36(10)	61(7)
C(18)	200(9)	381(11)	270(8)	4(7)	77(7)	99(8)

Table 6. Hydrogen coordinates (x 10^4) and isotropic displacement parameters ($Å^2$x 10^3) for **AHZ4** (CCDC 162496).

	x	y	z	U_{iso}
H(3)	2127(11)	2222(17)	2749(10)	17(4)
H(5)	700(12)	-636(17)	983(10)	21(4)
H(7)	4647(13)	-279(17)	1724(11)	25(4)
H(8)	4718(14)	1349(19)	503(11)	31(5)
H(9)	3244(13)	742(17)	-877(11)	25(4)
H(10)	2290(13)	-1182(16)	-441(10)	19(4)
H(11A)	1282(17)	-2940(20)	462(14)	56(6)
H(11B)	1338(16)	-3740(20)	1223(13)	45(6)
H(11C)	2034(15)	-4118(19)	683(12)	34(5)
H(12A)	3330(15)	-3480(20)	2982(13)	42(5)
H(12B)	4247(14)	-2744(18)	2779(11)	29(5)
H(12C)	3848(15)	-3890(20)	2165(13)	41(6)
H(13)	4088(12)	-351(17)	3152(10)	19(4)
H(14A)	4253(16)	2010(20)	3258(14)	49(6)
H(14B)	4730(16)	1330(20)	4161(13)	42(5)
H(14C)	3643(17)	2040(20)	4003(14)	58(7)
H(15A)	2850(17)	-50(20)	4402(14)	51(7)
H(15B)	3904(17)	-780(20)	4641(14)	49(6)
H(15C)	2985(15)	-1500(20)	3978(12)	41(5)
H(16)	-176(12)	1799(16)	837(11)	21(4)
H(17A)	702(15)	3833(18)	2030(13)	36(5)
H(17B)	-177(15)	4087(19)	1241(12)	36(5)
H(17C)	858(17)	3710(20)	1091(14)	49(6)
H(18A)	-789(13)	872(19)	1982(11)	25(5)
H(18B)	-1158(14)	2354(19)	1869(11)	31(5)
H(18C)	-256(15)	1970(20)	2653(14)	47(6)

Appendix H

^{13}C NMR Spectra of Polypropylene Produced by 1c, 2a, 2b, 3a and 3b/MAO (Chapter 2) and 2b/MAO (Chapter 3)

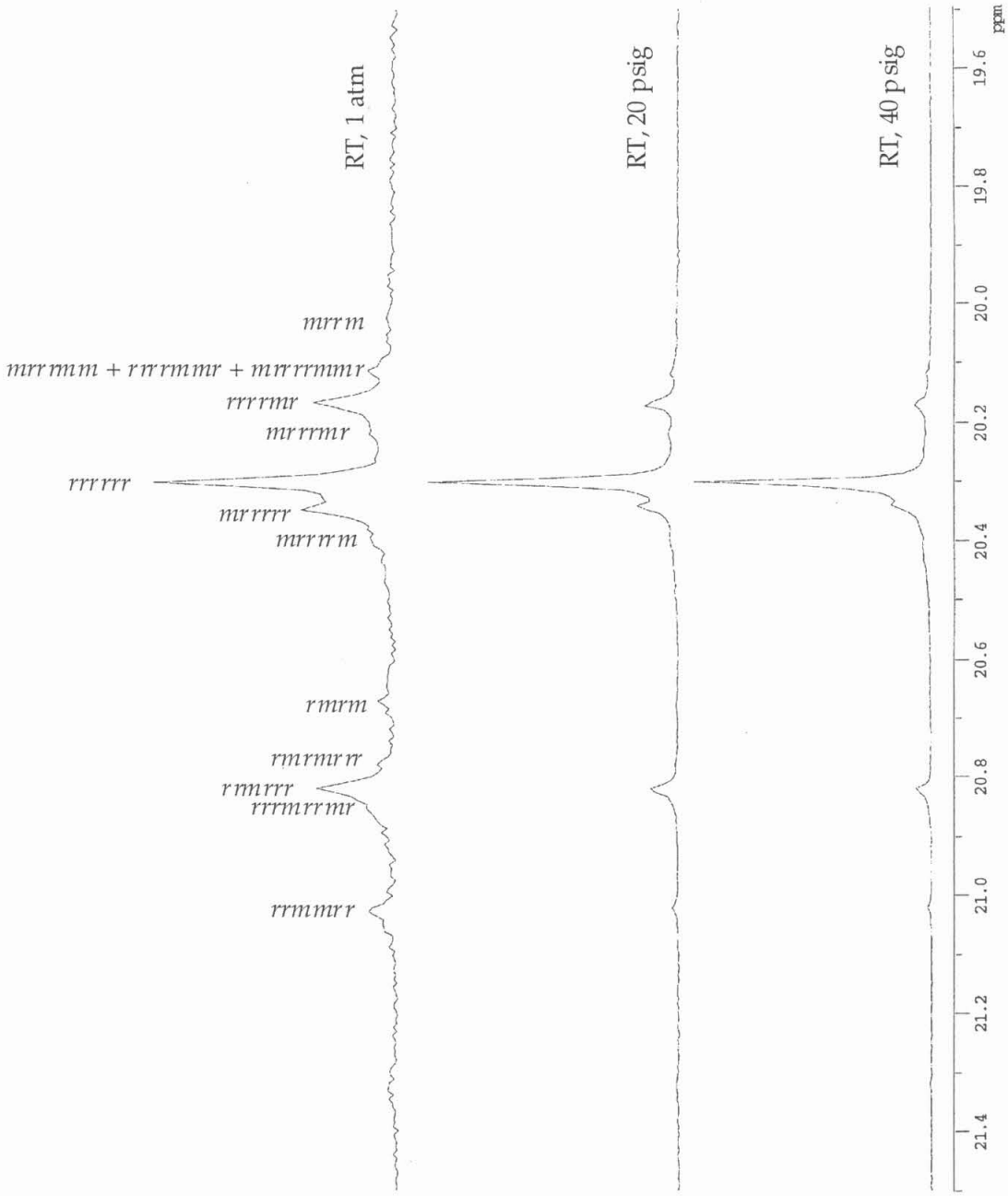

Figure 1. The methyl region of the ^{13}C NMR spectra, showing the pentad distributions of the polypropenes prepared by **1c**/MAO under various propene pressure at room temperature.

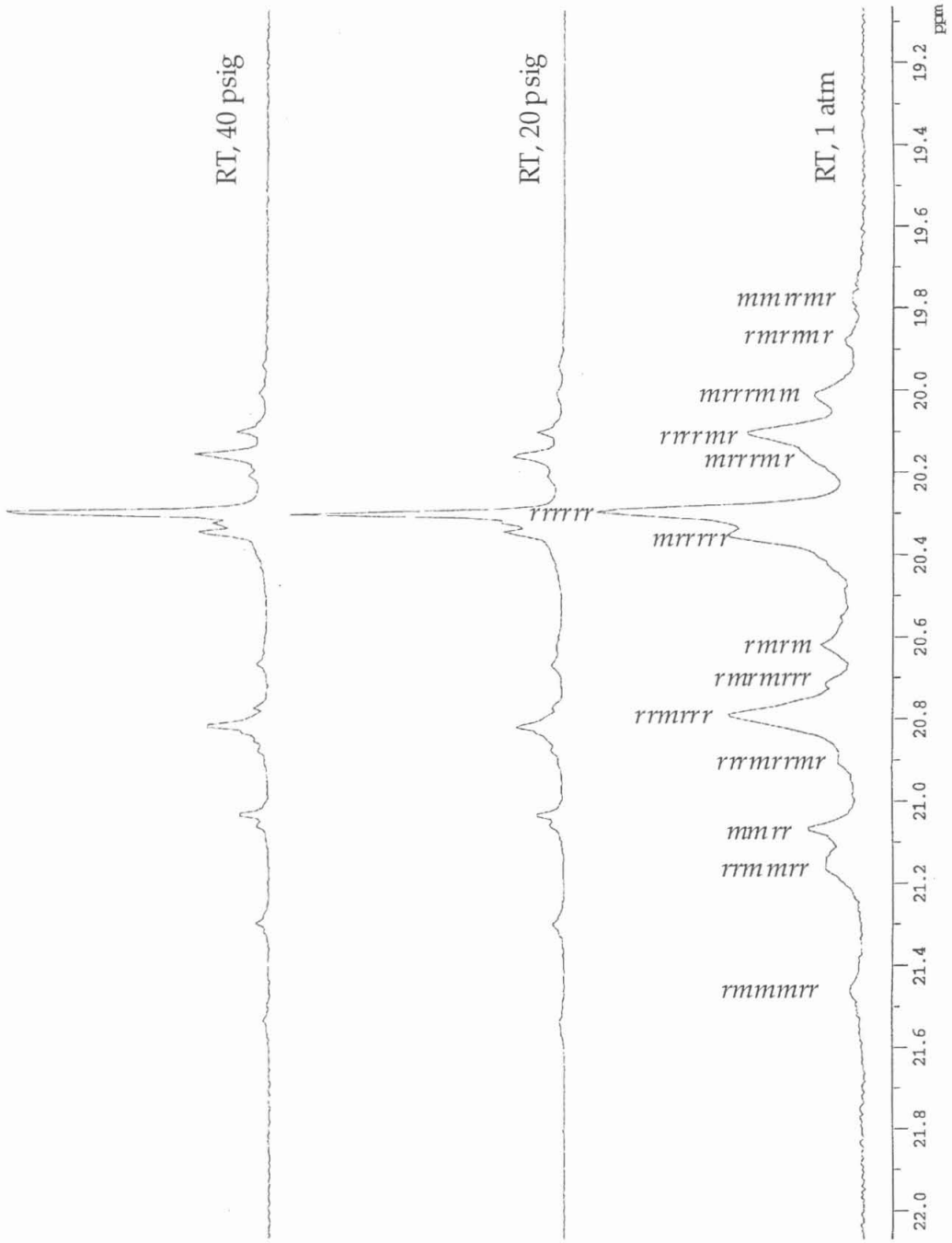

Figure 2. Methyl region of the ^{13}C NMR spectra of polypropylenes prepared by **2a**/MAO under various conditions.

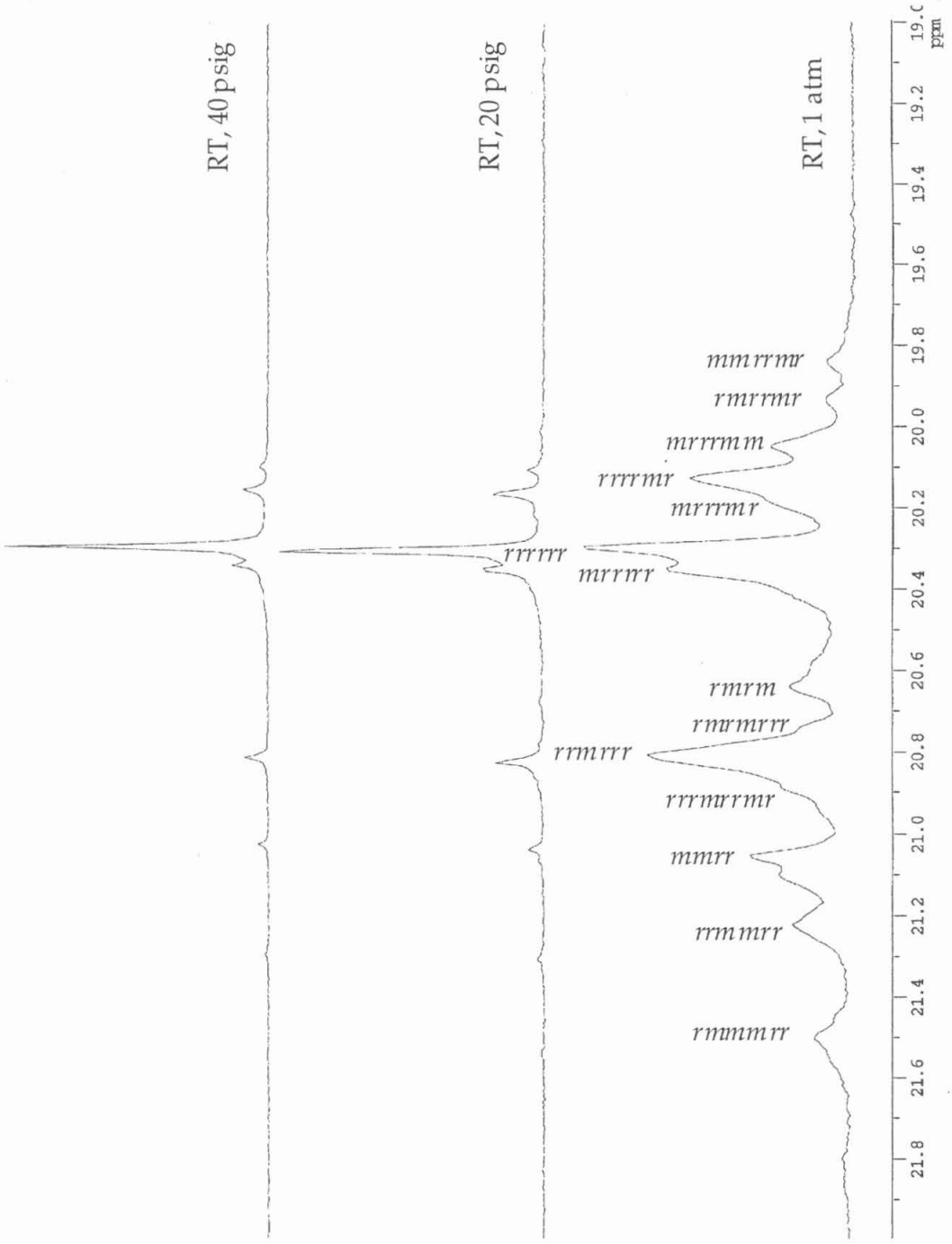

Figure 3. Methyl region of the ^{13}C NMR spectra of polymers prepared by **2b**/MAO under various conditions.

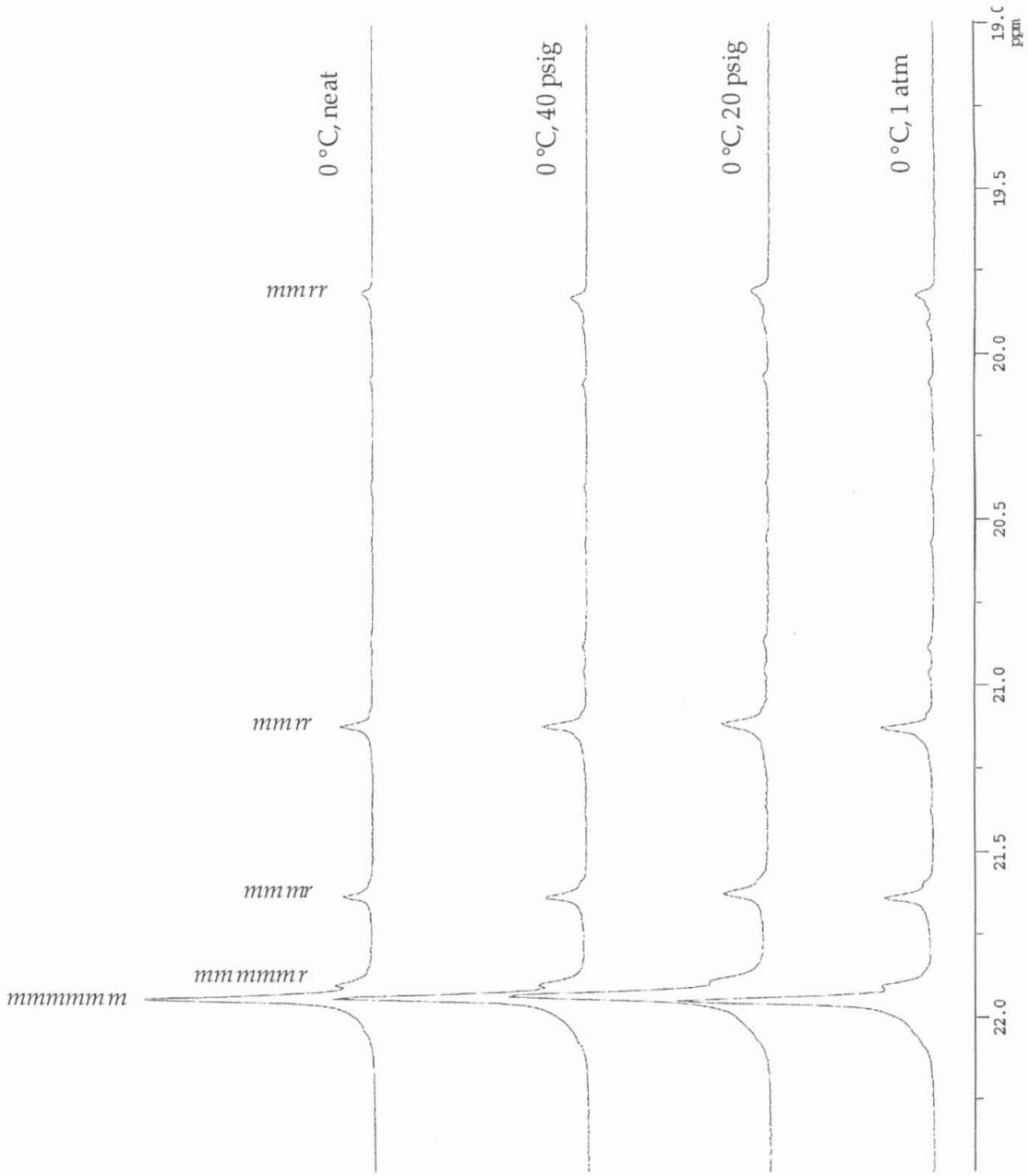

Figure 4 Methyl region of the ^{13}C NMR spectra of polymers prepared by **3a**/MAO under various conditions.

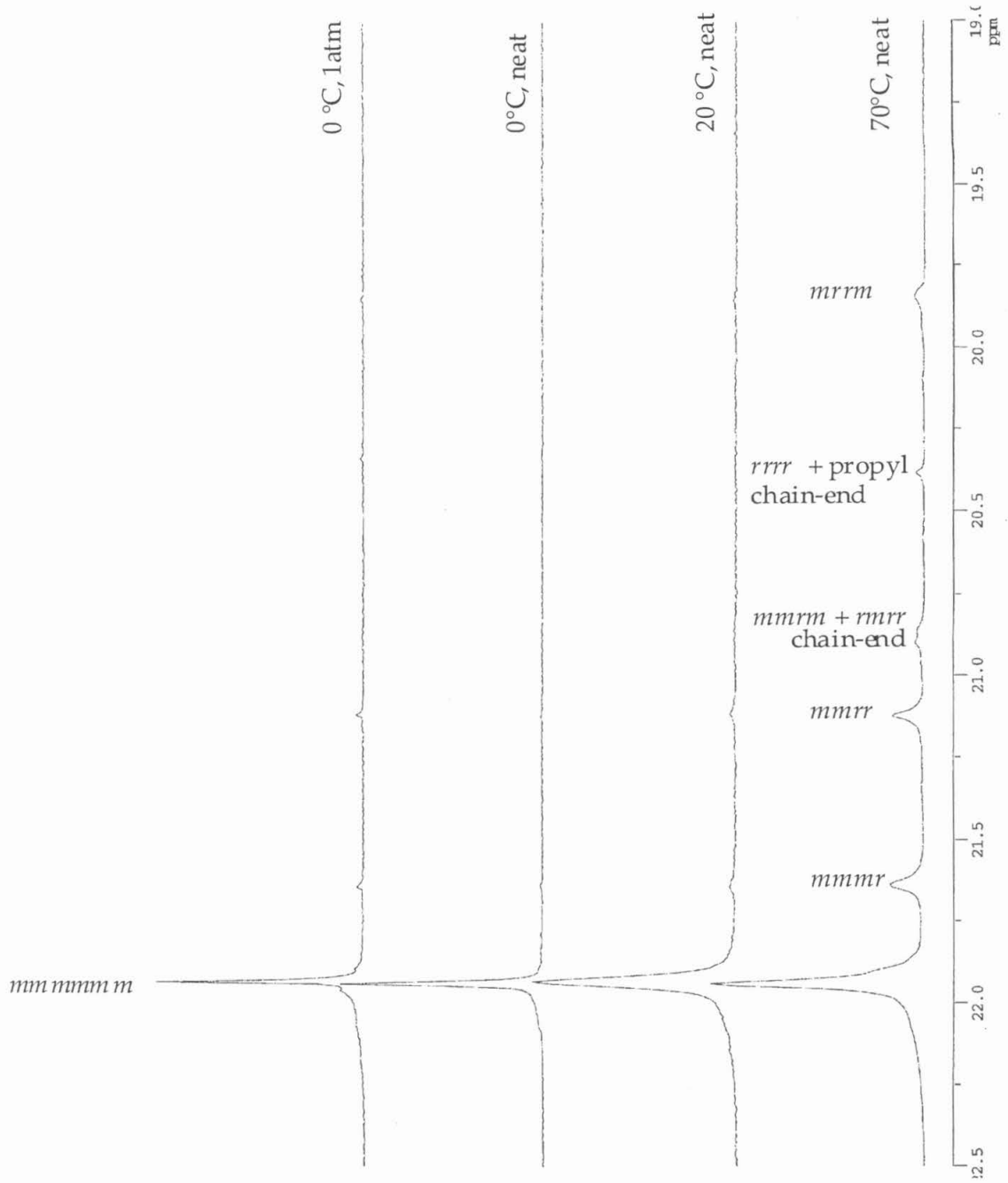

Figure 5. Methyl region of the ^{13}C NMR spectra of polymers prepared by **3b**/MAO under various conditions.

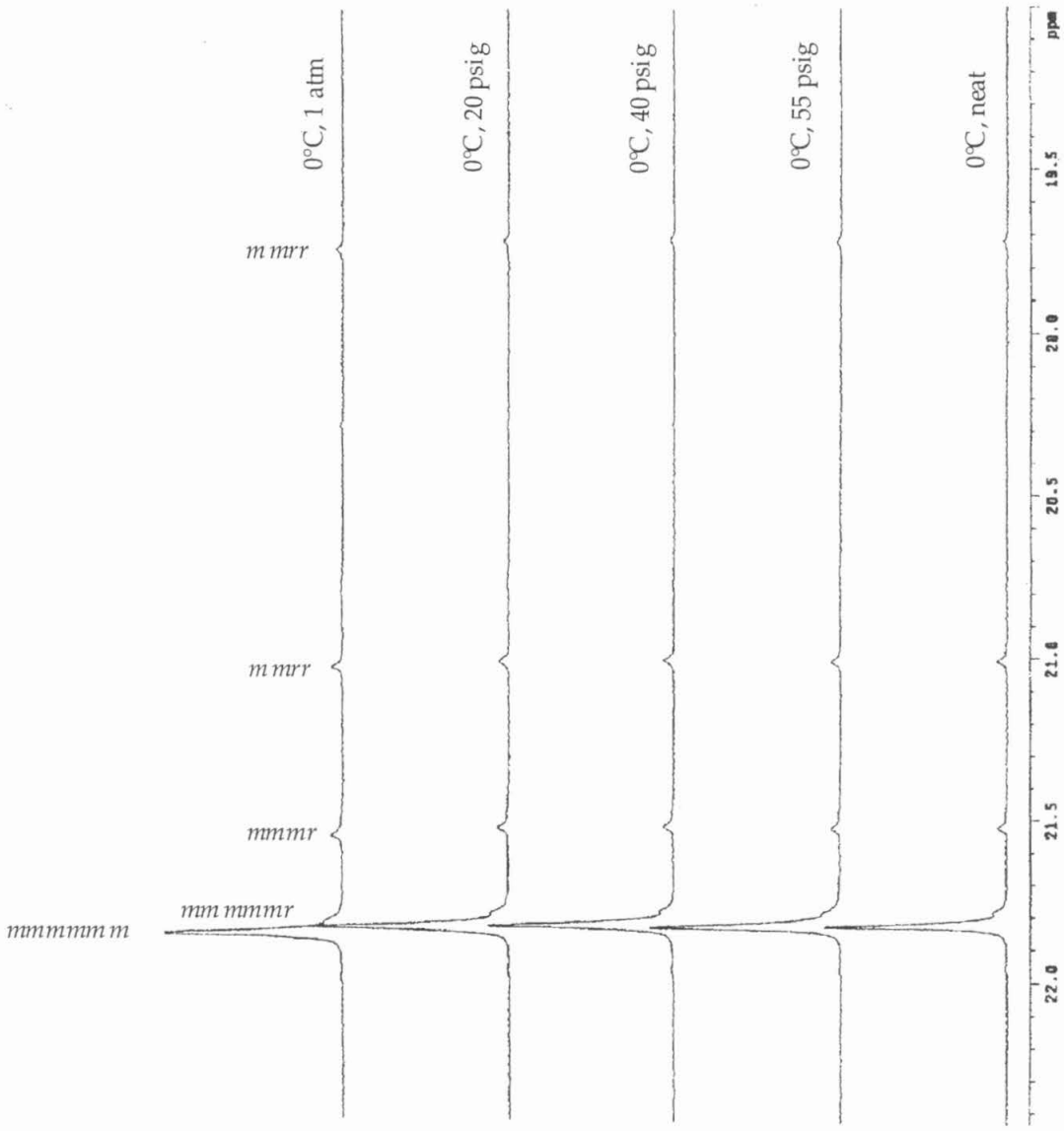

Figure 6. Methyl region of the ^{13}C NMR spectra of polymers prepared by **2b (Chapter 3)**/MAO under various propene pressure at 0–5 °C.